NMR studies of ionic mobility in PVDF based polymer gel electrolytes

Peter Michael Richardson

School of Physics and Astronomy

University of Leeds

Submitted in accordance with the requirements for the degree of

Doctor of Philosophy

September 2013

Declaration

The candidate confirms that the work submitted is his/her own, except where work which has formed part of jointly-authored publications has been included. The contribution of the candidate and the other authors to this work has been explicitly indicated below. The candidate confirms that appropriate credit has been given within the thesis where reference has been made to the work of others.

Chapters 4, 6 and 7 are partially based on work in Ref. [1], with chapters 4 and 5 also based respectively on work in Refs. [2] and [3], all co-authored with A.M. Voice and I.M. Ward (the supervisors), with the candidate as first author.

This thesis is dedicated to my mum, dad and brother for keeping me going throughout the course of this research.

Acknowledgements

I would like to thank all those who have helped me throughout the course of this research. My supervisors Dr. A.M. Voice and Professor I.M. Ward for valuable guidance and discussion throughout the entire project and for help with understanding the physical background of this project. I would also like to thank Dr. P.J. Hine, Dr. M.E. Ries and Dr. R.M.L. Evans for being my support team throughout this research and for providing extremely interesting and illuminating discussions. For help with the experimental side of this research I would like to thank Dr. R.A. Damion for helping with initial training and help with the NMR spectrometer with problems encountered. I would also like to thank Mr. S.C. Wellings for help with general glovebox training and sample preparation. Finally, I would like to thank Dr. J. Fisher from the School of Chemistry for allowing access to the NMR spectrometer and help with setting up the spectrometer to take relevant measurements.

Abstract

The pulsed-field gradient nuclear magnetic resonance (PFG-NMR) method of measuring self diffusion has been employed to understand the ionic mobility of liquid electrolytes and polymer gel electrolytes based on poly(vinylidene) fluoride (PVDF), propylene carbonate (PC) and lithium tetrafluoroborate ($LiBF_4$). Self diffusion measurements were carried out using the resonant frequencies of hydrogen (^{1}H), lithium (^{7}Li) and fluorine (^{19}F) to track the solvent molecules, lithium cation and fluorinated BF_4 anion, respectively. The order of diffusion constants was $D_{^1H} > D_{^{19}F} > D_{^7Li}$, since all entities are moving through the same medium the lithium had the largest radius, which was attributed to a large solvation shell. The NMR-PFG measurements of the polymer gel electrolytes using the lithium and hydrogen resonant frequencies revealed two distinct diffusive species which were attributed to a solvated amorphous polymer phase and pure solvent liquid phase of the polymer gel electrolytes.

Ionic conductivities were measured using impedance spectroscopy for the liquid and polymer gel electrolytes. It was found that increasing the polymer concentration significantly decreased the ionic conductivity. The conductivity was observed to undergo a maximum with salt concentration due to the competition between the increase in ion carriers and viscosity as well as ionic association between the anion and cation. Peaks in the conductivity were analysed using the semi-empirical Casteel-Amis equation which revealed that the conductivity mechanisms were similar in the liquid and polymer gel electrolytes. The ionic conductivity was predicted using the Nernst-Einstein equation with the NMR-PFG diffusion measurements. The predicted values were observed to be significantly greater than the directly measured conductivity, suggesting a high level of ionic association between the cation and anion. For the liquid electrolytes it was observed that ionic association increased with temperature and salt concentration which was attributed to the lowering of the free energy of ion-pair formation at high temperatures. The ionic association for the gels was observed to be significantly higher than the corresponding liquid electrolytes.

The conductivity measurements of the polymer gel electrolytes showed that there are multiple phases contributing to the conductivity, corresponding most likely to a solvated amorphous phase and pure liquid electrolyte phase. It was observed that the total conductivity was an average from these phases which were observed to converge with an increase in temperature, revealed by ratios of gel and liquid conductivities.

The NMR longitudinal (T_1) and transverse (T_2) relaxation times were measured. The liquid and polymer gel electrolytes exhibited similar T_1 and T_2 values, suggesting that the systems were in the extreme narrowing regime (tumbling regime) on the high temperature side of the T_1 minimum. By comparing the longitudinal relaxation

times with the NMR diffusion measurements it was possible to predict the degree of translational and rotational motion of the molecules in solution. It was concluded that the hydrogen and lithium relaxations were predominantly due to translational motion and the fluorine relaxation was predominantly due to rotational motion.

The transverse relaxation measurements of the polymer gel electrolytes revealed at least three different phases containing hydrogen ions and two phases containing lithium ions. These were attributed to interlamellar amorphous PVDF, a solvated amorphous PVDF phase and a pure liquid electrolyte phase for the hydrogen measurements, where the lithium interlamellar amorphous polymer phase was not observed, implying no noticeable association with the polymer.

Viscosity measurements were taken for the liquid electrolyte at varying temperatures and salt concentrations. The ionic radius of each nucleus for the liquid electrolytes were determined using the Stokes-Einstein equation. The hydrogen and lithium effective radii were observed to decrease with salt concentration, whereas the fluorine radii increased. This was attributed to increased ionic association causing loss of the lithium solvation shell at higher salt concentrations.

Abbreviations

$A.C.$	Alternating current
a	Hydrodynamic radius
α	Ionic association
B	Magnetic field (static)
c	Molar salt concentration
D	Diffusion constant
$D.C.$	Direct current
Δ	NMR diffusion time
δ	Gradient pulse duration
E	energy/activation energy (with subscript)
E'	VTF energy term (with subscript for different processes)
ΔE	Energy difference
G	Magnetic field gradient
γ	Gyromagnetic ratio
h	Planck's constant
$\hbar$	Planck's constant divided by 2π
I	Spin
J	Angular momentum
k_B	Boltzmann's constant
$LiBF_4$	Lithium tetrafluoroborate
ln	Logarithm base e
M	Macroscopic magnetisation
μ	Magnetic moment
N_A	Avagadros number
NMR	Nuclear magnetic resonance
PC	Propylene carbonate
$PVDF$	Poly(vinylidene) fluoride
PFG	Pulsed-field gradient
R	Universal gas constant
RF	Radio frequency
r	Distance
SNR	Signal to noise ratio
t	Time
T	Absolute temperature
T_1	Spin-lattice/longitudinal relaxation time
T_2	Spin-spin/transverse relaxation time

$T*_2$	Effective spin-spin/transverse relaxation time
τ	Time interval
τ_c	NMR correlation time
η	Viscosity
σ	Conductivity/ionic conductivity
ω_0	Larmor frequency

Note: these are the most commonly used abbreviations in this thesis. Others appear in particular chapters, but are always introduced and described at the point of use.

Contents

List of Figures

List of Tables

Chapter 1

Introduction

1.1 Polymer Gel Electrolytes

A polymer gel electrolyte (PGE) is a membrane which consists of a polymer, an organic solvent and a salt. Polymer gel electrolytes have been developed over the last thirty years. The stages of this development were (i) dry solid-state polymers, (ii) plasticized gel and (iii) polymer composites [5]. They are of interest due to their uses in advanced secondary lithium batteries and other electrochemical devices.

Research into dry solid-state polymers was first carried out by Wright [6; 7] and Armand [8] which were produced from poly(ethylene oxide) (PEO) with alkali salts. These samples did not contain any liquid and the salt was dissolved by the polymer. The absence of liquid in these solid-polymers resulted in ionic conductivities in the range of 10^{-8} S cm^{-1} for the original research at ambient temperatures; therefore these materials could not be used in electrochemical devices due to the low ionic conductivity. The solid-polymers based on PEO and alkali salts exhibited both crystalline and amorphous polymer phases, concluding that the ionic conduction takes place in the amorphous region of the polymer[9; 10]. PEO based solid-polymers contain a significant amount of crystalline material at ambient temperatures; which is the cause of these low conductivities.

In order to increase the mobility of the ions within the polymer structure it was required to reduce the crystallisation of the polymer, allowing more amorphous regions to serve as pathways for conduction. One method was to use a very low molecular weight version of PEO, termed poly(ethylene glycol) (PEG), which reduces the crystalline polymer and enhances the ionic conductivity [11]. There is another method which has been explored to lower the crystallinity of PEO, which involves the introduction of comb polymers, which has the effect of lowering the glass transition temperature, and produces conductivities as high as 10^{-4} S cm^{-1} [12–15].

Other ways to enhance the mobility of the ions in the polymer structure are to use plasticisers such as low mass oligomers or solvents [16; 17]. This led to the invention polymer gel electrolytes - polymers which are dissolved in organic solvents with a salt. The introduction of solvent to the polymer-salt complexes had the effect of significantly increasing the ionic conductivity to around 10^{-3} S cm^{-1} at ambient temperature. In order for a polymer gel electrolyte to be used in lithium batteries it must exhibit high ionic conductivity at ambient temperatures, good mechanical

strength, high lithium transference number, to be thermally and electrochemically stable and compatible with the electrodes [18].

The third stage in the development of these gels is the composite polymer gel electrolytes. These gels contain nano-particles which have been seen to increase the ionic conductivity[5; 19–21]. However, composite gels will not be considered within this research, however a detailed review by Stephan has been published [5].

There are several different polymers which have been used in the production of PGEs for use in lithium batteries and therefore a considerable amount of research has been carried out. The most popular polymers are PEO, poly(vinylidene fluoride) (PVDF) [22–25], poly(vinylidene fluoride-hexafluoro propylene) (PVDF-HFP) [26; 27], poly(acrylonitrile) (PAN) [28], poly(methyl methacrylate) (PMMA) [29] and poly(vinyl chloride) (PVC) [30].

In this thesis, PVDF thermo-reversible gel electrolytes are investigated. These are semi-crystalline, distinct from gels formed from amorphous polymers such as PMMA. The semi-crystalline gels form crystalline junctions within the solution below the melting temperature. The crystalline junctions will melt again if the melting temperature is exceeded due to the absence of chemical cross-links, allowing the gels to be thermo-reversible [18]. This has particular implications for the practical processability, a process that has been patented at the University of Leeds, known as extrusion lamination [31; 32], relies on this feature. The extrusion lamination process involves keeping a heated source of all constituents at the top of the machine, maintained at the temperature above the melting temperature to hold the PGE in its molten state. The molten gel is then fed into rollers which are coated with electrodes. The molten gel then cools and seals the electrodes together. The PGE acts as the separator meaning there is no need for any addition material or heavy casing for the cells [32].

The aim of this research is to understand how the dynamics change between liquid electrolyte and polymer gel electrolyte and the effect of salt concentration and temperature on the system, therefore focus will be turned to only considering PGEs that contain PVDF. There are several comprehensive reviews on the topic of polymer gel electrolytes containing the polymers previously mentioned [5; 18; 33].

1.2 Polymer Gel Electrolyte Structure

It has already been stated that polymer gel electrolytes consist of a polymer mixed with a solvent and salt mixture. These gels are created by mixing the constituents and heating above the dissolution temperature of the polymer, so that the mixture becomes a homogeneous solution. As the solution cools, phase separation occurs producing a multi-phase complex structure. The phases that are believed to exist in the polymer gel electrolytes are crystalline regions, an interlamellar amorphous polymer phase, a solvated amorphous phase and a pure liquid electrolyte phase as described by Hubbard *et al* [34]. There are many contributing factors that affect the structure and morphology of these gels which will be briefly discussed in this section.

The polymer network in PVDF based polymer gel electrolytes are quite commonly made up of spherulites. Spherulites consist of highly ordered crystalline polymer lamellae which are connected by amorphous regions to form spheres. The highly ordered lamellae give the spherulites an increase in tensile strength, while the interlamellar amorphous regions give the spherulite a

degree of elasticity. The spherulites pack together to form the polymer network, usually deforming at the boundary between two neighbouring spherulites due to their inherent elasticity. The morphology of the spherulites are highly dependent on the cooling rate of the solution[35]. If the cooling rate of the gels is rapid then the amorphous polymer regions are essentially locked in place and can not form these complex spherulite structures, however under a slow cooling rate the lamellar regions can nucleate and grow radially producing spherulites. Although the term spherulite is commonly used in the literature regarding the gelation process, it is not clear the means by which these spherulites are formed and indeed of what they consist. It has been suggested by Chou *et al* [36] that the gelation process has four steps; nucleation and growth into spherical structures, aggregation of the spherical structures, diffusion controlled coarsening which is a fast process and finally Ostwald ripening which is a much slower process [36]. Also in this paper the authors suggest that the spherulite structure commonly observed are compact spheres of crystalline micro-colloids which minimise the surface energy [36]. In an earlier paper by Chou *et al* [37] they state the spherulites may not be crystalline and the structure of the gel consists of an aggregation of spherulitic structures, however it has been observed by Voice *et al* [22] that there are clearly crystalline regions within the gel structure. The exact structure of the PGEs is not fully understood and there is some debate.

There are many publications on the structure of polymer gel electrolytes based on PVDF, some of which will be discussed here. A paper by Shimizu *et al* [38] details gels which have been prepared using dried PVDF membranes, which were subsequently swelled using several different organic solvents, including diethyl carbonate (DEC), γ-butyrolactone (GBL) and propylene carbonate (PC). They found that for all of the solvents used, spherulites were present and that the three dimensional polymer structure is a result of an aggregation of spherulites. They also found that the gelation conditions have significant effects on the size and morphology of the spherulites. They report that using DEC as the solvent resulted in rough edged spherulites, whereas using GBL and PC resulted in very smooth spherulites. They measured both unsalted and salted gels using $LiBF_4$ and found that the spherulite diameter is dependent on the salt concentration. Unsalted PVDF gels were found to have spherulites of around 10 μm in diameter and with 1.0M $LiBF_4$ around 2 μm [38]. It can therefore be noted that the introduction of salt into the system nucleates smaller crystal structures. The research in this thesis concerns polymer gel electrolytes which are allowed to cool at ambient temperature from 160°C. This would therefore allow the formation of spherulites most likely in the micrometer range [38].

Research carried out by Kim *et al* [35] on PVDF-PC based polymer gel electrolytes also showed that spherulites were formed. They took measurements of gels with 15%wt and 25%wt PVDF and were formed by cooling at a controlled rate of 10 K/min and also 1 K/min. They found that the cooling rate had a significant affect of the diameter of the spherulites formed in the polymer network. Much larger spherulites were obtained with the slower cooling rate and were also covered in a 'mesh-like' fibrous substance, for which they did not offer an explanation [35].

Tazaki *et al* [39] have also probed the effect of applying different cooling rates to PVDF based polymer gel electrolytes. They produced two identical samples, however one sample was cooled at a slow steady rate of 0.1 K/min and the other was immersed in a water bath which was held steady at 30°C and therefore rapidly cooled. The result is somewhat counter intuitive, for the

rapidly cooled gel the resulting solution was a turbid gel which was rich in spherulites. The slow cooling rate sample produced a clear gel which contained no visible spherulites, but rather a fibrous polymer structure.

Yang *et al* [40] have investigated thermally induced phase separations of PVDF based polymer gel electrolytes with cyclohexanone (CO) and PC. Again it was observed that the solvent used in the polymer gel electrolytes dictated the structure of the polymer network. For the PC smooth spherulites were observed just as described above [38], for the CO solvent gels a rough edged spherulite was observed, which is comparable to Shimizu *et al* [38] studies using DEC. Yang *et al* [40] have stated that there are two different phase separation mechanisms for CO and PC, respectively. For the gels containing CO the mechanism is thought to occur via a solid-liquid phase separation after the destruction of the polymer-solvent interactions [40], whereas the gels containing PC are believed to firstly go through a liquid-liquid phase separation before the crystallisation takes place.

For solvents such as GBL and PC it is believed that the there is an interaction between the C=O carbonyl group of the solvent and the C-F bond of the PVDF which is considered to be a crucial factor in the gelation of PVDF based gels. These high polarity solvents seem to all exhibit large smooth spherulites [40]. PVDF chains which have been dissolved in PC are known to be in a state which does not allow crystallisation at high temperatures, however at lower temperatures liquid-liquid phase separation will occur once the polymer-solvent interactions have weakened [40].

Magistris *et al* [41] have reported PVDF based polymer gel electrolytes produced using phase inversion, which involves firstly producing a porous PVDF network, drying it out and then swelling with a liquid electrolyte. They report that a two step gelation process is occurring with the majority of the liquid filling voids in the polymer network, with a non-negligible fraction of the electrolyte swelling the amorphous regions of polymer [41]. They achieved gels with both fibrous and spherulitic structures with porosities of up to around 80%. They report pore sizes of around 30 μm, allowing high conductivities to be achieved. They also observed multiple phases for the diffusion measurements and attrbiute them to the liquid filled cavities and a solvated amorphous polymer phase.

In summary the predicted structure of the PVDF/PC/$LiBF_4$ polymer gel electrolytes used in this thesis comprise of smooth spherulites which are densely packed to form a porous polymer network. The spherulites are made up of highly ordered crystalline lamellae which are held together with interlamellar amorphous polymer chains. The packing of the spherulites leaves cavities in the structure which are occupied entirely by liquid electrolyte. There are also likely regions of amorphous polymer which are mixed with liquid electrolyte which will be referred to as a solvated amorphous phase. Therefore the polymer gel electrolytes are assumed to contain four distinct phases; a crystalline lamellar polymer phase, an inter-lamellar amorphous phase, a solvated amorphous PVDF phase and a pure liquid electrolyte phase[34].

1.3 Experimental Techniques

1.3.1 Sample Preparation

PVDF was chosen for this research due to its semi-crystalline thermo-reversible nature and therefore processability advantages. However, PVDF has other advantages, for instance, it contains a strong electron withdrawing functional group (C-F) which allows the polymer to be anodically stable [5; 18]. It also exhibits a moderate dielectric constant which is helpful in the dissolving of the salt anion and cation which enhances the ionic conductivity with less neutral pairs.

The solvent is used as a plasticiser; the plasticisation effect of adding an organic solvent to the polymer is to decrease the glass transition temperature of the polymer. This decrease in glass transition temperature helps to soften the polymer chain and has a positive effect on segmental motion. The increased segmental motion creates voids or free volume cavities which the pure liquid electrolyte can fill. This has the effect of increasing the ionic mobility through the material in the presence of an electric field [42]. The desirable properties of the organic solvents are; a high boiling point, low viscosity and high dielectric constant. The high dielectric constant is needed in order to dissociate the salt into charge carriers to enhance the ionic conductivity of the system. Other high boiling solvents used include dimethyl formamide (DMF), ethylene carbonate (EC), γ-butyrolactone (GBL) and diethyl carbonate (DEC) [43; 44].

The salt that was used in this research was lithium tetrafluoroborate ($LiBF_4$). In order to achieve high ionic conductivity, a low degree of ionic association is required. Lithium based salts are a popular choice since lithium is a charge dense ion. The anion is also of importance and usually a fluorinated anion is chosen as they are relatively large, causing an uneven size distribution which promotes ionic dissociation. Other popular salts include $LiCF_3SO_3$, $LiPF_6$ and LiBOB [44–46]. The LiBOB salt is relatively new and has been found elsewhere to produce high conductivities despite its high viscosity due to the ability of enhanced ionic dissociation [46]. It has also been shown that by adding a small amount of LiBOB to a PC/$LiBF_4$ system, it enhances the performance of the Li-ion cell [47].

The polymer gel electrolytes were produced using the thermo-reversible gel crystallisation technique [18; 22; 48]. This method involved mixing the salt and solvent together until fully dissolved to produce the liquid electrolyte. Then the liquid electrolyte was added to the polymer and throughly mixed. Once heated up past the melting point of the polymer solution (160°C), it was stirred and allowed to cool. As the molten solution cooled it formed the crystalline junctions and became the flexible polymer gel electrolyte. Other preparations of these gels involved a technique known as phase inversion which involves being dissolved in a solvent, which is then washed out with a non-solvent leaving a porous membrane which can be swelled with any liquid electrolyte [49].

1.3.2 NMR-PFG Measurements

Pulsed-field gradient NMR has been widely used in the analysis of the transport properties of both liquid and polymer gel electrolytes. This technique involves using radio frequency (RF) pulses to excite the nuclear spins which will decay with time. However this pulse sequence applies two magnetic field gradients, one to give spatial encoding of the spins and one to remove

the encoding after a set time (Δ). The attenuation of the signal is then dependent on the diffusion of the spins and can be determined from fitting. The classic PFG sequence was first designed by Stejskal and Tanner [50], however it has been found that a modification of this classic pulse sequence can enhance the data by use of a stimulated echo version of the sequence [51]. The pulse sequence used in this research was a complex version of the Stejskal and Tanner sequence designed by Cotts [52], which involved bipolar magnetic gradient pulses to account for any background field gradients caused by field inhomogeneities.

It is possible to measure the diffusion constant for different nuclei by applying the resonant frequency of the relevant nucleus. This technique is a powerful tool in understanding the dynamics of each constituent in the liquids and gels. In the polymer gel electrolytes the organic solvents usually contain hydrogen; the cation of the salt is usually lithium and the anions are usually fluorinated. Common measurements of these gels are carried out using ^{1}H, ^{7}Li and ^{19}F to detect the solvent molecules, cation and anion, respectively [25; 53–56]

This method has been commonly used to determine the diffusion constants of liquid electrolytes [56], however the focus of most research in this field is to determine few temperatures and salt concentrations of many different combinations and mixtures of materials. In this research only a single solvent and single salt are used in order to gain a comprehensive understanding of the system with both salt concentration and temperature. The polymer gel electrolyte diffusion measurements carried out in this thesis were more novel and thought provoking than the corresponding liquid electrolyte, however they are helpful in understanding the dynamics of the ions in the gels. It was observed that two distinct diffusive species could be identified via the PFG-NMR measurements, which were attributed to two different phases within the gels. This has been seen briefly by one group which observed this for some PVDF and PVDF-HFP based gels containing 1.0M $LiPF_6$ in a mixed solvent of EC:DEC (1:1) [41]; however the authors only witnessed two diffusion constants for gels that had high levels of porosity.

The presence of multiple phases has been witnessed using various techniques by different research groups. Capiglia *et al* [26] underwent measurements on polymer gel electrolytes based on PVDF-HFP with EC/DEC mixtures using $LiN(C_2F_5SO_2)_2$ for a range of different polymer concentrations. They found that the diffusion measurements increased as the solvent content increased; they also determined via scanning electron microscopy (SEM) that at polymer:solvent ratios of 50:50 no cavities were observed. However for polymer:solvent ratios 40:60 and 30:70 cavities of the order of 10 μm were observed. This group concluded that for high solvent containing polymer gel electrolytes, interconnected cavities existed which allows the free liquid to flow. A similar result was observed by Song *et al* [27] for PGEs containing PVDF-HFP with 1.0M $LiPF_6$ and EC, that an EC rich phase was present at a content level of 60wt.% of EC. The porosity was reported to change from 32% at low solvent content to 62% at high solvent content. Therefore the mobility of the gels is dependent on the amount of solvent contained, however as the solvent amount is increased the mechanical properties of the gel decrease [48]. The presence of multiple diffusive species and therefore phases is discussed in detail in this thesis (Chapter 5).

1.3.3 NMR Relaxation Times

In this research the NMR relaxation times were measured using saturation recovery (T_1) and Carr-Purcell-Meiboom-Gill (CPMG) (T_2) pulse sequences. It has been shown in this research

that by comparing the diffusion and longitudinal relaxation times that translational and rotational contributions of the relaxation can be determined for the liquid electrolytes, this was achieved by following the strategy of Williamson *et al* [57]. NMR relaxation times have been used to determine translational and rotational contributions on different systems elsewhere [57; 58].

The T_2 values for the polymer gel electrolytes can be used to detect the number of phases present in the polymer gel electrolytes. The presence of multiple phases has been observed in other measurements of NMR relaxation times. It was observed by Hubbard *et al* that by measuring the $T_{1\rho}$ NMR relaxation times of PVDF based polymer gel electrolytes revealed multiple phases [34]. The authors witnessed at least four different phases within the gels. The phases were attributed to a crystalline PVDF, interlamellar amorphous PVDF, solvated chains of the PVDF and a pure liquid electrolyte component [34].

A publication by Ali *et al* [59] presents T_1, T_2 and $T_{1\rho}$ measurements for plasticised amorphous PEO-PPO with $LiCF_3SO_3$ with PC and DMF as the plasticising agents. They found that in the presence of 50% PC the $T_{1\rho}$ measurements exhibited two different values, which were attributed to two different phases within the gel [59].

1.3.4 Impedance Spectroscopy

The ionic conductivity has been determined for the liquids and polymer gel electrolytes using impedance spectroscopy. Conductivity is a common measurement as this value is of great importance to the practical lithium battery application. The understanding of the ionic conductivity for these liquids and gels is crucial as a high ionic conductivity is needed for use in lithium batteries. The conductivity of gels is observed to significantly decrease with the addition of polymer [18]. It is therefore important to understand the location of the ions. It has been stated elsewhere, that the ionic conductivity of a porous membrane is essentially the conductivity of the electrolyte contained within [60; 61]. Therefore, the membranes porosity and tortuosity dictate the ionic conductivity. The ionic conductivity of the liquids and polymer gel electrolytes have been measured in this thesis. By comparing these two values some insight into the conduction mechanisms can be obtained. It is also proposed in this thesis that the conduction arises from multiple regions of gel and not simply from liquid channels within the gel.

1.3.5 Ionic Association

The ionic association is an important factor as it dictates the ionic conductivity of the system. The ionic association is the fraction of ions which are unable to contribute to the conductivity due to ion pairing. This factor can be determined by calculating the predicted conductivity using the diffusion constants of the cation and anion along with the Nernst-Einstein equation which has the form;

$$\sigma = \frac{N_A e^2 c}{k_B T} \left[D_{Li} + D_{BF_4} \right] \tag{1.1}$$

where c is the salt concentration, e is the fundamental charge on an electron, N_A is the Avagadro number, k_B is Boltzmann's constant, T is the absolute temperature and D_{Li} and D_{BF_4} are the diffusion constants for the cation and anion, respectively. The ratio of the predicted and measured conductivity is the ionic association of the system. This method is widely used to determine the ionic association of both liquid and polymer gel electrolytes [43; 54; 56; 62; 63].

The ionic association was determined by Aihara *et al* [56] for liquid electrolytes containing six different salts in PC and GBL. The salts that were measured were found to be in order of association $LiSO_3CF_3$>$LiBF_4$>LiBETI≈LiBOB≈LiTFSI≈$LiPF_6$. Therefore the system used in this research was analysed and found to exhibit one of the highest ionic associations. It was observed that all of the salts exhibited a rise in ionic association with increasing salt concentration. This was also measured for the PC/$LiBF_4$ liquid electrolytes in this thesis, where the temperature dependence has also been determined.

There is an alternative way of determining the ionic association more directly, used by Kataoka *et al* [64; 65] which employs an electric current while measuring the PFG-NMR diffusion constants. Since only the conducting ions will be affected by the electric field the ionic association can be determined. Using this technique, the authors were also able to determine the individual mobilities of the anion and cation. In this research the ionic association was only determined via the Nernst-Einstein equation.

1.4 Aims and layout

The main aim of this research, as discussed above, was to investigate the dynamics of PVDF based polymer gel electrolytes and the corresponding liquid electrolytes they are based upon. It is important to understand the dynamics within the liquid electrolyte before the polymer gel electrolytes can be discussed, as the polymer is viewed as a porous container of the liquid electrolyte. The techniques which were used in this research were NMR pulsed-field gradient diffusion, T_1, T_2, impedance spectroscopy and viscosity measurements. The diffusion measurements allowed determination of three different resonant frequencies ^{1}H, ^{7}Li and ^{19}F which corresponded to the solvent molecules, lithium cation and fluorinated anion. By comparing the diffusion and viscosity measurements, values of the ionic radii can be determined. It was also possible to predict the conductivity of the system by using the diffusion constants of the anion and cation. This produced a conductivity much higher than the directly measured values due to ionic association, therefore a ratio of the two values yielded the fraction of salt not able to contribute to the conductivity.

The measurements taken throughout the course of this research have allowed determination of a lot of key factors which affect the mobility of the ions in solution. For the battery applications, for which this is the primary application, the conductivity and ionic association must be understood. The phase separation of the polymer gel electrolytes is also of interest as the pore size and tortuosity of the polymer structure has a direct effect on the mobility of the ions within the gels, this issue has not been directly addressed here but rather some thought provoking discussions have been carried out based on the ionic conductivity and diffusion measurements. Most of these issues have been addressed in this thesis to form a comprehensive discussion on the dynamics of PVDF based polymer gel electrolytes.

1.4.1 Thesis Layout

The thesis is laid out as follows: in Chapter 2 the basic theory of nuclear magnetic resonance is discussed, as well as the experimental pulse sequences which were utlilised. Details on the spectrometers used throughout the course of this research can also be found in Chapter 2. In

Chapter 3 a detailed description of the the sample preparation is reported as well as the the background theory and experimental detail of the impedance spectroscopy and viscosity measurements. In Chapter 4 the liquid NMR results are discussed, including both longitudinal (T_1) and transverse (T_2) NMR relaxation times and translational diffusion constants. This chapter contains a detailed analysis of the data as a function of salt concentration and temperature; with a comparison between the T_1 and diffusion data which gives insight into translational and rotational contributions of the relaxation. This led into Chapter 5 which discusses the corresponding polymer gel electrolytes NMR results. Measurements of T_2 and diffusion yield interesting discussions on the phase separation of the gels as a function of salt and temperature. In Chapter 6 the ionic conductivity measurements are discussed for both liquid and polymer gel electrolytes. The temperature and salt concentrations dependences have been comprehensively studied and a comparison between the gel and liquid conductivities suggests multiple phase conductivity contributions. Finally, in Chapter 7 the diffusion and conductivity data are analysed to determine the ionic association of the liquids and gels. The viscosity measurements of the liquid electrolytes are also reported. This allows determination of the ionic radii with the use of the Stokes-Einstein equation. The final conclusions of the research as well as possible direction for future work can be found in Chapter 8.

1.5 Publications

The work presented in this thesis has resulted in three papers, co-authored with my supervisors A.M. Voice and I.M. Ward. Chapters 4, 6 and 7 are based on Refs. [1]. Chapters 4 and 5 also based, respectively, on work in Refs. [2] and [3]. Details of the contribution of each of us to these papers is given in the declaration at the start of this thesis.

Chapter 2

Nuclear Magnetic Resonance

2.1 Nuclear Spin

All protons and neutrons, the components of the atomic nuclei, have the quantum intrinsic property spin. This intrinsic property of the protons and neutrons arises from the composition of the quarks that are the building blocks of these particles [4]. There are six known types of quarks, all of which are believed to have spin-1/2, three of which have a charge of $-e/3$ and the other three have a charge of $+2e/3$. Protons and neutrons each comprise of three quarks held together by gluons. The proton is made up of one quark with the charge $-e/3$ and two quarks with charge $+2e/3$ which gives an overall charge of 1. Two of the quarks have spins antiparallel to each other which cancel each other out leaving a sole spin-1/2 quark contributing to the total spin of the proton. Therefore this yields a spin-1/2 for the proton. The neutron is also comprised of three quarks; this time two with charge $-e/3$ and one with charge $+2e/3$ resulting in a neutral charge. As with the proton the neutron contains two quarks with antiparallel spins resulting in an overall spin-1/2. The quark configuration of the proton and neutron are shown in figure 2.1.

Since all nuclei that can be addressed in NMR are simply compositions of differing number of protons and neutrons, the spins of any nuclei can be determined. When combining two spins,

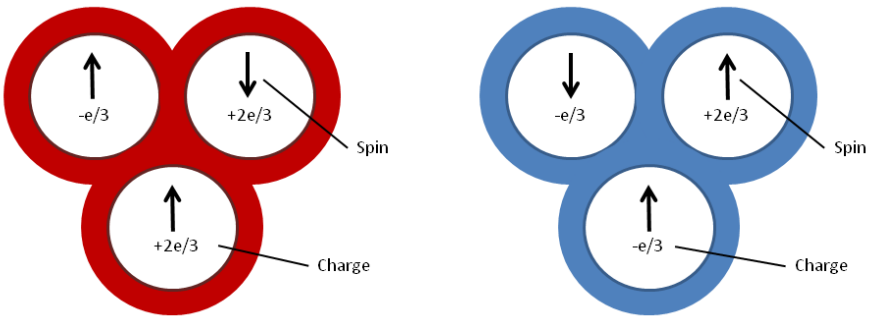

(a) Proton (b) Neutron

Figure 2.1: Quark configuration of proton and neutron. Figure adapted from reference [4]

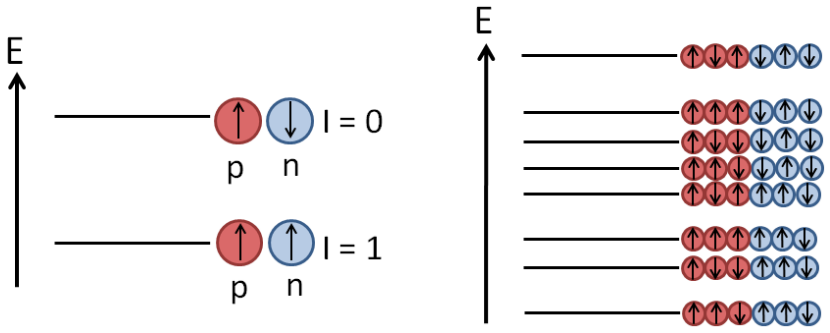

(a) ^{2}H energy levels. (b) ^{6}Li energy levels.

Figure 2.2: Energy levels of the possible spin states of the ^{2}H and ^{6}Li nuclei. Figure adapted from reference [4]

each of spin-1/2, the general rule of possible values that can be taken are;

$$S_{Total} = \begin{pmatrix} |S_1 - S_2| \\ |S_1 - S_2| + 1 \\ \vdots \\ |S_1 + S_2| \end{pmatrix} \tag{2.1}$$

where S_1 and S_2 are the spin values of the two spins that have been placed together with S_{Total} as the resulting spin [4]. Therefore two spin-1/2 particles placed together can take the values of S_{Total}=0 and S_{Total}=1; this example is synonymous with a deuterium (^{2}H) nucleus as it consists of a proton and a neutron both with spin-1/2. Electrons are bound by the Pauli exclusion principle which states that two fermions cannot have the same quantum state, i.e. could not have two parallel spins. However, the intrinsic spin property of a nucleus does not abide by the same rules, therefore two parallel spins can occur. Although the parallel and antiparallel situations are possible, the ground state is the most likely configuration as it requires a lower amount of energy to occupy. Figure 2.2(a) shows the relative energy that each state takes up for the ^{2}H nucleus; the energy for the antiparallel case is significantly higher than that of the parallel state, an energy gap so significant that it means the higher states cannot be reached via normal chemical reactions or electromagnetic fields. In NMR the spin of nuclei is defined by the ground state energy level arrangement due to the stability of this state. Figure 2.2(b) shows the possible arrangements of the ^{6}Li nucleus which contains three protons and three neutrons, showing that the ground state spin of the ^{6}Li is I=1.

There are no set rules for which of the spin states is the ground state energy level and they are traditionally determined empirically, however there are some general rules to govern the spin a nucleus will exhibit. If the number of protons and neutrons are both even numbers then the ground state spin is I=0 and is NMR silent; as NMR exploits the intrinsic spin; two examples are the ^{12}C and ^{16}O nuclei. If the number of protons and neutrons are both odd then an integer value of the spin is achieved. If the nucleus has a mass number which is even, then the spin has to be an integer and if the mass number is odd, then the spin will have a half-integer value. Examples of odd mass number nuclei are ^{1}H, ^{7}Li and ^{19}F which have spin of 1/2, 3/2 and 1/2,

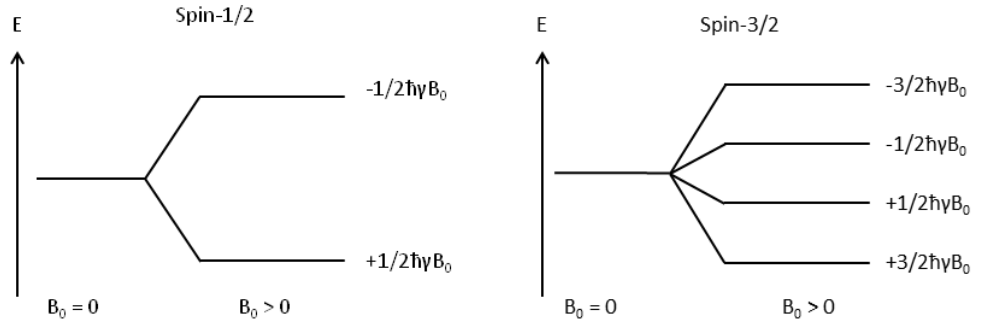

(a) Zeeman splitting for spin-1/2 nuclei. (b) Zeeman splitting for spin-3/2 nuclei.

Figure 2.3: Zeeman splitting energy levels of the possible spin states of the spin-1/2 and spin-3/2 nuclei.

respectively; these three nuclei are the ones used in this research.

2.2 Single Spin

It is logical to start by considering a single ^{1}H nucleus as this is a simple spin-1/2 case. The presence of the intrinsic spin property introduces a non-zero magnetic moment, μ. The spin quantum number I and magnetic moment are related to each other in the form;

$$\vec{\mu} = \gamma \vec{J} = \gamma \hbar (I(I+1))^{\frac{1}{2}} \tag{2.2}$$

where γ is known as the gyromagnetic ratio, which has a unique value for each nucleus and $\hbar(I(I+1))$ is the spin angular momentum term ($\vec{J}$). This spinning motion has certain quantised angular momentum values. In the absence of a magnetic field, all of the spin states have the same value and are degenerate. When a non-zero spin system is placed in the presence of a magnetic field, the degenerate states become non-degenerate due to Zeeman splitting. The number of occupied states is given by;

$$\#ofSpinStates = (2I+1) \tag{2.3}$$

where I is the spin quantum number, for spin 1/2 nuclei, I=1/2. Along with the number of accessible states, there are also a list of discrete values that each state can possess. These are governed by the quantum number m and is defined by;

$$m = -I, -I+1, ..., I-1, I \tag{2.4}$$

which dictates that the values that can be taken for m are from $-I$ to I with integer spacing. For a ^{1}H nucleus with spin-1/2, there are two possible states with values of m=-1/2,+1/2, shown in figure 2.3(a). The nuclei of ^{7}Li with spin-3/2, will exhibit four different energy levels during the Zeeman splitting; two parallel and two antiparallel states shown on figure 2.3(b).

When the spins are in the presence of a magnetic field the energy of the magnetisation can be expressed as;

$$E_{Mag} = -\vec{\mu}.\vec{B} \tag{2.5}$$

where $\vec{B}$ is the magnetic field strength of the static field applied to the system. The dot product in equation 2.5 means that the direction of the magnetic moment is relative to that of the magnetic field. The magnetic moment can now either align parallel or antiparallel to the magnetic field. It is clear that the lower energy state is when the magnetic moment is parallel to the magnetic field, indicated by the negative sign in equation 2.5. The two states can be labeled as α and β for the parallel and antiparallel configurations, respectively. Equation 2.2 for the magnetic moment can now be written in terms of the z-direction, which is defined as the direction of the static field, in the form;

$$\mu_z = \gamma J_z = \gamma \hbar m \tag{2.6}$$

where μ_z and J_z are the magnetic moment and spin angular momentum in the z direction, respectively. By combining equation 2.5 and 2.6 the energy of magnetisation becomes;

$$E_{Mag} = -\gamma \hbar B_z m \tag{2.7}$$

where B_z is the magnetic field in the z-direction, as it is standard to define the static magnetic field to be applied in the +z direction. For a spin-1/2 nucleus the two possible m values available are -1/2 and +1/2 and therefore the difference in energy between the two states can be expressed as;

$$\Delta E_{Mag} = E_\beta - E_\alpha = \hbar \gamma B_z \tag{2.8}$$

where E_α and E_β are the energies for the parallel and antiparallel states, respectively. This splitting produces two states, α and β with different energies described by equation 2.8 which shows that the difference in energy of the two states is dependent on the magnitude of the magnetic field applied to the system. In order for the spins to change state, the system must absorb or emit energy that is equal to ΔE_{Mag} which in terms of frequency ν_0 is;

$$\nu_0 = \frac{\Delta E_{Mag}}{h} = \frac{\gamma B_z}{2\pi} \tag{2.9}$$

which can also be expressed as an angular velocity ω_0 given by the equation;

$$\omega_0 = 2\pi\nu_0 = \gamma B_z \tag{2.10}$$

this is known as the Larmor frequency. When the spins are subjected to a static magnetic field they will occupy a state located either parallel or antiparallel to the magnetic field and precess at a rate equal to the Larmor frequency.

The presence of the static magnetic field causes a torque on the magnetic moment that forces them to precess around the field at some angle from the field which can be described by;

$$\vec{\tau} = \mu \times \vec{B} \tag{2.11}$$

where $\vec{\tau}$ is the torque felt by the magnetic moment $\vec{\mu}$, when they are placed in a static magnetic field $\vec{B}$. This results in the spins following a cone shaped motion about the magnetic field. For each of the $2I+1$ states a different cone will be produced, therefore for the spin-1/2 nuclei there will be two cones one parallel and one antiparallel shown in figure 2.4(a). However, for a spin-3/2 nuclei there will be four cones, two parallel and two antiparallel, shown in figure 2.4(b).

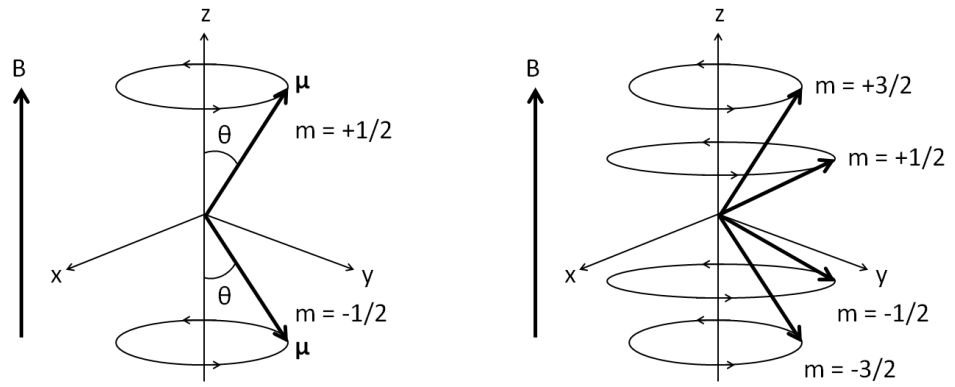

(a) 'Spinning top' model for spin-1/2 nuclei. (b) 'Spinning top' model for spin-3/2 nuclei.

Figure 2.4: Illustration of the semi-classical idea of a 'spinning top' like situation of a spin-1/2 and spin-3/2 system. Adapted from reference [66].

The only component of $\vec{B}$ is B_z as the applied field is always chosen to be applied in the z-direction on standard Cartesian co-ordinates. The dipole moment is moved by some angle θ away from the direction of the static magnetic field. The angle of the cone is determined by;

$$cos\theta = m\left[I\left(I+1\right)\right]^{-\frac{1}{2}} \tag{2.12}$$

where θ is the angle of the magnetic moment away from the static magnetic. The direction of this precession is determined by the gyromagnetic ratio which can be either positive or negative. A positive value means that the magnetic moment is in the same direction as the spin angular momentum. A negative sign of the gyromagnetic ratio means that the magnetic moment and spin angular momentum are antiparallel to each other. The sign of the gyromagnetic ratio determines whether the spin precesses the field clockwise or anticlockwise.

2.3 Multiple Spins

In section 2.2, a single spin was considered which is the simplest case; however, in a real system there are many spins, which will now be considered. In section 2.2, it was stated that in the presence of a static magnetic field, Zeeman splitting occurs resulting in two possible spin states α and β for the spin-1/2 nucleus which are parallel and antiparallel to the magnetic field. Each spin has to be in one of these states, with the α state having a lower energy, as it is easier for the spin to be aligned with the field. The states are filled according to the Boltzmann distribution;

$$\frac{N_\beta}{N_\alpha} = exp\left(\frac{-\Delta E_{\alpha\beta}}{k_B T}\right) \tag{2.13}$$

where N_α and N_β are the number of spins in α and β states, respectively, k_B is the Boltzmann constant and $\Delta E_{\alpha\beta}$ is the amount of energy needed to cause a transition from one state to another. The total number of spins can be defined as;

$$N = N_\alpha + N_\beta \tag{2.14}$$

as all spins must be in either one state or the other. Most spins are considered to have another spin in exactly the opposite direction with the same magnitude and therefore cancel out, resulting in no net magnetisation. Due to the presence of the field, and the fact that the α state has a lower energy there is a small excess of spins in the α state. This produces a net magnetisation parallel to the static magnetic field. Substituting equation 2.8 into equation 2.13 gives;

$$\frac{N_\beta}{N_\alpha} = exp\left(\frac{-\gamma\hbar B_0}{k_B T}\right) \tag{2.15}$$

where the population excess can be defined by[66];

$$n = \frac{\gamma\hbar N B_0}{2k_B T} \tag{2.16}$$

Where N is the number of spins in each state and T is the absolute temperature of the system. Therefore the population excess is dependent on the gyromagnetic ratio, which is different for every nucleus. The strength of the NMR signal is dependent on the population excess as this causes the net magnetisation. The net magnetisation can be considered as the sum of magnetic moments that have not been canceled out so net magnetisation is given as;

$$M = \sum \mu = n\mu = \frac{\hbar N B_0 \mu}{2k_B T} \tag{2.17}$$

In NMR experiments the energy difference between the two states is relatively small which has the consequence of making the equilibrium constant N_β/N_α very close to 1. An implication of this is that ΔN is very small, which is important to NMR as the signal intensity is related to the magnitude of ΔN. In the case where ΔN=0, no signal will be observed as NMR hinges on an excess of spins in either state. It can also be seen from equation 2.16 that the population excess is proportional to the magnetic field strength and total number of spins, therefore a stronger magnetic field will produce a larger population excess resulting in a better signal. It is important to have a large magnetic field in NMR experiments in order to obtain a large population difference and therefore increasing the signal to noise ratio (SNR).

2.4 Spin Interactions

In NMR, radio frequency (RF) pulses can be used in order to perturb the system away from thermal equilibrium and in some instances coherence can be imposed on the spins. In the thermal equilibrium state the spins are considered to have no coherence and be distributed according to the Boltzmann distribution explained by equation 2.15. After the spins have been perturbed by the RF pulses, there are two types of relaxation that occur. Firstly, there is the longitudinal (spin-lattice) relaxation which is the movement of the spin populations back to thermal equilibrium via interactions with the surroundings (or $'lattice'$). The second type of relaxation is the transverse (spin-spin) relaxation which involves the loss of coherence between adjacent spins in the xy plane.

In order to understand the following explanations of the relaxation processes it is important to define how the magnetisation changes with time, this is achieved with the Bloch equations. The Bloch equations describe the change in magnetisation with time for the x, y and z directions.

The magnetisation can have components in all three axes, the total magnetisation in all directions will have the form;

$$M = M_x\hat{i} + M_y\hat{j} + M_z\hat{k} \tag{2.18}$$

where M_x, M_y and M_z are the magnetisation in the x, y and z directions, respectively. At thermal equilibrium there is effectively no magnetisation in the x and y directions therefore $M_x = M_y$=0. The change in the angular momentum with time can be expressed as the value of torque in the form;

$$\frac{d\vec{J}}{dt} = \vec{\tau} = \mu \times \vec{B} \tag{2.19}$$

where $\vec{J}$ denotes the spins angular momentum. By combining equations 2.2 and 2.19 gives rise to the time dependent magnetisation in the form;

$$\frac{d\vec{M}}{dt} = \gamma\vec{M} \times \vec{B} \tag{2.20}$$

where this is known as the main Bloch equation [67]. By expanding equation 2.20 it can be stated that the magnetisation in the x, y and z directions are;

$$\frac{d\vec{M}_x}{dt} = \gamma(\vec{M} \times \vec{B})_x \tag{2.21}$$

$$\frac{d\vec{M}_y}{dt} = \gamma(\vec{M} \times \vec{B})_y \tag{2.22}$$

$$\frac{d\vec{M}_z}{dt} = \gamma(\vec{M} \times \vec{B})_z \tag{2.23}$$

where these equations are for a system which has no interactions. However in any real system there is interactions between the spins and the lattice. To account for these interactions equations 2.21, 2.22 and 2.23 can be expanded and have terms added which are first order relaxation terms, arising from the relative relaxation processes in each direction;

$$\frac{dM_x}{dt} = \gamma\left(M_yB_z - M_zB_y\right) - \frac{M_x}{T_2} \tag{2.24}$$

$$\frac{dM_y}{dt} = \gamma\left(M_zB_x - M_xB_z\right) - \frac{M_y}{T_2} \tag{2.25}$$

$$\frac{dM_z}{dt} = \gamma\left(M_xB_y - M_yB_x\right) - \frac{(M_z - M_0)}{T_1} \tag{2.26}$$

where M_0 refers to the magnetisation at thermal equilibrium, T_1 is the spin-lattice (longitudinal) relaxation time and T_2 is the spin-spin (transverse) relaxations time. These equations can now be further simplified by considering that $B_x = B_y$ =0 and that $B_z = B_0$, making these simplifications yield;

$$\frac{dM_x}{dt} = \gamma M_yB_z - \frac{M_x}{T_2} \tag{2.27}$$

$$\frac{dM_y}{dt} = -\gamma M_xB_z - \frac{M_y}{T_2} \tag{2.28}$$

$$\frac{dM_z}{dt} = -\frac{(M_z - M_0)}{T_1} \tag{2.29}$$

where these equations now consider the relaxation terms and a static magnetic field in the z direction. These are known as the Bloch equations and are used to describe the magnetisation in every direction. Since the static field is in the z-direction at thermal equilibrium there will be no magnetisation in the x and y directions. However it is possible to perturb the magnetisation away from the z-direction which will then cause the system to relax. The xy plane magnetisation decays with the characteristic time constant T_2, which is known as the spin-spin or transverse relaxation, as the decay in magnetisation is due to interactions between spins. The T_2 relaxation process will be discussed in more detail in section 2.5.2. The return of the magnetisation to the z-direction is described by the time constant T_1 which is known as the spin-lattice relaxation time, as the relaxation is caused by interactions with the surroundings, also known as the longitudinal relaxation time.

2.5 Spin-Lattice Relaxation

Thus far it has been considered that the magnetic moments precess about the z-axis at the Larmor frequency and the three axis are labeled x, y and z. However it is considered simpler to describe the interactions and pulse sequences in from a rotating frame of reference. The z-axis component will be unaffected, however the magnetisation would no longer appear to precess but rather stay stationary [68]. From here on all diagrams will show the system in the rotating frame of reference which will be assumed to be rotating at the Larmor frequency. The Cartesian coordinates x, y and z are distinct from the rotating frame coordinates labeled x', y' and z'. An example of a the magnetisation in thermal equilibrium represented in the rotating frame of reference is shown in figure 2.5 (left hand side), where the magnetisation is now stationary. Figure 2.5 also gives an example of a 90° (or $\pi/2$) RF pulse which perturbs the spins into the xy plane.

So far only single spins and ensembles of single spins that are non-interacting have been considered; however in reality these spins will form larger molecules containing multiple nuclei. In the example of a water molecule, the protons attached to the molecule undergo significant motion in the solution. These rather violent molecular surroundings are seen to slightly interfere with the nuclear spins and therefore the nuclear magnetism. Inside of every molecule are small magnets, as each spin electron and nucleus all produce magnetic fields. Due to thermal energy in the system, these small magnets are seen to fluctuate very randomly, which will vary in time and space. Each spin therefore experiences a slightly different fluctuating magnetic field. This results in a very small magnetic moment which is the key to observing nuclear magnetism. It is therefore possible for any given spin to wander around the different precessional cones allowing each spin to experience every possible cone. It is more probable for the spin to wander into the lower energy state which is parallel to the static magnetic field. This bias to the lower energy state is known as thermal equilibrium to which all spins will eventually adhere. This effect will occur when the sample is first placed inside the static magnetic field; it will also occur if the spins are excited away from thermal equilibrium. This return to the thermal equilibrium is known as the spin-lattice relaxation, also known as longitudinal relaxation.

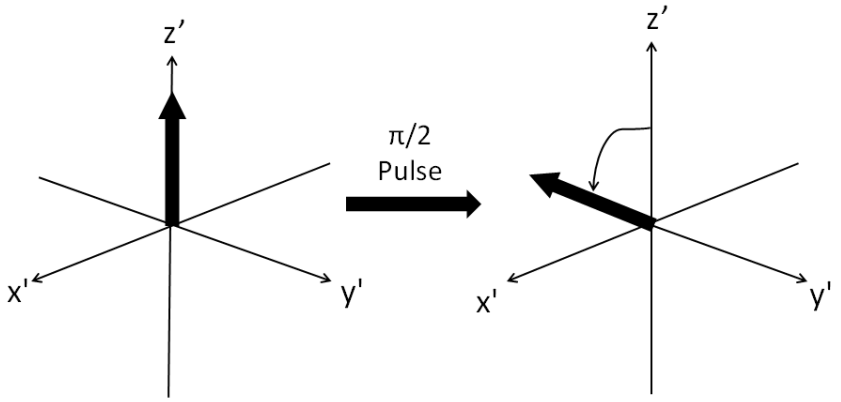

Figure 2.5: Magnetisation in thermal equilibrium, and the use of an $\pi/2$ RF pulse to move magnetisation from z-axis to the xy plane in the rotating frame of reference.

The longitudinal relaxation of the spins is described by an exponential as a function of time. The time taken for the individual spins to align themselves with the magnetic field is given by;

$$M_z = M_0(1 - Aexp\left[\frac{-t}{T_1}\right]) \tag{2.30}$$

where M_z is the net magnetisation in the z direction (i.e. direction of static magnetic field), M_0 is the maximum magnetisation that the sample can attain, i.e. when the nucleus is in thermal equilibrium, T_1 is the longitudinal relaxation time and is defined as the time taken for the equilibrium magnetism to be recovered to 63% of its total value and A is a constant which can either be 1 or 2 for the saturation and inversion recovery pulse sequences, respectively; which will be detailed in section 2.6. An example T_1 curve with time can be seen in figure 2.6, which is for a liquid electrolyte sample containing pure PC using the ^{1}H nucleus. It can be seen in figure 2.6 that immediately after magnetisation has been perturbed away from thermal equilibrium that the M_z is close to zero, as the time increases the magnetisation starts to align with the static field once more until it reaches the M_0 value.

Using radio frequency (rf) pulses can excite the spins into the higher energy state. This is achieved by using the resonant frequency for the nucleus in question given in equation 2.10 to excite these spins away from the static field. The spins will be perturbed by this rf pulse of strength $\vec{B_1}$ by some angle θ when the pulse is applied for some time τ_P given by equation 2.31 and then the return of the magnetisation is controlled by T_1.

$$\theta = \gamma \vec{B_1} \tau_P \tag{2.31}$$

If the pulse is held until the magnetisation is moved through an angle of $\pi/2$ there will be no net magnetisation left in the z-direction and now will have some measurable signal in the xy plane, referred to as a $\pi/2$ pulse. If the pulse duration is twice that of a $\pi/2$ pulse, then an angle of π would be attained. A perfect 180^o (π) pulse inverts the excess spins that were aligned with the

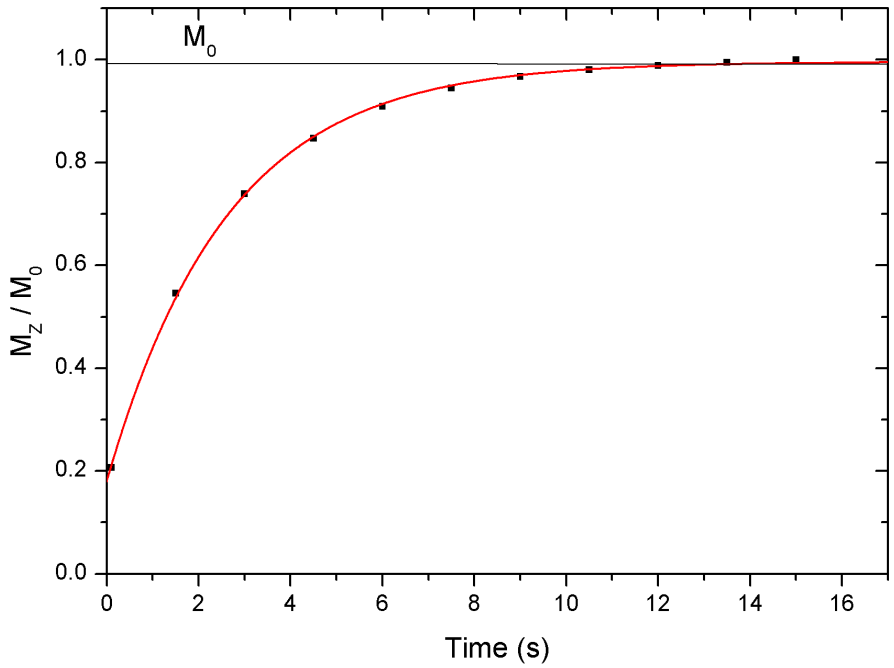

Figure 2.6: A saturation recovery T_1 relaxation curve for pure PC at 293 K using ^{1}H nucleus.

magnetic field to the higher state antiparallel to the field; this is known as an inversion pulse. During an inversion pulse the population of the states has flipped causing an excess of spins in the state opposing the field which will then relax.

2.5.1 Relaxation Mechanisms

In most forms of spectroscopy transitions between energy levels rely on the emission or absorption of photons or via collisions within the system. However, in NMR these methods are considered to be negligible. Instead NMR transitions are induced via interaction between magnetic fields within the sample. It has already been discussed that when a system of spins is placed inside a strong magnetic field the spins will tend toward thermal equilibrium. The thermal equilibrium state consists of a spin population with an excess of spins in the lower energy level (aligned with the static field). Most NMR experiments use radio frequency pulses to perturb the system in order to monitor the return to thermal equilibrium, which will be discussed in more detail in section 2.6. Since the NMR relaxations rely on magnetic fields in the sample, it is possible to gain understanding of the dynamics of the system. In order to have an effective relaxation process randomly fluctuating magnetic fields are required. In a real NMR system there are several different scenarios which will produce such fields and cause relaxations.

In the interest of completeness this section will cover most NMR relaxation mechanisms, however only a few are considered relevant and will be used later in this thesis. This section is designed to be an overview of these mechanisms, for the interested reader there are many detailed books published on these mechanisms in different systems [4; 68–71]. The relaxation mechanisms discussed in this chapter can occur simultaneously and are, by definition additive.

The relevant contribution of each mechanism is also discussed, as these can vary due to dynamics of the molecules or the spin number of the nucleus.

In this thesis NMR results have been taken using three different nuclei; ^{1}H, ^{7}Li and ^{19}F, which correspond to the solvent molecules, lithium cation and fluorinated BF_4 anion, respectively in the liquid electrolyte systems. In the polymer gel electrolytes the ^{1}H and ^{19}F nuclei also are contained in the polymer. In the case of the longitudinal relaxation times the exchange between the relevant sites of these nuclei are rapid on the timescale of the NMR experiment and therefore an average T_1 is obtained for all regions. In this section the liquid electrolyte case will be considered for ease of understanding.

2.5.1.1 Dipole-Dipole

Firstly spin-1/2 systems will be considered which corresponds to the ^{1}H and ^{19}F nuclei in this research. It is well known that the dominant relaxation mechanisms for the spin-1/2 system is dipole-dipole interactions. Each atom in a sample essentially behaves as a dipole which will have its own magnetic field. In a liquid the random motion and diffusion of the molecules in solution will result in each spin experiencing a random fluctuating magnetic field which can thus induce transitions between energy levels. Since the magnetic field experienced by each spin varies with both time and space and also the rate at which the molecules are tumbling in solution, information about the dynamics can be obtained by measuring the relaxation times. In Chapter 4 of this thesis the relative contributions of rotational and translational motion of the molecules are discussed, it is therefore important to define the possible motions of the dipoles which can result in relaxation. Taking for example the ^{1}H NMR measurements on a liquid electrolyte system containing PC/$LiBF_4$; it is possible to have relaxation via intramolecular and intermolecular motions. In order to have effective relaxation the distance between two nuclei or the orientation of the dipolar direction in B_0 must vary with time. In the case of intramolecular interactions, since all of the hydrogen sites translate as a molecule there is a constant distance between each site and therefore relaxation via translational intramolecular motions are not possible. However each hydrogen site of the PC molecule can rotate about its own axis, allowing relaxation from intramolecular rotation. Molecules in liquids will usually undergo fast molecular reorientation or tumbling and will translate as well as rotate. Therefore as a molecule passes neighbouring molecules the spins will experience a fluctuating magnetic field which will induce transitions, which are known as intermolecular interactions.

The magnetic field felt by the spins due to dipole-dipole interaction will, on average be zero as the field spends as much time in the negative as positive, so therefore;

$$\langle B_x(t) \rangle = 0 \tag{2.32}$$

where B_x is the fluctuating field observed by the spins. In order to analyse these fields there needs to be some measurable value and therefore the average of the square of the field can be used;

$$\left\langle B_x^2(t) \right\rangle \neq 0 \tag{2.33}$$

which will take a non-zero value. This value corresponds to the magnitude of the fluctuating fields, however the rate at which the field fluctuates also needs to be defined. The rate of

fluctuations is defined by the auto-correlation function;

$$G(\tau) = \langle B_x(t) B_x(t+\tau) \rangle \neq 0 \tag{2.34}$$

where this equation is true for the equilibrium situation and is not dependent on t, but rather is dependent on the difference denoted τ [4]; the brackets represent an average of all spins. If the time interval τ is zero, then equation 2.34 reduces to the mean square field represented in equation 2.33. The choice of τ is important, for short values of τ the values of B_x at time t and time $t+\tau$ are very similar, if the interval is short enough only one fluctuation would occur. At long intervals the system loses its 'memory' because if many fluctuations have occurred between time t and $t+\tau$ then the two values could have different signs and therefore will make the auto-correlation function close to zero.

The correlation function can be written in terms of the correlation time (τ_c) in the form of;

$$G(\tau) = \left\langle B_x^2 \right\rangle exp \left\{ \frac{-|\tau|}{\tau_c} \right\} \tag{2.35}$$

where the correlation time (τ_c) is defined as approximately the time it takes for the molecule to rotate 1 radian. Short correlation times cause the correlation function to decay rapidly whereas a long correlation time causes the function to decay much more slowly. The correlation time is mainly dependent on the size and shape of a molecule as well as the temperature and viscosity of the surrounding medium. τ_c is an indication of the rate that the fluctuating field changes sign.

It is now possible to Fourier transform the correlation function given in equation 2.34 in order to yield the spectral density, $J(\omega)$ given by;

$$J(\omega) = \int_0^\infty G(t) e^{-i\omega t} dt \tag{2.36}$$

This takes the system from a time dependent system to a spatial one and leaves the spectral density in the form of;

$$J(\omega) = \frac{2\tau_c}{1+\omega\tau_c} \tag{2.37}$$

where $J(\omega)$ is the spectral density, whereby for short correlation times give rise to a broad spectral density function and long correlation times give less broad spectral density. This result is intuitive, molecules that tumble very rapidly (i.e. short τ_c) can sample many different frequencies, therefore would have a broad spectral line, whereas more slowly tumbling molecules would only have the opportunity to sample fewer frequencies.

It is possible to estimate the longitudinal relaxation by considering the transitions between the two states due to the dipole-dipole interaction. This was first introduced by Bloembergen, Purcell and Pound which is known as BPP theory [72] and was stated that the longitudinal relaxation can be given by;

$$\frac{1}{T_1} = \frac{3}{2}\gamma^4 \hbar^2 I(I+1) \left[J_1(\omega_0) + J_2(2\omega_0) \right] \tag{2.38}$$

where $J_1(\omega_0)$ and $J_2(2\omega_0)$ are the spectral densities which have been derived from dipole-dipole interactions and are defined as;

$$J_0(\omega) = \left(\frac{24}{15r^6} \right) \frac{\tau_c}{1+\omega^2\tau_c^2} \tag{2.39}$$

$$J_1(\omega) = \frac{1}{6} J_0(\omega) \tag{2.40}$$

$$J_2(\omega) = \frac{2}{3} J_0(\omega) \tag{2.41}$$

from these equations T_1 can be determined. It should be noted that equation 2.38 is for homonuclear interactions. The spectral density functions are highly dependent on both the Larmor frequency ω_0 and the correlation time τ_c. By combining equations 2.39, 2.40 and 2.41 with equation 2.38 the relaxation rate for homonuclear interactions is given by;

$$\frac{1}{T_1} = \frac{2}{5}\gamma^4\hbar^2 I(I+1)[\frac{\tau_c}{1+\omega_0^2\tau_c^2} + \frac{4\tau_c}{1+4\omega_0^2\tau_c^2}] \tag{2.42}$$

where this equation is valid for homonuclear interactions. It is also possible to write down an equation for heteronuclear interactions which involve the interaction between two different nuclei.

$$\frac{1}{T_1} = DC_{A-B}\frac{2}{5}\gamma^4\hbar^2 I(I+1)[\frac{3\tau_c}{1+\omega_A^2\tau_c^2} + \frac{6\tau_c}{1+(\omega_A+\omega_B)^2\tau_c^2} + \frac{\tau_c}{1+(\omega_A-\omega_B)^2\tau_c^2}] \tag{2.43}$$

where ω_A and ω_B are the resonance frequencies for nuclei A and B which arbitrarily labeled and DC_{A-B} is the dipolar coupling constant for heteronuclear interactions experienced by nucleus A as a result of nucleus B and given by;

$$DC_{A-B} = \frac{8}{45}\frac{\gamma_A^2\gamma_B^2\hbar^2}{r_{A-B}^6} I_A(I_A+1) I_B(I_B+1) \tag{2.44}$$

where γ_A and γ_B are the gyromagnetic ratios of nuclei A and B respectively, I_A and I_B are the spin number for the relevant nuclei and r_{A-B} is the internuclear distance.

It should be noted that equation 2.42 will be used in Chapter 4 in order to calculate the longitudinal relaxation due to intramolecular motion. The other equation for heteronuclear interactions will not be used in the duration of the thesis but is present in the interest of completeness. It should be noted that in this system there is likely a significant interactions between the ^{1}H and ^{19}F nuclei, however this research is concerned with obtaining an indication of the relative contributions from translational and rotational motions of the molecules, not accurate calculations of the relaxation times.

In the high temperature (low correlation time) side of the T_1 minimum the correlation time can be given by;

$$\tau_c = \frac{4\pi\eta a^3}{3k_B T} \tag{2.45}$$

where a is the ionic radius, η is the bulk viscosity and T is the absolute temperature of the system. Therefore it can said that the correlation time is dependent on the size of the molecule and the bulk viscosity and absolute temperature of the medium. The T_1 relaxation is therefore dependent on the rate of tumbling (τ_c) and frequency of the motion, where molecular motion close to the resonant frequency produces the most efficient relaxation time. Since the frequency is dependent on the magnetic field strength, so is the longitudinal relaxation time.

It should be noted that equations 2.42 and 2.43 are for intramolecular homonuclear and heteronuclear interactions, respectively. Intermolecular interactions can also take place as two

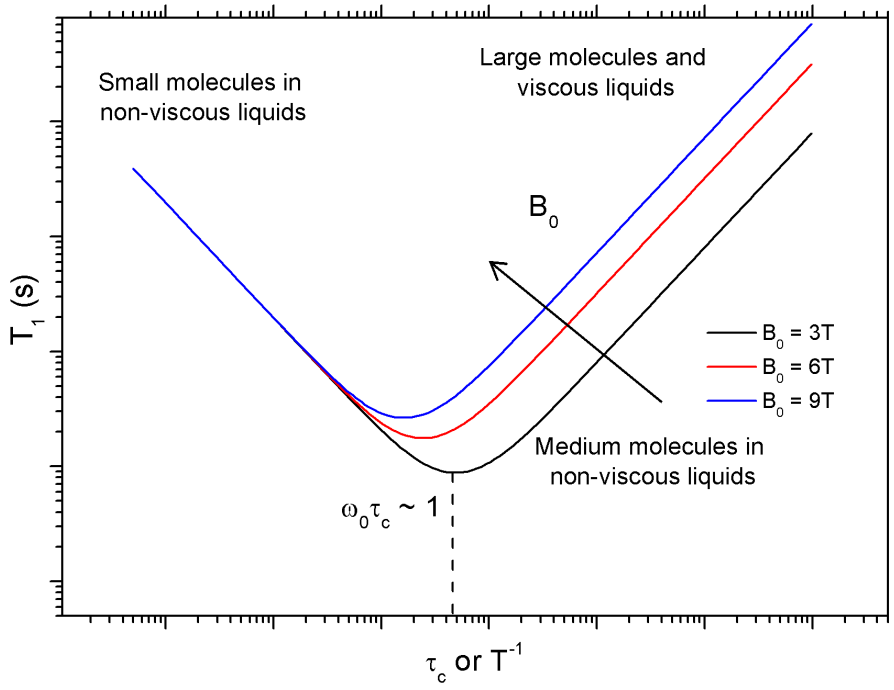

Figure 2.7: Calculated T_1 from BPP theory as a function of correlation time and inverse temperature for 3T, 6T and 9T static B_0 field [72].

neighbouring molecules pass each other, this interaction can be described by;

$$\frac{1}{T_1(inter)} = \frac{4\pi}{15}\frac{N\gamma^4\hbar^2 I(I+1)}{aD} \tag{2.46}$$

where N is the concentration of spins and a is the effective radius of the relevant molecules and D is the translational diffusion constant. This equation will be considered in more detail in Chapter 4 and used to calculate the intermolecular translational component of the longitudinal relaxation. It should be noted that this is for homonuclear interactions.

Figure 2.7 shows the calculated longitudinal relaxation using equation 2.38 as a function of both the correlation time and the inverse of temperature. At very low correlation times, which refer to small molecules in non-viscous liquids, the T_1 values are quite large. As the correlation time increases the T_1 value decreases until the condition $\omega_0\tau_c \approx 1$ is satisfied; at this point, the T_1 will undergo a minimum. This minimum occurs as the timescale of the motions of the molecules are the same as the resonant frequency of nucleus in question and therefore produces the most efficient relaxation possible. Increasing the correlation time further into the medium/large molecules region of figure 2.7, the value of T_1 will increase again. When on the left hand side of the minimum (in figure 2.7), increasing the temperature will have the effect of raising the longitudinal relaxation times; however, if we are in a system on the other side of the minimum increasing the temperature will lower the longitudinal relaxation times. The systems analysed in this thesis are on the low correlation (high temperature) side of the minimum for all measurements. The values of ω_0 used in figure 2.7 are 128 MHz, 256 MHz and 384 MHz which are the resonant frequencies for a ^{1}H nucleus at magnetic fields of 3 T, 6 T and 9 T, respectively.

At low correlation times, the longitudinal relaxation is independent of magnetic field, however at high correlation times the longitudinal becomes field dependent and seen to increase with increasing field strength.

In summary the dipole-dipole interaction is the most significant relaxation mechanism for spin-1/2 nuclei. The interaction is highly dependent on the distance between two neighbouring spins and also the molecular reorientation rate.

2.5.1.2 Chemical Shift Anisotropy

This relaxation mechanism is particularly strong for certain nuclei including ^{13}C, ^{19}F and ^{31}P. Therefore this is a possible effective relaxation when using the ^{19}F resonant frequency to detect the anion in the liquid electrolytes. It should also be noted that this relaxation rate for this mechanism is proportional to B_0^2 and therefore is more substantial for large magnetic fields. In this research a 9.4 T NMR spectrometer was used to measure the ^{19}F longitudinal relaxation times and therefore could have a non-negligible contribution from the chemical shift anisotropy (CSA). The other two nuclei used in this research (^{1}H and ^{7}Li) are likely to have a much lesser contribution. The application of this mechanism to the results is considered beyond the depth of this research and will not be applied.

In NMR measurements the magnetic field experienced by various nuclei will be less than the static external field B_0. Electrons surrounding the nucleus will precess, which results in a local magnetic field (B_E) which by definition opposes the static field. The electrons are therefore said to shield the nucleus. The magnetic field experienced by each nucleus becomes;

$$B = B_0 - B_E \tag{2.47}$$

where B_0 and B_E are the static and local magnetic fields, respectively. Since the Larmor frequency is dependent on the magnetic field experienced by the nucleus this changes the resonant frequency of the nucleus. Therefore it is possible for multiple ^{1}H nuclei to resonate at different frequencies. This effect makes it possible to distinguish between two different molecular locations of the same nuclei. This behaviour is highly important to chemists as it serves as a method to identify samples and the shielding of a nucleus can yield information about the structure of a molecule.

A screening constant (σ_s) can be defined, which is used to describe the chemical shift. The resonant frequency observed by a nucleus is then given by;

$$\nu = \nu_0(1 - \sigma_s) \tag{2.48}$$

where ν and ν_0 are the effective resonant frequency and the operational frequency for the spectrometer, respectively. The electronic screening constant consists of three parts: a diamagnetic term which arises from the circulation of undisturbed spherical electron precession, a paramagnetic term which arises from perturbed non-spherical electron precession and a term which is due to magnetic anisotropy of neighbouring molecules [70].

The electronic environment is usually anisotropic; meaning that the precession of the electrons around the nucleus is different on various sides of the nucleus. Therefore in order to quantify this effect a chemical shift tensor is used. The chemical shift tensor is defined in three dimensions

and has components σ_x, σ_y, σ_z. A chemical shift anisotropy can be defined by;

$$\Delta\sigma = \frac{2\sigma_z - (\sigma_x + \sigma_y)}{3} \tag{2.49}$$

where $\Delta\sigma$ is the chemical shift anisotropy [70]. In the case of rapidly tumbling molecules as characteristic in non-viscous liquids the chemical shift tensor is averaged out in each direction and the total screening constant (σ_s) becomes an average of the tensor in x, y and z directions.

In liquids, random molecular motions can give rise to fluctuating magnetic fields in the presence of a chemical shift anisotropy, the relaxation rates of these interactions to the spin-lattice is described by;

$$\frac{1}{T_1}(CSA) = \frac{1}{15}\gamma^2 B_0^2 \Delta\sigma^2 [\frac{2\tau_c}{(1+\omega_0^2\tau_c^2)}] \tag{2.50}$$

where τ_c is the correlation time, $\Delta\sigma$ is the chemical shift anisotropy, γ is the gyromagnetic ratio and ω_0 is the Larmor frequency.

2.5.1.3 Spin Rotation

Another relaxation mechanism that can affect the T_1 longitudinal relaxation is the spin-rotation (SR) mechanism. This mechanism is considered to be fairly weak compared to the dipole-dipole interactions and therefore for the duration of the thesis will be essentially ignored. This relaxation mechanism arises from fast molecular tumbling (molecular reorientation) which is characteristic of small molecules in low viscosity mediums, such as liquids. It has already been discussed that the motions of the dipoles with respect to neighbouring dipoles creates a dipole-dipole coupling which results in relaxation with molecular motions, however, the spin-rotation mechanism relies on the electrons surrounding the nuclei, which will create magnetic moments even in the absence of a static field. The relaxation rate is defined by;

$$\frac{1}{T_1}(SR) = \frac{I_r^2 C^2}{9\hbar^2\tau_c} \tag{2.51}$$

where I_r is the moment of inertia for the molecule, C is the spin-rotation constant and τ_c is again the correlation time [70]. This mechanism is likely to affect the ^{19}F more than the other two nuclei, as it most effective for heavy nuclei. That being said this relaxation mechanism is easily identifiable as $T_1(SR) \propto \tau_c \propto 1/T$, which therefore means that T_1 will decrease with increasing temperature if spin-rotation is a dominant factor. Since usually in a liquid T_1 increases with temperature this makes it easier to identify a possible contribution for this relaxation mechanism.

In this thesis the solvent used is propylene carbonate which has a methyl group on the molecule. The methyl group on PC molecules protrude from the molecule which allows them to rapidly rotate. This is a likely scenario in which the spin-rotation mechanism could be effective. This would have the effect of lowering the T_1 for that part of the molecule, this will be discussed later in Chapter 4.

2.5.1.4 Quadrupolar

The last mechanism that will be considered this section is the quadrupolar interaction relaxation mechanism. A quadrupole moment occurs in nuclei that have a spin number of I>1/2. In this research ^{7}Li NMR has been carried out to detect the salt ions, since ^{7}Li has is a spin-3/2 nucleus

it has a quadrupole moment and thus an uneven charge distribution. Therefore the measured T_1 values in this thesis using the ^{7}Li are assumed to be dominated by quadrupolar relaxation. However, the lithium T_1 values have not been calculated in this thesis and the equations found in this section will not be used. It is still possible to infer the contributions of intermolecular translational motion and rotational motions from measurements of T_1 without considering the specifics of this relaxation mechanism, as shown in Chapter 4. It is still likely that there will other contributing factors to the relaxation and the total rate of relaxation will be merely an addition of all these factors.

For quadrupolar nuclei the distribution of charges are non spherical and thus cause a quadrupole moment. The electric quadrupole moment (Q) will be zero for spin-1/2 nuclei as these are considered to have spherical charge distributions, a non-zero Q suggests either a prolate or oblate charge distribution which will yield a positive or negative Q, respectively [73]. This non-spherical charge distribution causes an electric field gradient. When a quadrupole nucleus is placed in the static magnetic field, the electric field gradients will interact with the magnetic field [70]. If the nucleus in question undergoes rapid molecular reorientation then this causes a fluctuating magnetic field which is needed to cause NMR relaxations.

To describe the electric field gradient a tensor is used which has components eq_{xx}, eq_{yy} and eq_{zz} which refer to the x, y and z directions, respectively. The component eq_{zz} is always defined along the chemical bond [70]. It is possible to determine an equation for the relaxation rate due to the quadrupolar interaction and it takes the form;

$$\frac{1}{T_1}(Q) = \frac{3}{10}\pi^2 \frac{(2I+3)}{I^2(2I-1)}\left(\frac{e^2 q_{zz} Q}{h}\right)^2\left(1+\frac{\eta_Q^2}{3}\right)\tau_c \tag{2.52}$$

where eq_{zz} is the major component of the electric field gradient tensor, Q is the quadrupolar moment, e is the charge of an electron, h is Planck's constant and η_Q is the shape factor which is defined by;

$$\eta_Q = \frac{|eq_{xx} - eq_{yy}|}{eq_{zz}} \tag{2.53}$$

where if eq_{xx} and eq_{yy} are equal the charge is symmetrical and the shape factor is equal to zero. It should be noted that equation 2.52 is for the extreme narrowing regime (i.e. when $\omega_0\tau_c << 1$). It should also be noted that for nuclei in this regime that exhibit a quadrupolar moment, this is the dominant relaxation mechanism.

2.5.2 Spin-Spin Relaxation

The transverse magnetisation relaxation occurs due to the de-phasing of the nuclear spins with time. When the spins are in thermal equilibrium there is no magnetisation perpendicular to the static field. This is because although the spins precess about the B_0 field at an angle, they are considered cylindrically symmetrical and therefore have no net magnetisation. As with the longitudinal relaxation, RF pulses can be used in order to perturb the spins away from thermal equilibrium.

A $\pi/2$ pulse is used to force the magnetisation into the x-y plane, if the signal was measured immediately after the pulse then the maximum intensity would be attained. However, as soon as the spins have been moved they will start to relax back to the static field direction. Unlike the T_1, where the relaxation was due to the release of energy to the surroundings, there will also be

relaxation due to loss of coherence. Ensembles of spins will exchange energy between themselves inducing spins with different precessional frequencies. The effect of this will be loss of coherence, causing relaxation. The decrease of magnetisation from the x-y plane is characterised by time constant T_2.

The $\pi/2$ pulse will rotate the net magnetisation into the -y axis, with some spins in the +y axis. Immediately after the pulse the spins will rotate about the z-axis in the xy plane with an angle θ away from the z-axis of $\pi/2$. As the spins relax back to thermal equilibrium the angle θ decreases until thermal equilibrium is restored. The initial $\pi/2$ pulse gives the spins coherence, the spins will then interact with each other causing the spins to precess at different frequencies. The transverse relaxation is the rate that the spins lose this coherence through interaction, this decay process is irreversible.

The magnetisation in the x and y-axis at time t after the $\pi/2$ pulse is defined by;

$$M_y(t) = -M_0 cos(\omega t)\, exp\left\{\frac{-t}{T_2}\right\} \tag{2.54}$$

$$M_x(t) = M_0 sin(\omega t)\, exp\left\{\frac{-t}{T_2}\right\} \tag{2.55}$$

where T_2 is the transverse relaxation time and M_0 is the magnetisation when the spins are in thermal equilibrium.

In real NMR systems there is a problem with field inhomogeneity which can cause the spins to dephase faster than expected purely from the relaxation mechanisms. This faster relaxation parameter is known as the effective transverse relaxation time and denoted T_2^* and is defined by;

$$\frac{1}{T_2^*} = \frac{1}{T_2} + \frac{1}{T_{2,inhom}} = \frac{1}{T_2} + \gamma \Delta B_0 \tag{2.56}$$

where $T_{2,inhom}$ is the relaxation term caused by the field inhomogeneity and ΔB_0 is the deviance from the static field which is the cause of the field inhomogeneity. There are methods in which T_2 can be measured without having to worry about field inhomogeneities; this is achieved by using spin echo pulse sequences, this is addressed in section 2.6.3.

As with the longitudinal relaxation, BPP theory [72] can also allow calculation of the transverse relaxation in terms of the spectral densities defined in equations 2.39, 2.40 and 2.41 in the form of;

$$\frac{1}{T_2} = \gamma^4 \hbar^2 I(I+1)\left[\frac{3}{8}J_0(0) + \frac{15}{4}J_1(\omega_0) + \frac{3}{8}J_2(2\omega_0)\right] \tag{2.57}$$

therefore now the value of T_2 can be calculated as a function of the correlation time τ_c and compared to the longitudinal relaxation.

Figure 2.8 shows the correlation time and inverse temperature dependence of the longitudinal and transverse relaxation times. As previously discussed, the longitudinal relaxation undergoes a minimum around $\omega_0\tau_c \approx 1$, however it can be seen that the transverse relaxation does not exhibit the same trend and instead carries on decreasing with increasing correlation time. At low correlation times and high temperatures the values of T_1 and T_2 converge and have equal values; this is due to the T_1 becoming very inefficient at correlation times much lower than resonance, and therefore the T_1 is controlled by the T_2 relaxation times. It is the case where $T_1 \geq T_2$ as the spin-spin interactions can contribute to the T_1 value but the T_2 values are independent of the

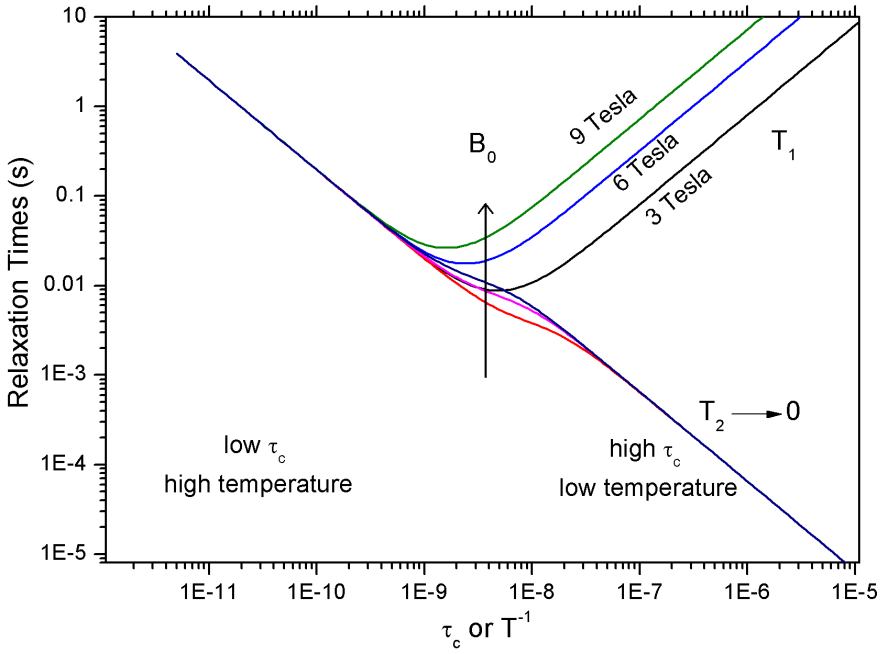

Figure 2.8: Calculated T_1 and T_2 from BPP theory as a function of correlation time and inverse temperature for 3T, 6T and 9T static B_0 fields.

spin-lattice relaxation. It can be seen from figure 2.8 that the field dependence of the T_2 values is much less significant than the T_1 dependence. For high and low correlation times, there is no field dependence of the transverse relaxation times, however there is some deviance near the T_1 minimum.

2.6 Pulse Sequences

In this section the pulse sequences that were used in this research will be discussed. These all involve using radio frequency pulses to perturb the system away from thermal equilibrium and the application of field gradients to measure diffusion of the molecules.

2.6.1 Inversion Recovery

When the sample is first placed in a static magnetic field in the z-axis, the spins will align either parallel or antiparallel dependent on the Boltzmann distribution with a bias toward the direction of the static field. The use of RF pulses perturb the system away from thermal equilibrium and can cause spins to change state. An inversion pulse, or π pulse, is when an RF signal is applied at the resonant frequency of the nuclei being observed for a time sufficient to invert the population excess. Once the pulse is removed the system will start undergoing relaxation via the mechanisms previously mentioned, eventually leading back to thermal equilibrium.

Figure 2.9 shows the the state of the net magnetisation at each point throughout the inversion recovery pulse sequence. It can be seen that initially there is an excess of spins and therefore

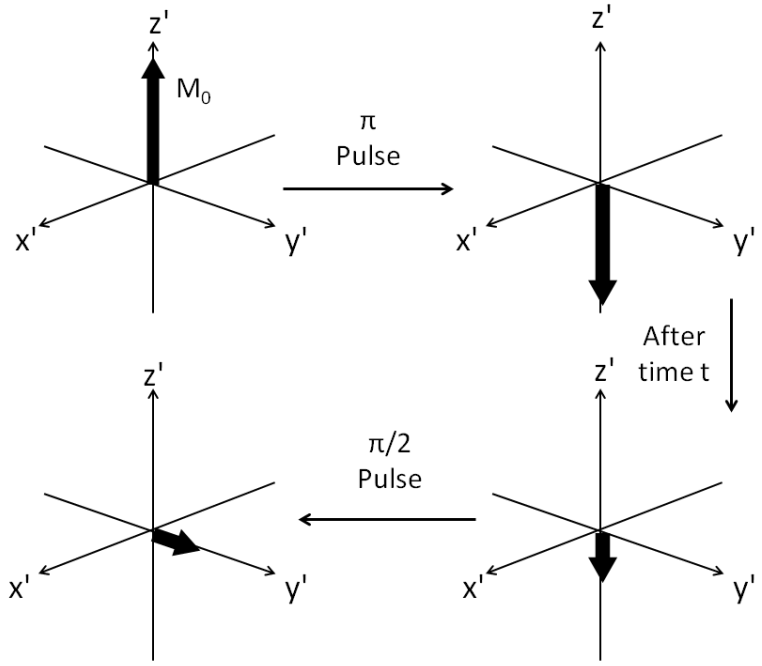

Figure 2.9: Inversion recovery pulse sequence used to measure longitudinal relaxation time T_1.

net magnetisation in the +z-axis. A π pulse is then applied to the system, this has the effect of inverting the spin populations and hence the net magnetisation. The system is then allowed to relax a given amount of time t, after which another RF pulse is used, however this time a $\pi/2$ pulse. The second RF pulse moves the magnetisation into the xy plane, sometimes referred to as a 'read' pulse, as NMR signals are undetectable in the z-axis and therefore need to be read in the xy plane. The experiment is then repeated several times, each time using different times t. As the time is increased the magnetisation will return to the thermal equilibrium. It should be noted that between each scan it is important to leave around $5T_1$ as the magnetisation must reach thermal equilibrium before the next one starts. Once the read pulse has been applied, the signal will undergo a free induction decay (FID). The equation that governs this pulse sequence is a simple exponential of the form;

$$M_z\left(t\right) = M_z\left(0\right)\left[1 - Aexp\left\{\frac{-t}{T_1}\right\}\right] \tag{2.58}$$

where M_z is the magnetisation aligned with the magnetic field and A is a constant that takes a value of 2 if the sequence has been setup correctly. The value of A for this sequence theoretically has a value of 2 because the at time t=0 s the the magnetisation will have a value of $-M_0$ and at infinitely long times the magnetisation will relax to M_0 and therefore the total difference in magnetisation throughout the inversion recovery sequence is $2M_0$; which is reflected by equation 2.58. There is an alternative pulse sequence that can be executed in order to measure the longitudinal relaxation time, this is known as saturation recovery.

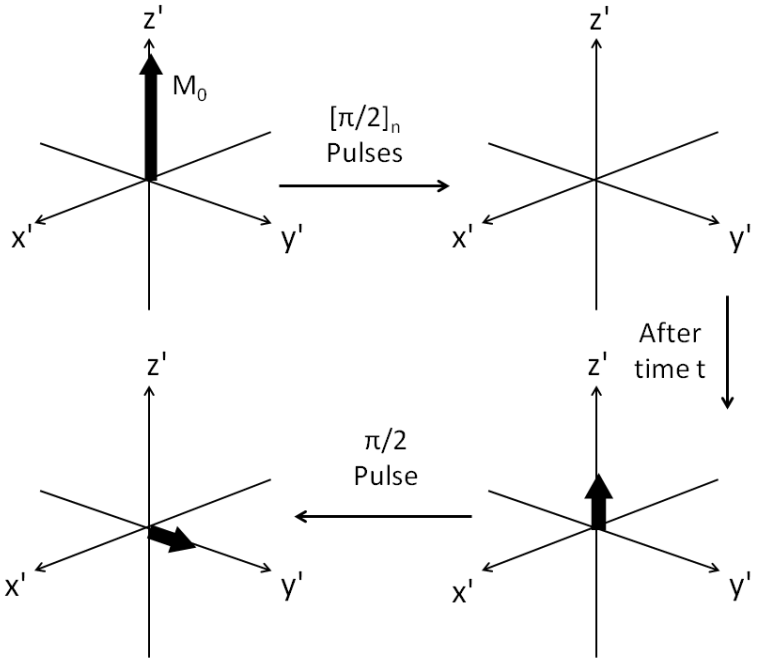

Figure 2.10: Saturation recovery pulse sequence used to measure longitudinal relaxation time T_1.

2.6.2 Saturation Recovery

Similar to the inversion recovery sequence, the saturation recovery pulse sequence is used in order to measure the longitudinal relaxation times. This pulse sequence begins with what are known as 'saturation' pulses which involves applying many $\pi/2$ pulses to the system spread out over a very narrow time. This has the effect of producing no net magnetisation in any direction.

Figure 2.10 shows, step by step, what is happening to the magnetisation of the system at each stage of the pulse sequence. The $\pi/2$ pulses are applied n times, effectively breaking down the net magnetisation as it randomly distributes the spins into the different spin states, canceling out all the spins. The system will then start to relax back to thermal equilibrium. After the initial set of $\pi/2$ pulses, the magnetisation is essentially zero; however if the sequence is not perfectly set up then the magnetisation will not be zero, which can be experimentally ignored by the use of an arbitrary constant. The spins will then undergo relaxation via the mechanisms previously outlined. As with the inversion recovery, several experiments must be run at different times after the initial $\pi/2$ pulses in order to map out the relaxation as a function of time. However, unlike the inversion recovery sequence this time there is no need to wait $5T_1$ in between experiments as the initial pulse scrambles the spins and therefore resets the system manually. As with the inversion pulse, a final $\pi/2$ pulse was used after a time t as the 'read' pulse. The value of A in equation 2.58 should now have a theoretical value of 1, as the magnetisation goes from zero at t=0 to M_0 at infinitely long times.

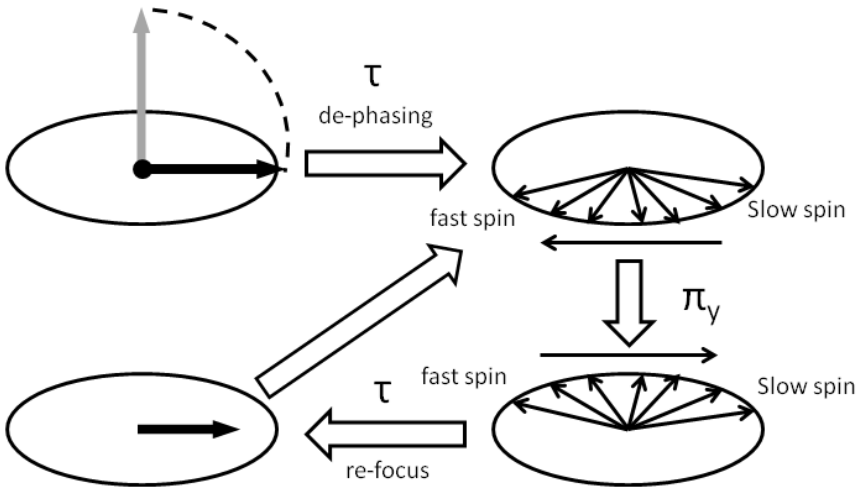

Figure 2.11: Schematic of the spins after each stage in the Hahn spin echo pulse sequence to measure T_2.

2.6.3 Hahn Spin Echo

The transverse relaxation is the de-phasing of spins in the xy plane, therefore the magnetisation must be allowed to relax in the xy plane. This is again achieved by the use of an RF pulse sequence. As previously mentioned, any real NMR machine will have field inhomogeneities and therefore the magnetisation will decay much faster than expected due to normal relaxation mechanisms. These effects can be eliminated by the use of spin echoes. Spin echoes are when the magnetisation is refocused after de-phasing, where the magnetisation decay caused by relaxation mechanisms are irreversible; however, the decay from the field inhomogeneities are reversible, therefore spin echoes allow measurements of the true transverse relaxation times. The concept of spin echoes was first introduced by Hahn [74] and has the form;

$$\frac{\pi}{2} - [\tau - \pi - \tau]_n \tag{2.59}$$

where $\pi/2$ is the duration of a 90^o pulse, π is the duration of a 180^o pulse, τ is the time the spins are allowed to dephase before the refocusing pulse is applied and n is the number of echoes.

Figure 2.11 shows a schematic of the spin at each stage of the Hahn spin echo pulse sequence. Immediately after the $\pi/2$ pulse has been applied to the system, all spins will be in phase with each other as the RF pulse has given the spins coherence. Due to the field inhomogeneities, each spin will precess at different frequencies, so that the spins are spreading out. After a time τ the spins will have significantly spread out from each other, effectively lowering the net magnetisation. An inversion pulse (π) is then applied to the system, this has the effect of inverting the spin populations and therefore the direction of precession. The slower spins are now in front of the faster spins and after time τ the spins will realign themselves producing a maximum in the magnetisation. This process is known as a spin echo and ultimately undoes the affects of the field inhomogeneities; however, the net magnetisation of the spins after the

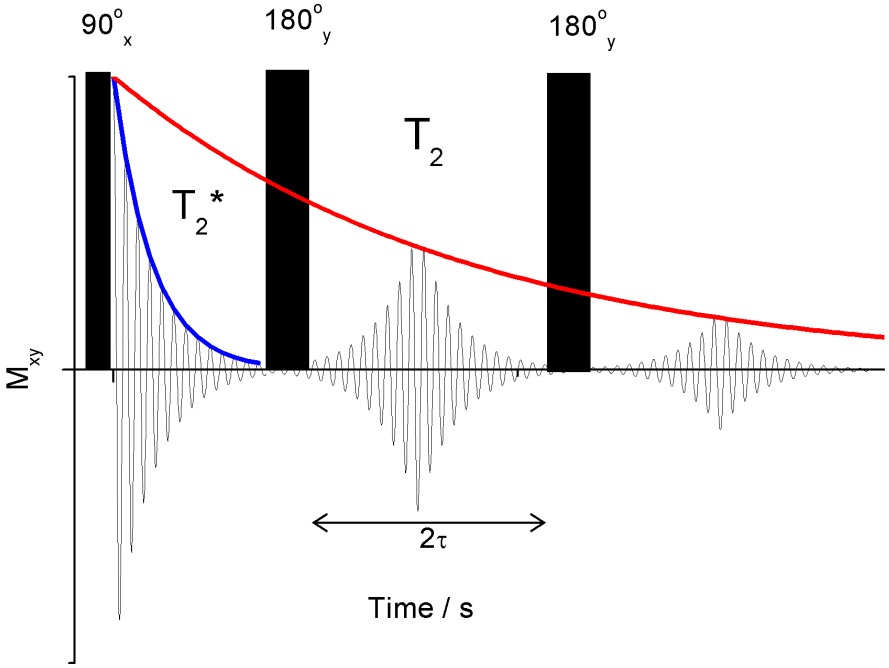

Figure 2.12: Magnetisation in the xy plane M_{xy} as a function of time for the Hahn spin echo pulse sequence.

spin echo will be less because the relaxation mechanisms are irreversible. The spins will start to dephase again; if another π_y pulse is applied the spins will be flipped again and after another time τ the spins will refocus again. This can be repeated many times until the magnetisation has decayed via the relaxation mechanisms.

The sequence has to involve multiple spin echoes and the intensity of the magnetic field is recorded after each spin echo so that the magnetisation can be mapped out as a function of time obeying a simple exponential;

$$M_{xy}(t) = M_0 exp\left\{\frac{-t}{T_2}\right\} \tag{2.60}$$

where M_0 is the magnetisation immediately after the $\pi/2$ pulse. The time t can then be calculated for each echo, as the echoes occur after a time τ followed by a π pulse and then another time τ for the spins to realign, therefore the total time of the experiment is give by;

$$t = \tau_{\pi/2} + n_{echo}(2\tau + \tau_\pi) \tag{2.61}$$

where $\tau_{\pi/2}$ and τ_π are the lengths of the $\pi/2$ and π pulses, respectively, τ is the time that the spins are allowed to dephase before being inverted and n_{echo} is the number of spin echoes. The choice of τ is clearly important for these measurements because in order to fit the data several echoes must be performed; if τ is too long then the magnetisation will decay too quickly before enough echoes can be recorded.

Figure 2.12 shows the free induction decay after each pulse. After the excitation pulse ($90°_x$ or $\pi/2_x$) the magnetisation will decay quickly due to the field inhomogeneities, which is shown in figure 2.12 by the blue line. The time constant is the effective transverse relaxation time

which is denoted T_2^*. Then after the π_{y} (180_{y}) pulse the magnetisation starts to increase due to the spins starting to refocusing until the magnetisation reaches a maximum, i.e. when the spins are perfectly refocused, however at a lower value than after the initial pulse. After refocusing, the spins will start to dephase again and thus the magnetisation in the xy plane starts to exponentially decrease. After a further time τ another π_y pulse can be applied to the system in order to flip the spins again and begin the refocusing which will again start to exponentially increase until it reaches another maxima. The peaks of these maximum due to spin echoes are the true transverse relaxation, this is shown by the red exponential fit in figure 2.12.

One consideration that has been omitted so far is the effect of an imperfect pulse being applied to the system. This would surely cause the value of T_2 to be incorrect. There is a solution in the form of the Carr-Purcell-Meiboom-Gill sequence.

2.6.4 Carr-Purcell-Meiboom-Gill (CPMG)

The Carr-Purcell-Meiboom-Gill (CPMG) sequence is based on the Hahn spin echo sequence shown in the previous section [75; 76]. There is an in-built quality of the CPMG sequence that is missing in the standard Hahn sequence. Instead of applying the sequence $(\pi/2)_x - \tau - \pi_y - \tau$ which is the standard Hahn sequence a second echo is taken. If we consider a pulse that is not perfectly set up and say a $175^{\mathrm{o}}{}_{\mathrm{y}}$ instead of a $180^{\mathrm{o}}{}_{\mathrm{y}}$ one, then for the standard Hahn sequence this would mean that the spins do not re-focus properly. If another echo is produced then this should be corrected because the system has been flipped and the same $175^{\mathrm{o}}{}_{\mathrm{y}}$ pulse has been applied. This involves producing a spin echo train and only measuring the intensity of the even number of spin echoes. Therefore the CPMG sequence has the same form as equation 2.59, however the value of n has to take an even number.

2.7 Diffusion

Diffusion is defined as the random translational motion (Brownian motion) of molecules. This motion is driven by the internal thermal energy of the molecules. Fick's law defines the flux of material across a plane as proportional to the concentration gradient,

$$J = -D\frac{\delta c\left(x,t\right)}{\delta x} \tag{2.62}$$

where J is the flux of material, D is the constant of proportionality known as the self diffusion coefficient and $\delta C\left(x,t\right)/\delta x$ is the concentration gradient. The negative sign indicates that the molecules diffuse in the direction of the lower concentration. Equation 2.62 is Fick's first law which omits the fact that the gradient and local concentration of impurities decreases with time.

Fick's second law states that the change in concentration is the same as the change in local flux of diffusion,

$$\frac{\delta c\left(x,t\right)}{\delta t} = \frac{-\delta J}{\delta x} \tag{2.63}$$

therefore by combining equations 2.62 and 2.63 we determine that;

$$\frac{\delta c\left(x,t\right)}{\delta t} = D\frac{\delta^2 c\left(x,t\right)}{\delta x^2} \tag{2.64}$$

where the diffusion coefficient is independent of the position of any one molecule. The diffusion constant can be described by the Stokes-Einstein equation in the form;

$$D = \frac{k_B T}{f} = \frac{k_B T}{6\pi\eta a} \tag{2.65}$$

where f is frictional force given by $6\pi\eta a$. Therefore by measuring the diffusion and viscosity of a solution the molecular radii can be determined. There are some issues with comparing macro-viscosity with micro-diffusion, which will be considered in Chapter 7.

The pioneering work of Hahn has already been considered in which he showed that spin echoes were possible in order to measure the transverse relaxation time T_2. However, Hahn also noted that the echo amplitude is affected by the Brownian motion of the molecules. As discussed in the previous section, the spin echo is produced by applying an excitation pulse ($\pi/2_x$) which shifts the magnetisation from the z-axis into the xy plane. The spins start to de-phase due to field inhomogeneities, after a time τ, an inversion pulse is used to re-focus the spins. If another magnetic field is added to this system, parallel to the B_0 field and label this additional field B_z, then the Larmor frequency of the spins becomes;

$$\omega_{eff} = \omega_0 + \gamma B_z \tag{2.66}$$

where $\omega_0 = \gamma B_0$ is the Larmor frequency of the spins and B_z is the field applied parallel to the B_0 field. If it is assumed that the field has a linear gradient equation 2.66 becomes;

$$\omega_{eff} = \omega_0 + \gamma z \frac{\delta B_z}{\delta z} \tag{2.67}$$

where this extra field is known as a field gradient and gives spatial encoding to each of the spins, since each spin is a sum of the static field (B_0) and the applied field gradient ($z\delta B_z/\delta z$).

In the presence of the field gradient, spins at different locations experience different local magnetic fields; it is this feature that gives the spatial encoding. As time goes on, the presence of the field gradient results in a magnetisation helix. A gradient of equal magnitude in the opposite direction would result in the spins reducing their magnetic field helix until they are once again aligned, thereby undoing the spatial encoding, known as a 'gradient echo'.

The most common type of diffusion measurement is to use these pulse field gradients (PFG) with a spin echo sequence (SE). This sequence was first proposed by Stejskal and Tanner[50], and involves the standard RF pulses of a Hahn sequence i.e. the initial excitation pulse ($\pi/2_x$) followed by an inversion pulse (π_y) after time τ in order to cause a spin echo. The first gradient pulse is applied in the de-phasing region of the pulse sequence and then in the opposite direction, during the re-focusing stage, where the magnitude and duration of the gradients are denoted G and δ respectively, shown in figure 2.13.

The effect of the gradient in figure 2.13 is to give the spins spatial encoding by giving each spin a different angular velocity about the z-axis. If the spins retain their exact positions when the gradient is removed by the second gradient application then the spin echo amplitude will be unaffected. However, if the spins have changed location between the two gradients, i.e. Δ, the diffusion time, then the re-focusing will be incomplete which will cause a decrease in the intensity of the spin echo.

In order to remove the magnetic gradients, a second gradient pulse is used in the opposite direction. In figure 2.13 both gradient pulses are in the same direction, this is because the

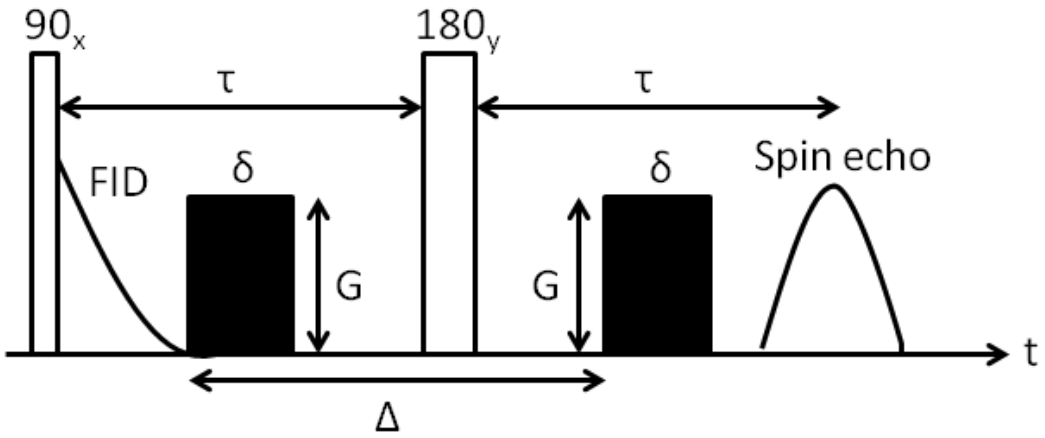

Figure 2.13: Stejskal-Tanner pulse field gradient spin echo (PFG-SE) NMR pulse sequence.

spins are flipped by the inversion pulse, therefore applying the gradient in the same direction is effectively in the opposite direction.

After the first gradient pulse a phase shift is defined as;

$$\phi_1 = \phi_0 + \int \gamma G z dt = \phi_0 + \gamma G z_1 \delta \tag{2.68}$$

where z_1 is the position of the spin, the phase shift after the second pulse is given as;

$$\phi_2 = \phi_0 + \gamma G z_1 \delta - \gamma G z_2 \delta = \phi_0 + \gamma G \delta \left(z_1 - z_2\right) \tag{2.69}$$

where the second gradient is just the negative magnitude of the first gradient pulse. Therefore if the spin has not translated then $z_1 - z_2 = 0$ and then $\phi_2 = \phi_0$. The Bloch equations can now be completed with the addition of the diffusion term in the form;

$$\frac{\delta M\left(r/t\right)}{\delta t} = \gamma \vec{M} \times \vec{B} - \frac{M_x \hat{i} + M_y \hat{j}}{T_2} - \frac{\left(M_z - M_0\right) \hat{k}}{T_1} + D \nabla . \nabla \vec{M} \tag{2.70}$$

where $\nabla . \nabla$ is the Laplace operator given by;

$$\nabla . \nabla \equiv \nabla^2 = \frac{\delta^2}{\delta x^2} + \frac{\delta^2}{\delta y^2} + \frac{\delta^2}{\delta z^2} \tag{2.71}$$

The intensity of the echo signal for the PFG-SE sequence is;

$$s\left(t\right) = exp\left(\frac{-2\tau}{T_2}\right) exp\left[-D\gamma^2 G^2 \delta^2 \left(\Delta - \frac{\delta}{3}\right)\right] \tag{2.72}$$

where G is the magnitude of the gradient used with duration δ spaced Δ apart with diffusion coefficient D. Equation 2.72 is the intensity for the PFG-SE sequence.

There is an alternative pulse sequence which can be used. This sequence is known as a pulse field gradient stimulated echo (PFG-STE) sequence. With the PFG-STE sequence the inversion pulse is replaced with two $\pi/2$ pulses, which has the effect of prohibiting any transverse relaxation

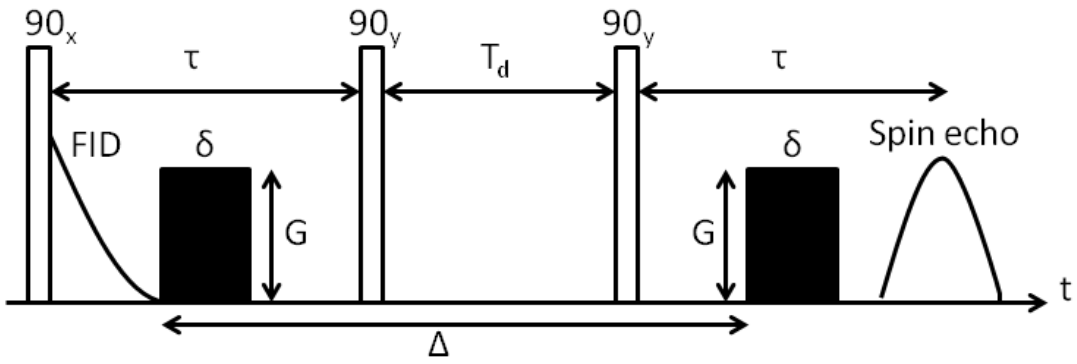

Figure 2.14: Pulse field gradient stimulated echo (PFG-STE) NMR pulse sequence.

to occur during the diffusion time. This sequence is shown in figure 2.14. During the diffusion time the spins are held in the -z-axis and therefore undergo longitudinal relaxation. The signal intensity for this sequence is given by;

$$s\left(t\right) = \frac{1}{2} exp\left(\frac{-T_d}{T_1}\right) exp\left(\frac{-2\tau}{T_2}\right) exp\left[-D\gamma^2 G^2 \delta^2 \left(\Delta - \frac{\delta}{3}\right)\right] \tag{2.73}$$

where T_d is the time between the two $\pi/2$ pulses. Each experiment must be carried out several times; usually the gradient strength is altered and the resulting intensity is monitored, while all other parameters are held constant, i.e. Δ, δ and T_d. This sequence has been shown to yield more reproducible data than the pulsed-field gradient spin echo sequence [51].

The stimulated echo pulse field gradient sequence is often preferred as usually T_2 can be much lower than T_1. In this case we need a sufficiently long relaxation time so that the signal does not decay on the same timescale as the diffusion time which is usually around $\approx 10\,\text{ms}$.

In any real system there will be a background field gradient G_0 present which will cause some discrepancy in the diffusion measurements. The pulse sequence used in this research is a complex five pulse sequence, this is a stimulated echo bipolar pulse and was originally designed by Cotts [52] in order to minimise the background gradient. The equation that describes the intensity with this varying pulse field gradient strength is:

$$I \propto exp\left[-\gamma^2 G^2 D\delta^2 \left(\Delta - \frac{\delta}{3}\right)\right] \tag{2.74}$$

where G is the gradient field strength, Δ is the time between subsequent gradient pulses and δ is the gradient pulse duration. Equation 2.74 is not complete as it is affected by the background magnetic gradients. This manifests itself in the form of cross terms of the applied magnetic gradients and the background magnetic gradients. This introduces terms into equation 2.74 and forms the equation;

$$I \propto exp\left[-\gamma^2 \left(G^2 + aGG_0 + bG_0^2\right) D\delta^2 \left(\Delta - \frac{\delta}{3}\right)\right] \tag{2.75}$$

where a and b are some arbitrary constants and all other terms are as in equation 2.74. As there is no need to know every term that is a constant, the G_0^2 term can be just incorporated

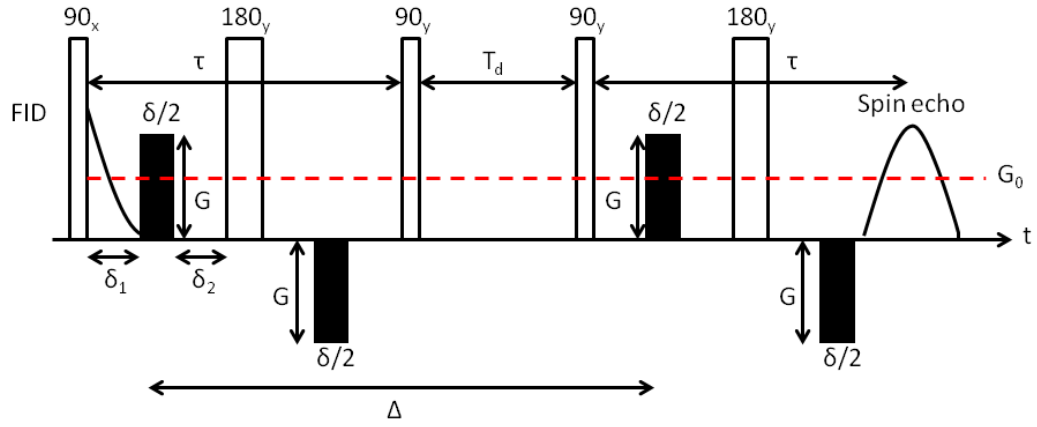

Figure 2.15: Cotts pulse field gradient stimulated echo bipolar (PFG-STE-BP) pulse sequence.

into the constant of proportionality. The GG_0 term makes it difficult to measure the diffusion coefficient as one would need to also know the background magnetic field gradient. However, the introduction of bipolar pulses resolves this problem and allows measurement of the self diffusion coefficients. The Cotts pulse sequence[52] shown in figure 2.15 has incorporated bipolar pulses in order to eliminate these cross terms.

A bipolar pulse is when the gradient is split into two gradient pulses of equal size with opposite sign which are used in order to eliminate the background gradient field. An inversion pulse between each of the two gradient pulses is needed in order to flip the system so when the negative gradient is applied it actually adds to the first gradient, so ultimately adding two halves together. The background field occurs due to the heterogeneities within the magnetic field causing a distribution of magnetic field gradients throughout the sample which, as a result creates a non uniform magnetisation in the sample.

In order for the Cotts pulse sequence in figure 2.15 to obtain the desired result of eliminating the cross term the value of a must be zero. This is the case when the gradient pulse is at equal distances from subsequent radio frequency pulses. When the time between the first RF pulse and gradient pulse (δ_1) and the time between the gradient pulse and first inversion pulse (δ_2) are equal (i.e. $\delta_1 = \delta_2$), then a=0 and the cross term is eliminated and the G_0 value is incorporated into the constant of proportionality. The modified equation when $\delta_1 = \delta_2$ is given as;

$$I = I(0)exp\left[-\gamma^2 G^2 D\delta^2\left(\Delta - \frac{\delta}{3}\right)\right] \tag{2.76}$$

where I(0) is the intensity of the magnetisation when $G = 0$, i.e. in the absence of the gradient which is usually normalised to give a value of 1.

The radio frequency pulses have to be on resonance with the nucleus of the material that is being detected, therefore it is possible to isolate the different parts of the salt such as the anion, and cation and can also track the solvent molecules. The value for Δ used in this research was 40ms and the value for δ was 10 ms; these values were used as they have been proven to work with this type of measurement [77].

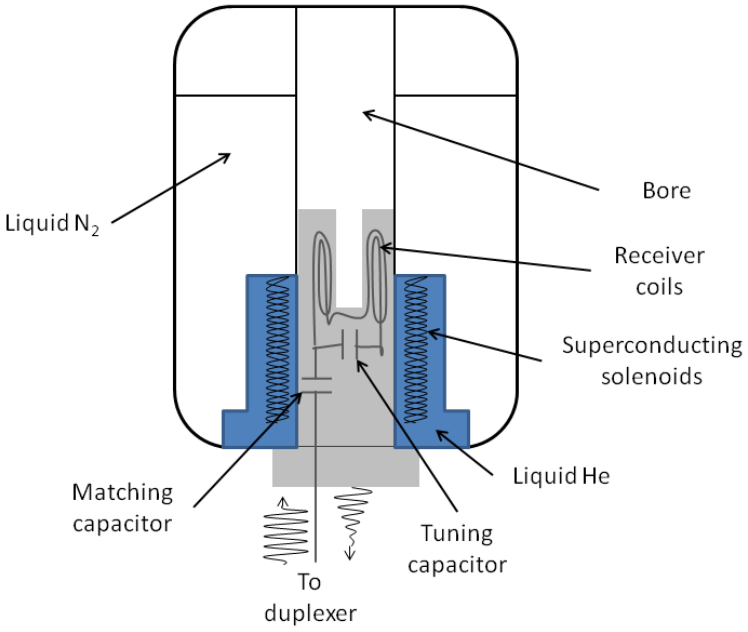

Figure 2.16: Schematic of NMR spectrometer magnet with probe inserted into the bore, adapted from reference [4].

2.8 NMR Spectrometer

A typical NMR spectrometer is comprised of many components, the most significant of which will be covered in this section. In this research, three different NMR spectrometers were used so there will not be an in depth explanation of each but rather an explanation of a general NMR spectrometer.

The most logical place to begin would be the magnet. As previously mentioned in NMR, a large magnetic field is required in order to cause a large difference between spin states, resulting in a strong signal. This magnet needs to produce a magnetic field which is both strong and highly homogeneous, i.e. independent of position. The magnetic field must be stable over the entire volume of the sample used. In most NMR spectrometers the large magnetic fields are produced using superconducting solenoids as they can accommodate large currents without electrical resistance. These superconducting coils are charged when they are installed; due to their lack of electrical resistance, they last indefinitely. Superconductors usually need to be kept at extremely low temperatures of around a few Kelvin, and therefore need to be cooled constantly. This cooling is achieved by immersing the solenoids in liquid helium, which is then surrounded by a further layer of liquid nitrogen. An NMR magnet also contains a bore down the centre, through which the sample probe will be entered. Figure 2.16 shows a schematic of the magnet and the NMR probe.

Inside the magnet there is a further two sets of coils, known as shim coils. These coils have the sole purpose of ensuring the magnetic field produced by the superconducting solenoids is homogeneous. The coils have the ability to change the homogeneity of the field; one set of coils

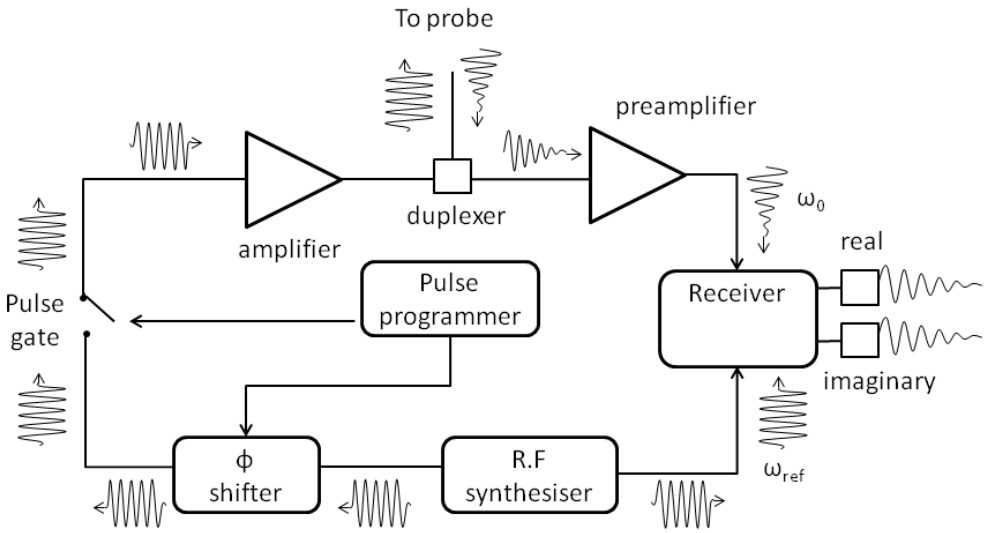

Figure 2.17: Schematic of NMR spectrometer circuitry for the emission and detection of the RF radiation, adapted from reference [4].

is placed in the liquid helium and is referred to as the 'superconducting shim coil' and is charged on installation of the magnet. There is another set of shim coils placed in the bore of the magnet used to adjust the homogeneity after the introduction of each sample. This is required as the spectrometer is highly sensitive to field inhomogeneities.

The NMR probe shown in figure 2.16, has to be very precisely manufactured from glass and contains the receiver coils, used to emit the RF radiation and to detect the very small signal from the sample. The probe is also designed so that the sample sits in the strongest part of the field. The probe contains two capacitors which are denoted C_M and C_T; they are the matching capacitor and the tuning capacitor, respectively. The matching capacitor is used in order to efficiently couple the probe to the magnetic field. The tuning capacitor has the purpose of increasing the strength of the current in the coil using magnetic resonance. This coil is extremely important as the signal from the sample decaying back to thermal equilibrium is extremely small and therefore needs to be boosted.

The next part to consider is the production of the radio frequency pulses. This circuitry is used not only to emit the RF radiation to excite the spins but also to detect the outgoing signal from the receiver coils in the NMR probe. Here a single channel NMR spectrometer is considered and a schematic is shown in figure 2.17.

The synthesiser is used to produce an oscillating radio frequency pulse which requires a very well defined frequency, as the spins will only respond to the resonant frequency for a given nuclei. The output of the synthesiser is given by;

$$I_{synth} \approx cos\left(\omega_{ref} t + \phi\left(t\right)\right) \tag{2.77}$$

where ω_{ref} is the reference frequency used by the spectrometer and $\phi(0)$ is the phase shift applied to the oscillating electric field produced by the synthesiser. The electric field is passed through

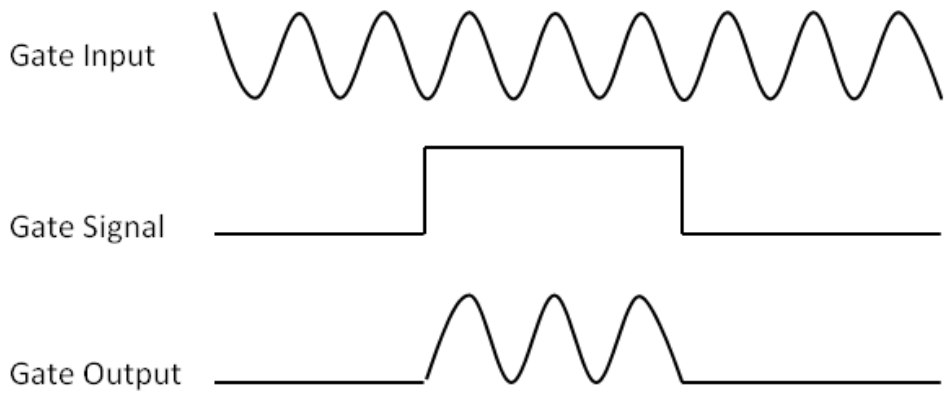

Figure 2.18: Function of the pulse gate, showing incoming signal, gate signal and the resulting output signal, adapted from reference [4].

the phase shifter which changes the phase of the signal from the synthesiser. This phase is very important as it decides the axis in which the RF pulse is applied. There are four different values that $\phi(t)$ can take which are $\phi = 0, \pi/2, \pi, 3\pi/2$. In previous sections of this chapter it was discussed that an RF pulse can be applied in the x-axis and y-axis, however the pulses can also be applied in the $-x$-axis and $-y$-axis. Each of the four values of $\phi(t)$ corresponds to each of the axes, the values of $\phi = 0, \pi/2, \pi, 3\pi/2$ correspond to the x, y, $-x$ and $-y$ axes, respectively.

Once the oscillating electric field has been created and the shift has been adjusted by the pulse programmer it then passes through the pulse gate. The pulse gate is also controlled by the pulse programmer, which is opened and closed in order to set the pulse duration. The input to the gate will be a constant oscillating field, where the gate signal can be switched on and off by the pulse programmer. When the gate is open the oscillating signal will be allowed to pass through; the functionality of the gate is shown in figure 2.18. It should be noted that it does not matter at what point in the oscillation the gate is opened and closed, but rather, the time the gate is left open.

Once the signal has passed through the gate, the next part of the process is the duplexer. The duplexer is shown in figure 2.17 and sorts the incoming and outgoing signals. The duplexer is connected to both the probe inside the magnet and the outgoing receiver. When the large signal comes from the synthesiser, the duplexer sends all of the signal up to the probe; however when the duplexer detects a very small signal, i.e. from the sample relaxing, it sends it to the receiver.

When the signal from the probe exits the duplexer the first stop is in to the preamplifier, which takes the very small signal and scales it up into a more manageable level. The signal is then passed to the computer in order to be analysed, which is the final stage of the measurement. The amplified signal is then passed to the quadratic receiver. The incoming signal will be at a frequency of ω_0 which will oscillate at frequencies in the range of 10^6 Hz which are too high for the receiver to handle. Therefore the reference frequency is subtracted from the Larmor

frequency, given by;

$$\Omega_0 = \omega_0 - \omega_{ref} \tag{2.78}$$

where ω_{ref} is the reference frequency. If we consider the free induction decay then the signal will be given by;

$$I_{Real}(t) = cos(\omega_0 t)\, exp\left[\frac{-t}{T_2}\right] \tag{2.79}$$

where T_2 is the dampening factor of the signal. Usually the reference frequency and the Larmor frequency are similar in value, which means that it is possible for the value of Ω_0 to be negative as the frequency of a single spin can be faster or slower than the Larmor frequency, as a result of the stronger and weaker local magnetic fields. Therefore the quadratic receiver splits the signal into a real and imaginary signal in the form of equations 2.80 and 2.81.

$$I_{Real}(t) = cos(\Omega_0 t)\, exp\left[\frac{-t}{T_2}\right] \tag{2.80}$$

$$I_{Imaginary}(t) = sin(\Omega_0 t)\, exp\left[\frac{-t}{T_2}\right] \tag{2.81}$$

These signals are then taken and converted from analogue to digital signals to be used by computers in order to analyse the signals.

2.9 Experimental Detail

In this research, three different NMR spectrometers have been used. The logic behind this decision was due to the high demand of each NMR spectrometer. The majority of the work was carried out on a 400 MHz Bruker AVANCE II NMR spectrometer, which allowed measurements of the longitudinal and transverse relaxation times as well as the self diffusion of multiple nuclei. Although three spectrometers were used, all measurements are self consistent and each set of data was taken on a single machine.

NMR spectrometers are usually classified by their magnetic field strength but are actually denoted as the resonant frequency of the ^{1}H nucleus which can be determined from the Larmor frequency. As mentioned above, the Bruker 400 MHz machine relates to a magnetic field strength of around 9.4 T.

2.9.1 400 MHz Bruker AVANCE II Ultrashield Spectrometer

The 400 MHz Bruker AVANCE II spectrometer was purchased from and installed by Bruker. It has x, y and z gradients installed, which allows imaging. Only the z-axis gradients are needed to make diffusion measurements; the imaging function was not used in this research. The measurements that were taken on this spectrometer are the longitudinal and transverse relaxation as well as the self diffusion. The probe used was a Diff60 which has interchangeable coils, depending on the nucleus that is required. The temperature of the samples is controlled by water cooling. The temperature can also be altered with compressed air that blows through a heater and past the sample.

There were limitations to this spectrometer, due to the spectrometer's ability to image, the water cooling is required to stop overheating. In this research, temperatures of around 353 K

were measured. With the liquid samples it was found that if the air was blowing at 353 K, the water could be raised to a maximum of 313 K and therefore created a temperature gradient. It was found that samples needed to be as small as possible in order to avoid any temperature gradients. It was clear when the temperature gradient was present due to rapid increases in the diffusion, suggesting correlated motion of the ions. The polymer gel electrolytes did not seem to exhibit this same correlated motion, therefore it is assumed that because the gels are separated into smaller pockets of liquid there was no temperature gradient.

Three different nuclei were used on this spectrometer - ^{1}H, ^{7}Li and ^{19}F, where ^{1}H and ^{19}F are spin-1/2 nuclei and the ^{7}Li is a spin-3/2 nucleus. The resonant frequency for the ^{7}Li and ^{19}F were 155 MHz and 376 MHz, respectively. The preamplifier used was changed depending on the nucleus as filters are used in order to omit frequencies outside of the range of the nuclei needed. The pulse durations used were τ_{90}=18.50 μs and τ_{90}= 19.6 μs for the ^{7}Li and ^{19}F nuclei, respectively, at a power level of 3 dB and τ_{90}= 6.47 μs at a power level of 0 dB for the ^{1}H nucleus.

The diffusion measurements were measured using a bipolar stimulated echo pulsed-field gradient pulse sequence. The settings of the diffusion time (Δ) and gradient duration (δ) were fixed at 40 ms and 10 ms, respectively, for all diffusion measurements, unless otherwise stated. The software that controlled the computer was Bruker Topspin 1.5 which had a function called 'diff' it would take an expected diffusion constant along with values for Δ and δ and would automatically set the maximum gradient strength.

2.9.2 50 MHz Maran Benchtop Spectrometer

The 50 MHz Maran benchtop spectrometer was used to measure the longitudinal and transverse relaxation times for the liquid and polymer gel electrolytes. This machine was not multi-nuclear and therefore could only be used to measure the hydrogen (^{1}H) nucleus which was used to detect the solvent molecules.

The spectrometer contained built in programs which were used to calibrate the receiver gain and pulse durations. The pulse duration was not changed through all measurements as it was well defined for the machine as $\tau_{90^{\circ}}$= 3.5 μs. The pulse sequence which was used to measure the T_1 values was a simple inversion recovery sequence, therefore a recycle delay was set as standard to $5T_1$, to ensure all magnetisation had dissipated. The values of τ for the inversion pulse sequence were determined based on initial measurements of the relaxation time in order to capture a representative recovery of the magnetisation.

The transverse relaxation measurements were measured with the CPMG pulse sequence. The control computer included an interactive setup for the transverse relaxation times. In order to observe the entire relaxation it was necessary to set the total experiment time. The total time was controlled by the the number of echoes and the time allowed to dephase and refocus (τ). If the value of τ was made too large then the value of T_2 would decrease due to relaxation between measurements; therefore the value of τ was kept short and the number of echoes was changed.

The temperature of the system was controlled with a flow of nitrogen gas over the sample combined with a heater controlled by a Eurotherm temperature controller. It was possible to reach temperatures of around 253 K confidently; the highest temperature used was 333 K.

2.9.3 500 MHz Bruker Avance Ultrashield Spectrometer

The only measurements taken with this spectrometer were the longitudinal relaxation times using the ^{1}H nucleus. With the benchtop spectrometer the different hydrogen sites were not distinguished, therefore this spectrometer was used in order to measure the relaxation times of each individual site on the propylene carbonate molecule.

The 500 MHz spectrometer had the capability to measure multiple nuclei, however only the ^{1}H longitudinal relaxation times have been observed using this spectrometer. The probe used was a Bruker issued quattro nucleus probe (QNP), containing two sets of coils, inner and outer. The inner coil was used to detect three predetermined nuclei - ^{19}F, ^{31}P and ^{13}C, while the outer coil was tuned to detect the ^{1}H nucleus. Therefore, in these measurements the outer coil was used in order to detect the hydrogen nucleus and the inner coils were not used.

The saturation pulse sequence was used for these measurements. The duration of the $\pi/2$ pulse was τ_{90}= 9.82 μs for a power level of -3 dB. Again, the values of τ were chosen after preliminary measurements of the T_1 values as they needed to be set for each measurement in order to observe the entire recovery. The fitting of the data was completed using the Topspin software which utilises the Levenberg-Marquardt [78; 79] algorithm. The spectrometer was calibrated by Bruker on regular inspections of the machine.

The temperature was controlled using a source of heated compressed air with a control unit built into the Bruker Topspin 1.3 software that the computer used for this spectrometer. The temperature range used for this spectrometer was 303-353 K.

Chapter 3

Experimental Techniques

3.1 Sample Preparation

3.1.1 Materials Selection

The aim of the research presented in this thesis is concerned with transport properties of liquid and polymer gel electrolytes based on poly(vinylidene fluoride) (PVDF), lithium tetrafluoroborate ($LiBF_4$) and propylene carbonate (PC). Polymer gel electrolytes are considered porous membranes which contain an organic solvent and a salt. The primary application of these polymer gel electrolytes is for their use in secondary lithium batteries. The original polymer electrolytes were solvent-free and consisted of a polymer with an alkali salt. These proved to not be suitable for battery applications since they exhibited very low conductivities (10^{-8} S cm^{-1})[6]. With the addition of an organic solvent as a plasticiser the glass transition temperature of the polymer is decreased and makes the polymer chain more flexible. The effect of the plasticiser has been to introduce channels or cavities containing liquid which allow for significantly higher conductivities [43]. There are many different polymers, solvents and salts that can be chosen when creating a polymer gel electrolyte, however this combination must be chosen carefully to enhance the conductivity for use in the electrochemical devices.

The choice of solvent will be discussed first. In order for the salt to dissolve, the correct solvent must be chosen. The solvent commonly used exhibit a high dielectric constant. Propylene carbonate (PC) has a very high dielectric constant of 61.7 at 313 K [80]. The salt ions are attached by electrostatic force F_C (Coulomb forces) defined by Coulomb's law;

$$F_C = \frac{q_1 q_2}{4\pi\epsilon_0\epsilon_r r^2} \tag{3.1}$$

where the equation describes the force F_C between two charges (q_1 and q_2) at a separation from each other of r, ϵ_0 is the permittivity of free space and ϵ_r is the dielectric constant or relative permittivity of the material that the charges are immersed. Therefore, if ϵ_r was increased then the force between the two charges would decrease and if the dielectric constant is of sufficient magnitude, the two charges could be dissociated from one another. The level of dissociation in a liquid electrolyte is important as this directly dictates the conductivity of the system. If the cations and anions are associated then they have a neutral charge and will not contribute to the

Solvent	T_M (°C)	T_B (°C)	η(25 °C) (mPa s)	ϵ_r	M_w (g mol^{-1})
Dimethyl carbonate	2.4	90	0.585	$3.12^{25\,°C}$	90.08
Diethyl carbonate	-43.0	126	0.748	$2.82^{24\,°C}$	118.13
γ-Butyrolactone	-43.3	204	1.7	$39.0^{20\,°C}$	86.09
Propylene carbonate	-48.8	242	2.53	$61.7^{40\,°C}$	102.09
Ethylene carbonate	36.4	48	$1.93^{40\,°C}$	$89.78^{40\,°C}$	88.06

Table 3.1: Physical properties of organic solvents commonly used in liquid electrolytes. Data taken from reference [61]. Superscript represents temperature at which this data was taken.

ionic conductivity, therefore a solvent with a high dielectric constant is required as the practical application of these gels is for advanced lithium batteries, which demand high ionic conductivity.

The choice of solvent is not solely dependent on the dielectric constant, as it must also exhibit other qualities. For instance, the dielectric constant of ethylene carbonate is 88.6 at 313 K [61] which is higher than for PC. It would be expected that EC would promote a higher level of ionic dissociation, however the boiling point of EC is much lower than that of PC, it is also a solid at room temperature and therefore conductivity would be extremely low. A list of organic solvents commonly used in the liquid electrolytes with relevant properties shown in table 3.1. From observing the properties in table 3.1 it can be seen that PC is a clear candidate for use in liquid and polymer gel electrolytes because it exhibits an excellent range of operational temperatures, where the melting and boiling temperatures are -48.8 °C and 242 °C, respectively [61]. The other solvents in table 3.1 such as dimethyl carbonate (DMC) and diethyl carbonate (DEC) have significantly lower dielectric constants and therefore do not promote ionic dissociation as well as PC.

It has been found that PC cannot be used in a Li-ion cell as it causes a passivation layer on the electrodes which in turn causes loss of ions [18]. This effect can be avoided by using a mixed solvent; at the University Leeds it has been shown that high conductivities can be obtained by using a mixture of EC:PC (2:1). The resulting solution has a mixture of the properties, it lowers the melting point and is not a solid at room temperature. Since they both exhibit high dielectric constants, the resulting mixture would also exhibit a high dielectric constant. In this thesis the liquid and polymer gel electrolytes were produced using a PC as a single solvent. Although the systems cannot be directly used in the commercial batteries due to the passivation effect, a single solvent is easier to gain a better physical understanding of the dynamics.

With solvents such as PC (which are polar), have been found to solvate the cation more favourably than the anion [81]. This is due to the cation's large charge density which is more attractive than the dispersed charge of the anion. Moreover, the structure of such solvents as PC contain rings with a carbonyl group which protrudes from the molecule, and contains a small negative charge which will easily bond with the lithium positive charge. However, the anion bonds with a less favourable part of the PC molecule, resulting in less anion solvation by the solvent molecule. The structures of the PC molecule and the BF_4^- anion are shown in figures 3.1(a) and 3.1(b), respectively.

An important question to address is how many solvent molecules attach to a single cation, this is important because it will affect the transport properties as with the solvated molecules on the lithium it will be a much larger entity and will therefore slow the lithium molecules down

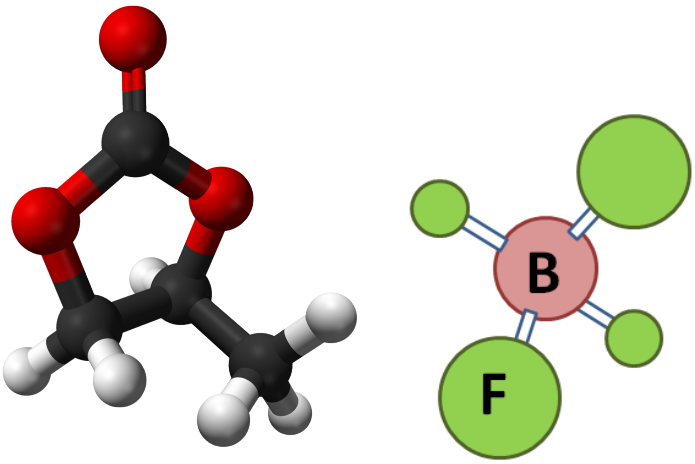

(a) Propylene Carbonate (b) Tetrafluoroborate

Figure 3.1: Chemical structure of PC and BF_4 anion. (a) Red, white and black corresponds to oxygen, hydrogen and carbon respectively. (b) Green and red correspond to fluorine and boron respectively.

when traveling through the medium. It has been found that the maximum of four PC molecules can solvate the lithium cation [82], this relatively high solvation number suggests that PC will dissolve the salt well. It is important to consider the ratio of solvent molecules to salt ions and see if there are enough solvent molecules to have four attached to each lithium ion. It is possible to calculate the ratio of PC molecules to lithium ions in a typical liquid electrolyte in the form;

$$\frac{Mass\ of\ 1L\ of\ PC}{Molar\ Mass\ of\ PC} = \frac{\rho V}{M_W} = \frac{(1.197g/ml)\,(1000ml)}{102.09g/mol} = 11.7Moles \tag{3.2}$$

where the values used are for a pure PC solution, showing that for every lithium ion there are around 11 PC molecules, which means that there are enough PC molecules to achieve solvation of 4 molecules around each lithium ion. The radius of the PC molecules, lithium ions and BF_4^- anions as well as the solvation numbers, will be discussed in Chapter 7.

The discussion above has outlined reasons for using PC as the solvent, however the choice of salt is also important. The salts commonly used tend to be lithium based as they have a large anion attached to the relatively small lithium cation. This uneven size distribution causes a somewhat dispersed charge, and hence low lattice energy and is therefore favourable for the salt molecule to split and dissolve in the solvent. For this reason the anions are usually fluorinated as they provide large anions. The radius of a single lithium ion and the BF_4 anions is 0.076 Å and 2.29 Å respectively [83]. The most important property for the salt to exhibit is that it needs to be miscible in the polymer and solvent otherwise the ions will not dissociate and conduct. The $LiBF_4$ was obtained from Sigma-Aldrich.

When choosing a polymer to use for the PGEs it is important that they satisfy the criteria needed. In order for the polymer gel electrolytes to be used in advanced batteries, the polymer must be chemically inert and stable under 4 V. Fluoropolymers are among the most chemically inert polymers, making them a good choice. PVDF is a fluorinated polymer which exhibits both

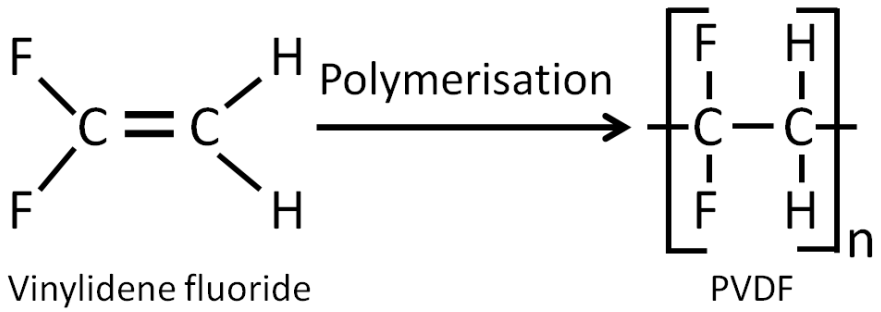

Figure 3.2: Structure of vinylidene fluoride and the polymer form PVDF.

Density (g cm^{-3})	T_m (°C)	M_W (g mol^{-1})	M_N (g mol^{-1})	Polydispersity Index (PDI)
1.78	160-172	573000	238000	2.4

Table 3.2: Properties of Solef ®PVDF 1015 used in the polymer gel electrolytes. M_W is the weight averaged molecular weight, M_N is the number averaged molecular weight and the polydispersity index is calculated using M_W/M_N. All data taken from Solvay Chemicals website.

pyroelectric and piezoelectric qualities due to the charged fluorine ions on the polymer backbone - PVDF is therefore a polar polymer. Figure 3.2 shows the structure of vinylidene fluoride (the monomer of PVDF) and PVDF. The polar properties of the polymer give it a high dielectric constant of between 8.15-10.46 [61] which aids in the dissociation of the anion and cation.

The PVDF used in this research was Solef ®(Solvay Chemicals) 1015 PVDF. The properties of the Solef ®PVDF 1015 are displayed in table 3.2 and highlight the melting temperature, weight averaged molecular weight (M_W), number averaged molecular weight (M_N) and the polydispersity index of the polymer used.

PVDF is a semi-crystalline polymer which forms crystalline junctions that are not chemically cross-linked. This semi-crystalline nature gives the resulting polymer gel electrolyte good mechanical properties which allows the gels to be thermo-reversible. The thermo-reversible properties of these gels are essential to the extrusion lamination process developed at the University of Leeds [31]. Once the gels are heated past their melting points, they will stay molten until allowed to cool; this allows for great manipulation of the gels compared with the corresponding crystalline polymer which are often used in polymer gel electrolytes. In fact, the thermo-reversible property is exploited in this research when mounting the gels into the various cells used which would be difficult with a crystalline polymer. The various polymers commonly used in polymer gel electrolytes have been listed in table 3.3. Most importantly, the solvent chosen must be able to dissolve the polymer otherwise the gelation process will not occur.

The polymer concentration must also be considered. For the practical battery application, the gels need to be flexible and therefore require a significant amount of solvent contained within the polymer. It has been observed that increasing the amount of solvent in the polymer gel electrolytes has a positive effect on the mobility of the ions; however there is also a significant decrease in the mechanical properties [84]. It has been observed by Capiglia *et al* [26] for PVDF-

Polymer	ϵ_r	T_g (°C)	T_m (°C)
Polyethylene (PE)	2.3	123	136-142
Polypropylene (PP)	2.2-2.3	-23	160-170
Polyvinylidene fluoride (PVDF)	8.15-10.46	-40	165-170
PVDF/HFP copolymer	7.9-10.0	-100-90	140-145
Polyacrylonitrile (PAN)	5.5	97	319
Poly(methyl methacrylate)	3.0	105	–

Table 3.3: Physical properties of polymer commonly used in polymer gel electrolytes. Data taken from refs. [61].

HFP polymer gel electrolytes, that when 50% solvent was present no significant voids were produced. By increasing the solvent to 70% they witness voids of up to 10 μm, with the formation of channels connecting these voids. Therefore allowing the ions to translate through the liquid regions of the gels creates a much higher diffusion constant, and as a result, conductivity. It has been seen at the University of Leeds that for the commerical extrusion lamination gels, solvent content of 70% produces both strong transport and mechanical properties [85], therefore a logical polymer:solvent ratio to use in this work was considered to be 30:70 (30% PVDF). Measurements have also been taken for another polymer:solvent ratio of 20:80 (20% PVDF) to compare the transport properties between the two polymer concentrations. There is going to be loss of mechanical properties with the addition of the extra solvent, however they will not be considered in this research. It should be noted that the 20% PVDF gels underwent the gelation process and were still suitably $'solid'$ at room temperature. Preliminary gels produced with 40% PVDF were too brittle and not easily manipulated and therefore considered not suitable. Polymer gel electrolytes were also made with less than 20% polymer; these gels were also found unsuitable as they did not gel properly and did not have the desired mechanical properties.

3.1.2 Preparation Process

The liquid electrolytes were prepared by mixing the $LiBF_4$ salt with PC at different concentrations using magnetic stirrer bars at room temperature. All chemicals were obtained from Sigma-Aldrich and were received vacuum sealed. All liquid electrolytes were prepared inside a nitrogen filled glove box, this was to prevent any moisture from being absorbed by the sample, as it would likely affect some of the measurements significantly.

The polymer gel electrolytes (PGE) were prepared by making the liquid electrolyte and adding a given amount of polymer - in this case PVDF. The polymer concentrations used here were 20% and 30% PVDF, by mass, with respect to the solvent. These polymer concentrations have been chosen as a balance so that there is ample polymer to form the gels with good mechanical properties; however there is still enough solvent for the lithium ions to travel through in order to produce decent transport properties.

Figure 3.3 shows a flow diagram of the production process of a polymer gel electrolyte. Firstly, the liquid electrolytes were made by measuring the desired amount of solvent and salt and mixing until fully dissolved. Then the polymer was added to the liquid electrolyte and heated to around 160°C (the temperature at which PVDF dissolves), until the gel turns clear.

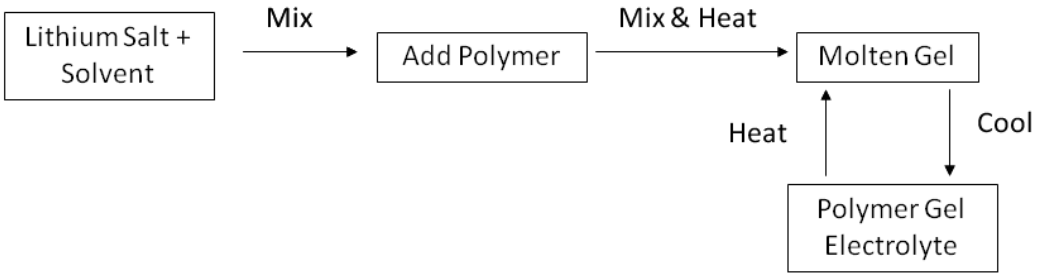

Figure 3.3: Flow diagram of the preparation of polymer gel electrolytes.

The liquid electrolyte and polymer slurry was placed inside a glass tube, which was placed inside a heated metal chamber, fully encasing the sample. It was important to wait until the centre of the gel turned fully clear due to it being heated from the outside. It was visibly clear when making the gels if it had not heated through as it would be opaque in the centre. At this point the solution needs stirring and then be allowed time to cool. As the molten gel cools it forms crystalline junctions (as well as amorphous PVDF regions) and contains cavities filled with pure liquid electrolyte; this is the complete polymer gel electrolyte. By using PVDF as the host polymer, this process is thermo-reversible since chemical cross-linking are not present. Therefore, the gels can be made to change state with the use of heating and cooling, allowing manipulation of the PGEs in the production stages. This property is of importance to the Leeds group extrusion lamination production [31] of polymer gel electrolytes as the bulk solution is kept in the molten stage until ready to be processed. However, the samples used throughout this research were not re-heated as this would likely cause loss in solvent and therefore a change in composition of the gels.

3.1.3 Sample Compositions

All liquid electrolytes in this research were made to a total volume of 10 ml, which allowed easy calculation of the mass of salt that would be needed as the molecular mass of the salt was well known, the mass of salt was determined using;

$$m_{salt} = \frac{M_{salt} c}{100} \tag{3.3}$$

where m_{salt} is the mass of salt required for the liquid electrolyte, M_{salt} is the molar mass of the salt being used, c is the salt concentration (in M, i.e. in mol dm^{-3} of solution) and the factor of 100 reduces the total volume to 10 ml. The total volume of the liquid electrolyte can be written as;

$$V_{Total} = V_{Solvent} + V_{Salt} \tag{3.4}$$

where $V_{Solvent}$ and V_{Salt} are the volumes of the solvent and salt, respectively. It was assumed that there was no volume change on the dissolution of the salt in equation 3.4. Since $V = m/\rho$,

equation 3.4 can be written,

$$V_{Total} = \frac{m_{Solvent}}{\rho_{Solvent}} + \frac{m_{Salt}}{\rho_{Salt}} \tag{3.5}$$

where $\rho_{solvent}$ and ρ_{salt} are the densities of the solvent and salt respectively. The molar mass of $LiBF_4$ is well known to be 93.74 g mol^{-1}, therefore the mass needed to make up a sample solution of 10 ml is m_{Salt}=0.9374 g for a 1.0M solution. The mass of solvent can then be calculated for the various salt concentrations needed by rearranging equation 3.5 using,

$$m_{Solvent} = \left(V_{Total} - \frac{m_{Salt}}{\rho_{Salt}}\right)\rho_{Solvent} \tag{3.6}$$

where the solvent density was taken as 1.197 g mol^{-1} which was measured as part of this research. The amount of polymer used was taken as a mass fraction (w) of the total solvent in solution, which can be defined by;

$$w_{polymer} = \frac{m_{polymer}}{m_{polymer} + m_{solvent}} \tag{3.7}$$

where $m_{polymer}$ is the mass of polymer added to the 10 ml liquid electrolyte solution. Equation 3.7 can be rearranged for the mass of polymer;

$$m_{polymer} = m_{solvent}\left(\frac{c_{Polymer}}{1 - w_{Polymer}}\right) \tag{3.8}$$

where $w_{polymer}$, the amount of polymer contained within the PGEs and in this research is limited to either 20% ($w_{polymer}$=0.2) or 30% ($w_{polymer}$=0.3) PVDF due to the reasons previously discussed.

The density of $LiBF_4$ has been measured here as (1.6±0.1) g cm^{-3}. This was achieved by rearranging equation 3.5 in the form of;

$$\rho_{LiBF_4} = \frac{m_{LiBF_4}}{\left(V_{total} - \frac{m_{PC}}{\rho_{PC}}\right)} \tag{3.9}$$

where $LiBF_4$ and PC were used as the salt and solvent, respectively. The mass of $LiBF_4$ used was a 1.0M solution made up to a total volume of 10 ml, which is 0.937 g. This was placed in a volumetric flask, where PC was added until filled up to the 10 ml line of the volumetric flask; the mass of the PC was also recorded. The density of the PC had been previously calculated using the volumetric flask as 1.197 g ml^{-1}. These values were used along with equation 3.9 to calculate the density of the $LiBF_4$. The assumption of this method is that the salt is completely miscible in the PC and that no change of volume occurs. This was measured at the ambient temperature of the lab which was around 20 °C.

In this section, the quantities used to produce the liquid electrolytes and PGEs are given for a range of salt concentrations in table 3.4 which have been calculated using equations 3.6 and 3.8 for liquid and gels, respectively.

The values in table 3.4 were measured out accurate to ± 0.005 g, however there was inherently some solvent loss when producing these samples. This loss was closely monitored for a range of concentrations. It was found that the most significant loss of materials occurred when removing the stirrer bar because it retained some liquid. However, this is assumed to be an even mix of liquid electrolyte so should not alter the composition of the samples. When making the PGEs some solvent was lost while heating the mixture past the PVDF melting temperature. This was

Salt Conc. (M)	m_{LiBF_4} (g)	m_{PC} (g)	$m_{PVDF}(20\%)$ (g)	$m_{PVDF}(30\%)$ (g)
0.0	0.000	11.970	2.993	5.130
0.2	0.187	11.830	2.957	5.070
0.4	0.375	11.689	2.922	5.010
0.6	0.562	11.549	2.887	4.950
0.8	0.750	11.409	2.852	4.890
1.0	0.937	11.269	2.817	4.829
1.2	1.125	11.128	2.782	4.769
1.4	1.312	10.988	2.747	4.709
1.5	1.406	10.918	2.730	4.679

Table 3.4: Quantities calculated using equations 3.6 and 3.8 for 10 ml solutions of liquid electrolytes based on PC and $LiBF_4$, with the corresponding masses to make either 20% or 30% PVDF polymer gel electrolytes.

not seen to be very significant compared to the bulk solution mass. By measuring the extremes of the solvent loss during the mixing of the liquid electrolyte and heating process (once the polymer has been added), it has been estimated that the polymer concentrations used were (0.20±0.03) and (0.30±0.03) for the 20% and 30% PVDF gels, respectively.

The samples discussed throughout this thesis will be denoted in the form; 20% PVDF/PC/ $LiBF_4$ (1.0M), where the 20% refers to the a polymer:solvent ratio of 20:80. The other PVDF concentrations used in this research are 30% (a polymer:solvent ratio 30:70) and 0%, which refers to the liquid electrolyte, which is sometimes written as simply PC/$LiBF_4$ (1.0M). The salt concentration is displayed in brackets at the end of the sample name, in this example 1.0M. The masses of each constituent can be determined using equations 3.3, 3.6 and 3.8 for the salt, solvent and polymer, respectively.

3.2 Ionic Conductivity

Electrical conductivity is comprised of two factors, the ionic conductivity which arises from the ions within the electrolyte solutions and the electronic conductivity which is due to the movement of electrons. The conductivity of a system is related to the resistivity, bulk resistance and geometrical factors such that:

$$\sigma = \frac{1}{\rho} = \frac{t}{AR_b} \tag{3.10}$$

where ρ is the resistivity, t is the thickness of the sample, A is the cross-sectional area of the electrodes and R_b is the bulk resistance of the sample. By placing a conducting sample between two electrodes, then applying an electric potential difference across them, the ions will translate to the relative electrode. A current occurs due to the free ions within the sample moving between the two electrodes. Conductivity can be measured by applying an alternating current (AC) and measuring the resulting impedance. It is implied that these measurements could be taken using a direct current (DC), however the use of a DC potential difference can cause an issue of polarisation, that is to say a build up of charges at each of the electrodes. Polarisation has the affect of repelling subsequent charges and thus reducing the conductivity, becoming more

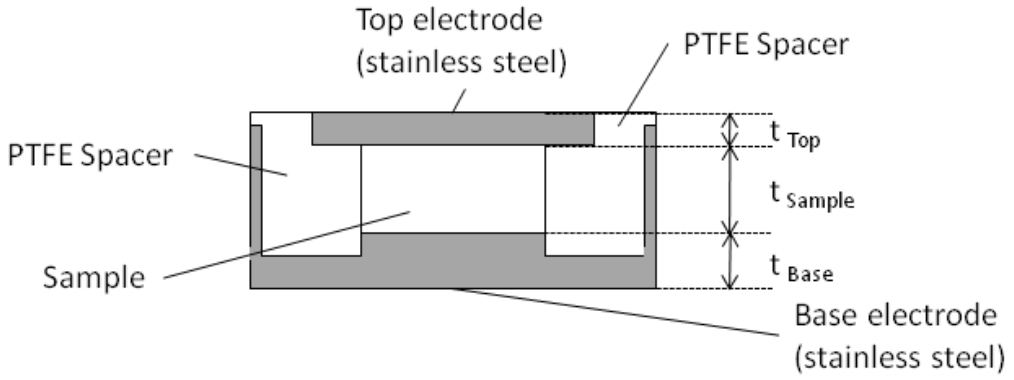

Figure 3.4: Schematic of the cell used for both liquids and gels. The base and top act as the electrodes with the sample in the middle and polytetrafluoroethylene (PTFE) spacer was used to support the structure without affecting the contact between the plates.

of an issue with increased conductivity. An AC source was used to avoid this problem as the ions are not given the opportunity to polarise, given that the frequency is sufficiently high.

There are two different types of material that can be used to produce the electrodes, blocking or non-blocking. Blocking electrodes are produced from inert materials such as platinum, or in this research, stainless steel, and therefore no chemical reaction occurs when the ions gather at the electrode. Non-blocking electrodes would usually be made from lithium based metals, when the lithium ions in the salt gather at the electrode a chemical reaction will occur at the surface and the ions can pass through the electrodes [86]. Since the conductivity of the samples was required in this research it was important to not lose any ions and therefore blocking electrodes were chosen.

3.2.1 Conductivity Cell & Novocontrol Conductivity Rig

The conductivity cell has to be made up of two electrodes produced from a highly conductive material, with an insulating material as the spacer. A few different cells have been tried and tested here in order to find the most optimum cell possible to carry out the conductivity measurements. It was decided that all of the conductivity cells would consist of inert blocking electrodes produced from stainless steel, meaning the lithium ions will not chemically react with the electrodes. The material chosen for the insulating spacer was polytetrafluoroethylene (PTFE), as it has a very high melting temperature, is extremely insulating, and relatively cheap and durable.

A few different cells were designed throughout the course of this research. It was decided that one cell performed better than the rest, and was used to measure the ionic conductivity. This was a circular cell consisting stainless steel base and sides with a raised bottom electrode. The PTFE was then inserted inside the cell, with the centre of the cell left vacant for the sample to be inserted. The cell had a sample thickness of (2.01±0.02) mm with a sample diameter of (11.14±0.02) mm, which corresponded to a cell constant of t/A of (0.22±0.01) cm^{-1}; a schematic of the cell can be seen in figure 3.4.

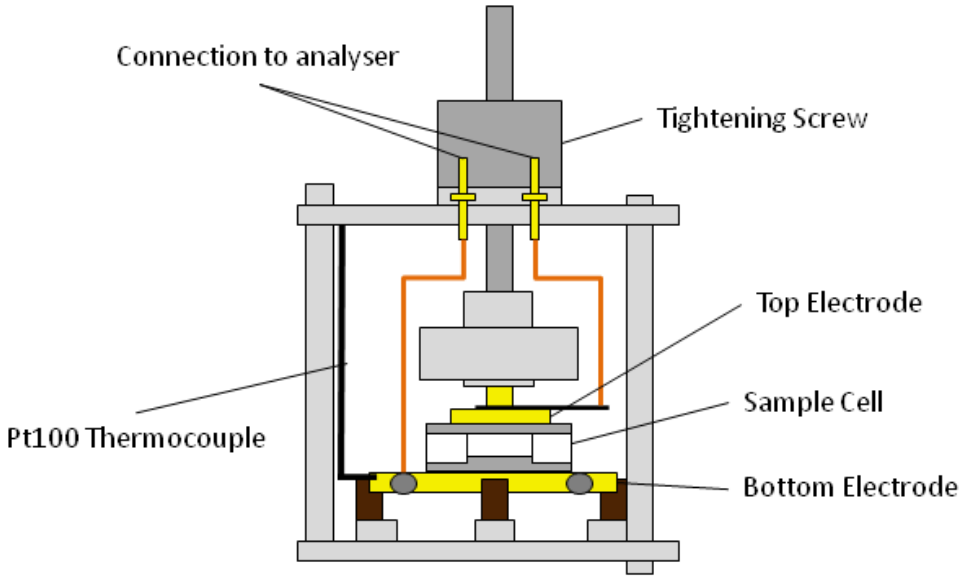

Figure 3.5: Conductivity cell inside the Novocontrol BDS1200 rig, Pt thermocouple was attached to the bottom plate. Figure adapted from reference [87].

The cell had to be throughly cleaned, as any contamination would affect the ionic conductivity. The cleaning process involved submersing the cell into acetone (for an extended period of time) and cleaned using a cotton bud, then immersed in acetone a second time, followed by drying in an oven at 383 K.

In order to measure the conductivity, the sample cell must be placed between two electrodes in a conductivity rig. By using a Novocontrol alpha beta frequency analyser an AC voltage can be applied at different frequencies in the operational range of 10^{-4} Hz to 10^{7} Hz and then the analyser recorded the resulting complex impedance. A Novocontrol BDS1200 standard sample cell rig was purchased from Novocontrol, housing the sample cell by clamping each electrode against a highly conductive brass electrode attached to the rig. A schematic of the cell housed in the rig is shown in figure 3.5.

The BDS1200 Novocontrol rig is shown in figure 3.6(a) and has an operating temperature range of 73 K to 673 K and is equipped with a Pt100 thermocouple which was attached to the base plate electrode of the rig. The schematic in figure 3.6(b) shows the Pt100 thermocouple placed inside the bottom electrode which is accurate to within 0.1 °C. The temperature was controlled by an external Eurotherm temperature controller which was connected to the Pt100 connection of the BDS1200. A nitrogen dewar was used to produce a steady flow of nitrogen over the sample and heated by a 400 W heater built in house. This allowed conductivity to be measured in the temperature range of -20 °C to 80 °C.

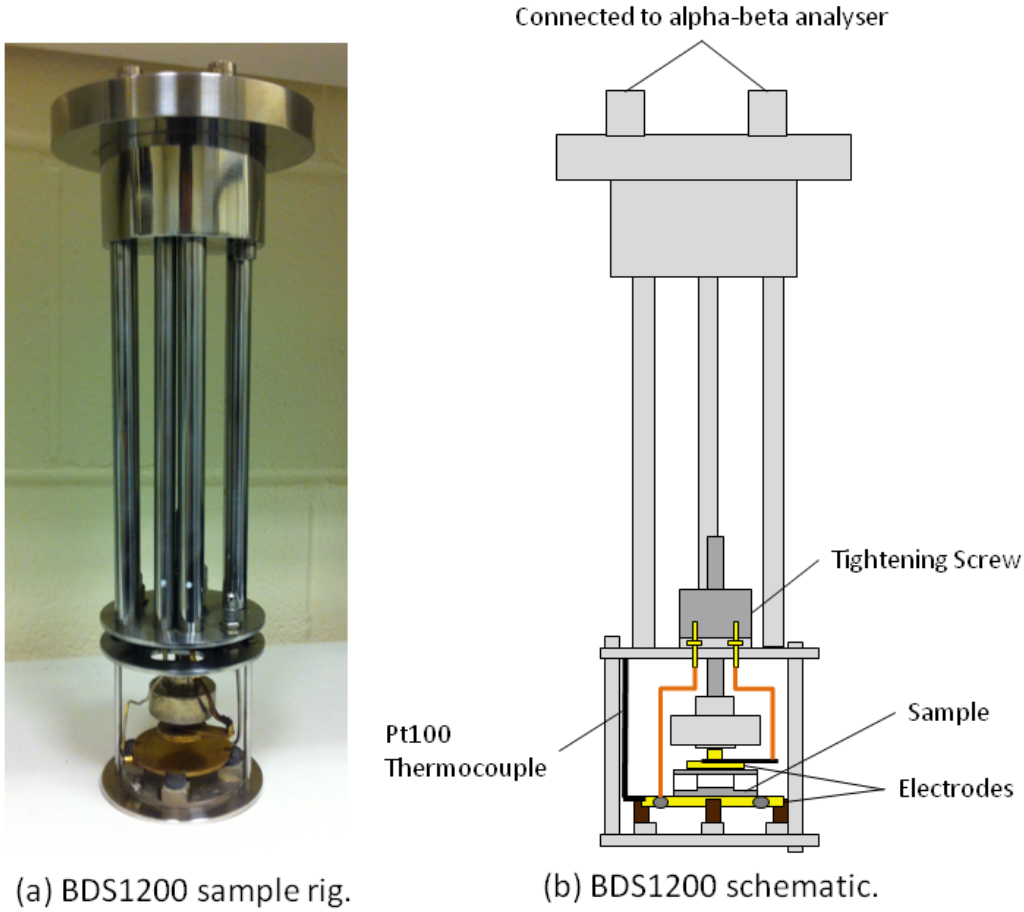

Figure 3.6: (a) Picture and (b) schematic of the BDS1200 Novocontrol standard sample rig used for all conductivity measurements. (b) adapted from reference [87]

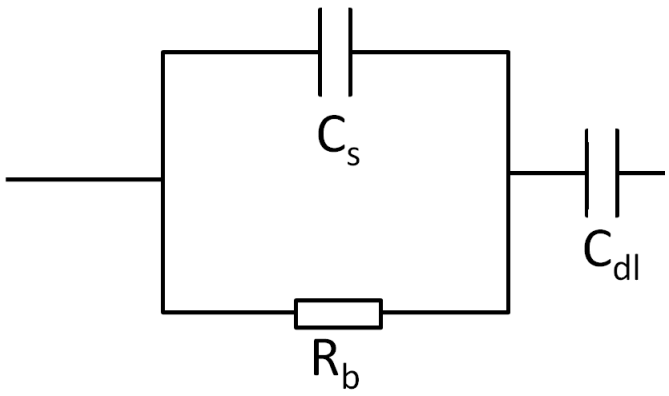

Figure 3.7: Equivalent circuit for two stainless steel electrodes separated by an insulating spacer with a sample between the electrodes. Figure adapted from references [88; 89].

3.2.2 Effective Circuit

The cell used here consisted of two stainless steel electrodes separated by an insulating spacer produced from PTFE. This type of cell gives an equivalent circuit which contains capacitances and resistances which is shown in figure 3.7, where C_s and R_b refer to the capacitance and resistance of the electrolyte, respectively and C_{dl} corresponds to a double layer formed at each electrode. The double layer capacitance arise due to the ions gathering at the electrodes and forming a layer with a very small thickness. Since capacitance is inversely proportional to separation, it produces a large response. This response becomes increasingly large at low frequency because at high frequency the ions do not have the opportunity to form a layer. This effect is called polarisation as the charges that have gathered at the surface of the electrode repel like charges and attract opposite charges, and therefore affects the conductivity by reducing its value[90].

Since the contribution from the ions in solution (ionic conductivity) is much greater than the contribution from the electrons (electronic conductivity) in electrolytic systems, the terms conductivity and ionic conductivity can be assumed to be synonymous for the duration of this thesis. The use of an alternating current produces a real (Z') and imaginary (Z'') component of the resulting impedance of the form:

$$Z = Z' - iZ'' \tag{3.11}$$

where i denotes a complex number and thus goes with the imaginary part of the impedance. With the correct setup, both the imaginary and real impedance can be measured as a function of frequency. Complex notation is usually depicted in Cartesian coordinates with the real part being on the x axis and the imaginary on the y axis, which is shown in figure 3.8. It should be noted that the angle ϕ in figure 3.8 is equal to ωt, where ω is the frequency, therefore the angle ϕ is frequency dependent. In general, an AC voltage will cause a phase difference ϕ between the current (I) and voltage (V) in the form:

$$Z' = \frac{V}{I} cos\phi \tag{3.12}$$

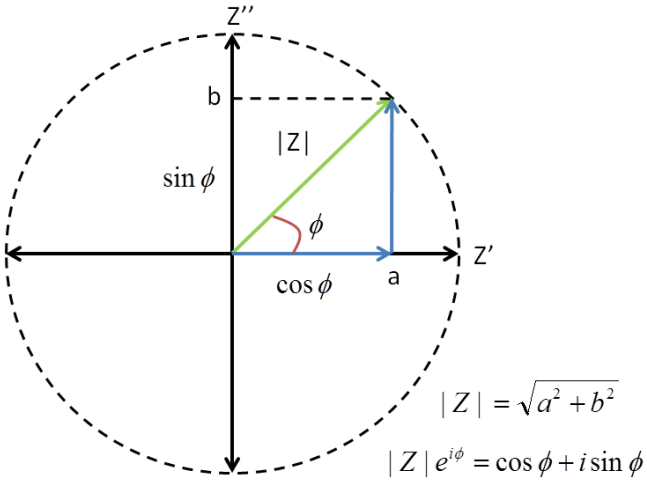

Figure 3.8: Argand diagram which defines the complex impedance notation.

$$Z'' = \frac{V}{I} sin\phi \tag{3.13}$$

therefore, by applying an alternating voltage across the electrodes and measuring the resulting current along with the phase difference between them, both the real and imaginary impedance can be determined. An AC voltage has the form;

$$\nu_R(t) = V_R sin(\omega t) \tag{3.14}$$

where ω is the angular frequency of the input voltage ν_R with magnitude V_R. The impedance contribution given from a resistor can be expressed in the form:

$$Z_{Resistor} = \frac{\nu_R(t)}{i_R(t)} = \frac{V_R sin(\omega t)}{I_R sin(\omega t)} = R_b \tag{3.15}$$

where i_R is the current through a resistor with magnitude I_R. Equation 3.15 shows that a ratio of the AC voltage and current is the resistance as the voltage and current are in phase when passing through a resistor. The alternating current flowing through a capacitor (i_C) has the form:

$$i_C(t) = C\frac{d\nu_C(t)}{dt} \tag{3.16}$$

where ν_C is the voltage through a capacitor with capacitance C. The impedance contribution from a capacitor is given by:

$$Z_{capacitor} = \frac{\nu_C(t)}{i_C(t)} = \frac{V_C sin(\omega t)}{C\omega V_C cos(\omega t)} \tag{3.17}$$

where V_C and I_C are the magnitude of the voltage and current through the resistor, respectively. Equation 3.17 can be simplified to give;

$$Z_{capacitor} = \frac{V_C sin(\omega t)}{C\omega V_C sin(\omega t + \pi/2)} = \frac{-i}{\omega C} \tag{3.18}$$

therefore the $Z_{capacitor}$ solely contributes to the imaginary part of the impedance.

From equations 3.15 and 3.18, it is now possible to calculate the impedance contribution of the conductivity cell. There are two factors contributing to the total impedance; the impedance from the electrolyte which consists of a parallel resistor-capacitor circuit which is in series with the capacitance from the electrodes in the form of a double layer. The total conductivity cell impedance can be given as the sum of these two factors:

$$Z_{cell} = Z_{electrolyte} + Z_{electrodes} \tag{3.19}$$

The impedance contribution from the sample ($Z_{electrolyte}$), will be considered first, which consists of a resistance and capacitance in parallel shown in figure 3.7. When impedances are in parallel to each other, the total impedance $Z_{electrolyte}$ is given by:

$$\frac{1}{Z_{electrolyte}} = \frac{1}{Z_{R_s}} + \frac{1}{Z_{C_s}} \tag{3.20}$$

therefore by using equations 3.15 and 3.18, equation 3.20 can be rewritten as:

$$\frac{1}{Z_{electrolyte}} = \frac{1}{R_s} - \frac{\omega C_s}{i} \tag{3.21}$$

which can be rearranged in the form of equation 3.22.

$$Z_{electrolyte} = \left[\frac{R_b}{1 + (\omega C_s R_b)^2}\right] - i\left[\frac{\omega C_s R_b^2}{1 + (\omega C_s R_b)^2}\right] \tag{3.22}$$

The impedance contribution from the electrodes is solely due to a double layer capacitance and is given by:

$$Z_{electrodes} = \frac{-i}{\omega C_{dl}} \tag{3.23}$$

which arises from the contribution from the double layer formed at the electrodes. The total impedance of the sample cell used here is given by:

$$Z_{cell} = \left[\frac{R_b}{1 + (\omega C_s R_b)^2}\right] - i\left[\frac{\omega C_s R_b^2}{1 + (\omega C_s R_b)^2} + \frac{1}{\omega C_{dl}}\right] \tag{3.24}$$

however, since $1/\omega C_s >> R_b$ the impedance can be simplified to be;

$$Z_{cell} \approx R_b - \frac{-i}{\omega C_{dl}} \tag{3.25}$$

therefore, the real part of the impedance is approximately the bulk resistance of the sample and the total impedance is equal to the bulk resistance when $Z'' = 0\,\Omega$. The impedance at this point will be used along with equation 3.10 to determine the value of the conductivity [88].

Using typical values for C_s, R_b and C_{dl} along with equation 3.24 it is possible to calculate the real and imaginary impedances at various frequencies, the resulting values of which are shown in figure 3.9. From figure 3.9 it can be seen that at high frequencies (left hand side) there is a semi-circle and at low frequencies there is a vertical linear line. At high frequencies the double layer capacitance tends to zero as the ions do not have the opportunity to form the layer. The high frequency semi-circle is characteristic of a parallel resistor-capacitor (RC) circuit which represents the sample capacitance (C_s) and resistance (R_b). The peak of the semi-circle should

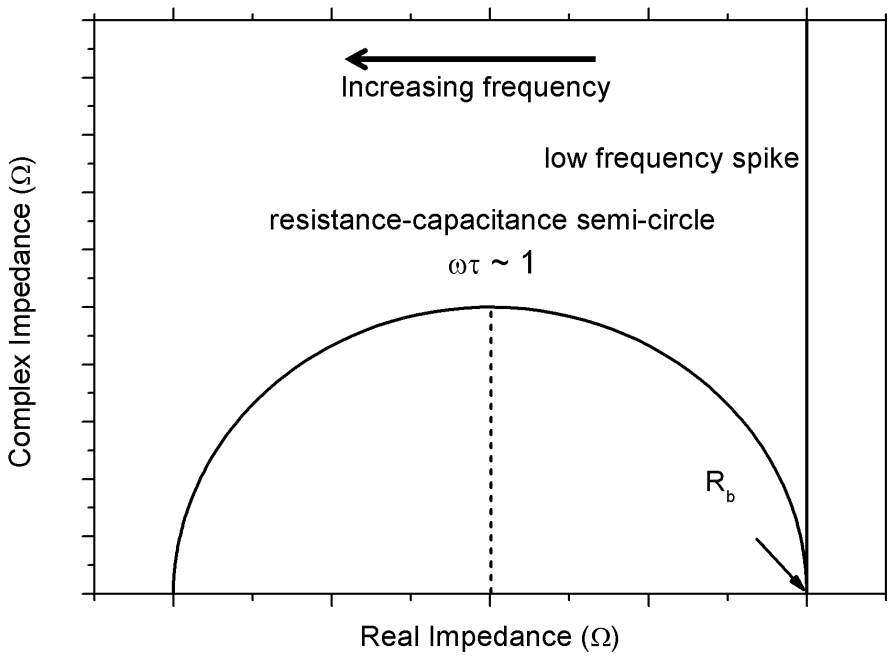

Figure 3.9: Theoretical Cole-Cole plot for sample cell used in this research.

theoretically appear at $\omega R_b C_s \approx 1$, i.e. when the time constant (τ) is equal to the frequency. The time constant of an RC circuit is defined as the capacitance times by the resistance ($\tau = R_b C_s$) and is defined as the time required to charge the capacitor through the resistor.

At low frequencies the double layer begins to become a factor which causes the vertical line in figure 3.9. Since the double layer capacitance does not have a resistance associated with it there is no real component as described by equation 3.17, therefore the imaginary part increases and the real part is constant. The position of the vertical line is determined by the sample and is situated at the end of the semi-circle and is by definition the bulk resistance of the sample (R_b).

The liquid and polymer gel electrolytes exhibit conductivities of the order of 1 mS cm^{-1}, which is relatively high, for this reason $Z'' = 0\,\Omega$ will occur at frequencies no lower than 10^5 Hz, thereby suggesting that there is no benefit to measuring at very low frequencies. When the imaginary part of the impedance is zero, the real part is equal to the bulk resistance which is needed in order to calculate the conductivity from equation 3.10. Therefore, the value of impedance taken is when the imaginary impedance is zero ($Z'' = 0\,\Omega$), this can easily be identified via a Cole-Cole plot (or Argand diagram) an example of which is shown in figure 3.9.

3.2.3 Polymer Gel Electrolytes

The mounting of the gels needed to be carried out differently to that of the liquids as it cannot simply be pipetted into the cell. One method consisted of the gel being cut into shape and then heated in the cell so that the gel melts. This caused the gel to fill the cell and give good contact between the electrodes. However, the difficulty here was that the solvent can be boiled off which will change the composition of the gel, so this mounting process needed to be carefully

monitored to ensure a significant amount of solvent was not lost.

An alternative, and improved method, was to pour the molten gel straight into the cell in the production stage and then place on the lid in order to make the gel cool into position. This method has been tried and tested and resulted in the least amount of solvent loss, making this the optimum method for accurately mounting the gels within the cell. This method was used in all gel conductivity measurements.

The geometry of the conductivity cell used here were (2.01±0.02) mm and (11.14±0.02) mm for the thickness and diameter of the circular cell, respectively. For the liquid electrolytes these geometrical factors did not change; however with the polymer gel electrolytes, the thickness was known to vary because of difficulty in mounting the sample due to an overlap of the gel out of the cell. Therefore, the thickness was measured for each PGE sample to ensure an accurate value of the thickness was used in the calculation of the ionic conductivity. The total thickness (t_{Total}) is given by;

$$t_{Total} = t_{Sample} + t_{Top} + t_{Base} \tag{3.26}$$

where t_{Sample}, t_{Base} and t_{Top} is the thickness of the sample, base electrode and the top $'penny'$ electrode. Equation 3.26 can be rearranged to determine the thickness of the sample;

$$t_{Sample} = t_{Total} - (t_{Top} + t_{Base}) \tag{3.27}$$

These thickness' are pictured in figure 3.4. By using equation 3.27, along with the constants t_{Top} and t_{Base} for each cell and the measured total thickness of the cell (t_{Total}) the sample thickness can be determined for each gel sample. It is crucial that the correct thickness is used as the conductivity is proportional to the thickness.

3.2.4 Calibration

The Novocontrol alpha-beta analyser has a built-in calibration sequence, consisting of a 'calibrate all', 'load-short' and 'low frequency' sequences. Here the 'calibrate all' and 'load-short' calibration sequences are used, the low frequency calibration is not needed as the measurements here only go down to 1 Hz and the sequence is designed for measurements below 1 Hz. The 'calibrate all' function calibrates the alpha-beta analyser and does not need to be performed regularly. The 'load-short' sequence is used to set the 'short' value which is when there is nothing between the electrodes and also a standard 100 Ω resistor is used to calibrate the 100 Ω. Before each conductivity measurement, a standard 100 Ω sample supplied from Novocontrol was measured in the frequency range of 1 Hz to 10^7 Hz. In the event that all frequencies displayed 100 Ω, the calibration was not employed.

3.2.5 Initial Measurements & Setup

It is crucial to understand what was being measured by the Novocontrol alpha beta analyser. The impedance as a function of frequency was measured for a PC/$LiBF_4$ (1.0M) liquid electrolyte sample; the frequency range covered for all conductivity measurements was 1 Hz-10 MHz. Using the conductivity cell discussed in section 3.2.1, the expected Cole-Cole plot was a semi-circle at high frequencies, with a low frequency spike as shown in figure 3.9. The Cole-Cole plot for the PC/$LiBF_4$ (1.0M) liquid electrolyte sample is shown in figure 3.10 as a function of temperature.

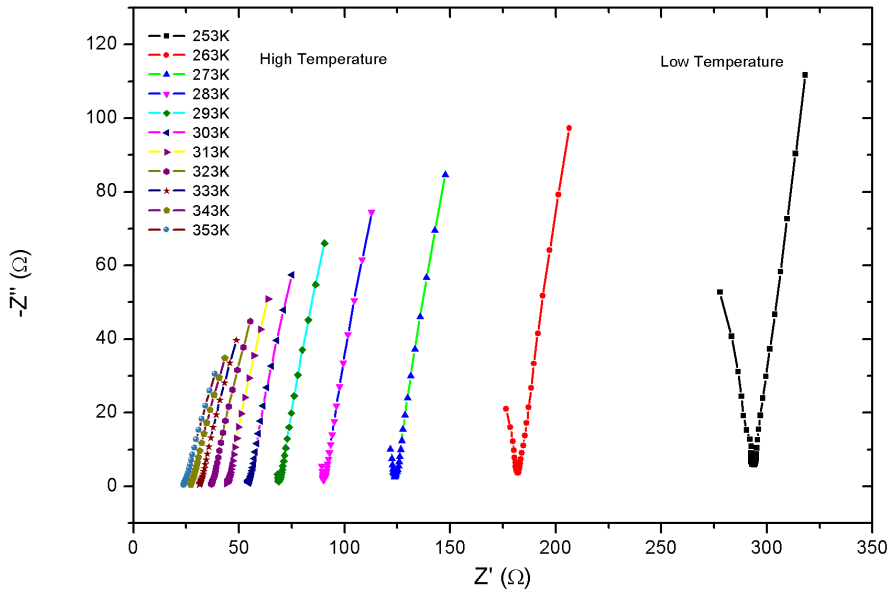

Figure 3.10: Cole-Cole plot (Argand diagram) for PC/$LiBF_4$ (1.0M) liquid electrolyte at various temperatures in the range 253 K-353 K.

The high frequency semi-circle was not observed in figure 3.10, this was attributed to the highly conducting liquid electrolytes. The position of the semi-circle is dependent on the conductivity of the sample, for highly conducting samples the semi-circle would be shifted to higher frequencies. It was assumed that the semi-circle would be revealed at higher frequencies, however the analyser was not capable of measuring these frequencies. For all samples the $Z'' = 0\,\Omega$ point of the Cole-Cole plot was observed so the conductivity could be measured. A preliminary measurement of the ionic conductivity of a PC/$LiBF_4$ (1.0M) liquid electrolyte at 20 °C gave a value of (2.99±0.05) mS cm^{-1}. Comparing this value to one measured elsewhere for PC/$LiBF_4$ (≈1.0M) liquid electrolyte at 19.5 °C which gave 2.968 mS cm^{-1} [91]. Although there is a 0.5 °C difference between these measurements, the two values were extremely close. The value measured in this thesis was slightly higher (by 0.022 mS cm^{-1}), this was attributed to the slight temperature difference.

To check that the high frequency semi-circle was present, a low conductivity sample was used, which should shift the semi-circle to lower frequencies. Figure 3.11 shows a Cole-Cole plot for a sample of pure propylene carbonate. The semi-circle is now present and therefore satisfies that the analyser was measuring the correct data. The Novocontrol analyser has a maximum operational frequency of 10^7 Hz. The area of interest here is the point at which the imaginary impedance is zero as this is when the real impedance is equal to the bulk resistance of the sample needed for equation 3.10 along with the cell geometry. For all electrolyte samples $Z'' = 0\,\Omega$ occurred below the maximum operational frequency. It should be noted that the low frequency spike in figure 3.11 is not a vertical line as predicted in figure 3.9, but is linear with a positive gradient. In a real system ions in the sample will attract and gather at the electrodes at low frequencies causing a double layer capacitance, as predicted, however as subsequent ions travel toward the layered electrodes they will feel a reduced force. At some distance away from the

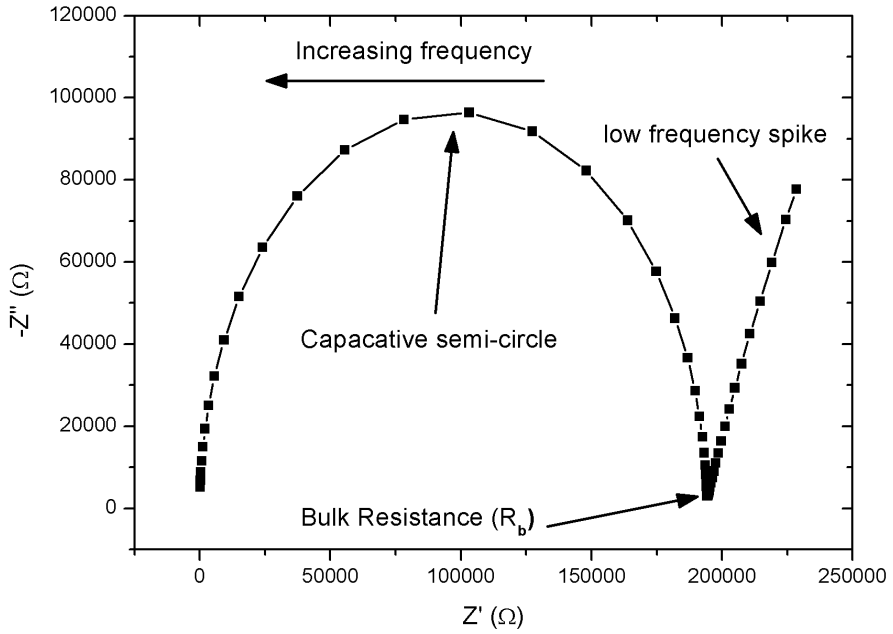

Figure 3.11: Cole-Cole plot for pure propylene carbonate at 273 K.

electrode the ions will diffuse, thus causing an additional real impedance term at low frequencies, resulting in a positive gradient, as the real impedance increases. At these low frequencies the real impedance due to the sample will be constant and the increase is due solely to the ions associated with the double layer and is therefore not of interest in this research.

The conductivity as a function of frequency for a PC/$LiBF_4$ (1.0M) liquid electrolyte at 293 K is shown in figure 3.12. At low frequency the conductivity is very low, almost non conducting, which was caused by the ions having the opportunity to gather at the electrodes and repel subsequent ions effectively reducing the conductivity. The conductivity starts to increase which can be seen in the mid range of frequencies in figure 3.12, suggesting that as the frequency was increased the effect of polarisation was reduced. At high frequencies the conductivity reaches a plateau, the conductivity is now completely out of the frequency range where polarisation is caused, and thus, is the true conductivity measurement. This frequency profile is dependent on the conductivity of the sample and for lower conducting samples the plateau will shift to lower frequencies as the ions translate more slowly and the time taken to reach the electrodes will increase, therefore polarisation will occur at a much slower rate.

3.3 Viscosity Measurements

The viscosity of a system is important to the understanding of the transport properties. It is a fundamental characteristic property of all liquids. The viscosity of a liquid is defined as the internal resistance to the flow of molecules and can be considered as a drag force on the motion of molecules. It plays a large role in the conductivity measurements especially with increasing salt concentration and temperature. It can also be related to the diffusion of the system which will be measured using the PFG-NMR method detailed in Chapter 2. The viscosity can be used

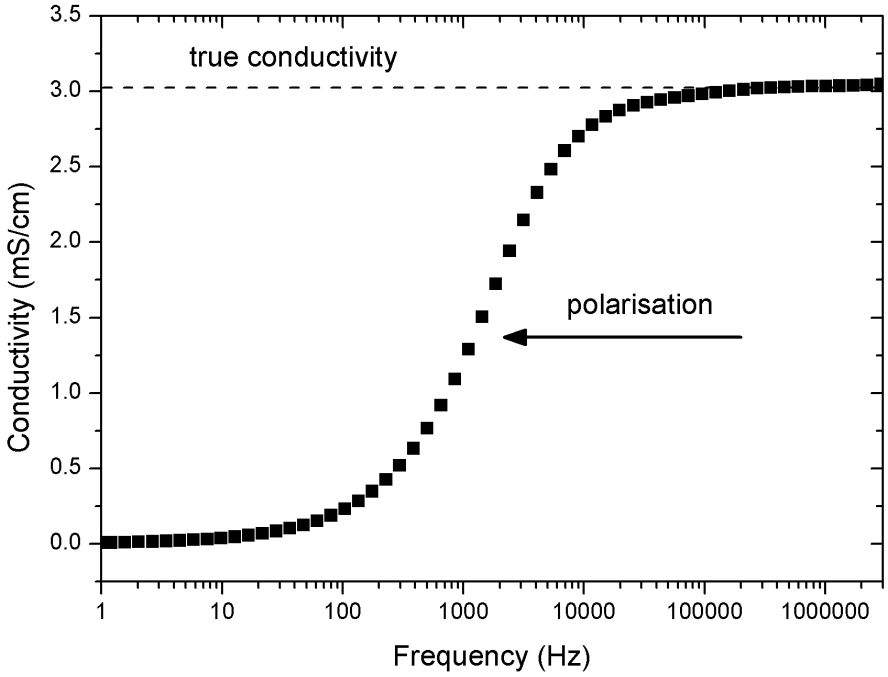

Figure 3.12: Conductivity frequency dependence for a PC/$LiBF_4$ (1.0M) liquid electrolyte at 293 K.

in the Stokes-Einstein equation along with the diffusion constants to determine the ionic radius of the diffusive species, this will be discussed in detail in Chapter 7.

The shear stress of a Newtonian fluid is given by;

$$\sigma_s = \eta \frac{d\nu}{dr} \tag{3.28}$$

where σ_s is the shear stress, η is the dynamic viscosity, ν is the velocity and r is an arbitrary distance away from the centre of the tube (shown in figure 3.13) [92]. A force balance equation of the cylindrical tube states that the change in pressure times by the area will be equal to stress times by the cross-sectional area which gives;

$$\sigma_s 2\pi r L = \Delta P \pi r^2 \tag{3.29}$$

where L is the length traveled through the cylindrical tube and ΔP is the pressure difference between the two ends. Now it is possible to substitute equation 3.28 into equation 3.29 which yields;

$$\frac{d\nu}{dr} = \frac{\Delta P}{2\eta L} r \tag{3.30}$$

It is assumed that the liquid is exhibiting laminar flow through the cylindrical tube which means that the velocity of the liquid increases towards the centre of the tube, with zero velocity at the outer boundaries. Therefore equation 3.30 can be integrated using the condition that $\nu(a)$=0, which gives;

$$\nu = \frac{\Delta P(a^2 - r^2)}{4\eta L} \tag{3.31}$$

The flow rate through the cylindrical tube can be determined by noting that, in a unit of time between the radii r and $r + dr$, the volume of the liquid flowing is given by $2\pi r\nu dr$ [92]. By integrating the volume over all space the volumetirc flow rate can be given by;

$$Q = \int_0^a 2\pi r\nu dr \tag{3.32}$$

where Q is the volumetric flow rate. If equation 3.31 is substituted into equation 3.32 and integrated the volumetric flow rate can be written as;

$$Q = \frac{V}{t} = \frac{\pi a^4 \Delta P}{8\eta L} \tag{3.33}$$

where t is the time taken for volume V to flow through the tube. Equation 3.33 is known as Pouiselle's equation, used to describe the laminar flow of liquids through a cylindrical tube.

The viscosity measurements carried out in this thesis used an Ostwald viscometer ($'U'\,tube$), vertically held in place so a fixed volume of liquid can be pumped around the tube and the descent back to equilibrium is monitored. Since the tube is vertical, the hydrostatic pressure difference is given as;

$$\Delta P = \rho g h \tag{3.34}$$

where ρ is the density of the liquid, g is the gravitational field strength and h is the height of the liquid. Therefore, the viscosity can be written as;

$$\eta = K\rho t \tag{3.35}$$

where K is a constant;

$$K = \frac{\pi g h a^4}{8LV} \tag{3.36}$$

Therefore if the liquid has a fixed length and volume then K is constant and there is no need to know the geometry of the Ostwald viscometer if a calibration liquid is used. Therefore by taking a ratio of the sample and calibrated viscosities gives;

$$\frac{\eta_{Sample}}{\eta_{Calibration}} = \frac{t_{Sample}\rho_{Sample}}{t_{Calibration}\rho_{Calibration}} \tag{3.37}$$

where this equation can therefore be used to measure viscosity without the geometric constants. However, a calibration liquid is required.

In this thesis, the calibration liquid used was pure PC as it is a well characterised solution. The viscosity was taken from a paper by Barthel [93] and the density of the pure PC was measured. Since the change in height is the driving force behind the displacement of the liquid in correspondence with potential energy, there must be a constant volume of liquid for all measurements. For the measurements taken in this research, a volume of 10 ml has been used, measured out using a 10 ml volumetric flask. There are some issues with using a simple Ostwald viscometer. As mentioned, the volume has to be kept constant, yet with these measurements it must be assumed that all samples measured have a similar change in density with temperature and thus a similar change in volume. Another issue with the Ostwald viscometer is that it needs to be kept as close to vertical as possible. This was achieved experimentally by clamping the viscometer in two places it keep the viscometer as steady as possible.

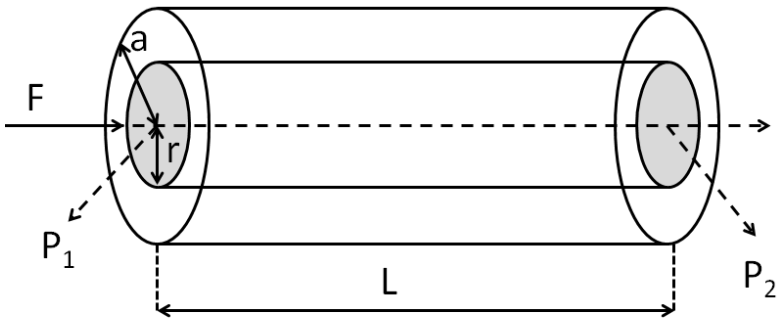

Figure 3.13: Derivation of Pouiseuille's equation, adapted from reference [92].

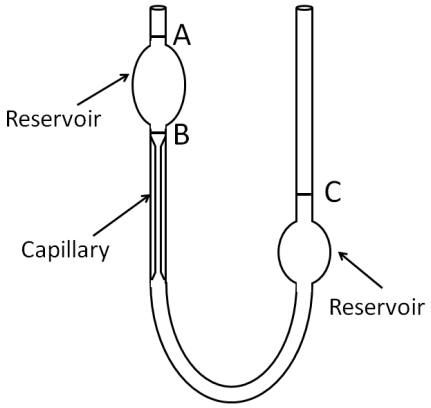

Figure 3.14: Schematic of Ostwald viscometer used in viscosity measurements.

The temperature of the sample was controlled via a water bath that was placed on a hotplate, operated by a thermocouple and Eurotherm temperature controller. This method produced an error of around 0.5 °C and was limited to temperatures between 20 °C and 60 °C. The limitations of the temperature were a result of using water as the method of heating as it is limited by the boiling point of water. An alternative method would have been to use an oil, however a reduced temperature range still yielded valuable information about the dynamics of the system. The temperature was monitored by two different thermocouples; one was placed at the top and bottom of the viscometer. The water was also stirred by a mechanical stirrer which was used to help circulate the water around the flask to obtain a constant temperature at all points in the sample.

The schematic of the Ostwald viscometer used is shown in figure 3.14. There are several markings on the Ostwald viscometer labeled A, B and C. The A and B markings indicate the volume over which the measurements should be timed in order to have a set length defined. The C marking was used as the total volume indicator, where at equilibrium the liquid should fall at this point in order to maintain a constant volume.

Chapter 4

Liquid Electrolyte NMR

4.1 Introduction

In this chapter the results of the NMR work carried out on the liquid electrolytes containing $LiBF_4$ will be reported and discussed. As discussed in Chapter 2, NMR is an excellent tool for investigating the transport properties of both liquids and solids. Measurements of the longitudinal (T_1) and transverse (T_2) relaxation times have been measured, as well as the self diffusion coefficients for the anion, cation and solvent. Due to the nature of NMR it is possible to use different frequencies (ω_0) in order to isolate a single nucleus as each element will exhibit a unique resonant frequency. Hydrogen (^{1}H), lithium (^{7}Li) and fluorine (^{19}F) nuclei have been used to detect the PC molecules, lithium ions and BF_4 anions, respectively.

Three spectrometers have been used in this research - a 50 MHz Maran bench top, a 400 MHz Bruker Avance II Ultrashield and a 500 MHz Bruker Avance. The measurements taken on each machine is self consistent and there are no overlap in measurements between machines, to ensure that no field affects are taken into consideration. Three spectrometers were used as there was a high demand for the machines and therefore to maximise the data that could be taken all three were used. The temperature limitations on the spectrometers were 253-333 K, 283-353 K and 293-353 K for the 50 MHz, 400 MHz and 500 MHz spectrometers, respectively. When using the lithium and fluorine resonant frequencies it was important to remember that these nuclei are only found in the salt and therefore at low salt concentrations the signal to noise ratio (SNR) decreases. It was found that the fluorine nuclei had a larger SNR than the corresponding lithium. The sensitivity of the NMR experiments is dictated by the populations between the different states discussed in Chapter 2. The population excess is dependent on the static magnetic field strength and the gyromagnetic ratio of the relevant nuclei. The fluorine and lithium gyromagnetic ratios are 103.962(10^6 rad s^{-1} T^{-1}) and 251.662(10^6 rad s^{-1} T^{-1}), therefore the fluorine exhibits a larger SNR due to the larger gyromagnetic ratio. It was observed that the fluorine measurements could measure in the range of 0.1-1.5 M whereas the lithium could measure 0.3-1.5 M. Since the vast majority of the sample was propylene carbonate which contains 6 hydrogen ions per molecule the SNR for hydrogen was strong for every sample and had no limitations and therefore the operational range was between 0.1-1.5 M.

4.2 NMR Relaxation Times

4.2.1 Low Field Hydrogen Longitudinal Relaxation

The low field 50 MHz Maran bench top NMR spectrometer was used to measure the longitudinal and transverse relaxation times. The schematic of the magnet in Chapter 2 (figure 2.16) was for a larger spectrometer, however the main components are still present here. This machine is known as a 50 MHz spectrometer due to the resonant frequency of the ^{1}H nucleus being 50 MHz at this magnetic field. This machine does not have the multi-nuclear capability of measuring different nuclei and therefore only ^{1}H measurements were taken on this machine. This spectrometer can carry out longitudinal and transverse relaxation measurements as well as standard free induction decay (FID) and solid echoes.

The spectrometer has a maximum sample diameter of 10 mm, therefore samples were placed in glass tubes of 10 mm diameter. Since it is important that no moisture is allowed to enter the samples as it could affect the results the samples were created in a nitrogen filled glove box and sealed inside the air tight glass tube inside the glove box. Each sample was made and measured within 24 hours to ensure that the sample did not degrade. It is important in NMR measurements to have sufficient sample in order to attain a good signal to noise ratio (SNR) however the sample should not be too large either as then it is possible to produce a temperature gradient in the sample. The height of the sample was around 2 cm which was judged by eye.

The temperature of the system was moderated using liquid nitrogen gas blown over the sample along with a heater controlled by a Eurotherm temperature controller. It was possible to reduce the temperature of the sample to around 223 K. Any lower than this was not achieved due to loss of gas to the surroundings. The lowest temperature used here in measurements was 253 K, which is significantly higher than the lowest possible. The highest temperature used was 353 K. This was chosen as a safe temperature to heat the spectrometer and sample without the risk of injury or damage to the spectrometer.

The spectrometer needed to be calibrated after each sample had been introduced to the magnetic field. This calibration involved matching and tuning the sample into the spectrometers magnetic field, as discussed in Chapter 2 in section 2.9. The receiver gain had to be set to ensure that the signal strength was not too high otherwise the signal can be 'clipped' and possibly distorted. These processes were carried out by the program incorporated on the computer used to control the spectrometer. The duration of the $\pi/2$ or 90^o pulse is well defined on this machine and did not need to be altered throughout the experiments, the value of was $\tau_{90} = 3.5\ \mu$s.

The pulse sequence that was used to measure the longitudinal relaxation time was the inversion recovery sequence. This sequence was described in Chapter 2 section 2.6.1 and consists of a π_x or 180^o_x pulse to invert the spin populations and then allow a time τ for the spins to relax along the z-direction. Then, a 90^o_y pulse is used in order to cause an FID which can be detected by the NMR spectrometer. The experiment is repeated multiple times with various values of τ where increasing this value increases the magnetisation in the +z-axis due to relaxation back to thermal equilibrium. The values of τ to be used were determined by carrying out a preliminary T_1 measurement and then set the maximum τ above the value of T_1.

With the inversion recovery pulse sequence it is essential to leave a certain amount of time after each value of τ as the magnetisation needs to have fully relaxed back to thermal equilibrium

	T_1(s)								
Temp. (K)	0.0 M	0.1 M	0.3 M	0.5 M	0.7 M	1.0 M	1.1 M	1.3 M	1.5 M
253	0.62	0.53	0.44	0.31	0.27	0.17	0.16	0.13	0.10
263	0.94	0.81	0.67	0.52	0.43	0.27	0.27	0.22	0.17
273	1.31	1.17	0.96	0.76	0.62	0.43	0.40	0.33	0.26
283	1.73	1.58	1.33	1.06	0.90	0.62	0.59	0.48	0.40
293	2.22	2.05	1.72	—	1.23	0.86	0.83	0.67	0.57
303	2.76	2.55	2.15	1.82	1.57	1.08	1.10	0.90	0.78
313	3.38	3.09	2.66	2.26	1.98	1.36	1.40	1.18	1.03
323	3.96	3.66	3.18	2.77	2.40	1.68	1.71	1.48	1.29
333	4.57	—	3.75	3.22	2.84	1.91	2.10	1.79	1.57

Table 4.1: ^{1}H Longitudinal relaxation times for PC/$LiBF_4$ (0.0-1.5 M) liquid electrolytes in temperatures range of 253-333 K.

before the next measurement starts. Not allowing the magnetisation to fully relax can cause an incomplete inversion of the populations and therefore result in an incorrect value of T_1. The time between successive experiments is known as the recycle delay and was set to be $5T_1$, this allows more time than required to reach thermal equilibrium. When taking these measurements it is possible to take different numbers of scans, which refers to the number of times an experiment is repeated i.e. same value of τ used multiple times and then the signals are added together. As standard 8 scans per point were used which seemed sufficient to get reliable data. For a few of the samples, 16 scans were employed resulting in the same value of T_1 to within <1%.

From figure 2.7 in Chapter 2 it can be seen that the value of T_1 undergoes a transition with both temperature and correlation time (τ_c) in the form of a minimum. It is important to understand which regime that this system is a part of in order to understand the dynamics of the molecules. The temperature dependence of the longitudinal relaxation will either exhibit a decrease in T_1 with temperature or an increase depending which side of the minimum the system falls. It is also possible to observe the T_1 minimum when increasing temperature if the system is close to the transition point. This minimum occurs when $\omega_0\tau_c \approx 1$, where ω_0 is the Larmor frequency and for the ^{1}H at this magnetic field strength $\omega_0 = 50$ MHz. Therefore if the value of the correlation time is of the order of $\tau_c \approx 10^{-7}$ s then one would expect to observe the T_1 minimum.

The longitudinal relaxation times for the liquid electrolytes containing PC/$LiBF_4$ using ^{1}H nucleus can be seen in table 4.1. All salt concentrations exhibited the same temperature dependence and were seen to increase with increasing temperature. This temperature trend would suggest that the liquid electrolytes are on the low correlation (high temperature) side of the T_1 minimum, meaning that $\omega_0\tau_c << 1$. This region of the minimum is reserved usually for small molecules in non-viscous liquids; it is therefore reasonable that the liquid electrolytes are in this regime. This means that the molecules are in the tumbling (extreme narrowing) regime as discussed in Chapter 2.

	T_2(s)								
Temp.(K)	0.0 M	0.1 M	0.3 M	0.5 M	0.7 M	1.0 M	1.1 M	1.3 M	1.5 M
253	0.60	0.46	0.37	0.29	0.23	0.15	0.14	0.10	0.08
263	0.71	0.75	0.58	0.44	0.36	0.26	0.24	0.19	0.14
273	1.22	1.12	0.93	0.70	0.60	0.36	0.39	0.31	0.24
283	1.65	1.52	1.26	1.02	0.85	0.60	0.57	0.46	0.37
293	2.12	1.97	1.67	—	1.18	0.83	0.79	0.64	0.53
303	2.61	2.31	2.10	1.66	1.51	1.06	1.05	0.86	0.73
313	3.10	2.79	2.56	1.92	1.88	1.32	1.33	1.11	0.95
323	3.61	3.29	3.03	1.81	2.25	1.60	1.64	1.38	1.21
333	4.27	—	3.54	2.01	2.66	1.85	1.94	1.69	1.47

Table 4.2: ^{1}H Transverse relaxation times for PC/$LiBF_4$ (0.0-1.5 M) liquid electrolytes in temperatures range of 253-333 K.

4.2.2 Low Field Hydrogen Transverse Relaxation

The transverse relaxation times were measured using a standard Carr-Purcell-Meiboom-Gill (CPMG) sequence as discussed in Chapter 2. This sequence involves using an initial excitation pulse ($\pi/2_x$ or 90^o_x) to perturb the spins into the xy plane, where they will undergo relaxation in the form of the spins losing phase as the spins precess at different frequencies. After a time τ an inversion pulse was used in to flip the spins, leaving the faster spins behind the slower spins allowing them to catch up (or re-focus) after a further time τ, known as a spin echo. Spin echoes are used in order to remove the reversible process of the field inhomogeneity.

For this sequence the number of echoes and the time τ needs to be defined. These two values are obviously responsible for the total experimental time as the total time can be given by;

$$t_{Total} = \tau_{\pi/2} + n_{echoes}\,(2\tau + \tau_\pi) \tag{4.1}$$

where n_{echoes} is the number of echoes and $\tau_{\pi/2}$ and τ_π are the durations of the $\pi/2$ and π pulses respectively. Therefore these values need to set such that the signal does not decay too quickly or too slowly. If the value of τ was set too high then the signal would decay too quickly and would prove difficult to analyse.

The transverse relaxation times for PC/$LiBF_4$ (0.0 M, 1.0 M and 1.5 M) liquid electrolytes are shown in table 4.2 for the ^{1}H nucleus. The values of the transverse relaxation times are very close to the longitudinal relaxation times. This agrees with the hypothesis that the system is in the low correlation time (high temperature) side of the T_1 minimum as the two relaxation times converge at low correlation times. This is due to the tumbling regime which dominates both relaxations and therefore they relax at a very similar rate. In the tumbling regime $T_1 \geq T_2$ as the longitudinal relaxation is caused by the transverse relaxation. An example of this relation can be observed if values from table 4.1 and 4.2 are extracted, for example at a salt concentration of 1.0M $LiBF_4$ at a temperature of 253 K were 0.17 s and 0.15 s for T_1 and T_2, respectively. At the same concentration at a temperature of 333 K, the values were 1.91 s and 1.85 s for T_1 and T_2, respectively. At the two temperature extremes the relaxation values are comparable and the dynamics can be attributed to tumbling.

A problem in measuring the transverse relaxation time occurred due to the increase of T_2 with temperature, which then required an increase of either the value of n_{echoes} or τ to be increased to accommodate the difference. Initially as T_2 increased with temperature the value of n_{echoes} was left constant and the value of τ was increased. At high temperatures the trend with temperature was seen to change and the T_2 values started to decrease with increasing temperature which was unexpected. It was deduced that the cause of this anomaly was that the value of τ was set too large and between echoes relaxation was occurring which was effectively reducing the resulting signal. Therefore the value of τ was not allowed above 1500 μs and the number of echoes was increased instead.

4.2.3 Low Field Relaxation Temperature Dependence

Tables 4.1 and 4.2 show that the T_1 and T_2 values increase with temperature, however it is possible to further categorise the temperature dependence. If the data follows a simple exponential then it is considered Arrhenius and in the form of;

$$T_1 = A_{T_1} exp\left[\frac{E_{T_1}}{RT}\right] \tag{4.2}$$

where A_{T_1} is the pre-exponential factor and E_{T_1} is the activation energy of the longitudinal relaxation. Similarly the equation for the transverse relaxation can take the form;

$$T_2 = A_{T_2} exp\left[\frac{E_{T_2}}{RT}\right] \tag{4.3}$$

where E_{T_2} is the activation energy of the transverse relaxation and R is the universal gas constant which gives the activation energy in units of J mol^{-1}. Figure 4.1 shows both the natural log of the longitudinal and transverse relaxation times against $1000/T$. If the data is plotted in this manner and a linear fit can be employed then it can be said that the data has Arrhenius type behaviour, however if the data is non-linear then it is more likely described by the Vogel-Tamman-Fulcher (VTF) [94–96] temperature dependence.

Figure 4.1 has both a linear (dashed line) and a non-linear (solid fits) applied to the data, in order to test if the rate of relaxation is Arrhenius or non-Arrhenius. The Arrhenius equation was initially used to describe the rates of chemical reactions, which brought about the concept of an activation energy which in its original case was the energy required for the reaction to occur. When liquids are high above their glass transition temperature (T_g) they tend to exhibit Arrhenius type behaviour and at lower temperatures start to deviate from this behaviour due to reduced mobility of the ions. It can be seen that the non-linear fit in figure 4.1 was better than the linear fit, which suggests that the rate of relaxation cannot be described by the simple case represented in equations 4.2 and 4.3. Therefore the T_1 and T_2 data will be fitted using the Vogel-Tamman-Fulcher (VTF)[94–96] equation of the form;

$$T_1 = A_{T_1} exp\left[\frac{B_{T_1}}{R\left(T - T_0\right)}\right] \tag{4.4}$$

and

$$T_2 = A_{T_2} exp\left[\frac{B_{T_2}}{R\left(T - T_0\right)}\right] \tag{4.5}$$

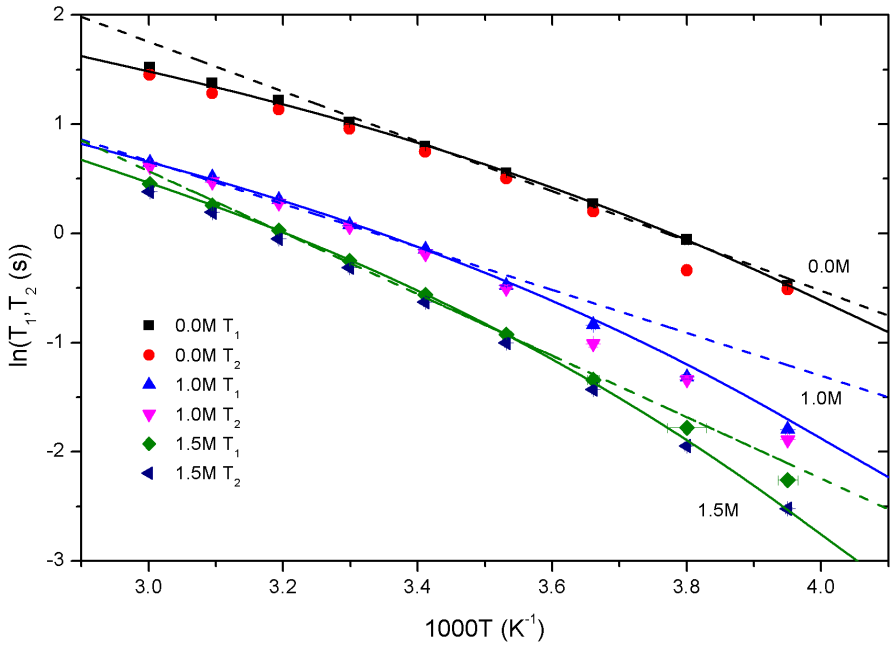

Figure 4.1: ^{1}H Arrhenius plot of T_1 and T_2 for PC/$LiBF_4$ (0.0 M, 1.0 M and 1.5 M). Both linear (dashed fits) and non-linear (solid) fits have been employed.

where T is the absolute temperature of the system, B_{T_1} is a temperature dependent energy term, as opposed to E_{T_1} which describes a physical energy barrier that must be overcome and is constant at all temperatures and T_0 is the ideal glass transition temperature and is usually related to the glass transition temperature T_g by $T_0 \cong T_g - 50$.

Initially, the T_1 and T_2 data were fitted to equations 4.4 and 4.5 respectively and the resulting T_0 values from this fitting were found to have no trend with salt concentration. Therefore an average value of T_0 was taken for both the T_1 and T_2 data and refit with equations 4.4 and 4.5 again, this time holding T_0 constant and allowing the other parameters to be freely fitted. The average T_0 values were found to be 147 K and 157 K for the T_1 and T_2 data, respectively. Figure 4.2 shows the activation energies, E_{T_1} and E_{T_2} of the data, the T_2 data was fitted with holding T_0 to both 147 K and also 157 K, to compare the activation energies. It can be seen from figure 4.2 that the activation energies of T_1 and T_2 data when fixed to an ideal glass transition temperature of 147 K were very similar. This was expected as in this regime the longitudinal and transverse relaxation times are comparable. The activation energy is a quantity which refers to the activation of a certain mechanism, in this case the relaxation of the spins. The activation energies were observed to increase with salt concentration for both the longitudinal and transverse relaxation times. This was attributed to an increase of the viscosity thus making it more difficult for the molecules to translate, therefore requiring more energy to activate the relaxation.

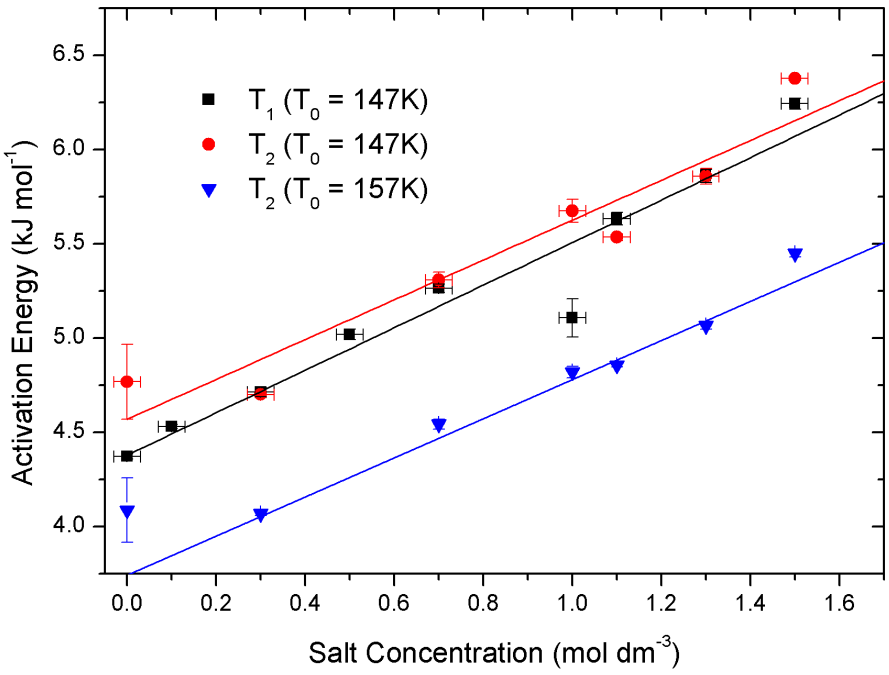

Figure 4.2: ^1H activation energies from T_1 VTF fits with $T_0 = 147$ K and T_2 with both $T_0 = 147$ K and $T_0 = 157$ K for PC/$LiBF_4$ liquid electrolytes.

4.2.4 High Field Hydrogen Longitudinal Relaxation

The 500 MHz Bruker Avance Ultra Shield spectrometer has been used to measure the high field hydrogen longitudinal relaxation times of the liquid electrolytes. The previously discussed low field T_1 measurements did not have the capability to separate the individual peaks corresponding to the different hydrogen sites of the propylene carbonate molecule. The hydrogen nucleus has been used here in order to understand the role of the solvent molecules within the liquid electrolytes. The propylene carbonate structure has 6 protons per molecule and contains a C-H, C-H_2 and C-H_3 bond. The use of a high field in an NMR spectrometer allows the separation of these sites which are identifiable. The NMR spectrum shown in figure 4.3 exhibits four clearly defined peaks which have been labeled 1-4 in order of their ppm (parts per million) values. The inset of figure 4.3 shows a ball and stick model of a propylene carbonate molecule. The intensity of peaks 1-3 were, due to the fact that there was one hydrogen atom per peak as the first peak was due to the lone C-H bond, with peaks 2 and 3 resulting from the C-H_2 bond where the position of each peak was different allowing separation. Peak 4 was seen to exhibit a much larger intensity than the other peaks, due to the C-H_3 methyl group which protrudes from the ring, as this peak contains three hydrogen atoms it is reasonable to assume this is the cause for the increased intensity.

The inversion and saturation recovery pulse sequences were both used, as described in Chapter 2. The inversion recovery uses an initial inversion pulse (π or 180^o) to invert the spin populations which will then start to relax back to thermal equilibrium, after a time τ a 'read' pulse ($\pi/2$) will be applied to move the magnetisation into the measurable xy plane. The satu-

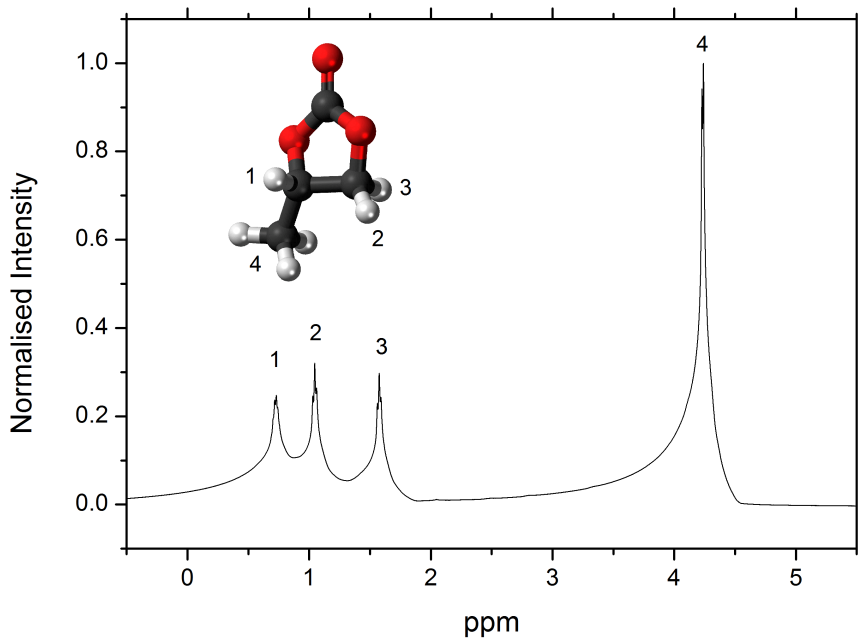

Figure 4.3: ^{1}H NMR spectrum for a PC/$LiBF_4$ (1.0 M) liquid electrolytes at 303 K. Inset shows the structure of propylene carbonate structure.

ration pulse sequence involves applying multiple $\pi/2$ pulses to the system in order to scramble the magnetisation so there is no net magnetisation in any direction. After a time τ the magnetisation will have relaxed back at which point a 'read' pulse is used again to measure the magnetisation. If setup correctly, these two pulse sequences should yield the same result. Since the saturation recovery sequence applies the multiple $\pi/2$ pulses at the beginning of each measurement there is no need to wait the time for the recycle delay (RD), so it was set as 1 second as standard. Both sequences were initially used for each sample at each temperature to ensure that there was no discrepancy between using the two sequences. The difference between the two sequences was nominal and therefore the data reported in this section are from saturation recovery measurements.

For each nucleus the pulse durations have to be determined in order to produce accurate $\pi/2$ and π pulses, otherwise the measurements would be incorrect. It was possible by using the software to have the machine run a continuous spectrum, allowing the user to change parameters and observe the effect on the spectrum in real time. If the pulse duration τ_{90} was altered until there was a maximum in magnetisation, the value would correspond to a $\pi/2$ pulse and by definition $2\tau_{90} = \tau_{180}$. However, the Topspin 1.3 software contained a sequence called 'popt' which is a parameter optimisation sequence. It was possible to tell the software to use different τ_{90} values and measure the resulting spectrum intensity. The expected outcome of this would be a sine wave with the maximum being the true value of τ_{90} and the points with zero magnetisation being τ_{180}. The software is told to search for a minimum i.e. the duration of the π pulse; this value was then halved in order to determine the duration of the $\pi/2$ pulse. The duration of the pulse was also proportional to the power of the RF pulse applied. The power level had a maximum value of -6 dB, the power used here was -3 dB, for this power level the pulse duration

	T_1 (s)											
	0.0 M				0.7 M				1.5 M			
Temp (K)	1	2	3	4	1	2	3	4	1	2	3	4
303	5.20	3.62	3.37	2.58	3.12	2.19	2.14	1.77	2.55	1.51	1.47	1.29
313	6.15	4.24	4.10	3.09	3.92	2.67	2.55	2.42	2.81	1.64	1.60	1.54
323	7.52	5.25	4.95	3.74	4.74	3.22	3.10	2.75	3.44	2.00	1.97	1.90
333	8.31	5.93	5.60	4.29	5.50	3.68	3.52	3.39	4.06	2.40	2.26	2.25
343	9.44	6.89	6.41	4.98	6.49	4.39	4.26	3.82	4.74	2.86	2.64	2.72
353	10.61	7.87	7.52	5.89	7.53	5.24	5.11	4.43	5.63	3.35	3.30	3.25

Table 4.3: Longitudinal relaxation times for individual peaks numbered 1-4 of the NMR spectrum for PC/$LiBF_4$ (0.0 M, 0.7 M and 1.5 M) liquid electrolytes using ^{1}H nucleus.

was $\tau_{90} = 9.82\,\mu$s.

Table 4.3 shows the longitudinal relaxation times with each of the four peaks listed individually and denoted 1-4. The data was measured and analysed using the Bruker Topspin 1.3 software, much the same as for the 400 MHz spectrometer. The Bruker Topspin 1.3 software used a least squares fit sequence based on the Levenberg Marquardt algorithm [78; 79]. For each experiment, 8 scans were performed meaning that for each point on the T_1 recovery curve the FID was repeated 8 times and added together. Each temperature was measured a minimum of three times and an average was taken of repeat readings.

For a spin 1/2 nucleus such as hydrogen the most significant relaxation mechanism is due to dipole-dipole interactions. This can be further subcategorised into homonuclear and heteronuclear which involve interaction between two hydrogen atoms and two different atoms, respectively. It should also be noted that the relaxation can consist of either intramolecular (inside the molecule) or intermolecular (between neighbouring molecules) interactions. In this chapter there will be some discussion into the relevant contributions from translational motion and rotational motion. In the intramolecular case it is impossible for there to exist a translational component to the relaxation as all of the atoms are moving together on a single molecule and therefore the relative distances do not change and therefore do not cause relaxation. However, it is possible for the atoms to rotate, therefore creating a rotational contribution to the relaxation due to intramolecular interactions. The intermolecular interactions can be both translational and rotational as the atoms can relax as they pass neighbouring atoms in solution. Table 4.3 shows the longitudinal relaxation times for three different salt concentrations at various temperatures. Since the spectra could be resolved into four different peaks, four values of T_1 were determined. It was observed that the four different T_1 values had varying values. Taking for example the unsalted PC from table 4.3, the T_1 values were 5.20 s, 3.62 s, 3.37 sand 2.58 s for peaks 1-4, respectively. Since all four peaks arise from various sites on the PC molecule it is assumed that on average the contribution from the intermolecular translational interactions are roughly equal for each site. Therefore presumably there is some difference in rotational motion for each site. As previously stated there are two types of rotational effects that can cause relaxation intramolecular and intermolecular. The intramolecular interaction concerns the internal rotational motion of the molecule, whereas the intermolecular interaction is due to the rotation

	Activation energy (kJ mol^{-1})			
Salt Concentration (M)	Peak 1	Peak 2	Peak 3	Peak 4
0.0	12.64	13.91	13.95	14.48
0.3	11.18	12.56	12.91	12.80
0.5	14.87	14.90	15.57	15.53
0.7	11.94	15.24	15.28	15.70
1.0	15.45	12.48	12.55	14.55
1.3	15.39	16.06	16.12	17.39
1.5	15.66	16.43	16.07	17.01

Table 4.4: Activation energy for longitudinal relaxation times for individual peaks numbered 1-4 of the NMR spectrum for PC/$LiBF_4$ liquid electrolytes using ^{1}H nucleus.

of the entire molecule within which the atoms reside. Since each ^{1}H site of the PC molecule has a different inter-nuclear distance, as the PC molecules rotate each atom can feel a different interaction, this is known as anisotropic molecular reorientation. For example the C-CH_3 methyl bond protrudes much more significantly than the others and would therefore observe a different interaction when undergoing molecular reorientation (rotation of the molecule). The varying T_1 values could also be due to intramolecular rotational interactions. The internal rotations of the PC molecule are related to the inter-nuclear distance. In fact the relaxation due to rotation in this way is highly dependent on this distance, which will be discussed more in section 4.5.1 of this chapter. This difference in inter-atomic separation is most likely the cause of the different T_1 values obtained for the various sites of the PC molecule.

The methyl group is well known to display rapid internal rotation; however this would have the effect of increasing the longitudinal relaxation time due to the spin-rotation relaxation mechanism discussed in Chapter 2. Since the T_1 relating to the methyl group is the shortest relaxation time it can be assumed that this rapid internal rotation is not a significant effect of the relaxation. It should be noted that for the duration of this chapter the term 'translational' motion with regards to relaxation refers to the intermolecular translational effect and that 'rotational' motion refers to a combination of internal rotation (intramolecular) and rotation of the molecules (intermolecular).

The temperature dependence of the longitudinal relaxation has been observed. The NMR spectrometers sample temperature was controlled by a flow of compressed air which at equilibrium produced a sample temperature of around 298 K, therefore the lowest temperature that was possible here was 303 K. The highest temperature used was 353 K which was selected to match the data previously taken.

Figure 4.4 shows an Arrhenius plot for a PC/$LiBF_4$ (0.5 M) liquid electrolyte using the ^{1}H nucleus for the four separate peaks of the NMR spectrum. Linear fits have been applied to the data in figure 4.4 and are shown to fit the data well, suggesting that the temperature dependence is Arrhenius. The activation energy of each peak can be determined by using the gradient of the linear fits in figure 4.4 and multiplying by the universal gas constant R.

Activation energies of the longitudinal relaxation times for the individual peaks denoted 1-4 are shown in table 4.4. If the activation energies of the relaxation and diffusion are comparable

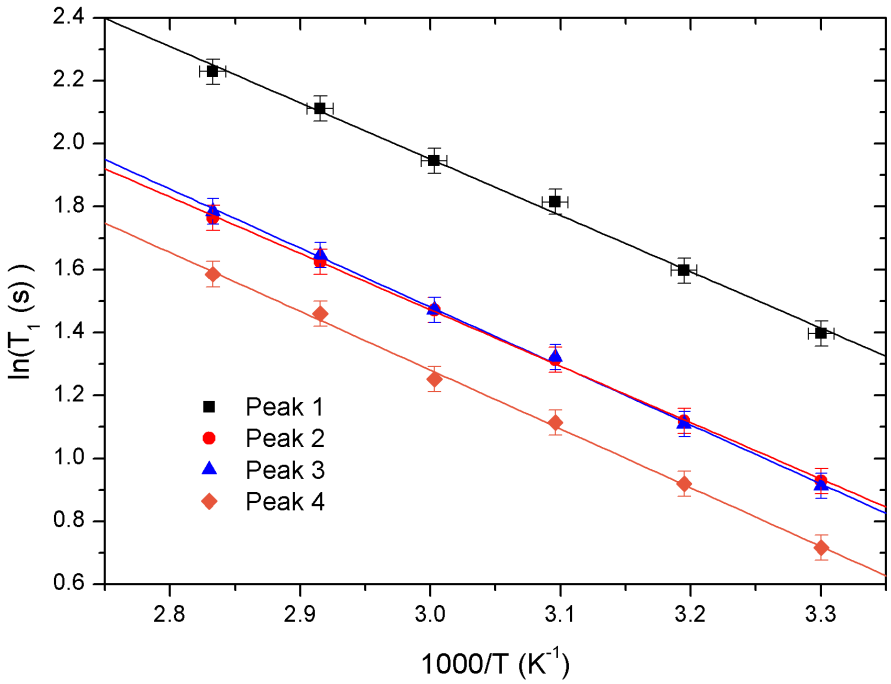

Figure 4.4: ^{1}H Arrhenius plot for longitudinal relaxation times for individual peaks numbered 1-4 of the NMR spectrum for PC/$LiBF_4$ (0.5 M) liquid electrolyte.

then it is reasonable to assume that the relaxation process is largely due to translational motion. The activation energies of the relaxation are always less than that of the diffusion activation energy; however, the values for the relaxation and diffusion are comparable suggesting that there was a strong translational component to the longitudinal relaxation. This will be investigated in more detail in section 4.4.

4.2.5 Lithium Longitudinal Relaxation

By using the multi-nuclear high field 400 MHz Bruker Avance II Ultrashield spectrometer it was possible to investigate the relaxation of different nuclei to detect different parts of the system. The Bruker spectrometer is also equipped with an x, y and z gradient system which is essential for imaging, however imaging was not measured in this research. Only the z gradient was used in order to measure the self diffusion of the molecules. The spectrometer is able to probe multiple nuclei by changing the coil on top of the Diff60 probe which has been supplied by Bruker and was used to measure longitudinal and transverse relaxation times as well as diffusion measurements.

The temperature of the sample was partially controlled via water cooling and also heated compressed air, using a built in heater in the diff60 probe. There were some issues with temperature gradients within the sample as the water cooling could only be raised to 313 K maximum and the samples were heated to a maximum of 353 K via air heating and therefore introduced possible temperature gradients. This led to possible contributions to the diffusion constant from correlated motion (convection). This was overcome by ensuring samples were of a small size, around 0.5 cm in height. The hydrogen coil had a bore of 5 mm and the lithium and fluorine

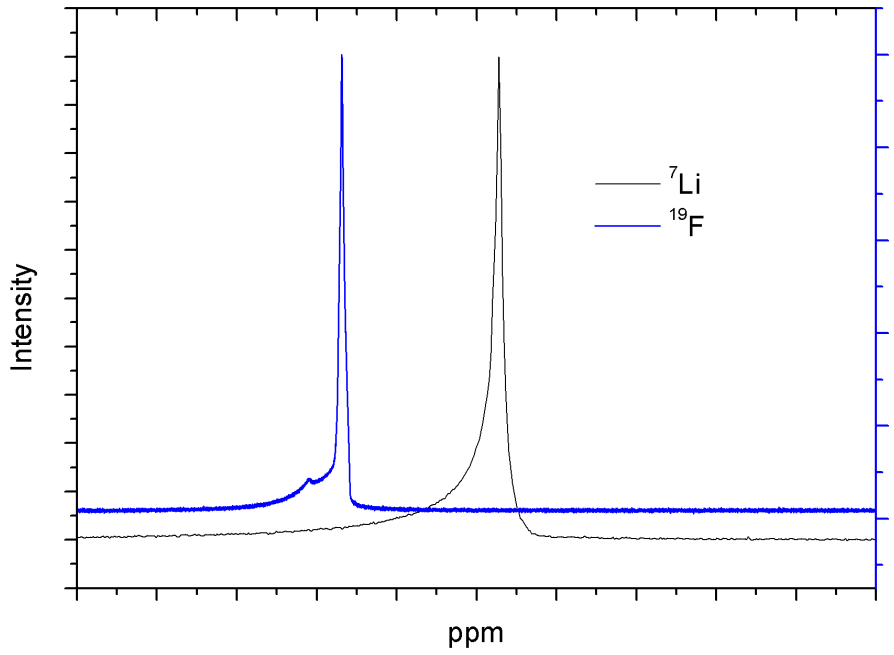

Figure 4.5: NMR spectra for ^{7}Li PC/$LiBF_4$ (1.0 M) and ^{19}F PC/$LiBF_4$ (0.7 M) liquid electrolyte at 303 K. Arbitrary chemical shift used.

coils had a bore of 10 mm, therefore two different sized glass tubes were used in order to fit inside the coil.

In section 4.2.4 the ^{1}H nucleus was used in order to track the solvent molecule in the system, however it is also of interest to investigate the behaviour of the salt ions, both cation and anion. The salt used was lithium tetrafluoroborate ($LiBF_4$) and therefore has a Li^+ cation and a BF_4^- anion, where the boron has four fluorine ions in a tetrahedral structure. By using the 400 MHz Bruker Avance II high field spectrometer it was possible to alter the nuclei by changing the receiver coil located at the top of the diff60 probe.

The spectrometer had to be set up to be able to measure the lithium resonant frequency. Firstly the hardware needed to be setup which involved using the correct amplifier and pre-amplifier connections to allow for the frequency of 155 MHz, the resonant frequency of lithium, to be used. Filters were used to ensure that minimal stray signal affected the spectrum. The Bruker Topspin1.5 software was used to tell the spectrometer that a ^{7}Li nucleus was being used which sets the resonant frequency of the nuclei. Once the sample was entered into the magnetic field it would first need to be 'wobbled' which refers to using the matching and tuning capacitors in order to tune the coil into the static magnetic field to ensure that the resonant frequency is set correctly. These capacitors needed to be altered by hand and tuned by eye with help from both the software and also the display on the pre-amplifier.

The pulse durations were determined in the same manner as for the 500 MHz spectrometer using the 'popt' sequence. As with the 500 MHz spectrometer the T_1 measurements were carried out using mainly the saturation recovery pulse sequence and a few inversion recovery measurements to test the validity of the saturation measurements. The spectrometer's control computer

	T_1(s)					
Temp. (K)	0.3 M	0.5 M	0.7 M	1.0 M	1.3 M	1.5 M
283	1.79	1.67	1.44	1.27	1.09	0.99
293	2.24	2.07	1.83	1.51	1.29	1.15
303	2.47	2.37	2.04	1.79	1.50	1.32
313	3.01	2.86	2.52	2.13	1.79	1.56
323	3.63	3.40	2.98	2.51	2.11	1.85
333	4.24	3.95	3.47	2.90	2.46	2.16
343	4.80	4.43	3.90	3.26	2.78	2.48
353	—	4.72	4.08	3.47	3.09	2.74

Table 4.5: ^{7}Li longitudinal relaxation times for PC/$LiBF_4$ (0.3-1.5 M) liquid electrolytes in temperatures range of 283-353 K.

ran Bruker Topspin 1.5, which is a later version of the software used on the 500MHz spectrometer, therefore the setup of the system was very similar to that explained for the 500 MHz spectrometer. The same parameters were also used, however a different magnetic field strength would result in different pulse durations. The duration that was used here was $\tau_{90} = 18.50\,\mu$s at a power level of 3 dB. Examples of typical spectra for lithium and fluorine PC/$LiBF_4$ liquid electrolytes are shown in figure 4.5. It can be observed that both the lithium and fluorine nuclei exhibited a single peak.

Table 4.5 shows the longitudinal relaxation times for the PC/$LiBF_4$ (0.3-1.5 M) liquid electrolytes using the lithium (^{7}Li) nucleus. The 0.3 M sample contained the lowest amount of $LiBF_4$ that could be used here as in order to obtain NMR data there needs to be a significant NMR signal which will clearly decrease as the number of lithium ions are reduced. A signal was still seen below 0.3 M, however the data was not reliable as the SNR was too low. The maximum salt concentration was chosen as the maximum amount of salt that can be confidently dissolved by the solvent while still being slightly away from saturation in order to ensure full miscibility. The trends with salt concentration and temperature are similar to the hydrogen (^{1}H) measurements taken on the low field Maran bench top NMR spectrometer. The value of T_1 was seen to increase with increasing temperature which is understood by observing the correlation time dependence of the longitudinal relaxation time in the fast tumbling regime the current system is located. Decreasing the correlation time increases the value of T_1 and since the temperature is inversely proportional to the correlation.

The temperature dependence for the lithium longitudinal relaxation times can be determined in the same manner as in section 4.2.4 regarding the hydrogen nucleus T_1 measurements. Figure 4.6 shows an Arrhenius plot for the PC/$LiBF_4$ (0.3 M, 1.0 M and 1.5 M) liquid electrolytes using the ^{7}Li nucleus. It can be seen that unlike the hydrogen nucleus the lithium longitudinal relaxation seems to exhibit Arrhenius type temperature dependence and therefore can be described by equation 4.2. The data taken for the hydrogen nucleus was taken on the bench top NMR spectrometer which allowed measurements at much lower temperatures than the high field spectrometer. The difference in temperature behaviour is attributed to the temperature range of the samples, as the temperature dependence tends to exhibit non-Arrhenius type behaviour once

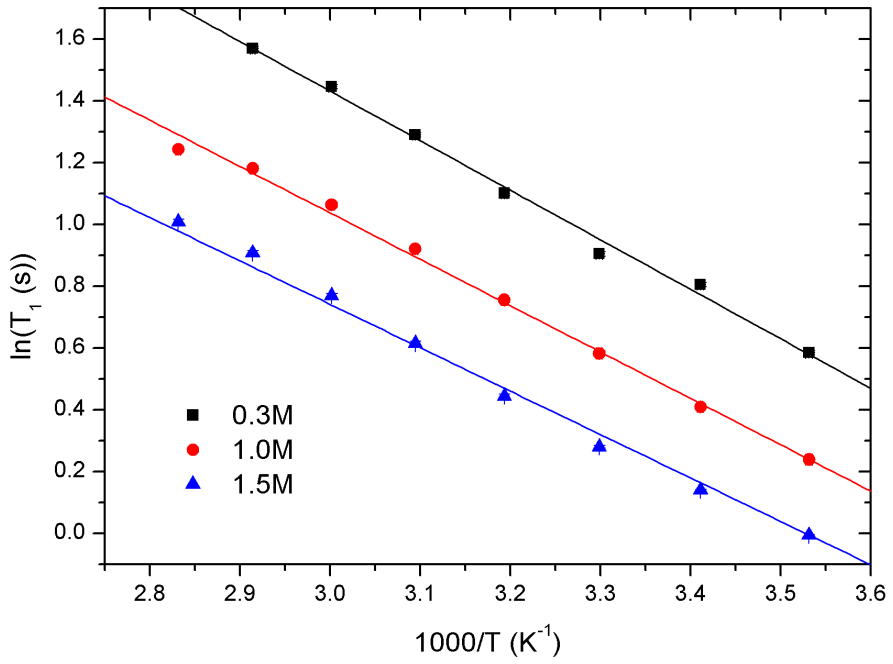

Figure 4.6: ^{7}Li T_1 Arrhenius plot for PC/$LiBF_4$ (0.3 M, 1.0 M and 1.5 M) liquid electrolytes.

they reach cold temperatures that are near their glass transition temperatures; i.e. when the system 'locks' up. The measurements here only go down as low as 283 K and therefore far from the glass transition temperature, so for this range of temperatures the dependence was assumed to be Arrhenius.

T_1 decreased with increasing salt concentration, a similar explanation can be employed as that used for the temperature dependence. As the salt concentration was increased the viscosity of the system will clearly increase. The correlation time is dependent on the size of the molecules and also the viscosity of the medium in which they translate and rotate. Therefore as the viscosity is increased the correlation time is increased as the motion of the molecules is slowed down. This has the effect of enhancing the value of $\omega_0\tau_c$ i.e. moving the motion of the molecules closer to the resonant frequency of the spins and therefore provide a more efficient relaxation and thus T_1 decreases. The correlation time is defined for spherical molecules in liquids by BPP theory [72] in the form of;

$$\tau_c = \frac{4\pi\eta a^3}{3k_B T} \tag{4.6}$$

where a is the radius of the molecule in solution with viscosity η at an absolute temperature T with k_B being the Boltzmann constant. It is clear that as the temperature is increased the correlation time will decrease and as the viscosity is increased the correlation time would increase, this explains the trends with both temperature and salt concentration.

4.2.6 Fluorine Longitudinal Relaxation

The fluorine nucleus (^{19}F) has been used here in order to track the anion which is a boron ion surrounded by four fluorine ions in a tetrahedral structure. Fluorine produces a fairly strong

	T_1(s)					
Temp. (K)	0.3 M	0.5 M	0.7 M	1.0 M	1.3 M	1.5 M
283	2.21	1.92	1.67	1.39	1.20	1.09
293	2.56	2.22	1.92	1.48	1.35	1.22
303	2.44	2.22	1.87	1.66	1.41	1.27
313	2.73	2.43	2.16	1.79	1.55	1.39
323	3.01	2.67	2.41	1.93	1.70	1.54
333	3.29	2.97	2.67	2.08	1.85	1.70
343	3.60	3.25	2.90	2.29	2.06	1.86
353	3.72	3.84	3.12	2.46	2.21	2.04

Table 4.6: ^{19}F longitudinal relaxation times for PC/$LiBF_4$ (0.1-1.5 M) liquid electrolytes in temperatures range of 283-353 K.

signal in NMR and has spin-1/2 like the hydrogen nuclei. It would have been possible to use ^{11}B in order to track the anion, however there are four times as many fluorine ions than boron per anion and will therefore produce a stronger signal. The spectrometer was setup in the same manner as for the lithium nucleus, with the only difference being, that the receiver coil had to be switched and the connections on the pre-amplifier changed.

The resonant frequency of the ^{19}F nuclei on this spectrometer is 376 MHz where the resonant frequency of ^{1}H on the same spectrometer is 400 MHz. The setup of the inversion and saturation recovery sequences were exactly the same as for the lithium nucleus with the exception that the fluorine nucleus had a different pulse duration. At the same power level of 3 dB the pulse duration of the $\pi/2$ pulse was $\tau_{90} = 19.6\ \mu$s.

Table 4.6 shows the data for the longitudinal relaxation times for PC/$LiBF_4$ (0.1-1.5 M) liquid electrolytes in temperatures range of 283-353 K using ^{19}F nucleus. The relaxation times were again seen to increase with increasing temperature and decrease with increasing salt concentration. The same explanation is used here to explain the trends as were used previously for the lithium measurements. The correlation time is proportional to the viscosity and inversely proportional to the temperature, shown in equation 4.6. The molecules in non-viscous liquids are characteristically on high temperature side of the T_1 minimum, therefore reducing the correlation time moves the motion away from resonance, producing a less efficient relaxation.

The Arrhenius plot for the PC/$LiBF_4$ (0.3 M, 1.0 M and 1.5 M) liquid electrolytes using ^{19}F nucleus is illustrated in figure 4.7, which shows similar to the lithium measurements in this temperature range the relaxation temperature dependence appears to be Arrhenius. The activation energy for the lithium and fluorine nuclei can be determined by fitting straight lines on an Arrhenius plot as the gradient of the line is given by;

$$Gradient_{Arrhenius} = \frac{E_{T_1}}{R} \tag{4.7}$$

where E_{T_1} is the activation energy of the longitudinal relaxation and R is the universal gas constant, leaving the units of the activation energy as kJ mol^{-1}. Table 4.7 shows the Arrhenius parameters pre-exponential and activation energy for the lithium and fluorine nuclei for the longitudinal relaxation times. It can be noted that the activation energy of the lithium ions are

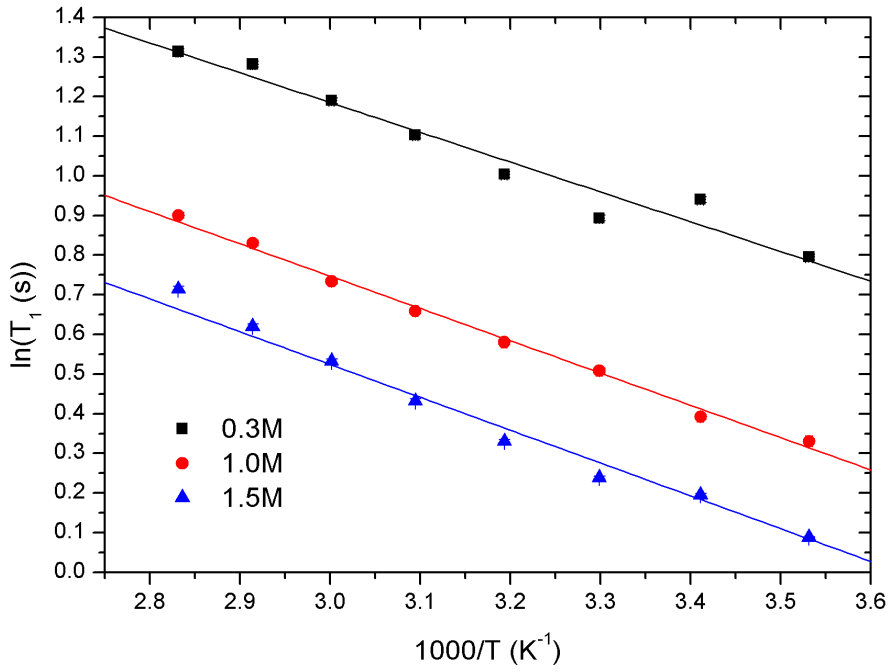

Figure 4.7: ^{19}F T_1 Arrhenius plot for PC/LiBF$_4$ (0.3 M, 1.0 M and 1.5 M) liquid electrolytes.

significantly larger than the corresponding fluorine ions, suggesting that the lithium has a more significant translational component to the relaxation than fluorine, this has been assessed by comparing the T_1 and diffusion activation energies in section 4.4.

4.3 Diffusion Measurements

4.3.1 Introduction

Diffusion measurements have been taken for both liquid electrolytes and polymer gel electrolytes containing PC/LiBF$_4$ and PVDF as the host polymer. In this chapter, only the diffusion of the

	A_{T_1} (s)		E_{T_1} (kJ mol^{-1})	
Salt Concentration (M)	^{7}Li	^{19}F	^{7}Li	^{19}F
0.3	1061	56	15.3	7.7
0.5	549	69	13.7	8.7
0.7	474	64	13.6	8.8
1.0	287	20	13.1	7.0
1.3	232	32	12.6	8.1
1.5	304	39	13.7	8.4

Table 4.7: ^{7}Li and ^{19}F Arrhenius fitting parameters, activation energies (E_{T_1}) and pre-exponential factor (A_{T_1}) for the longitudinal relaxation times for PC/LiBF$_4$ liquid electrolytes.

liquid electrolytes will be considered as it is important to first understand the liquids before considering the more complex polymer gel electrolytes.

As mentioned in Chapter 2, the diffusion of molecules can be measured by using pulsed-field gradient NMR (PFG-NMR). PFG-NMR involves using magnetic field gradient pulses along with a normal spin echo sequence in order to give the spins spatial encoding. Using the Stejskal-Tanner [50] sequence to measure diffusion has been observed to cause issues with some measurements, as highlighted by Annat *et al* [51], which showed that using the sequence resulted in different values obtained for multiple hydrogen sites on a single molecule. It was stated that the use of a stimulated echo PFG sequence was more successful. In a stimulated sequence the π RF pulse was replaced with two $\pi/2$ pulses, this was designed to stop any relaxation caused by T_2, as the during the diffusion time Δ the spins are in the z-direction.

The pulse sequence used in this thesis was a version of a stimulated PFG sequence by Cotts [52], which was modified to counter any background field inhomogeneities which may be present This was achieved by splitting each of the gradient pulses into two halves with equal and opposite magnitudes, placing an inversion pulse between them. The bipolar gradient pulse cancels out the background field (more detail on this pulse can be found in Chapter 2).

The parameters used here have been proved useful in measuring diffusion of liquids in previous publications [43]. The value for δ, the duration of the gradient pulse was fixed at 10 ms, this was not altered throughout the entire diffusion measurements. The diffusion time, Δ was the time between applying the first gradient set and the removal of the gradient by the second set and was fixed at a value of 40 ms. The time between the first gradient and inversion pulse of the first gradient set was denoted δ_1 and the time between the inversion pulse and the second half of the gradient was denoted δ_2, to eliminate the background field effectively $\delta_1 = \delta_2$, these were set to value of 1 ms. The maximum gradient that was used in each experiment was based on the expected diffusion coefficient. The Topspin 1.5 software contains a 'diff' setup window which allows the user to insert an expected diffusion coefficient and then the software will automatically set the maximum gradient strength based on this value. The maximum gradient needs to be set according to the diffusion otherwise the signal will decay too slowly or too quickly and the data will not be fitted well. The number of points used for most scans was 16 over a range of gradient strengths, at each gradient strength 8 measurements were taken, however for the lower intensity measurements such as lithium with low salt concentration 16 scans were employed.

The fitting of the resulting intensity profile could be performed using the Bruker Topspin 1.5 software. This allowed the user to set the gyromagnetic ratio of the nucleus being investigated and also the diffusion time (Δ) and the pulse duration (δ). An initial guess of the diffusion coefficient was used and then the software used an iterative process based on the Levenberg Marquardt algorithm (LMA) [78; 79] which is used for least squares fitting problems. One limitation of this fitting procedure is that the algorithm only finds a local minimum and not a global minimum which means that the initial guess has to be close to the final answer, however the diffusion constant are well known for liquids and is not considered an issue here.

Diffusion measurements have been performed for the solvent molecule (^{1}H), anion (^{19}F) and cation (^{7}Li) using different receiver coils for each nuclei and therefore each set of data was taken before moving onto the next set to avoid inconsistency in measurements. The diff60 probe was used for these diffusion measurements same as for the longitudinal relaxation times measured

on the 400 MHz Bruker AVANCE II spectrometer. Therefore the pulse durations used for the lithium and fluorine nuclei were $\tau_{90} = 18.5\ \mu$s and $\tau_{90} = 19.6\ \mu$s respectively and set at the same power level 3 dB. The pulse duration for the hydrogen nucleus was set at $\tau_{90} = 6.47\ \mu$s at a power level of 0 dB. The same heating system was also used which means that there was a chance of inducing correlated motion due to a temperature gradient, which would have a dramatic effect on the diffusion constant. This was seen in some initial measurements on the liquid diffusion with larger samples, in order to eliminate this factor as much as possible the sample size was decreased significantly. The correlated motion affecting diffusion measurements is a known problem which has caused Hayamizu *et al* [97] to design a new type of cell which uses a small annular volume to avoid this problem; however standard glass tubes were used here.

Pulsed-field gradient NMR measurements has been used extensively to probe the dynamics of different lithium salts in organic solvents [43; 57; 63; 98–102] including systems containing PC and $LiBF_4$ [56]. Here the diffusion constants are measured for a whole range of salt concentrations and temperatures, in other publications there seems to be more a focus on observing many different systems rather than any one system in detail, such as the work by Aihara *et al* [56] which reports the diffusion constants as measured by PFG for six different lithium based salts in PC and γ-butyrolactone (GBL).

4.3.2 Hydrogen Diffusion

It was shown in section 4.2.4 that the hydrogen spectra exhibited four peaks which were attributed to different sites of the PC molecules. Since each of these peaks corresponds to a single molecule which in theory should be translating with one another then the diffusion constant for each peak should be equal to the diffusion of the entire spectrum. Table 4.8 shows the data taken for a PC/$LiBF_4$ (1.0 M) liquid electrolyte where each peak has been investigated individually to obtain a value of the self diffusion constant. Only one sample has been displayed here to serve as an example. It should be noted from table 4.8 that at every temperature all of the peaks exhibited similar diffusion constants. For all other diffusion measurements in this section the entire spectrum was used to determine the final value of diffusion. If the data for the lowest temperature of 293 K from table 4.8 is observed it can be seen that the diffusion constants are 2.07, 2.06, 2.06 and 2.06 (10^{-10} m^2 s^{-1}) for peaks 1-4 respectively, therefore showing that there is no change when considering individual peaks, where the entire spectrum yielded a result of $(2.06\pm\ 0.02)\times10^{-10}$ m^2 s^{-1}. It seems at higher temperatures there is slight variation between the different peaks as at the highest temperature of 343 K the diffusion values were 6.60, 6.55, 6.45 and 6.51 (10^{-10} m^2 s^{-1}) for peaks 1-4 respectively, it can be stated that all values satisfy $(6.5\pm0.1)\times10^{-10}$ m^2 s^{-1} where the value using the entire spectrum was found to be $(6.51\pm0.03)\times10^{-10}$ m^2 s^{-1}, where this error was determined by taking repeat readings and using the standard deviation to determine the absolute error.

The entire diffusion data taken for the hydrogen nucleus for the PC/$LiBF_4$ liquid electrolytes is shown in table 4.9 which includes data using several different salt concentrations (0.0 M, 0.3 M, 0.5 M, 0.7 M, 1.0 M, 1.3 M and 1.5 M) at a temperature range of 293 K-343 K. The temperature range here was quite limited due to convection at temperatures above 343 K, which began to exhibit signs of correlated motion as the diffusion constants increased at a much faster rate. The lower temperature limit was set by the water cooling system. Also at temperatures below

	Diffusion (10^{-10} m^2 s^{-1})			
Temperature (K)	Peak 1	Peak 2	Peak 3	Peak 4
293	2.07	2.06	2.06	2.06
303	2.80	2.79	2.78	2.79
313	3.52	3.53	3.53	3.54
323	4.46	4.48	4.46	4.49
333	5.28	5.29	5.30	5.31
343	6.60	6.55	6.45	6.51

Table 4.8: ^{1}H Diffusion constants for peaks 1-4 for a PC/$LiBF_4$ (1.0 M) liquid electrolyte.

	^{1}H Diffusion (10^{-10} m^2 s^{-1})						
Temperature (K)	0.0 M	0.3 M	0.5 M	0.7 M	1.0 M	1.3 M	1.5 M
293	4.96	3.87	3.20	2.68	2.06	1.48	1.24
303	6.18	5.00	4.11	3.49	2.79	2.04	1.74
313	7.73	6.18	5.22	4.48	3.54	2.74	2.28
323	9.23	7.43	6.28	5.39	4.49	3.37	2.91
333	12.69	8.86	7.59	6.69	5.31	4.21	3.63
343	—	—	9.06	7.92	6.51	5.05	4.53

Table 4.9: ^{1}H diffusion constants for PC/$LiBF_4$ liquid electrolytes, representing the PC (solvent) molecules.

293 K the probe started to have a condensation problem, this caused the tuning and matching capacitors to stop working, therefore they would no longer tune the frequency. They had to be fully dried before they would once again operate correctly. There was no method of overcoming this on the timescale of this research so a limited temperature range was acquired.

The diffusion coefficients exhibited an exponential rise with increasing temperature. This effect can be attributed to the solvent molecules having more thermal energy at elevated temperatures. The viscosity of the system would also decrease as the temperature was increased, meaning that the energy required to translate would be reduced. Also from table 4.9 it can be seen that an increase in salt concentration causes the diffusion constant to fall, which can also be explained in terms the viscosity of the system, which increased as more salt ions were added to the solution.

4.3.3 Lithium Diffusion

Next the cation will be considered which was detected using the ^{7}Li nucleus. The same parameters were used for all nuclei, however when switching between nuclei, the software and hardware must be slightly altered. Unlike the hydrogen nucleus, the lithium ions only exhibit a single peak in the NMR spectrum shown in figure 4.5.

Table 4.10 shows the diffusion constants for the lithium nucleus. This time the temperature range was 283-353 K which was a bigger range than used for the hydrogen. Firstly because the

	^{7}Li Diffusion (10^{-10} m^2 s^{-1})					
Temperature (K)	0.3 M	0.5 M	0.7 M	1.0 M	1.3 M	1.5 M
283	1.22	1.02	0.82	0.61	0.43	0.34
293	1.64	1.37	1.14	0.86	0.63	0.51
303	2.17	1.84	1.55	1.19	0.89	0.72
313	2.75	2.34	2.00	1.56	1.19	0.97
323	3.35	2.89	2.50	1.97	1.53	1.26
333	4.06	3.51	3.05	2.44	1.93	1.63
343	5.63	4.43	3.63	2.96	2.43	2.15
353	—	6.47	4.69	3.63	3.18	2.86

Table 4.10: ^{7}Li diffusion constants for PC/$LiBF_4$ liquid electrolytes, representing the cations.

lithium ions are diffusing more slowly than the solvent molecules the correlated motion seemed to affect the lithium measurements less and was not observed here. Unsurprisingly, the diffusion data for the lithium measurements exhibited the same temperature and salt concentration trends, due to the reasons stated above, which were thermal energy and viscosity contributions to the system.

The lithium diffusion is the average of all the lithium species within the liquid electrolyte as the NMR spectrum can not distinguish between different species. Lithium ions within liquid electrolytes containing propylene carbonate are known to interact with the solvent molecules as the carbonyl group on the PC molecule is slightly negatively charged which would attract the lithiums' positive charge. This solvation is well understood and it has been shown that on average between 2-4 PC molecules can electrostatically interact with a single lithium ion [82; 103]. By taking the ratio of solvent and ion diffusion the solvation number can be estimated for lithium, was found to be around 2.2 on the timescale of the diffusion measurements [56]. These ratios have been calculated in regards to this research in Chapter 7. Other possible species containing lithium ions would be electrostatically attached to a BF_4^- anion producing a neutral entity, known as ionic association and will also be considered in Chapter 7. Therefore the final value of diffusion is simply an average of all these possible species which contain lithium ion(s).

4.3.4 Fluorine Diffusion

Lastly the diffusion constants for the liquid electrolytes were measured using the ^{19}F nucleus in order to measure the anion behaviour with both salt concentration and temperature. Again the temperature and salt concentration trends are the same as the hydrogen and lithium trends, which will be considered in greater detail in section 4.3.6. As with lithium, fluorine exhibits a single peak in the NMR spectrum as previously shown for the longitudinal relaxation measurements. As previously mentioned for the lithium ions, the fluorine diffusion is the average of all species that the fluorine ions are included. The fluorine can be either in the form of the anion of the salt which in this case is BF_4^- or attached to lithium ions in some manner whether it be with a single lithium ion or as part of a cluster of ions and molecules. This research will include some conjecture with regards to the possible association of the salt molecules in Chapter 7.

	^{19}F Diffusion (10^{-10} m^2 s^{-1})					
Temperature (K)	0.3 M	0.5 M	0.7 M	1.0 M	1.3 M	1.5 M
283	2.18	1.65	1.26	0.86	0.57	0.43
293	2.87	2.21	1.71	1.19	0.82	0.63
303	3.64	2.84	2.25	1.60	1.11	0.87
313	4.52	3.54	2.84	2.07	1.46	1.17
323	5.59	4.35	3.56	2.55	1.85	1.51
333	7.02	5.25	4.71	3.25	2.39	1.95
343	8.12	6.45	5.46	3.94	2.93	2.41
353	9.37	7.92	6.71	4.90	3.69	3.05

Table 4.11: ^{19}F diffusion constants for PC/$LiBF_4$ liquid electrolytes, representing the anion.

4.3.5 Diffusion Temperature Dependence

As with the longitudinal relaxation time measurements, the diffusion can be characterised by Arrhenius or VTF type temperature dependence. A graph of $ln(D)$ against $1000/T$ was plotted, if the resulting behaviour is linear then the trend is considered Arrhenius. It is important to note that here a somewhat limited temperature range was used due to limitations of the NMR spectrometer.

Arrhenius plots can be found in figure 4.8 for PC/$LiBF_4$ (1.0 M) liquid electrolytes using all three nuclei ^{1}H, ^{7}Li and ^{19}F. Linear fits have been applied in figure 4.8 which fitted the data well, suggesting that the diffusion temperature dependence was Arrhenius for all nuclei. However, as it has already been noted the temperature range is quite limited and would therefore most likely appear to be Arrhenius. It is likely that as the glass transition temperature is approached the system will start to 'lock' up and the temperature dependence would become non-Arrhenius (VTF). A good example of this has been shown in section 4.2.3 with the longitudinal relaxation times, on the low field machine the ^{1}H measurements exhibited a non-Arrhenius temperature behaviour , however the lithium and fluorine (^{7}Li and ^{19}F) exhibited Arrhenius dependence due to the limited temperature range. The temperature dependence of the diffusion data in this temperature range can therefore be fitted in the form;

$$D\left(T\right) = D_{\infty} exp\left[\frac{E_D}{RT}\right] \tag{4.8}$$

where D_∞ is the pre-exponential factor for the diffusion which relates to the diffusion at infinite temperature and E_D is the activation energy of the diffusion process. Therefore for each salt concentration an activation energy and pre-exponential factor can be determined for each nucleus, shown in table 4.12. Arrhenius type temperature dependence has been observed in other lithium based salts in organic solvents such as DMF with $LiCF_3SO_3$ [43].

Firstly the activation energy will be considered, from table 4.12 it can be observed that the activation energies have a positive trend with salt concentration. For diffusion the physical meaning of the activation energy is the amount of thermal energy per molecule that is required for each molecule to translate within the liquid electrolyte it is contained within. Therefore it is reasonable to assume that as the viscosity is increased the molecules, on average, would

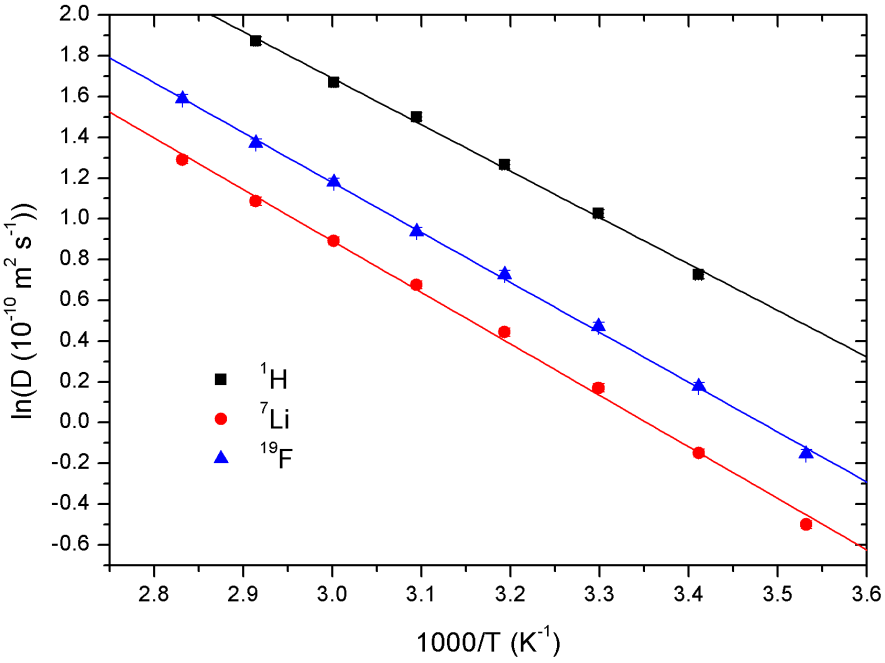

Figure 4.8: Arrhenius plot for diffusion constant for PC/$LiBF_4$ (1.0 M) liquid electrolytes using ^{1}H, ^{7}Li and ^{19}F nuclei which represent the solvent molecules, cation and anion respectively.

	E_D (kJ mol^{-1})			D_∞(10^{-7} m^2 s^{-1})		
Salt Concentration (M)	^{1}H	^{7}Li	^{19}F	^{1}H	^{7}Li	^{19}F
0.0	17.0	—	—	5.23	—	—
0.3	16.9	19.4	17.8	4.03	4.71	4.30
0.5	17.5	20.4	18.7	4.16	6.00	4.78
0.7	17.9	21.5	19.9	4.23	7.61	5.89
1.0	19.9	21.9	22.3	7.22	7.13	11.2
1.3	20.6	23.6	22.2	7.00	10.2	7.45
1.5	22.5	24.0	23.2	12.6	9.73	8.49

Table 4.12: Arrhenius parameters activation energy and D_∞ for diffusion constants for PC/$LiBF_4$ liquid electrolytes using ^{1}H, ^{7}Li and ^{19}F nuclei, representing the solvent molecules, cation and anion, respectively.

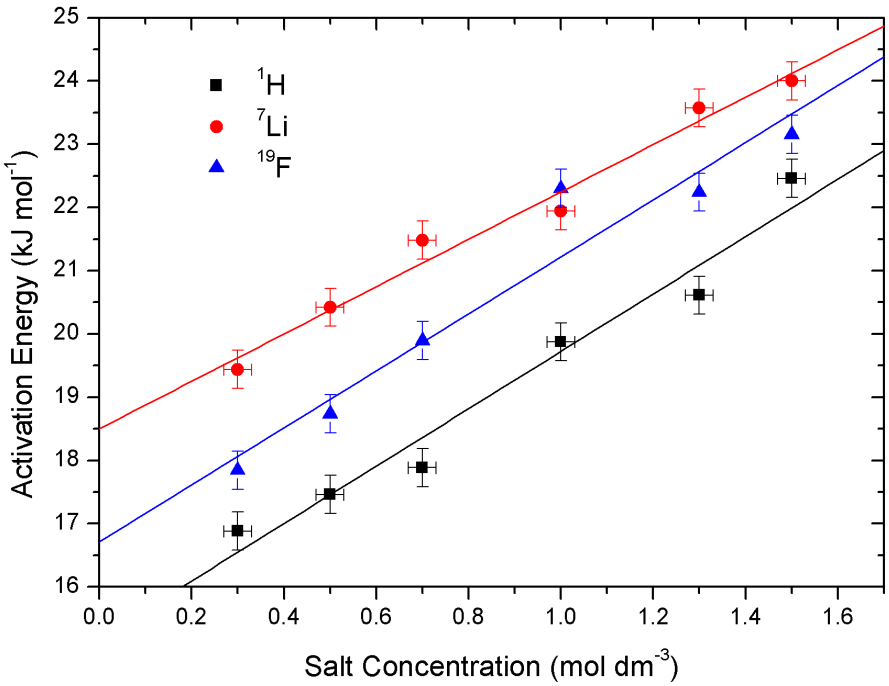

Figure 4.9: Arrhenius activation energies for diffusion for PC/$LiBF_4$ liquid electrolytes using ^{1}H, ^{7}Li and ^{19}F nucleus which represents the solvent molecules, cation and anion respectively.

require more energy to translate, explaining the rise in activation energy with increasing salt concentration. Figure 4.9 shows the activation energy of diffusion for the three nuclei. It can be seen that they all exhibit a somewhat linear relationship with salt concentration, however the gradient of the linear lines differ for each nucleus. Comparing the linear fit for the three nuclei gives values of (3.8±0.1), (3.7±0.1) and (4.5±0.1) for the hydrogen, lithium and fluorine nuclei respectively. Since all of these entities have the same bulk viscosity the variation in gradient of the linear fits were most likely due to the relative sizes of the molecules, suggesting that the radius of the BF_4 ions is increasing in size with salt concentration. At higher salt concentrations all three activation energies of the three nuclei are somewhat converging suggesting that, at this point, viscosity is dominating the system.

Since all three nuclei are in the same medium with the same bulk viscosity the relative activation energies can be used to indicate the average radii of each nuclei. Since in general $E_{D_H} < E_{D_F} < E_{D_{Li}}$, this implies that $a_{Li} > a_F > a_H$, where a_{Li}, a_F and a_H are the effective radii of the lithium, fluorine and hydrogen nuclei respectively. The order of diffusion constants was observed here to be $D_H \approx D_F < D_{Li}$, this trend is well understood and frequently observed in similar electrolytes containing lithium based salts in organic solvents [56; 99–101; 103]. This has been attributed to the lithiums tendency to be solvated several solvent molecules. Since the radii of a single lithium ion and BF_4^- ion have been determined to be 0.78 Å[104] and 2.29 Å[83] respectively there must be significant solvation for the lithium ion. The effective radii of the each constituent has been discussed in more detail in Chapter 7.

The empirical meaning of the Arrhenius parameter D_∞ is the diffusion constant when the

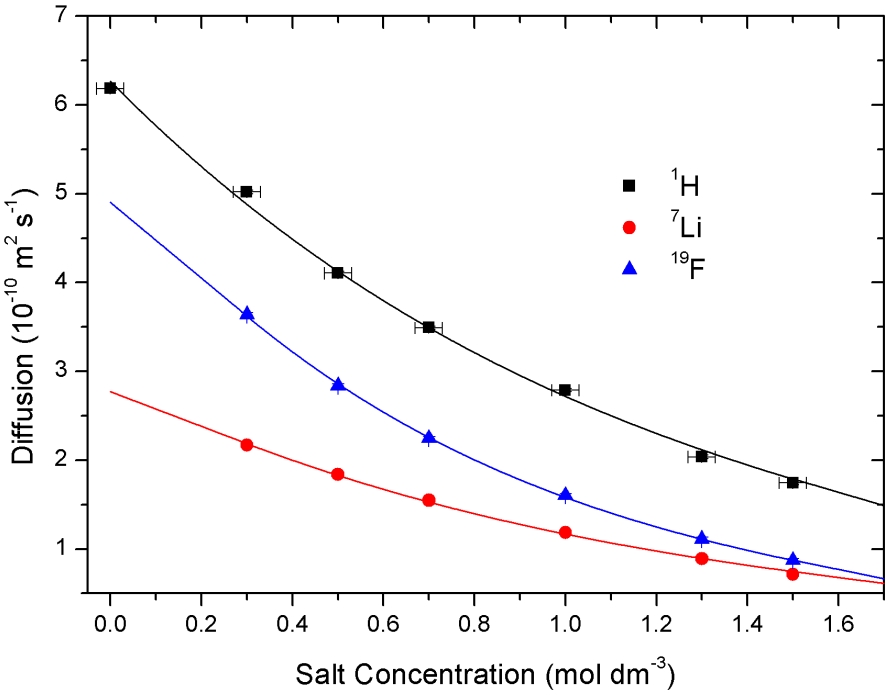

Figure 4.10: Diffusion constant as a function of salt concentration for PC/$LiBF_4$ liquid electrolytes using ^{1}H, ^{7}Li and ^{19}F nuclei which represent the solvent molecules, cation and anion respectively. All data was taken at 303 K and fitted with equation 4.9.

exponential term is equal to one, i.e. at infinite temperature. This parameter was observed to increase with increasing salt concentration, however, the data were quite scattered so no physical significance was placed on this parameter and the main focus was kept on the activation energies.

4.3.6 Diffusion Salt Concentration Dependence

The diffusion is inversely proportional to the viscosity, therefore as the salt concentration was increased the viscosity would increase which would in turn cause a decrease in the diffusion of the ions. As part of the activation energy discussion it was mentioned that each molecule experiences the same bulk viscosity so if the decrease was due to purely viscosity it would be expected that the decrease with salt concentration to be very similar. Figure 4.10 shows the diffusion constant as a function of salt concentration, it can be noted that the diffusion decay for each nucleus was not equal. The data in figure 4.10 was fitted using a simple exponential in the form of;

$$D\left(c\right) = D_0 exp\left[\frac{-c}{A_D}\right] \tag{4.9}$$

where D_0 was the diffusion at zero salt concentration and A_D was the decay constant for the salt concentration dependence of the diffusion. The value of A_D dictates the rate of the decrease with salt concentration, a smaller value for A_D produces a faster decrease with salt concentration.

The fitting parameter A_D obtained from the data in figure 4.10 took the values of (1.20±0.03), (1.12±0.02) and (0.85±0.01) for the hydrogen, lithium and fluorine, respectively. These values

	D_0 (10^{-10} m^2 s^{-1})			A_D (M)		
Temperature (K)	^{1}H	^{7}Li	^{19}F	^{1}H	^{7}Li	^{19}F
283	—	1.74	3.19	—	0.93	0.76
293	5.00	2.36	4.13	1.12	0.98	0.80
303	6.27	2.86	5.17	1.20	1.12	0.84
313	7.78	3.72	6.19	1.26	1.14	0.90
323	9.06	4.35	7.67	1.36	1.22	0.91
333	10.9	5.23	9.43	1.38	1.29	0.95
343	12.8	5.76	10.8	1.41	1.52	1.00
353	—	7.62	12.9	—	1.46	1.04

Table 4.13: Salt concentration fitting parameters A_D and D_0 for diffusion constants for PC/$LiBF_4$ liquid electrolytes using ^{1}H, ^{7}Li and ^{19}F nuclei which represent the solvent molecules, cation and anion respectively.

represent the decline in diffusion with salt concentration with the hydrogen being the least significant drop and fluorine the most significant. This data highlights that there are other mechanisms occurring alongside the viscosity increasing with salt concentration. As previously mentioned, the diffusion is dependent on the temperature of the system, viscosity and effective radius of the molecules, therefore it is likely that a change in radius of the BF_4 ions is producing the accelerated drop in diffusion with increasing salt concentration. It appears that at high salt concentrations (1.5M) the fluorine ions are diffusing at a very similar rate to the lithium ions, suggesting that they have comparable radii, and that the fluorine is associating with the lithium clusters, which has been seen in other systems and attributed to increased ion pairing [98].

Table 4.13 shows the data for the salt concentration fitting parameters A_D and D_0 from equation 4.9 for PC/$LiBF_4$ liquid electrolytes using ^{1}H, ^{7}Li and ^{19}F nuclei. These fitting parameters have been determined for all temperatures measured for the diffusion and it can be noted that both of these parameters increase with temperature. As previously stated if the value of A_D is increased then the rate at which the salt concentration decreases the diffusion is reduced. Figure 4.11 shows the salt concentration fitting parameter A_D as a function of temperature for all three nuclei. In figure 4.11 A_D was observed to increase with temperature, implying that the decay in diffusion is less significant at higher temperatures, which is considered reasonable due to the obvious decrease of viscosity that will be experienced by the molecules at higher temperatures.

4.4 Longitudinal Relaxation and Diffusion Comparison

In this section the results of the diffusion constants and longitudinal relaxation (T_1) will be compared in order to determine the relevant contributions of the translational and rotational components of the longitudinal relaxation. As previously discussed in this chapter the relaxation mechanisms can be broken down into intramolecular and intermolecular interactions. The intramolecular interactions are those internal to the molecule such as rotation of an atom on the molecule. Whereas the intermolecular interactions are the translational and rotational motion with respect to neighbouring atoms. As noted previously it is not possible for a translational in-

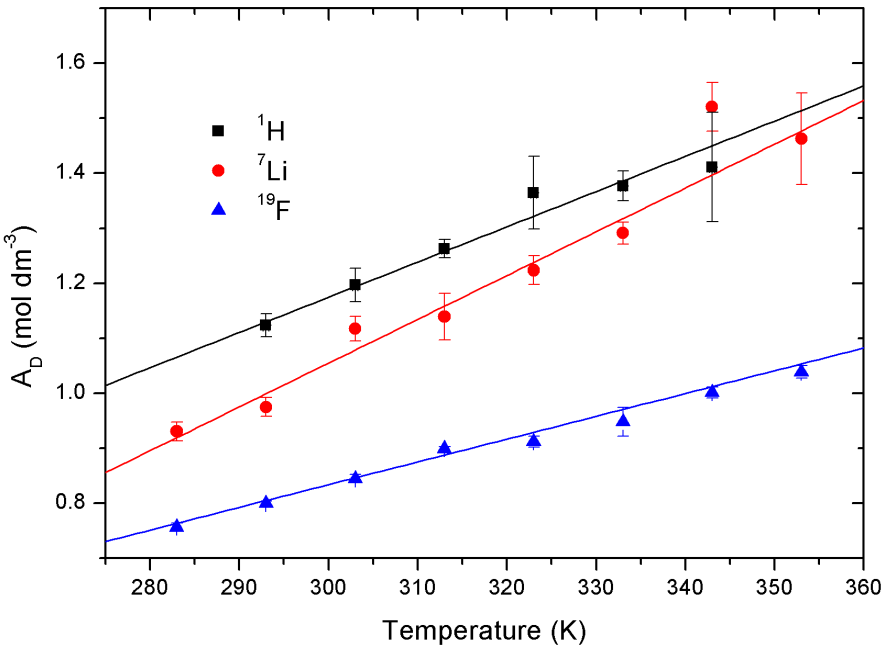

Figure 4.11: Salt concentration fitting parameters A_D for diffusion constants for PC/$LiBF_4$ liquid electrolytes using ^{1}H, ^{7}Li and ^{19}F nucleus representing the solvent molecules, cation and anion respectively.

tramolecular interaction to occur as all of the atoms translate together. Therefore in this section the term 'translational' motion refers to the intermolecular translational interactions. Whereas the 'rotational' motion can be thought of as a combination of intramolecular and intermolecular interactions. This section will not conclude the exact contributions but rather an indication of the relevant contributions. The strategy followed in this section is similar to the one carried out previously at the University of Leeds by Williamson *et al* on $LiCF_3SO_3$ in DMF [57].

Firstly, it was important to test the validity of a possible translational component of the longitudinal relaxation, by assuming that the molecules in the liquid electrolyte undergo Brownian motion caused by thermal energy of the system. The mean displacement of a molecule undergoing Brownian motion [105] is given by;

$$\langle r \rangle = \sqrt{6Dt} \tag{4.10}$$

where D is the self diffusion constant and t is the timescale of the diffusion. If it is assumed that the timescale of the experiment is that of the Larmor frequency which are 500 MHz, 155 MHz and 376 MHz for the hydrogen, lithium and fluorine nuclei respectively. For each nucleus the maximum and minimum mean displacement was calculated as 1.22-3.90 nm, 1.14-4.66 nm and 0.83-3.64 nm for the hydrogen, lithium and fluorine, respectively. The effective radii here can be calculated using viscosity measurements and diffusion measurements, these results can be found in Chapter 7 along with the bulk viscosity of the system; however, all values were seen to be of the order of Angstroms. Therefore the mean displacement is an order of magnitude larger than the ionic radii. This suggests that a intermolecular translational component of the longitudinal relaxation is possible, however this does not mean there has to be a translational component.

	Activation energy ($kJ\,mol^{-1}$)				
	Diffusion	T_1			
Salt Concentration (M)		Peak 1	Peak 2	Peak 3	Peak 4
0.0	17.0	12.64	13.91	13.95	14.48
0.3	16.9	11.18	12.56	12.91	12.80
0.5	17.5	14.87	14.90	15.57	15.53
0.7	17.9	11.94	15.24	15.28	15.70
1.0	19.9	15.45	12.48	12.55	14.55
1.3	20.6	15.39	16.06	16.12	17.39
1.5	22.5	15.66	16.43	16.07	17.01

Table 4.14: ^{1}H Activation energy for longitudinal relaxation times and diffusion for individual peaks numbered 1-4 of the NMR spectrum for PC/$LiBF_4$ liquid electrolytes.

From this point it was assumed that a translational component was possible and there is most likely some rotation of the molecules albeit from both intermolecular and intramolecular interactions. If this rotation is near the Larmor frequency then it would efficiently cause longitudinal relaxation.

It was logical to first compare the values of the activation energies of the diffusion and longitudinal relaxation times. If the activation energies for diffusion and longitudinal relaxation times are comparable then it can be assumed that the relaxation is caused primarily due to translational motion; since diffusion is a purely translational property. Table 4.14 shows the activation energies of the longitudinal relaxation times and also the diffusion for the hydrogen measurements. It can be noted that the activation energies of each the hydrogen peaks were comparable. They are also comparable to the diffusion constant activation energies. At low salt concentrations the values of the longitudinal relaxation times are (12.64, 13.91, 13.95 and 14.48) $kJ\,mol^{-1}$ for peaks 1-4 respectively, and the diffusion activation energy was 17.0 $kJ\,mol^{-1}$. This means that the longitudinal relaxation activation energies were between 74% and 85% of the diffusion activation energies, suggesting that the hydrogen relaxation was mainly due to intermolecular translational motion at low salt concentrations. At the higher salt concentration of 1.5M, the values of the relaxation activation energies were (15.66, 16.43, 16.07 and 17.01) $kJ\,mol^{-1}$ for peaks 1-4, respectively, with a diffusion activation energy of 22.5 $kJ\,mol^{-1}$. This corresponds to 70% and 76% of the diffusion activation energies, therefore suggesting that at higher concentrations there is a slightly reduced translational component. This was attributed to the increase in viscosity at higher salt concentrations. The increased viscosity would result in a higher activation of translational motion and therefore making the rotational component more prominant.

Therefore it can be concluded from comparing the activation energies of the hydrogen nucleus that the solvent molecules have a predominantly translational component with a non negligible rotational component. The lithium ion activation energies are shown in table 4.15 for both the longitudinal relaxation times and the self diffusion. At low salt concentrations (0.3M) the value of the activation energies are 19.4 $kJ\,mol^{-1}$ and 15.3 $kJ\,mol^{-1}$ for the diffusion and relaxation times, respectively. The relaxation activation energy was around 79% of the diffusion activation energy. This value is comparable to the hydrogen result suggesting that, as with the hydrogen,

	E_D (kJ mol^{-1})		E_{T_1} (kJ mol^{-1})	
Salt Concentration (M)	^{7}Li	^{19}F	^{7}Li	^{19}F
0.3	19.4	17.8	15.3	7.7
0.5	20.4	18.7	13.7	8.7
0.7	21.5	19.9	13.6	8.8
1.0	21.9	22.3	13.1	7.0
1.3	23.6	22.2	12.6	8.1
1.5	24.0	23.2	13.7	8.4

Table 4.15: ^{7}Li and ^{19}F activation energy of diffusion and NMR longitudinal relaxation for PC / $LiBF_4$.

the relaxation was predominantly due to translational motion but seems to have a definite rotational component. At the higher concentration the values of the activation energies are 24.0 kJ mol^{-1} and 13.7 kJ mol^{-1} for the relaxation and diffusion, respectively, which corresponds to 57%, suggesting that the translational component becomes much less dominant at high salt concentrations, allowing the rotational contribution to increase.

The fluorine diffusion and relaxation activation energies are also shown in table 4.15. The activation energy of the longitudinal relaxation for the BF_4 ions are much smaller than for the lithium and hydrogen whilst the E_D are comparable for the three nuclei, suggesting that the relaxation of the BF_4 ions predominantly undergo rotational motion. At low salt concentrations the diffusion and longitudinal relaxation activation energies are 17.8 kJ mol^{-1} and 7.7 kJ mol^{-1} respectively for the fluorine nucleus, corresponding to the relaxation being around 43% of the diffusion value. At higher salt concentrations (1.5M) the values of the activation energies are 23.2 kJ mol^{-1} and 8.4 kJ mol^{-1} for the diffusion and relaxation, respectively, which results in the relaxation being 36% of the diffusion activation energy. The fluorine relaxation times are therefore dominated by rotation at all salt concentrations; however, there is still a further reduction in translational contribution at higher salt concentrations, as seen with the lithium and hydrogen measurements.

Another approach to comparing the diffusion with the longitudinal relaxation times is to do so directly. If both values are scaled by their maximum values so all diffusion and relaxation times exhibit values between 0 and 1 it would be possible to draw a comparison. If the longitudinal relaxation behaved in the exact same manner as the diffusion then it would be reasonable to assume that the relaxation process was mainly due to translational motion. Figure 4.12 shows the normalised values for the diffusion and the longitudinal relaxation times for the PC/$LiBF_4$ liquid electrolytes at 303 K for the ^{1}H nucleus (solvent molecules). It can be noted that all of the T_1 values for the hydrogen sites on the PC molecule do not overlap the diffusion values, suggesting that there is a non-negligible rotational component present in the longitudinal relaxation. The data in figure 4.12 has been fitted with a simple exponential with the main purpose of a point of reference for the eye. It can be noted that the peak which deviates most away from the diffusion decay is peak 4, this peak corresponds to the methyl group of the PC molecule. This has been previously stated to be the most likely to have rotation since it protrudes from the main structure of the PC molecule. Peaks 2 and 3 have similar values to each other, shown in figure

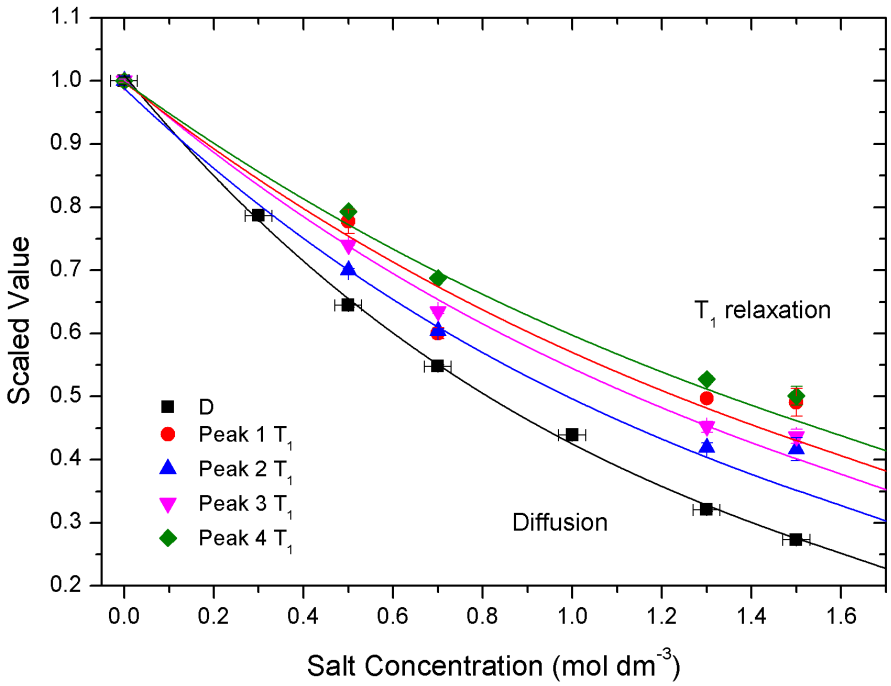

Figure 4.12: ^{1}H normalised diffusion and longitudinal relaxation for PC/$LiBF_4$ liquid electrolytes at 303 K.

4.12, suggesting that they have a similar rotational component; this was not surprising since they are part of the same site of the PC molecule. Peak 1 which refers to the C-H bond of the PC molecule seems to be affected by the increase in salt concentration most significantly. This could be attributed to a greater rise in rotational component at higher salt concentrations since the other peaks seem to exhibit a fairly prominent rotational contribution at all salt concentrations.

The lithium and fluorine were explored in the same manner and shown in figure 4.13. The longitudinal relaxation times for the lithium ions and the BF_4 ions were observed to be comparable, however the diffusion behaviour observed in figure 4.13 for the lithium and fluorine nuclei were seen to be quite different. The diffusion for the BF_4 ions was seen to decrease at a much faster rate than for the lithium ions. Since the longitudinal values for each are relatively similar this suggests that the fluorine has a much more significant rotational component than the lithium, however it seems that both the lithium and fluorine both exhibit some rotation. It has been seen in previous research that the fluorinated anions have a greater rotational component than the lithium cations [57]. For the application of batteries it is essential that the lithium ions have a high translational component as they are the dense charge carriers and therefore dictate the conductivity of the liquid, therefore the stronger the translational component the higher the conductivity possible. These results are not designed to yield definitive answers for the rotational and translational contributions but rather give an indication of the presence of each and to merely state which was the stronger source of longitudinal relaxation. From the methods currently stated it seems that the lithium and hydrogen relaxation times are dominated by translational motion and the fluorine relaxation times are dominated by rotational motion.

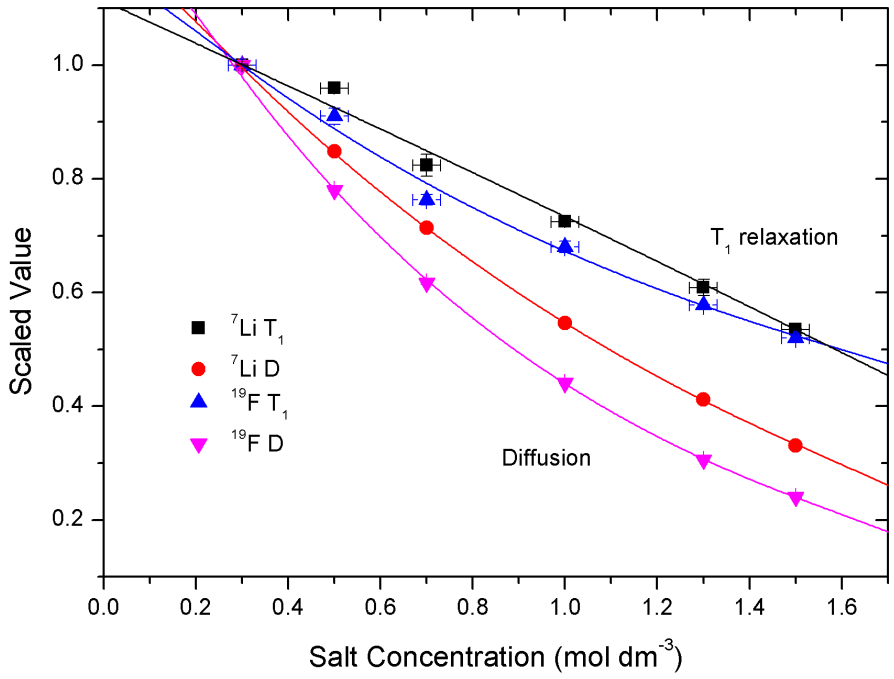

Figure 4.13: ^{7}Li and ^{19}F normalised diffusion and longitudinal relaxation for PC/$LiBF_4$ liquid electrolytes at 303 K.

Another approach to comparing the longitudinal relaxation with the diffusion constants was to take the natural log of both values and then produce a plot of them against one another. This would most likely produce a straight line and from this the gradient could give an indication of the relaxations translational motion contribution. If the relaxation times and diffusion behave exactly the same over a given temperature range then the gradient would be one, however if the value was less than unity then it is logical to assume that the discrepancy was caused by a rotational component. The ln(longitudinal relaxation) against ln(diffusion) plot is displayed in figure 4.14 for PC/$LiBF_4$ (1.0M) liquid electrolytes for the hydrogen (^{1}H), lithium (^{7}Li) and fluorine (^{19}F) nuclei. Figure 4.14 shows that the gradients of ln(T_1)-ln(D) were linear and therefore the gradient values were determined. From a simple observation of figure 4.14 it can be seen that the lithium and all four hydrogen peaks exhibit comparable gradients and the fluorine measurements exhibited a lower gradient. As previously stated from the other comparative measures it was believed that the hydrogen and lithium exhibited mainly translational motion, however fluorine was seen to be dominated by rotational motion.

The gradients of figure 4.14 were (0.62±0.03), (0.82±0.07), (0.66±0.05) and (0.78±0.01) for the hydrogen peaks 1-4, respectively, and (0.66±0.01) and (0.33±0.01) for the lithium and fluorine gradients, respectively. Firstly observing the hydrogen peaks it was seen that all had gradients <1 suggesting the presence of an intramolecular and intermolecular rotation. Based on this theory, the data suggests that peak 4 would have the smallest rotational component, however other previously stated results are contradictory. Therefore this implies that the difference in T_1 values from the different hydrogen sites of the PC molecule, are likely caused by different internuclear distances, rather than different rotational contributions. The important point is

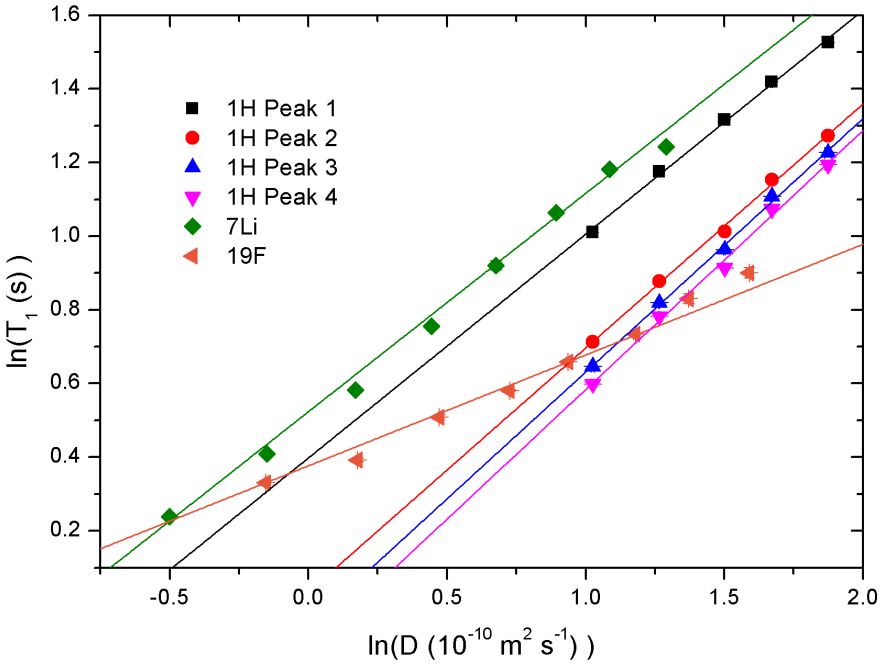

Figure 4.14: Natural log of longitudinal relaxation times against diffusion for PC/$LiBF_4$ (1.0M) liquid electrolyte using ^{1}H, ^{7}Li and ^{19}F nuclei.

that all peaks show a gradient which suggests a translational motion dominated system. The lithium gradient from figure 4.14 was 0.66±0.01. This value was quite similar to the hydrogen values suggesting again, that the lithium is dominated by translational motion. The fluorine measurements exhibited a gradient of 0.33±0.01 which was much lower than the hydrogen and lithium nuclei therefore suggesting that rotational motion dominated the longitudinal relaxation of the BF_4 ions. It was observed by Williamson *et al* that in a system containing tetraglyme (TG) with $LiCF_3SO_3$ gave gradients of 0.97, 0.46 and 0.51 for the ^{1}H, ^{7}Li and ^{19}F, respectively [57]. Therefore suggesting in their system the solvent molecules exhibited practically no rotational contribution where as the cation and anion were observed to exhibit a significant rotational contribution. Williamson *et al* also showed for $LiCF_3SO_3$ in DMF that the gradients gave 0.54, 1.04 and 0.43 for the ^{1}H, ^{7}Li and ^{19}F, respectively [57]. This result was quite different to the TG system, as in the DMF system the solvent molecules appeared to exhibited a significant intramolecular rotational contribution to the relaxation. Williamson *et al* attributed this difference to the presence of two methyl groups contained in each DMF molecule compared with the chain-like structure of the TG molecules. Therefore for the PC solvent molecules which contain a single methyl group in each molecule, it might be expected to observe an intramolecular rotational component between the TG and DMF molecules. This was in agreement with the average hydrogen gradient measured here of 0.72 which does fall between the two systems measured by Williamson *et al* [57].

The data in figure 4.14 were for a 1.0M liquid electrolyte, however there was likely a change in gradient with salt concentration. Table 4.16 shows the gradients of the ln(T_1) against ln(diffusion) for the hydrogen, lithium and fluorine nuclei for liquid electrolytes containing vari-

	Gradient of $ln(T_1)$-$ln(D)$					
Salt Concentration (M)	^{1}H				^{7}Li	^{19}F
	Peak 1	Peak 2	Peak 3	Peak 4		
0.0	0.66	0.78	0.95	0.80	—	—
0.3	0.79	0.93	0.87	0.87	0.87	0.47
0.5	0.94	0.88	0.85	0.92	0.73	0.51
0.7	0.88	0.85	0.84	0.95	0.75	0.45
1.0	0.62	0.82	0.66	0.78	0.66	0.33
1.3	0.73	0.84	0.85	0.90	0.59	0.38
1.5	0.71	0.69	0.63	0.78	0.60	0.39

Table 4.16: Gradient values of ln(T_1) against ln(diffusion) using ^{1}H (peaks 1-4), ^{7}Li and ^{19}F nuclei for PC / $LiBF_4$ liquid electrolytes.

ous amount of $LiBF_4$. The gradients for the four ^{1}H peaks of the PC molecule were seen to be roughly independent of salt concentration. However, it can be noted from this result was that the PC molecules were dominated by translational motion with a small rotational component. The lithium and fluorine exhibited a stronger trend with salt concentration than the hydrogen. At low salt concentrations (0.3M) the gradient yielded a value of 0.87 and 0.47 for the lithium and fluorine respectively. Remembering that a value of 1 would suggest a relaxation process that entirely depended on translational motion, a value of 0.87 for the lithium suggests that the relaxation was heavily dependent on translational motion however it seemed a rotational component was also present. The value of 0.47 for the BF_4 ions suggests that there was some translational motion, however was not the most significant contribution and therefore dominated by rotation. The gradient value was seen to fall with increasing salt concentration in both cases to 0.60 and 0.39 for the lithium and fluorine respectively, suggesting as the viscosity was increased the translational component of the T_1 relaxation was decreased and therefore the rotational component became more significant. Figure 4.15 shows the lithium and fluorine gradients with salt concentration, it can be seen that there was a definite negative gradient, however no quantitative values have been taken into consideration.

4.5 Longitudinal Relaxation Calculations

Using BPP theory [72] and the theories of Abragam [106] it is possible to calculate longitudinal relaxation for rotational molecular motion and also the relaxation caused by translational motion. The aim of this section was to calculate the contributions of rotation and translation where possible and then to compare these calculated components with the measured values of longitudinal relaxation times in order to observe the validity of the equations devised by Abragam and BPP theory.

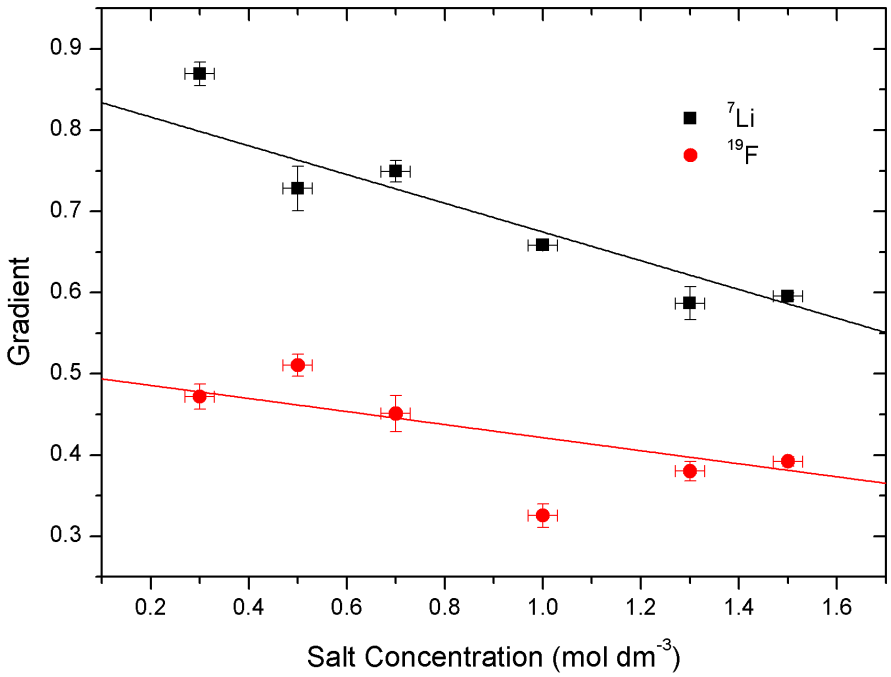

Figure 4.15: Gradient of $\ln(T_1)$-$\ln(D)$ plots as a function of salt concentration for PC/$LiBF_4$ liquid electrolyte using ^1H, ^7Li and ^{19}F nuclei.

4.5.1 Rotational Calculation

In order to derive the rotational component of the longitudinal relaxation, the auto-correlation function must first be determined. The rotation is thought of as random and therefore a random fluctuation function must be defined in the form;

$$\overline{f(t)} = \int p(y,t)f(y)dy \tag{4.11}$$

where $\overline{f(t)}$ which is a function based on $y(t)$ and $p(y,t)$ is the probability that the value of the function will be y at time t. As seen in Chapter 2 the correlation function takes the form;

$$G(t_1,t_2) = \overline{f(t_1)f^*(t_2)} \tag{4.12}$$

since the values are random but do show correlation only two times were used t_1 and t_2 where the function $p(y_1,t_1;y_2,t_2)$ is the probability of y taking the value y_1 at time t_1 and then taking value y_2 at time t_2. A second function is defined here which is the probability that y takes value y_2 at time t_2 when we know that the value of y was y_1 at t_2, this function is denoted $P(y_1,t_1;y_2,t_2)$ and the relationship between the probability function takes the form;

$$p(y_1,t_1;y_2,t_2) = P(y_1,t_1;y_2,t_2)p(y_1,t_1) \tag{4.13}$$

now by combining equations 4.11, 4.12 and 4.13 the auto-correlation function can take the general form;

$$G(t) = \int\int p(y_1,t_1)P(y_1,t_1\ ;y_2,t_2)f(y_1)f^*(y_2)dy_1dy_2 \tag{4.14}$$

where the function defines the random function $f(y)$ at times t_1 and t_2. Since the probability function $p(y,t)$ is time independent, there is only need to consider a difference in time rather than two separate times and therefore can be made in terms of τ where $\tau = t_2 - t_1$ in the form;

$$G(\tau) = \int\int p(y_1)P(y_1, y_2, \tau)f(y_1)f^*(y_2)dy_1dy_2 \tag{4.15}$$

where this is the complete general case for the auto-correlation function.

Now for a rotational case between two rotating molecules at angles θ and ϕ which define the in the case of hydrogen the proton-proton axis, where the direction of the axis is denoted Ω. The diffusion constant for rotation is given by the Stokes formula and is similar to the translational diffusion constant previously discussed and in the form;

$$D_{rot} = \frac{k_B T}{8\pi a^3 \eta} \tag{4.16}$$

where a is the radius of the molecule in a medium of viscosity η. Therefore we can now define the diffusion via the Debye diffusion equation which takes the form;

$$\frac{\delta\Psi(\Omega,t)}{\delta t} = D_{rot}\Delta_s\Psi(\Omega,t) \tag{4.17}$$

where D_{rot} is the rotational diffusion constant defined in equation 4.16. Abragam states that in order to solve equation 4.17 the probability that the axis of the two spins has the orientation of Ω at time t, when the value of Ω was Ω_0 at time zero. This probability function was determined from considerations of spherical harmonics, which is beyond the scope of this research and therefore was quoted as;

$$P(\Omega, \Omega_0, t) = \sum_{l,m} Y_l^{*m}(\Omega_0)Y_l^m(\Omega)exp\left[\frac{-t}{\tau_l}\right] \tag{4.18}$$

where $Y_l^{*m}(\Omega)$ is the normalised spherical harmonic. By using equations 4.15 and 4.18 and noting that the probability $p(\Omega_0)$ has the value of $1/4\pi$ the auto-correlation function becomes;

$$G(t) = \frac{1}{4\pi}\int\int F^*(\Omega)F(\Omega_0)Y_l^{*m}(\Omega_0)Y_l^m(\Omega)exp\left[\frac{-t}{\tau_l}\right]d\Omega d\Omega_0 \tag{4.19}$$

where random functions $F^{(1)}$ and $F^{(2)}$ are in terms of the spherical harmonics $Y_l^m(\Omega)$ by;

$$F^{(1)}(\Omega) = \frac{1}{b^6}\sqrt{\frac{8\pi}{15}Y_2^{(1)}(\Omega)};\ F^{(2)}(\Omega) = \frac{1}{b^6}\sqrt{\frac{32\pi}{15}Y_2^{(2)}(\Omega)} \tag{4.20}$$

where b is the distance between two neighboring spins and therefore the correlation functions $G^{(1)}(t)$ and $G^{(2)}(t)$ can be determined in the form;

$$G^{(1)}(t) = \frac{1}{b^6}\frac{2}{15}exp\left[\frac{-t}{\tau_c}\right];\ G^{(2)}(t) = \frac{1}{b^6}\frac{8}{15}exp\left[\frac{-t}{\tau_c}\right] \tag{4.21}$$

therefore by taking the Fourier transform of these correlation functions gives rise to the spectral density functions;

$$J_1(\omega) = \frac{1}{b^6}\frac{4}{15}\frac{\tau_c}{1+\omega^2\tau_c^2};\ J_2(\omega) = \frac{1}{b^6}\frac{16}{15}\frac{\tau_c}{1+\omega^2\tau_c^2} \tag{4.22}$$

where τ_c is the correlation time.

Remembering that the longitudinal relaxation takes the form of;

$$\frac{1}{T_1} = \frac{3}{2}\gamma^4\hbar^2 I\left(I+1\right)\left[J_1\left(\omega_0\right) + J_2\left(\omega_0\right)\right] \tag{4.23}$$

it can therefore stated via BPP theory that when two like spins are separated by a distance b and are in the high temperature (low correlation) side of the T_1 minimum, i.e. when $\omega_0\tau_c << 1$ then the rotational component is calculated from,

$$\left(\frac{1}{T_1}\right)_{rot} = \frac{2\gamma^4\hbar^2}{b^6} I(I+1)\tau_c \tag{4.24}$$

where τ_c is the correlation time and γ is the gyromagnetic ratio and I is the spin. The measurements are in the high temperature regime and therefore can use equation 4.24 to calculate the rotational contribution of the longitudinal relaxation times. BPP theory also shows that for spherical molecules in a liquid electrolyte, τ_c can be calculated using,

$$\tau_c = \frac{4\pi\eta a^3}{3kT} \tag{4.25}$$

where η is the viscosity and a is the effective radius of the molecules.

4.5.2 Translational Calculation

As with the rotational theory it is important to first define the correlation function. The correlation function will take the same form as equation 4.15 as this equation is the general form of the correlation function. It is again assumed that the diffusion equation will describe the motion of the molecules through solution. The diffusion equation which is similar in form to equation 4.17 the diffusion of rotation and is given by;

$$\frac{\delta\Psi(r,t)}{\delta t} = D\Delta\Psi(r,t) \tag{4.26}$$

where $\delta\Psi(\mathbf{r},0) = \delta(r-r_0)$ which is from classical diffusion theory which leads to;

$$\Psi(r,r_0,t) = (4\pi Dt)^{-\frac{3}{2}} exp\left[\frac{-(r-r_0)^2}{4Dt}\right] \tag{4.27}$$

where r represents the distance $(r_1 - r_2)$ between two identical spins then the probability of a spin being at location r at time t when it was known that the spins was at r_0 at time zero which is similar to equation 4.18 for the rotational case takes the form;

$$P(r,r_0,t) = (8\pi Dt)^{\frac{-3}{2}} exp\left[\frac{-(r-r_0)^2}{8Dt}\right] \tag{4.28}$$

where simply Dt was replaced with $2Dt$ in equation 4.27 in order to obtain the probability in equation 4.28. The auto-correlation function for the translational motion is given by;

$$G^{(m)}(t) = \alpha_m N(8\pi Dt)^{\frac{-3}{2}} \int\int \frac{Y_2^{(m)*}(\Omega_0)}{r_0^3}\frac{Y_2^{(m)}(\Omega)}{r^3} exp\left[\frac{-(r-r_0)^2}{8Dt}\right] d^3r_0 d^3r \tag{4.29}$$

where this equation describes the correlation function for all of the random functions $F^{(0)}$, $F^{(1)}$ and $F^{(2)}$ where the alpha values are given by;

$$\alpha^{(1)} = \frac{8\pi}{15},\ \alpha^{(2)} = \frac{32\pi}{15},\ \alpha^{(0)} = \frac{48\pi}{15} \tag{4.30}$$

therefore these factors can be used to switch between random fluctuations and also later spectral densities. In order to determine the spectral densities, firstly a Fourier expansion and transform must be applied; these steps have been omitted as they are above the scope of this research. However, there are limitations to the values that r can take because in this model, it was assumed that the molecules behave as hard spheres and therefore the closest approach of these molecules would be equal to $2r$ which is the diameter of the molecules denoted d. The spectral density was given by;

$$J(\omega) = J(0) = \frac{2}{15}\frac{N}{dD} \tag{4.31}$$

where this has been simplified by assuming that again the system is in the low correlation times (high temperature) side of the T_1 minimum where $\omega_0\tau_c << 1$. Therefore by using equations 4.23 and 4.31 the translational component of the longitudinal relaxation time[106] is given by,

$$\left(\frac{1}{T_1}\right)_{trans} = \frac{3}{2}\gamma^4\hbar^2 I\left(I+1\right)\left[J_1\left(\omega_0\right) + J_2\left(\omega_0\right)\right], \tag{4.32}$$

where

$$J_1\left(\omega_0\right) = \alpha^{(1)}J(0) = \frac{8\pi}{15}\left(\frac{2N}{15dD}\right);\ J_2\left(\omega_0\right) = \alpha^{(2)}J(0) = \frac{32\pi}{15}\left(\frac{2N}{15dD}\right), \tag{4.33}$$

where d is the distance of closest approach of two species which for a spherical molecule system would be $2a$ with self diffusion coefficient D and N spins per unit volume. Therefore using equations 4.32 and 4.33 the translational longitudinal relaxation time can be determined by

$$\left(\frac{1}{T_1}\right)_{trans} = \frac{4\pi}{15}\frac{N\gamma^4\hbar^2}{aD}I(I+1) \tag{4.34}$$

therefore this allows calculation of the intermolecular translational component of the longitudinal relaxation.

4.5.3 Calculation of fluorine relaxation values due to rotational and translational motion

The rotational component can be calculated using equation 4.24 and 4.25. The effective radius (a) was calculated using the bulk viscosity and diffusion constants along with the Stokes-Einstein equation; the ionic radius calculations will be addressed in detail in Chapter 7. The value of b for the inter-fluorine distance was 2.25 Å, this value which was determined from the geometry of a perfect tetrahedron[107] with a Li-F bond length of 1.4 Å[108]. Fluorine is a spin-1/2 (I=1/2) nucleus and therefore equation 4.24 can be reduced to;

$$\left(\frac{1}{T_1}\right)_{rot} = \frac{3}{2}\frac{\gamma^4\hbar^2}{b^6}\tau_c \tag{4.35}$$

where γ was the gyromagnetic ratio and for fluorine takes a value of 251.7×10^6 rad s^{-1} T^{-1} which is a well defined constant.

The translational component of the longitudinal relaxation was calculated , since the fluorine nuclei are spin 1/2 (I=1/2) using equation 4.34 the translational longitudinal relaxation time can be determined by;

$$\left(\frac{1}{T_1}\right)_{trans} = \frac{\pi}{5}\frac{N\gamma^4\hbar^2}{aD} \tag{4.36}$$

	Calculated			Measured
Salt Concentration (M)	T_1^{Trans} (s)	T_1^{Rot} (s)	T_1^{Total} (s)	T_1 (s)
0.3	20.59	8.42	5.97	2.44
0.5	10.32	5.73	3.68	2.22
0.7	6.16	4.05	2.45	1.87
1.0	2.98	3.10	1.52	1.66
1.3	1.71	1.85	0.89	1.41
1.5	1.16	1.47	0.65	1.27

Table 4.17: ^{19}F calculated translational, rotational and total longitudinal relaxations for PC/$LiBF_4$ liquid electrolytes. The measured T_1 are also included. All data calculated and measured at 303 K.

where the number of fluorines per unit volume N. The equation for the number of spins per unit volume N was given by;

$$N = \frac{N_{19F}\rho N_A}{M_W} \tag{4.37}$$

where N_{19F} is the number of fluorine ions per molecule, ρ_{LiBF_4} is the density of the $LiBF_4$ with a molecular weight M_W and N_A is Avagadros number. The number of fluorine atoms per $LiBF_4$ molecule was N_{19F}=4, the density of $LiBF_4$ was measured as 1.60 g cm^{-3} and has a molecular weight of 93.75 g mol^{-1}. The effective radii a was calculated using the Stokes-Einstein equation which required the knowledge of the viscosity (η) and diffusion constant (D) at an absolute temperature T. The viscosity data has been measured and will be displayed in Chapter 7.

When there are multiple relaxation mechanisms causing the longitudinal relaxation the rates can be simply added together, the rates of each mechanism are the reciprocal of the relaxation times. If the longitudinal relaxation times contain contributions from both translational and rotational motion then the total relaxation time T_1^{Total} is given by;

$$\frac{1}{T_1^{Total}} = \frac{1}{T_1^{Trans}} + \frac{1}{T_1^{Rot}} \tag{4.38}$$

where T_1^{Trans} and T_1^{Rot} are the longitudinal relaxation times for the translational and rotational contributions, respectively.

Table 4.17 shows the calculated longitudinal relaxation times for the translational and rotational contributions, the total calculated relaxation time and the measured relaxation time for PC/$LiBF_4$ liquid electrolytes using the ^{19}F nucleus. In the previous sections it has been discussed that it is believed that the fluorine species are being dominated by rotational rather than translational motion. It can be seen from table 4.17 that at low salt concentrations the measured T_1 values are around a quarter of the calculated rotational relaxation time. As the salt concentration is increased the calculated rotational component and the measured T_1 value converge. This result is within good agreement with figure 4.15 which shows that the gradient of the lnT_1 against lnD decreases at high salt concentration suggesting a higher contribution from the rotational component.

The calculated translational component of the fluorine T_1 was seen generally to be much higher than the rotational component. Since the rate of decay is defined as the reciprocal of

	Calculated	Measured
Salt Concentration (M)	T_1^{Trans} (s)	T_1 (s)
0.0	6.22	2.92
0.3	4.66	2.32
0.5	3.89	2.45
0.7	3.26	1.94
1.0	2.25	1.67
1.3	1.68	1.24
1.5	1.31	1.45

Table 4.18: ^{1}H calculated translational and measured NMR longitudinal relaxation for the PC/$LiBF_4$ liquid electrolytes. The measured T_1 have been taken as a weighted average of the four peaks. All data calculated and measured at 303 K.

the relaxation time the larger the value of T_1 the slower the rate of decay therefore suggesting a stronger rotational component because the rotational motion decays at a much faster rate than the translational motion. The total calculated T_1 has also been shown in table 4.17. The values of the total calculated T_1 are surprisingly close to the measured values considering the number of assumptions made in these calculations. The fact that the translational values are much higher at lower concentrations results in the rotational contribution being the more significant in the calculation of the total relaxation time.

4.5.4 Calculation of hydrogen relaxation values for translational motion

In this section the hydrogen translational component is calculated using equation 4.36. The number of spins per unit volume N was calculated for hydrogen using equation 4.37 where the value of N_{1H} was 6 per PC molecule with a density of 1.21 g cm^{-3} at room temperature and molecular weight of 102.09 g mol^{-1}.

In previous sections, the lithium and hydrogen species were seen to exhibit signs of a dominant translational component of the longitudinal relaxation with a rotational contribution which was deemed much weaker. Table 4.18 shows the calculated translational component determined using equation 4.36. The results for the calculated translational component were observed to be of the same magnitude of the measured values, which are considered reasonably close considering the number of assumptions made in these calculations. For instance the bulk viscosity (used in the calculation of the radius (a)) was used along with the micro-diffusion so there is some argument that these values should not be used in calculations together; however, for a comparison it was assumed adequate since the absolute calculated values have the purpose of checking theory rather than obtaining accurate results. Therefore equations 4.24 and 4.36 as proposed by Abragam can be considered to predict good first estimates for the translational and rotational components, respectively. The measured T_1 values in table 4.18 have been taken as a weighted average of the four peaks.

When using the equations to calculate the translational and rotational contributions of the

longitudinal relaxation it should be noted that the rotational component of the T_1 is dominated by the viscosity of the system and the translational component is dominated by diffusion. However there is likely overlap between these two and it remains true that the translational component is not independent of viscosity, nor is the rotational component independent of the diffusion measurements.

4.6 Conclusions

In this chapter nuclear magnetic resonance has been used to understand the mobility and dynamics of molecules in a liquid electrolyte. The liquid electrolytes used contained propylene carbonate with $LiBF_4$ at various concentrations. It was possible using different resonant frequencies to isolate single nuclei. The three nuclei used here include hydrogen (^{1}H), lithium (^{7}Li) and fluorine (^{19}F) which were used in order to track the solvent molecule, cation and anion (BF_4^-), respectively. Three different spectrometers were used in this chapter which included a 50 MHz, 400 MHz and 500 MHz machines where the frequency of the spectrometer refers to the resonant frequency of the ^{1}H nucleus at that magnetic field strength.

The longitudinal and transverse relaxation times were measured on the 50MHz NMR spectrometer using the ^{1}H nucleus. This spectrometer was a bench top Maran NMR machine and did not have the capability to change the nucleus and only hydrogen measurements could be measured. Measurements were made in the temperature range of 253-333 K. It was observed that the values of the longitudinal (T_1) and transverse (T_2) relaxation times were very similar, suggesting that the system was in the low correlation time (high temperature) side of the T_1 minimum.

The values of T_1 and T_2 increase with increasing temperature, which was attributed to a shift in the correlation time to lower times (i.e. tumbling faster) as the correlation time is inversely proportional to the temperature of the system. Therefore as the temperature was increased the system moved away from the minimum making the relaxation less efficient. It was determined that the mechanism was non-Arrhenius and in this case used the VTF equation to fit the data.

The relaxation times were seen to decrease with salt concentration, this was attributed to moving the system closer to the T_1 minimum as the correlation time is directly proportional to the viscosity of the system. Therefore if the viscosity rises then so will the correlation time which physically means that the molecule was tumbling at a slower rate and is shifted more towards the resonant frequency of the nucleus and has a more efficient relaxation.

Longitudinal relaxation times were also measured for the lithium (^{7}Li) and fluorine (^{19}F) nuclei, however since the bench top spectrometer could not measure different nuclei a high field 400MHz Bruker AVANCE Ultrashield was used for these measurements. The same trends were seen as with the hydrogen; they increase with temperature and decrease with salt concentration, the same logic was applied to explain these trends. However, where the hydrogen relaxation times exhibited VTF temperature dependence, these measurements exhibited Arrhenius type temperature dependence, this was attributed by the much smaller range of temperatures available when measuring on the high field spectrometer. The activation energies were seen to increase with salt concentration which was attributed to the increase in viscosity. It was noted that the activation energy of the T_1 values for the lithium ions were much higher than the corresponding

fluorine ions, suggesting that the lithium ions had a larger translational component than the fluorine ions, as translational activation energies are usually higher than that for rotational motion.

On the same 400MHz spectrometer, translational diffusion constants were measured for the hydrogen, lithium and fluorine nuclei at various temperatures and salt concentrations. These were measured by using pulsed-field gradient NMR (PFG-NMR). The diffusion constants were observed to increase with temperature due to the increased thermal energy and lowered viscosity. The diffusion constants were seen to decrease with increasing salt concentration, this was attributed to simply a rise in the viscosity of the system resulting in a slower diffusion of the molecules. The three nuclei exhibited the same trends with temperature and salt concentration, the order of diffusion of the nuclei was $D_{^1H} > D_{^{19}F} > D_{^7Li}$, suggesting a rough size order of the molecules containing each of these nuclei as they all experience the same bulk viscosity. This result yields that the lithium ions had the largest effective radii, followed by fluorine, with the smallest radii belonging to the hydrogen molecules. Due to lithiums small ion size, this was attributed to a large solvation shell of PC molecules.

The temperature dependence of the diffusion measurements was observed to be Arrhenius, similar to the longitudinal relaxation of the lithium and fluorine measured on the 400MHz spectrometer due to the limited temperature range available on the high field spectrometer. For all nuclei the activation energies were seen to increase with salt concentration which was attributed to the molecules needing more energy to diffuse in a higher viscosity medium. The activation energies of the diffusion were seen to be much higher than the longitudinal relaxation time energies, this was attributed to the presence of another relaxation process other than for translational motion. If the relaxation and diffusion activation energies were the same then it would be logical to assume that the relaxation was solely due to translational motion. The lithium relaxation was observed to be dominated by translational motion and the fluorine relaxation was dominated by rotational motion.

The diffusion was seen to fall exponentially with increasing salt concentration which was attributed to the rise in viscosity, however at each temperature the concentration decay of the diffusion was fitted with a simple exponential and the decay factor denoted A_D was determined for each nucleus at varying temperature. It was observed that the A_D values for each nuclei followed the general trend, ^{1}H>^{7}Li>^{19}F, where a larger value of A_D would result in a slower rate of decay with salt concentration. Therefore it was noted that the fluorine reduced much faster with salt concentration than the other two nuclei. If the viscosity was the sole reason for reduction of diffusion then this A_D factor would be equal for all nuclei, it was observed that the lithium and hydrogen values were quite similar. The reduced fluorine factor was attributed to a change in effective radius with salt concentration, most likely the anions containing fluorine are associating with the lithium structures. On observing the diffusion constants it was seen that the lithium and fluorine values converged at high salt concentrations which supports this hypothesis.

High field longitudinal relaxation measurements were also taken. The spectrum was seen to exhibit four different peaks relating to the different bonds of the PC molecule. The diffusion was determined for each peak and was found to be the same for all peaks, suggesting that they are indeed part of the same molecule and will therefore diffuse at the same rate. Each peak displayed

a different value for the longitudinal relaxation, since all peaks were diffusing at the same rate they would all have the same intermolecular translational contribution to the relaxation and could therefore be due to different rotational components. An alternative explanation is that each hydrogen site on the PC molecule experienced a different relaxation time due to anisotropic reorientation of the PC molecule.

The longitudinal relaxation has also been calculated, and was shown by using Abragam and BPP theory that it was possible to obtain reasonable estimations of the longitudinal relaxations for the rotational and translational motion. For the fluorine, the translational and rotational contributions were determined and for the hydrogen the translational relaxation time was calculated. The rotational contribution of the relaxation for the hydrogen nucleus was difficult to calculate as the distance between like spins was required, as each part of the spectrum would require a different distance. The lithium relaxation was not calculated due to a lack of information required. However the calculated values of longitudinal relaxation for the fluorine and hydrogen nuclei gave the same order of magnitude as the corresponding calculated values, which converged at higher salt concentrations.

Chapter 5

Polymer Gel Electrolyte NMR

5.1 Introduction

In Chapter 4, nuclear magnetic resonance was used to probe the dynamics of the PC/$LiBF_4$ liquid electrolytes. In this chapter, the NMR results for the polymer gel electrolytes based on poly(vinylidene) fluoride (PVDF), propylene carbonate and $LiBF_4$ are presented and discussed. It is logical to first consider the liquid electrolytes as the essential factors determining ionic mobility and hence dynamics of the polymer gel electrolytes are closely related to those shown by the corresponding liquid electrolytes which form the solvent phase in the gel. Two different polymer concentrations have been investigated here, 20% and 30% PVDF as a mass fraction of the solvent. The polymer gel electrolytes must have sufficient amount of polymer to have the desired mechanical properties but not too much that the transport properties are hindered. It was found that any less than 20% polymer resulted in a polymer gel electrolyte which was not fully formed and lacked mechanical stability. A 40% polymer gel electrolyte was found to be too brittle and was not easily manuipulated, therefore could not be easily mounted in the NMR tubes. Therefore 20% and 30% gels were made at various salt concentrations. The liquid electrolytes in the previous chapter contained 0.0-1.5M of $LiBF_4$ in PC, however now with the introduction of the polymer there was a competition between the salt and polymer in the solvation process. The amount of salt that can be used here was determined by a trial and error process. It was found that for the 20% PVDF gels 1.1M of $LiBF_4$ could be dissolved, however in the 30% gels only 1.0M of $LiBF_4$ could be dissolved. The lower limit for the salt concentration was set as 0.0M, 0.3M and 0.1M for the hydrogen (^{1}H), lithium (^{7}Li) and fluorine (^{19}F) measurements, respectively. The hydrogen was the most abundant element in the samples and therefore was easily detected at all salt concentrations. The lithium and fluorine were clearly present only in the salt and therefore 0.1M was the least possible in order to get a signal for the NMR spectrum. However in the case of the lithium the signal to noise ratio (SNR) was too low to obtain decent results and therefore not taken. The gyromagnetic ratios of the three nuclei used were $(42.576, 16.546, 40.053)$ MHz T^{-1} for the ^{1}H, ^{7}Li and ^{19}F, respectively. Therefore the lower gyromagnetic ratio made the SNR smaller for the lithium than the fluorine measurements and therefore the smallest salt concentration used was 0.3M for the lithium measurements.

Two spectrometers were used for the polymer gel electrolyte measurements, the low field

50 MHz bench top spectrometer and the 400 MHz high field spectrometer. The low field machine was used to measure the longitudinal and transverse relaxation times of the gels, however as stated previously this spectrometer can only measure spectra using the ^{1}H resonant frequency. In the case of the liquid electrolytes, this would only detect the various sites on the PC molecule, however PVDF also contains two hydrogen ions per monomer. Since the vast majority of these gels were made up of the solvent the most significant signal would be from the solvent molecules.

The 400 MHz spectrometer was used in order to measure the longitudinal and transverse relaxation times as well as the translational diffusion of the molecules using the ^{1}H, ^{7}Li and ^{19}F nuclei which were used in order to detect the solvent molecules, lithium cation and fluorinated BF_4^- anion, respectively.

This chapter will frequently revert back to the results from Chapter 4 in order to compare the polymer gel electrolytes with the liquid electrolytes. This will prove to be a useful tool as it known that during the phase separation of the gels there are parts that are entirely liquid (i.e. liquid electrolyte as described in the Chapter 4), areas of crystalline polymer and amorphous regions of polymer mixed with liquid (i.e. an intermediary phase), which will be discussed at some length in this chapter. It has been revealed by a mixture of T_2 and $T_{1\rho}$ measurements that there are at least three phases contained within these semi-crystalline thermo-reversible gels. It has been shown by Hubbard *et al* [18; 34] that the use of NMR $T_{1\rho}$ measurements that PVDF based polymer gel electrolytes contain four distinct phases. These phases were attributed to the crystalline PVDF (very short times), an interlamellar amorphous PVDF, solvated chains of PVDF (intermediate times) and a pure solvent component (long times).

5.1.1 Sample Preparation

The gels were produced using the technique detailed in Chapter 3, the NMR tubes were 10 mm in diameter and therefore fairly narrow. When dealing with the liquid electrolyte, the samples were merely pipetted into the tubes, however with the gels it was necessary to choose a mounting procedure that did not change the sample homogeneity significantly. The gels were considered to be mechanically stable, however if the gels were squeezed with any significant force then they expel liquid which would change the composition of the gel and thus introduce discrepancies into the data. A few different techniques of mounting were addressed in this thesis. Once the gel has been produced it can be cut into the desired shape in order to fit down the 10 mm tube; the sample preparation tubes were much larger than the 10 mm tubes as the gels needed to be stirred. It was visibly noticeable that when the gel was being cut, a lot of liquid was being expelled, therefore this method was disregarded due to solvent/liquid electrolyte loss.

The second method was to use a hot press which consisted of two hot steel plates with spacers of varying thickness which were used to obtain the desired thickness of the sample, in this case slightly less than 10 mm. There were two issues with this process; firstly, the gel still needed to be cut as the thickness was correct but the width needed to be less than 10 mm as the glass tubes were cylindrical which would again cause loss in solvent. Secondly, the actual pressing technique caused a noticeable loss in solvent in the form of significant amount of liquids left on the plates. Therefore this process was again considered unsuitable for use in the mounting of the gels.

The third and final technique, which was used here, involved manipulation of the polymer

gel electrolytes when they are above their melting temperatures and are able to flow. After the heating process a small amount of gel was separated from the bulk sample and allowed to cool. However while the gel was cooling it was possible to shape the gel into the thickness and size that was needed for the 10 mm tube diameter. This was carried out on a steel surface which was vigorously cleaned in between sample production, using a clean spatula to shape the gel. This method proved very useful in mounting the gels for the NMR experiments as very little solvent was expelled from the gel as shaping the gel while not fully cooled resulted in no noticeable loss of solvent. The gel was then carefully placed inside the glass tube and sealed while in the nitrogen filled glove box to avoid any moisture being present in the sample.

5.2 Transverse Relaxation

5.2.1 Hydrogen Measurements

Both longitudinal and transverse relaxation times have been measured using the bench top Maran 50 MHz spectrometer for the hydrogen (^{1}H) nucleus. Unlike the liquid case now there are multiple sites that the hydrogen can be involved, including the PC solvent molecule, polymer backbone and also an intermediary stage involving the amorphous regions of the polymer and the solvent. The transverse relaxation times were useful in determining the number of different phases within the polymer gel electrolytes.

The low field spectrometer does not allow much user interface with regards to the spectra, therefore the total spectra was taken automatically by the computer and analysed. The purpose of measuring the transverse relaxation times was to attempt to understand the number of phases present in the polymer gel electrolytes and to quantify the significance of each constituent.

The transverse relaxation times were measured using the CPMG pulse sequence [75; 76] previously described in Chapter 2. This pulse sequence involves the use of an initial excitation pulse which drives the net magnetisation into the measurable xy plane, where the spins start to dephase and hence relax. After a time τ an inversion pulse was used to flip the system causing the spins to re-focus and undo any effect on the relaxation caused by field inhomogeneities. This is known as a spin echo and here large numbers of echoes were used of the order of 1000. The decay of the magnetisation from the measurable xy plane back to the z-axis can be determined from;

$$M_{xy}(t) = M_{xy}(0)exp\left[\frac{-t}{T_2}\right] \tag{5.1}$$

where $M_{xy}(t)$ is the magnetisation in the xy plane as a function of time and $M_{xy}(0)$ is the magnetisation in the xy plane immediately after the excitation which is defined as time zero. As previously shown in Chapter 4 when the transverse relaxation times were measured for the liquid electrolyte systems the T_2 decay curves were very well described by equation 5.1. However when it came to the polymer gel electrolytes equation 5.1 was not sufficient to fit the data. Therefore this suggested that there was more than one phase present in the polymer gel electrolytes. In order to investigate this further the decay curves were fitted with equation 5.1 which will be referred to as '1 *parameter fit*' as well as equations with series of exponentials in the form;

$$M_{xy}(t) = M_{xy}^{(1)}(0)exp\left[\frac{-t}{T_2^{(1)}}\right] + M_{xy}^{(2)}(0)exp\left[\frac{-t}{T_2^{(2)}}\right] \tag{5.2}$$

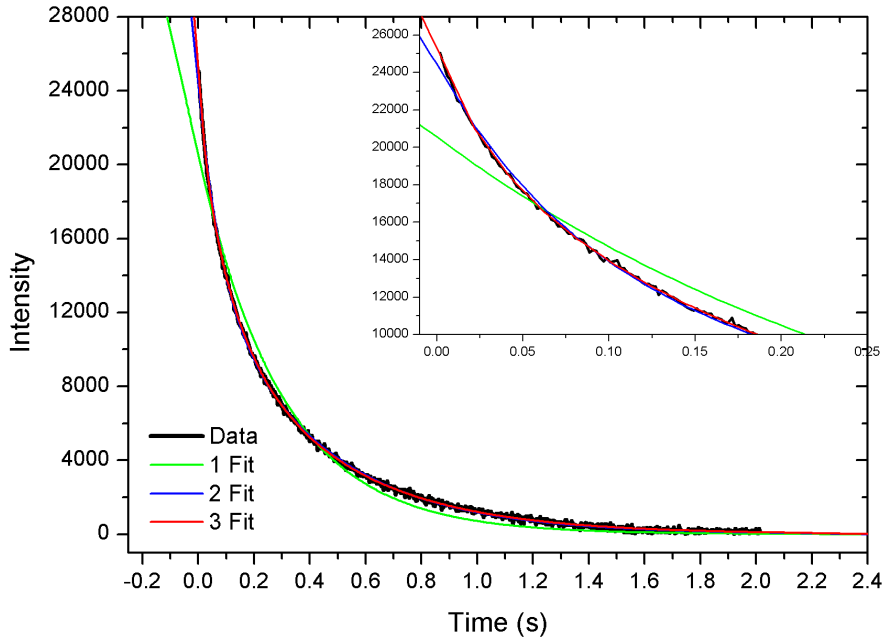

Figure 5.1: T_2 decay curve for a 20% PVDF/PC/LiBF$_4$ (0.5M) polymer gel electrolyte at 293 K. Inset shows zoomed view of graph for very short times between 0-250 ms.

	$T_2^{(1)}$ (ms)	$T_2^{(2)}$ (ms)	$T_2^{(3)}$ (ms)	I_1	I_2	I_3
one parameter fit	297	—	—	1.00	—	—
two parameter fit	399	76	—	0.59	0.41	—
three parameter fit	419	107	22	0.52	0.36	0.13

Table 5.1: Summary of fitting procedure of the hydrogen transverse relaxation decay for 20% PVDF/PC/LiBF$_4$ (0.5M) polymer gel electrolyte at 293 K. Where the (1), (2) and (3) refers to the liquid, amorphous polymer and interlamellar amorphous polymer phases, respectively.

and

$$M_{xy}(t) = M_{xy}^{(1)}(0)exp\left[\frac{-t}{T_2^{(1)}}\right] + M_{xy}^{(2)}(0)exp\left[\frac{-t}{T_2^{(2)}}\right] + M_{xy}^{(3)}(0)exp\left[\frac{-t}{T_2^{(3)}}\right] \tag{5.3}$$

where each additional exponential term added on in series represents a phase in the polymer gel electrolyte, where the $M_{xy}^{(1)}(0)$, $M_{xy}^{(2)}(0)$ and $M_{xy}^{(3)}(0)$ are the intensities of the decay for each phase denoted simply 1-3 for the time being all with corresponding transverse relaxation times $T_2^{(1)}$, $T_2^{(2)}$ and $T_2^{(3)}$, respectively.

The computer used to measure the NMR data on the 50 MHz spectrometer was not equipped with the facilities to fit more than one exponential to the transverse relaxation decay curve. Therefore the data was extracted, transfered to another computer, and analysed using OriginPro8.5 computer software. The fitting procedure used by this program is an iterative process based on the least squares fit using the Levenberg Marquardt algorithm (LMA)[78; 79]. The LMA allows fitting of curves even with initial guesses which are not very close to the final result.

The transverse relaxation decay curve for a 20% PVDF/PC/LiBF$_4$ (0.5M) polymer gel elec-

trolyte is shown in figure 5.1. The decay curve was fitted using equations 5.1, 5.2 and 5.3 which are refered to as the one parameter fit, two parameter fit and three parameter fit, respectively. The single parameter fit (green line) was shown to be insufficient to fit the data and therefore required more phases to explain the decay. The two parameter fit (blue line) was shown to greatly improve the fit of the data, suggesting two unique phases contributing to the transverse relaxation. However equation 5.2 failed to explain the result for very short times as the two parameter fit deviated from the data. Therefore a three parameter fit (red line) was employed which was seen to fit the very short times of the decay. The inset of figure 5.1 shows the data at very short times between 0-250 ms in order to highlight the difference between the two and three parameter fits at short times. The result of the single parameter fit was a tranvserse relaxation time of (297±2) ms, which was not considered to be relevant due to the poor fit of the data using a single parameter. The result of two parameter fit gave (76±2) ms and (399±2) ms with intensities of (0.41±0.03) and (0.59±0.03), respectively. The intensities here have been normalised so that they add together to give 1. The three parameter fit gave transverse relaxation times of (22±2) ms, (107±3) ms and (419±2) ms with intensities of (0.13±0.04), (0.36±0.03) and (0.52±0.03), respectively. In Chapter 1 it was stated that the polymer gel electrolytes are comprised of spherulites which are made up of crystalline lamellae connected by amorphous polymer chains. These spherulites pack together to create the polymer network and are held together with amorphous chains. Between these spherulites exist cavities which are entirely filled with liquid electrolyte. The three phases were therefore attributed to the inter lamellar PVDF phase of the spherulites, an amorphous PVDF phase which is solvated by PC molecules and a pure liquid electrolyte phase, as observed by Hubbard *et al* [34]. The T_2 for crystalline PVDF is typically around 20 μs [109] which is three orders of magnitude lower than the shortest time observed. Therefore it was assumed that the crystalline PVDF phase was not observed in these measurements. The crystalline phase is certainly present, however the very short times can not be fitted as the long liquid T_2 values over power the short crystalline times. The polymer gel electyrolytes formed here are only 20% and 30% polymer of which only a proportion will be crystalline and therefore contributes to the difficulty in detecting the crystalline lamellae.

From observing the transverse relaxation dependence on the correlation time it can be noted that as the viscosity was increased the correlation time would increase causing a lower T_2. Therefore the mid range T_2 of (107±3) ms was attributed to the solvated amorphous polymer phase, with the (419±2) ms T_2 referring to the liquid phase. The fitting parameters have been summarised in table 5.1. From the intensities it can be seen that the short interlamellar polymer phase was responsible for around 13% of the signal, the amorphous polymer region was responsible for 36% and the liquid electrolyte phase was around 52% of the signal. These values were considered reasonable since there was only 20% PVDF by mass contained in the gels. The amorphous phase was most likely comprised of amorphous polymer mixed with liquid electrolyte which would explain the 36% signal from this region and therefore the polymer was assumed to be solvated by the solvent molecules. As previously mentioned PVDF based gels have been observed to exhibit multiple phases including a crystalline PVDF, interlamellar amorphous phase, a solvated amorphous and pure liquid electrolyte phase [18; 34]. Therefore the transverse relaxation times have revealed in this thesis that all phases were observed except the crystalline PVDF phase. The effect of the amorphous polymer was to increase the viscosity of that phase

	$T_2^{(1)}$ (ms)	$T_2^{(2)}$ (ms)	$T_2^{(3)}$ (ms)	I_1	I_2	I_3
one parameter fit	173	—	—	1.00	—	—
two parameter fit	255	41	—	0.51	0.49	—
three parameter fit	263	49	5.1	0.44	0.42	0.14

Table 5.2: Summary of fitting procedure of the hydrogen transverse relaxation decay for 30% PVDF/PC/$LiBF_4$ (0.5M) polymer gel electrolyte at 293 K. Where the (1), (2) and (3) refers to the liquid, amorphous polymer and interlamellar amorphous polymer phases, respectively.

compared to the liquid electrolyte phase therefore reducing the transverse relaxation times due to an increased correlation time. Since the liquid electrolyte comprised 80% by mass of the sample the 52% contribution was not surprising, especially since some of the liquid electrolyte was assumed to be mixed with the intermediary amorphous polymer phase.

A system containing PVDF-HFP with EC:DEC (2:3) and $LiN(CF_3SO_2)_2$ has been studied by Capiglia *et al* in which they changed the solvent to polymer ratio and measured the ionic conductivity and PFG diffusion [26; 110]. They revealed for a 50:50 polymer:solvent ratio that there were no visible pores via scanning electron microscopy (SEM), however with an increase in solvent to 40:60 cavities started to occur around the micrometer size. By the time they had reached a polymer:solvent ratio of 30:70 there were pores with an average diameter of 10 μm [26; 110]. Their conclusions were that at high solvent content the gels exhibited interconnected cavities which were purely liquid. They also determined that there was a significant uptake of liquid into the amorphous region of the polymer. Research from a different group working on similar gels containing PVDF-HFP with EC found that the cavities of pure solvent were not present until around 60% EC, they found that the porosity ranged from 23% up to 68% with the increase of solvent content [27]. Therefore the polymer gel electrolytes here are for polymer:solvent ratios of 30:70 and 20:80 and since these are well above the 50:50 ratio it is reasonable to assume that there are large interconnecting cavities.

The transverse relaxation measurements gave a good indication of the number of phases present in the system as well as a rough estimate of the contribution of each phase. Both T_2 and $T_{1\rho}$ techniques have been applied to different polymer gel electrolytes in order to determine the relevant phases of the gel electrolytes [25; 54]. It was observed in previous studies at the University of Leeds by Ward *et al* [54] that for a gel containing PVDF/DMF/$LiCF_3SO_3$ the T_2 values were observed to yield 48 ms and 209 ms, with a corresponding liquid measurement of 348 ms. The longest time of 209 ms was attributed to the liquid phase of the polymer gel electrolyte and was observed to yield an intensity of around 64% [54].

Figure 5.2 shows the T_2 decay curve for a 30% PVDF/PC/$LiBF_4$ (0.5M) polymer gel electrolyte at 293 K which has had the same three fitting procedures employed as just shown in figure 5.1. It was observed that the single parameter fit was not sufficient and with the aid of the inset of figure 5.2, that the two parameter fit did not fit the very short times of the T_2 decay curve. It is logical to assume that the three phases present in the 20% PVDF polymer gel electrolytes would also be present in the 30% PVDF gels. The single fit here produced a transverse relaxation time of (173±2) ms which is lower than the equivalent value of (297±2) ms for the 20% PVDF gel. The two parameter fit produced relaxation times of (41±1) ms and (255±2) ms

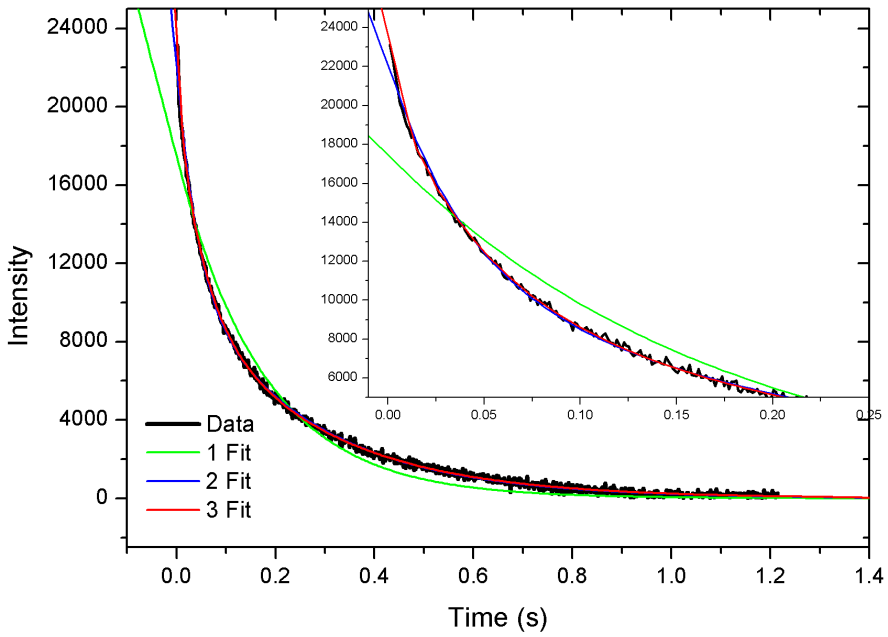

Figure 5.2: T_2 decay curve for a 30% PVDF/PC/$LiBF_4$ (0.5M) polymer gel electrolyte at 293 K. Inset shows zoomed view of graph for very short times between 0-250 ms.

with intensities of (0.493±0.003) and (0.507±0.003), respectively. These relaxations were both significantly lower than that for the 20% PVDF gels, this has been attributed to a rise in the viscosity of the system causing a higher correlation time of the molecules. The three parameter fit yielded relaxation times of (5.1±0.5) ms, (49±1) ms and (263±2) ms with intensities of (0.138±0.008), (0.422±0.004) and (0.440±0.004), respectively. Again these values of relaxation are much lower than the 20% PVDF gels suggesting a higher viscosity of each of the phases. The constituents of the 30% PVDF gels were observed to be around 14% for the interlamellar PVDF phase, 42% for the solvated amorphous phase and 44% for the pure liquid electrolyte phase. Therefore an increase in polymer concentration resulted in an increase of the two polymer phases and a reduction in the pure liquid electrolyte phase. This result was reasonable as it has been observed elsewhere that introducing more polymer into the system would result in smaller pores and cavities of liquid [27]. The fitting parameters from figure 5.2 are summarised in table 5.2.

Since the shortest T_2 value attributed to the interlamellar PVDF phase was usually less than 50 ms, it was quite difficult to determine as the signal decays within the first few points of the decay curve. However observing the results above it seems that in the two parameter fit and the three parameter fit the values for the intermediate phase and the liquid phase were comparable. The next stage was to observe the temperature dependence of each of the phases, this is shown in figure 5.3 for a 20% PVDF/PC/$LiBF_4$ (0.0M) (unsalted) polymer gel electrolyte. Here the data was denoted short T_2, intermediate T_2 and long T_2 which refer to the interlamellar, amorphous phase and the pure liquid electrolyte phase, respectively. It can be noted from figure 5.3 that the transverse relaxation times of all phases were seen to increase with temperature. Since there is no minimum present for the T_2 relaxation times an increase in temperature has the effect of

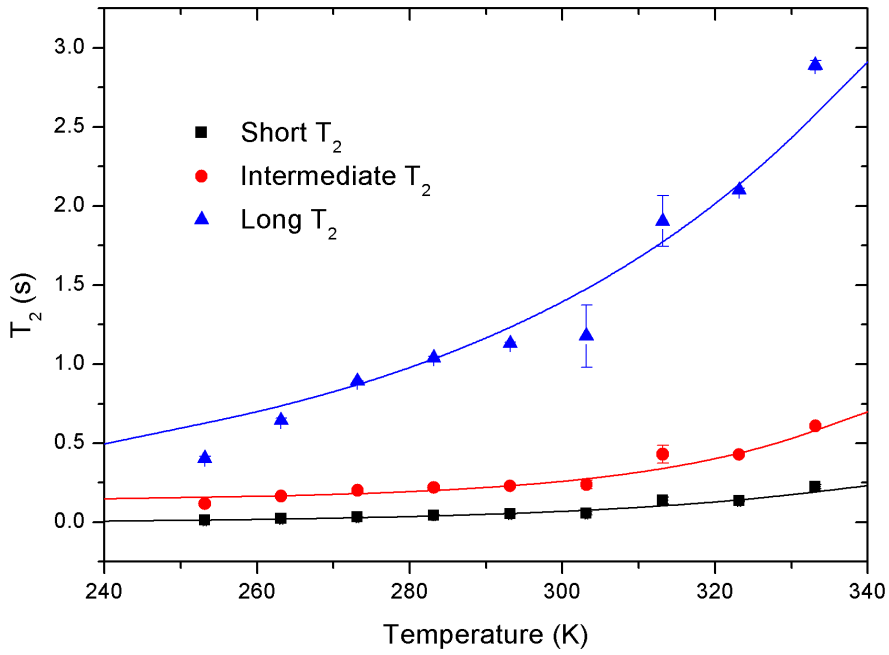

Figure 5.3: T_2 relaxation times for a 20% PVDF/PC/$LiBF_4$ (0.0M) (unsalted) polymer gel electrolyte for the three different phases present. The short, intermediate and long correspond to the interlamellar amorphous PVDF, solvated amorphous PVDF and liquid electrolyte phases , respectively. Data was fitted with equation 5.4.

decreasing the correlation time which in turn causes an increase in the relaxation time. However it can also be noted that the liquid electrolyte phase was more temperature dependent that the other two phases. In Chapter 2, figure 2.8 showed that at low correlation times the increase in temperature (decrease in correlation time) has a much greater effect of the transverse relaxation times than at very high correlation times. Therefore since the liquid electrolyte phase would have much lower correlation times than the other two phases this faster increase with temperature was reasonable. The fitted lines in figure 5.3 were just a simple exponential of the form;

$$T_2(T) = Aexp\left[\frac{t_{T_2}}{T}\right] \tag{5.4}$$

where A is simply a pre-exponential factor that corresponds to the transverse relaxation time at $T = \infty$ and t_{T_2} is the exponential factor which determines the rate of growth with temperature. A larger value of t_{T_2} would result in a faster rate of growth. For the 20% PVDF/PC/$LiBF_4$ (0.0M) (unsalted) polymer gel electrolyte shown in figure 5.3 the values of t_{T_2} were (50±5), (25±5) and (33±5) for the liquid electrolyte phase, amorphous phase and interlamellar phase, respectively. It should be noted here that although a quantity for the shortest T_2 has been given, this value was considered unreliable due to the limited number of points at short times that were used to determine the relaxation times.

A similar plot has been produced for a 30% PVDF/PC/$LiBF_4$ (0.0M) (unsalted) polymer gel electrolyte, this is shown in figure 5.4. Here the shortest T_2 was seen to be practically unchanged by temperature, also the values for the transverse relaxation times were observed to

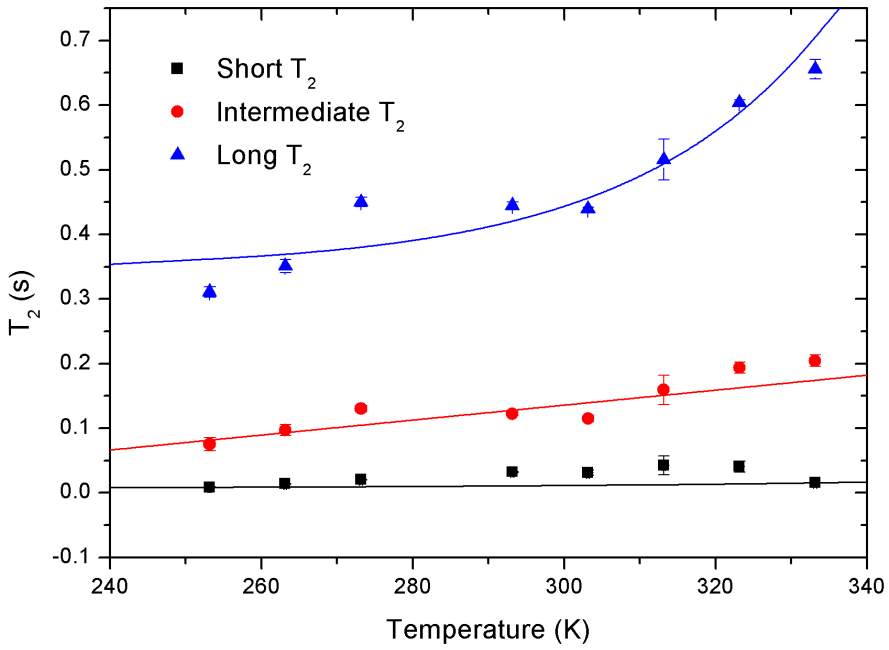

Figure 5.4: T_2 relaxation times for a 30% PVDF/PC/$LiBF_4$ (0.0M) (unsalted) polymer gel electrolyte for the three different phases present. The short, intermediate and long correspond to the interlamellar amorphous PVDF, solvated amorphous PVDF and liquid electrolyte phases , respectively. Data was fitted with equation 5.4.

be significantly lower than that of the 20% unsalted gel.

The conclusions of the transverse relaxation times have shown that there was certainly more than one phase present in the polymer gel electrolytes. It was possible to conclude that there are likely at least three phases, a contribution from the interlamellar PVDF, a solvated amorphous polymer phase and a liquid electrolyte phase. It proved impossible to detect the contribution from the crystalline polymer as there was very little crystalline PVDF in the sample, PVDF is roughly around 50% crystalline and here there was only 20% and 30% PVDF by mass of solvent. Secondly, the transverse relaxation times for solids are usually very short of the order of microseconds and therefore since the liquid phase was likely on a timescale of seconds would over power the signal from the crystalline PVDF. $T_{1\rho}$ measurements have been measured elsewhere as the solid components of multi-phase systems are shifted to a timescale closer to the other phases [18; 34]. $T_{1\rho}$ is the longitudinal relaxation time in the rotating frame of reference and is measured using a 'locking' pulse which is applied for different amounts of time τ, where the magnetisation is related to the time that the 'locking' pulse is applied. This spectrometer did not have the capabilities to measure $T_{1\rho}$ so only the T_2 measurements have been performed. However the transverse relaxation times give a good estimate of the contributions from each phase and the number of phases.

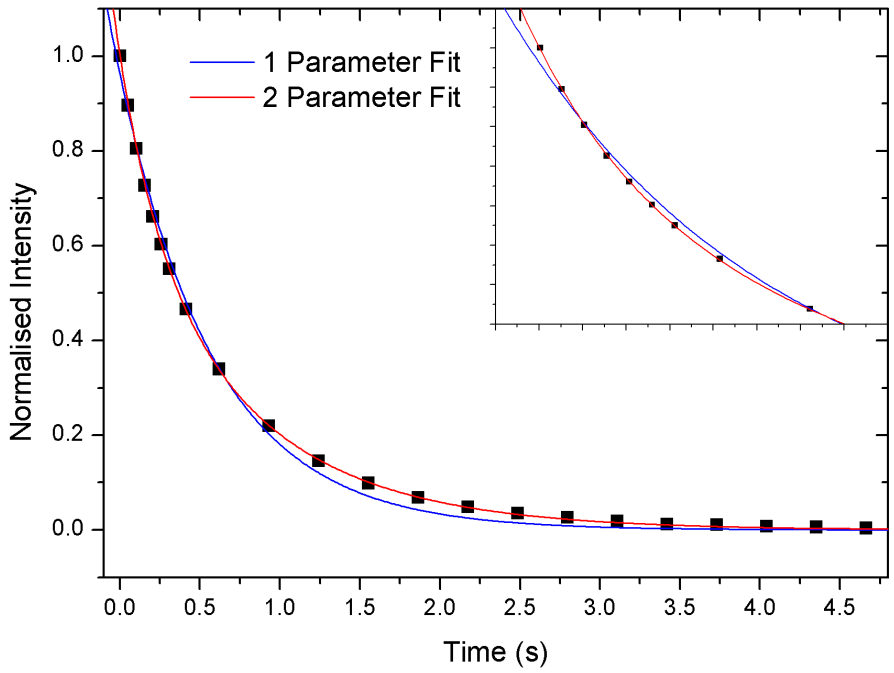

Figure 5.5: Lithium (^{7}Li) T_2 relaxation times for a 30% PVDF/PC/LiBF$_4$ (1.0M) polymer gel electrolyte at 303 K.

5.2.2 Lithium Measurements

Measurements of the lithium transverse relaxation times have been carried out on the 400 MHz Bruker Avance II Ultrashield NMR spectrometer in order to observe the number of phases that can be detected. The same CPMG pulse sequence was used to measure the relaxation times. However the benchtop NMR spectrometer took a continuous spectrum as the number of spin echoes were produced, where as the high field 400 MHz spectrometer required a discrete number of spin echoes to be chosen. These were chosen to reflect the measured relaxation time in order to obtain the entire decay. The value used for the pulse duration was the same as the lithium liquid diffusion in Chapter 4, which was $\tau_{90} = 18.50\ \mu$s for the $\pi/2$ pulse at a power level of 3 dB.

Figure 5.5 shows the transverse relaxation magnetisation decay for the lithium nucleus for a 30% PVDF/PC/LiBF$_4$ (1.0M) polymer gel electrolyte at 303 K. It was observed that the single exponential fit (blue line) in the form of equation 5.1 was not sufficient. As with the hydrogen measurements, a successive exponential term was added in series to describe a second phase within the gel in the form of equation 5.2 (red line). The inset of figure 5.5 shows the fitting at low times in order to highlight the deviance of the fitting of equation 5.1

The value of the single fitting procedure gave (600±20) ms for the transverse relaxation time. The two parameter fit gave values of (260±10) ms and (840±20) ms for the transverse relaxation times. It was observed that the two exponential fitting procedure described the data well and an addition of a third parameter did not increase the fit further. Therefore it can be stated that the lithium ions were predominantly found in two different phases within the polymer gel electrolytes; the values obtained from figure 5.5 are concluded in table 5.3. The two phases detected for the

	T_2^{liquid} (ms)	$T_2^{polymer}$ (ms)	I_{liquid}	$I_{polymer}$
one parameter fit	600	—	1.00	—
two parameter fit	840	260	0.64	0.36

Table 5.3: Summary of fitting procedure of the lithium transverse relaxation decay for 30% PVDF/PC/$LiBF_4$ (1.0M) polymer gel electrolyte at 303 K.

lithium fitting were likely for the solvated amorphous PVDF and liquid electrolyte phases.

It can be observed from table 5.3 that the intensity of the dual fitting gave values of (0.64±0.02) and (0.36±0.02) for the liquid electrolyte and solvated amorphous polymer phases, respectively. Therefore it can be noted that as with the hydrogen transverse relaxation measurements the liquid electrolyte phase was the most dominant which was expected due to the amount of each constituent. These values were in good agreement with the hydrogen values suggesting a similar number of ions of each type were located in the amorphous region of the gels.

5.3 Longitudinal Relaxation

5.3.1 Hydrogen Measurements

Unlike with the transverse relaxation times the longitudinal relaxation usually only exhibits a single value. This is due to the a fast exchange of energy to the lattice, therefore an average is determined from all of the phases. This makes it more difficult to analyse the longitudinal relaxation times for the polymer gel electrolytes. This average will encompass the various PC sites, as the solvated PC and free PC molecules can not be distinguished and will also include any contribution from the PVDF.

The longitudinal relaxation times were measured using the Bench top NMR spectrometer for the hydrogen nuclei using the inversion recovery sequence which was detailed for liquid electrolytes in Chapter 4. The experiments were also set up in the same manner using the same pulse lengths as previously used for the liquid electrolytes. The temperature range used here was 253-333K which was the same for the liquid electrolytes, allowing a comparison between the two systems.

Table 5.4 shows the longitudinal relaxation times for 0% (liquid), 20% and 30% PVDF/PC/ $LiBF_4$ (0.1M, 0.5M and 1.0M) polymer gel electrolytes in temperatures range of 253-333 K using ^1H nucleus. It can be readily observed from table 5.4 that as the polymer concentration was increased the longitudinal relaxation times decreased. At low salt concentration (0.1M) the longitudinal relaxations were 2.55 s, 1.26 s and 0.81 s for 0% (liquid), 20% and 30% PVDF PC/$LiBF_4$, respectively at 303 K. This shows that the decrease in T_1 with the introduction of 20% polymer was quite large (around 49% of the liquid value) and a further drop was observed for 30% PVDF (31% of the liquid value). At the highest salt conentration (1.0M) the relaxations times decreased to 1.08 s, 0.71 s and 0.56 s for 0% (liquid), 20% and 30% PVDF PC/$LiBF_4$, respectively at 303 K. There are multiple phases within the gels which contribute to the relaxation including a crystalline component of the PVDF, a solvated amorphous region and a pure liquid electrolyte

	T_1(s)								
	0.1M			0.5M			1.0M		
Temperature (K)	0%	20%	30%	0%	20%	30%	0%	20%	30%
253	0.53	0.33	0.24	0.31	0.23	0.19	0.17	0.14	0.12
263	0.81	0.47	0.33	0.52	0.33	0.26	0.27	0.21	0.18
273	1.17	0.61	0.41	0.76	0.46	0.35	0.43	0.30	0.24
283	1.58	0.79	0.51	1.06	0.60	0.45	0.62	0.41	0.33
293	2.05	1.00	0.69	—	0.76	0.58	0.86	0.55	0.44
303	2.55	1.26	0.81	1.82	0.95	0.71	1.08	0.71	0.56
313	3.09	1.58	1.01	2.26	1.20	0.88	1.36	0.89	0.73
323	3.66	1.96	1.25	2.77	1.46	1.10	1.68	1.11	0.92
333	—	2.39	1.58	3.22	—	1.40	1.91	1.43	1.17

Table 5.4: ^{1}H longitudinal relaxation times for 0% (liquid), 20% and 30% PVDF/PC/$LiBF_4$ (0.1M, 0.5M and 1.0M) polymer gel electrolytes in the temperature range of 253-333 K. Measured using 50 MHz Maran benchtop NMR spectrometer.

phase. The reduction in relaxation time could be due to less free space available to the molecules and therefore an increased viscosity, which would essentially slow the molecules down moving them closer to the resonant frequency of the ^{1}H nucleus and therefore producing a more efficient relaxation.

Table 5.4 also shows that the longitudinal relaxation times of the polymer gel electrolytes increased with increasing temperature. This suggests that the system was still on the low correlation time (high temperature) side of the T_1 minimum. As stated in the previous section this minimum occurs when the motion of the spins are equal to the resonant frequency of the nucleus under examination. As the correlation time is increased or decreased from this minimum the motion of the spins move away from resonance causing a less efficient relaxation and hence longer T_1 values. Since the correlation times and temperature are inversely proportional an increase in temperature would cause a decrease in the correlation time, and an increase in the molecular motion. Therefore the longitudinal relaxation was not decreasing with decreasing correlation time it logically leaves the system already beyond the minimum toward the high temperature side.

Figure 5.6 shows an Arrhenius plot for the longitudinal relaxation times for 0% (liquid), 20% and 30% PVDF/PC/$LiBF_4$ (1.0M) polymer gel electrolytes using the ^{1}H nucleus. The liquid electrolyte (0%) data have been included from Chapter 4 as a basis for comparison for the gels. Both linear (solid) and non-linear (dashed) fits were applied to determine if the temperature dependence was Arrhenius or non-Arrhenius. It can be noted from figure 5.6 that the liquid (0%) shows a definite non-linear realtionship and that the gels show a much more linear dependency. Obviously the gel system was much more complex than the liquid electrolyte system as now there are believed to be multiple phases in which the hydrogen spins can be located, this could be the reason for the Arrhenius type of behaviour. The different phases within the polymer gel electrolyte would likely have different T_1 values, however with longitudinal relaxation there is always a fast exchange of energy and therefore the measureable T_1 only ever displays a single

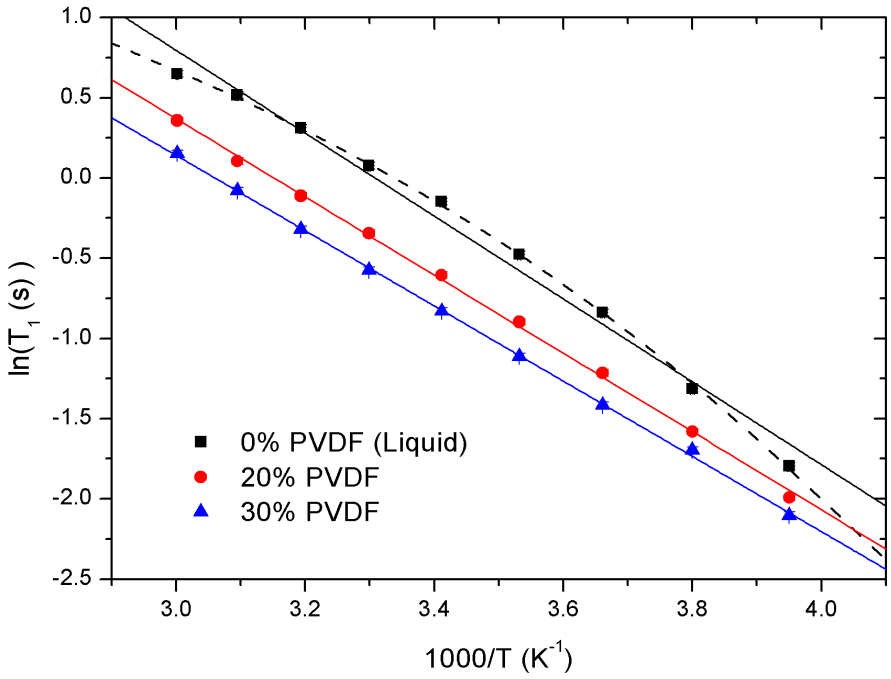

Figure 5.6: ^{1}H longitudnal relaxation Arrhenius plot for 0% (liquid), 20% and 30% PVDF/PC/$LiBF_4$ (1.0M) polymer gel electrolytes. Both linear (solid fits) and non-linear (dashed fits) have been employed.

value which is an average of the different contributions.

All of the longitudinal relaxation times for the gels exhibited Arrhenius type temperature dependence, therefore the activation energy was determined by fitting linear lines on the Arrhenius plots, an example of which is shown in figure 5.6 for all the different salt concentrations measured. As seen in Chapter 4 for Arrhenius systems the relaxation times obey;

$$T_1(T) = A_{T_1} exp\left[\frac{-E_{T_1}}{RT}\right] \tag{5.5}$$

where E_{T_1} is the activation energy of the longitudinal relaxation, A_{T_1} is the pre-exponential factor which is essentially the T_1 value at $T = \infty$ and R is the universal gas constant. Table 5.5 displays the activation energies and pre-exponential factors for the 20% and 30% PVDF/PC/$LiBF_4$ polymer gel electrolytes using ^{1}H nucleus at various salt concentrations. The activation energies are observed to increase with salt concentration, this was attributed to an increase in viscosity which resulted in a higher activation energy as it would require more energy for the molecules to move. Since the activation energies of the longitudinal relaxation are quite high, this suggests that the relaxation had a significant translational motion as it takes more energy to translate than rotate in the medium. As previously stated, the longitudinal relaxation measurements are now an average of all relaxation occuring within the different phases of the polymer gel electrolyte, however the most significant phase of these gels remains the liquid electrolyte phase as the gels contain 70% solvent by mass of the gel.

The longitudinal relaxation times were again observed to decrease with increasing salt con-

	E_{T_1} (kJ mol^{-1})		A_{T_1} (s)	
Salt Concentration (M)	20%	30%	20%	30%
0.0	15.2	15.3	534	449
0.1	17.1	16.5	1145	417
0.3	—	16.2	—	514
0.5	17.8	16.3	1116	532
0.7	—	17.2	—	669
0.9	—	16.5	—	343
1.0	20.3	19.5	2170	1306

Table 5.5: ^{1}H longitudinal relaxation Arrhenius parameters, activation energy E_{T_1} and pre-exponential factor A_{T_1} for 20% and 30% PVDF/PC/$LiBF_4$ polymer gel electrolytes.

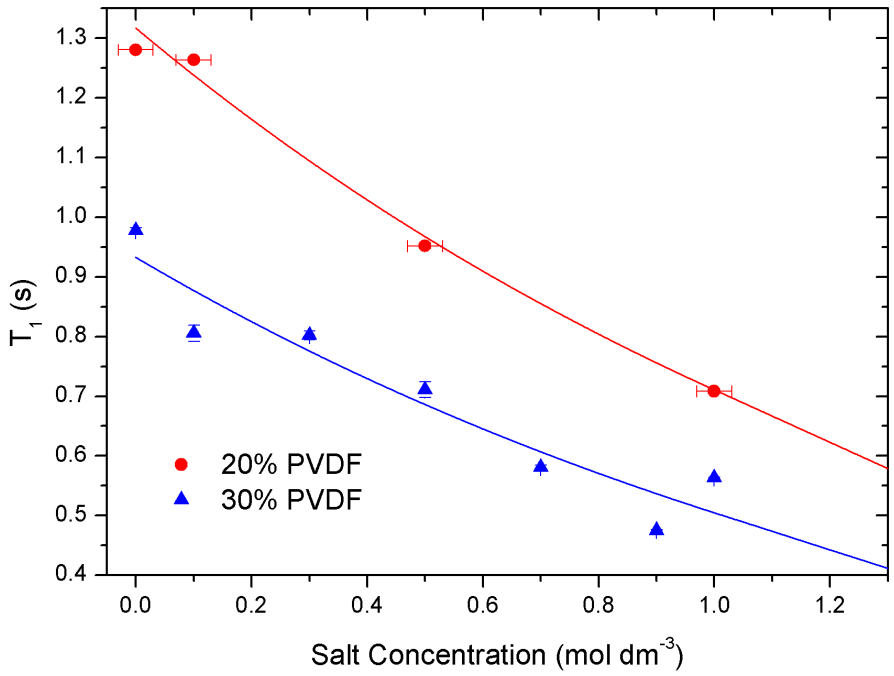

Figure 5.7: ^{1}H T_1 relaxation times for 20% and 30% PVDF/PC/$LiBF_4$ polymer gel electrolytes. Data were taken at 303 K.

	T_1 (s)						
Salt Conc.(M)	0.3M	0.5M	0.6M	0.7M	0.8M	0.9M	1.0M
283	—	1.62	1.24	1.46	1.40	1.28	—
293	—	1.94	1.54	1.74	1.64	1.54	1.45
303	2.43	2.04	1.97	1.98	1.80	1.73	1.69
313	2.86	2.37	2.28	2.26	2.08	2.02	1.96
323	3.23	2.67	2.60	2.60	2.27	2.33	2.28
333	3.54	2.91	2.88	2.84	2.43	2.58	2.53
343	3.76	3.07	3.10	3.00	2.46	2.82	2.79
353	3.95	3.12	3.27	3.16	2.36	3.03	3.04

Table 5.6: ^{7}Li longitudinal relaxation times for 20% PVDF/PC/$LiBF_4$ polymer gel electrolytes.

centration as with the liquid electrolytes. This was again attributed to an increase in viscosity and therefore an increase in correlation time (slowing molecular tumbling), bringing the correlation time closer to the T_1 minimum and resonant frequency of the nucleus. Figure 5.7 shows the longitudinal relaxation times for polymer gel electrolytes containing 20% and 30% PVDF/PC/$LiBF_4$ at 303 K. As with the liquid electrolytes there was an exponential decrease in T_1 with salt concentration. So far the results of the polymer gel electrolytes have shown very similar trends to the liquid electrolyte system, suggesting that the liquids are merely contained within the polymer structure.

5.3.2 Lithium Measurements

The lithium longitudinal relaxation times have been measured using the 400 MHz Bruker Avance II Ultrashield spectrometer for the 20% and 30% PVDF polymer gel electrolytes over temperature range of 283-353 K. Saturation recovery measurements were carried out using the same settings as for the lithium measurements of the liquid electrolytes discussed in Chapter 4. The saturation pulse sequence involved applying multiple $\pi/2$ pulses to the thermal equilibrium state which scrambles the magnetisation yielding a net magnetisation of zero, in this case the number of saturation pulses were chosen to be 100 spaced 500 μs apart. Then after a time τ a $\pi/2$ 'read' pulse was applied to perturb the magnetic field into the measureable xy plane. This was a two dimensional measurement meaning that the experiment was carried out using varying values of τ and recording the intensity of the free induction decay. The values of τ were chosen based on preliminary measurements of the longitudinal relaxation as they need to be spaced to observe the entire recovery.

The longitudinal relaxation of the liquid electrolytes were simpler than the corresponding polymer gel samples. Earlier in this chapter it was discussed that the transverse relaxation measurements exhibit several components to the decay curve, however this was not the case for the longitudinal relaxation recovery curves. The values of T_1 have a fast exchange of energy which means that the measured relaxation times are merely an average of all phases contained within the polymer gel electrolyte and thus prove difficult to analyse based on the fact the phases cannot be separated with these measurements. Table 5.6 shows the longitudinal relaxation times

	T_1 (s)				
Salt Conc.(M)	0.5M	0.6M	0.7M	0.8M	1.0M
303	2.05	1.97	1.90	1.76	1.53
313	2.38	2.28	2.17	2.04	1.77
323	2.68	2.60	2.50	2.32	2.03
333	2.89	2.84	2.76	2.54	2.28
343	3.01	3.05	3.00	2.69	2.51
353	3.14	3.17	3.16	2.81	2.72

Table 5.7: ^{7}Li longitudinal relaxation times for 30% PVDF/PC/$LiBF_4$ polymer gel electrolytes.

for the 20% PVDF/PC/$LiBF_4$ gels at all temperatures and salt concentrations measured. It can be noted readily that the relaxation times decrease with increasing salt concentration. This was attributed to the rise in viscosity with salt concentration which increases the correlation times towards the T_1 minimum, i.e. resonance and therefore produces a more efficient relaxation. Even though it has been stated that the relaxation times are an average of all phases the increased salt concentration would rise the viscosity of all regions and therefore reduce the relaxation times of each region and therefore the overall value of T_1. The temperature dependence of the relaxation times was observed to increase with increasing temperature. Employing the same argument for the salt concentration dependence, as the correlation time decreases with temperature, the timescale of the motion of the molecules deviates from the resonant frequency, thus causing a less efficient relaxation.

The longitudinal relaxation times were also measured for the 30% PVDF/PC/$LiBF_4$ polymer gel electrolytes, the values are displayed in table 5.7. As with the 20% PVDF gels the longitudinal relaxation was observed to increase with temperature and decrease with salt concentration, which have been attributed to the variation in correlation times.

Arrhenius plots of the longitudinal relaxation times have been displayed in figure 5.8, which shows four example samples containing 20% and 30% PVDF/PC/$LiBF_4$ (0.6M and 1.0M). It can be noted that for the 20% PVDF/PC/$LiBF_4$ (0.6M) sample and both 1.0M samples Arrhenius temperature dependence was observed. There was some slight curvature to the 30% PVDF/PC/$LiBF_4$ (0.6M) sample, however all samples were considered to have Arrhenius type temperature dependence for the duration of the analysis.

The activation energies of the longitudinal relaxation were determined from the Arrhenius plot linear fits an example of which was shown in figure 5.8. The activation energies and T_∞ of the longitudinal relaxation are displayed in table 5.8 for the 20% and 30% PVDF/PC/$LiBF_4$ polymer gel electrolytes.

The activation energies are quite scattered with increasing salt concentration. This is attributed to the production stage of the polymer gel electrolytes, however it can be noted that there is a general increase in relaxation time with salt concentration. This is attributed an increase in ions in solution causing an increase in viscosity. It can also be noted that the activation energies are quite similar for the 20% and 30% PVDF gels.

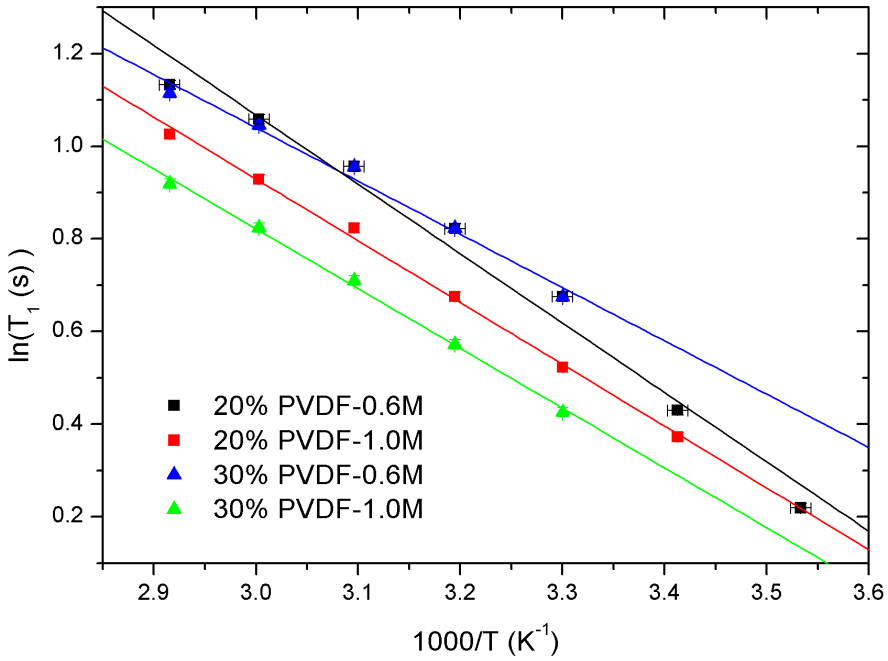

Figure 5.8: ^{7}Li longitudinal relaxation Arrhenius plot for 20% and 30% PVDF/PC/$LiBF_4$ (0.6M and 1.0M) polymer gel electrolytes.

	E_{T_1} (kJ mol^{-1})		T_∞ (s)	
Salt Conc.(M)	20%	30%	20%	30%
0.3	9.4	—	105	—
0.5	8.7	7.5	66	42
0.6	12.5	8.6	260	62
0.7	9.9	9.2	100	76
0.8	8.7	8.3	58	50
0.9	10.7	—	122	—
1.0	11.1	10.3	138	92

Table 5.8: ^{7}Li longitudinal relaxation Arrhenius parameters, activation energy (E_{T_1}) and T_∞ for 20% and 30% PVDF/PC/$LiBF_4$ polymer gel electrolytes.

5.4 NMR-PFG Diffusion

In Chapter 4, it was shown that the 400 MHz Bruker Avance II Ultrashield NMR spectrometer had the capability of measuring both the longitudinal relaxation and self diffusion coefficients for multiple nuclei. In this section the self diffusion constants for polymer gel electrolytes containing 20% and 30% PVDF with PC and $LiBF_4$ at various salt concentrations are reported and discussed. Three different frequencies were used to measure the hydrogen (^{1}H), lithium (^{7}Li) and fluorine (^{19}F) nuclei to detect the PC molecules, cation and anion of the salt, respectively. The salt concentration was again limited to 1.0M due to the competition between solvating the salt and polymer, if the salt concentration was too high phase separation occurs which is known as syneresis.

The polymer gel electrolytes are clearly more complex than the liquid electrolyte counterparts as they contain at least three phases which include the crystalline polymer, solvated amorphous polymer and liquid electrolyte phase [18; 26; 27; 34]. In this section the 400 MHz spectrometer has been used to determine the self diffusion of the various components of the gels. Earlier in this chapter, hydrogen and lithium transverse relaxation times exhibited at least two exponential components each corresponding to a distinct phase. It was expected that the fluorinated anions would also be found in at least two of the three phases. It has in fact been shown in this thesis that it was possible to detect multiple diffusive species of the lithium and hydrogen nuclei by using the Cotts [52] bipolar stimulated echo pulsed-field gradient (BPSTE-PFG) experiments.

The pulsed-field gradient method has proved a valuable tool in understanding the dynamics of polymer gel electrolytes [49; 54; 62; 111–113]. An interesting modification that has been applied by Kataoka *et al* was to use a cell which allowed a direct current to be applied to the sample [65]. This method was able to distinguish between the ions that were neutral pairs and those that were charged as they would respond differently to an electric field. This would allow determination of ionic association of the samples. However, in this thesis standard NMR tubes have been used and the diffusion will be an average of all species containing the relevant ions.

5.4.1 Fluorine Measurements

As previously discussed, the fluorine nucleus (^{19}F) was employed to understand the dynamics of the fluorinated anion of the salt molecules, in this case it was the BF_4^- anion in the liquid electrolyte samples. The polymer PVDF also contains two fluorine ions per monomer and therefore can be detected by NMR. However the content of PVDF was relatively low and therefore the fluorine anions of the salt would likely dominate the spectrum. In this section the self diffusion measurements have been reported for the fluorinated anions and compared with the corresponding liquid electrolytes. As previously mentioned the salt concentration for the polymer gel electrolytes were limited to a range of 0.0-1.0M $LiBF_4$. The temperature range used was 283-353 K, however there was slight concern regarding the data at 353 K as in the liquid electrolytes the samples displayed signs of correlated motion due to temperature gradients.

The pulsed field gradient measurements were carried out using the same method laid out in Chapter 2 using the same settings and parameters. The pulse sequence consisted of four gradient pulses and five RF pulses. The four gradients were in two sets of two pulses, designed to eliminate the background magnetisation of the spectrometer referred to as bipolar pulses.

	Diffusion (10^{-10} m^2 s^{-1})							
Temperature (K)	0.1M	0.3M	0.5M	0.6M	0.7M	0.8M	0.9M	1.0M
283	2.68	1.92	1.44	1.31	1.14	0.89	0.77	0.65
293	3.43	2.54	1.90	1.68	1.47	1.19	1.05	0.86
303	4.17	3.11	2.42	2.00	1.79	1.49	1.38	1.11
313	4.86	3.68	2.80	2.35	2.14	1.81	1.71	1.37
323	5.58	4.42	3.21	2.58	2.51	2.14	2.12	1.66
333	6.45	5.01	3.64	2.73	2.89	2.49	2.35	2.01
343	7.27	5.64	4.02	2.87	3.23	2.85	2.83	2.36
353	7.97	6.12	4.33	2.95	3.54	3.15	3.11	2.70

Table 5.9: ^{19}F self diffusion constants for 20% PVDF/PC/$LiBF_4$ polymer gel electrolytes.

The first set of gradients introduces spatial encoding while the second set remove the gradient. The RF pulses are applied to detect a measurable signal, these pulses were laid out in order to produce a spin echo as described by the CPMG sequence.

The fluorine self diffusion constants for the 20% PVDF/PC/$LiBF_4$ are displayed in table 5.9 for all temperatures and salt concentrations measured in this research. It can be readily observed that the diffusion constants increase with temperature and decrease with salt concentration. This trend was the same as for the corresponding liquid electrolytes and was attributed to the viscosity of the system. As the viscosity was decreased (increasing temperature) the molecules can move more freely and therefore, as the viscosity increased (increasing salt concentration) the molecules could less easily translate through the bulk solution.

The diffusion constants in table 5.9 were consistently lower than the corresponding liquid electrolyte values. For the sample containing $LiBF_4$ (1.0M) at 283 K the diffusion constants were measured as (0.86±0.01) and (0.65±0.03) (10^{-10} m^2 s^{-1}) for the 0% PVDF (liquid) and 20% PVDF polymer gel electrolyte, respectively. This result implied that as the polymer concentration was increased the viscosity of the bulk solution was increased. The polymer gel electrolytes were assumed to be consisting of a crystalline polymer phase, a solvated amorphous polymer phase and a pure liquid electrolyte phase. It was proposed here that the diffusion constants for the polymer gel electrolytes were for the pure liquid electrolyte phase. It was unlikely that there was a contribution to the diffusion from the crystalline polymer phase due to any movement of the polymer being significantly lower than the molecules translating through the liquid phase. It was therefore suggested that there might be a viscosity rise, however the introduction of the polymer would most likely introduce pockets of liquid throughout the polymer structure and therefore the liquid would be more confined than the free liquid measurements obtained from the liquid electrolyte samples. This single diffusion value obtained for the fluorine nuclei was assumed to be be an average of all diffusing species, however this value would clearly be dominated two factors. Firstly, the number of fluorine spins in each phase of the gel and also the rate at which they diffuse. Since the crystalline polymer will no doubt move on some scale it was assumed untraceable at present due to the very small movements relative to the liquid electrolyte anions translational motion. There was a possible contribution from the solvated amorphous polymer phase however they were not distinguishable. Therefore the diffusion con-

	Diffusion (10^{-10} m^2 s^{-1})							
Temperature (K)	0.1M	0.3M	0.5M	0.6M	0.7M	0.8M	0.9M	1.0M
283	2.72	1.80	1.28	1.12	0.98	0.84	0.75	0.59
293	3.39	2.22	1.65	1.54	1.31	1.12	1.00	0.86
303	4.14	3.02	2.10	1.78	1.65	1.47	1.31	1.08
313	4.80	3.55	2.57	2.00	2.04	1.81	1.56	1.41
323	5.64	4.17	2.98	2.12	2.34	2.13	1.83	1.67
333	6.45	4.61	3.38	2.47	2.67	2.39	2.17	1.87
343	7.27	4.98	3.75	2.80	2.96	2.72	2.49	2.12
353	8.13	5.47	4.14	2.93	3.23	3.04	2.73	2.32

Table 5.10: ^{19}F self diffusion constants for 30% PVDF/PC/$LiBF_4$ polymer gel electrolytes.

stants measured in this thesis for the fluorine nucleus were assumed to be the average of the anions in the liquid electrolyte and solvated amorphous polymer phases of the gels.

The diffusion constants were also measured for polymer gel electrolytes containing 30% PVDF by mass, these results are displayed in table 5.10. The temperature and salt concentration trends were the same as for the liquid and 20% PVDF electrolytes. The interesting point to note was that the diffusion constants for the 20% PVDF and 30% PVDF polymer gel electrolytes were quite similar. Taking again the 1.0M $LiBF_4$ samples as an example, the values for the various polymer concentrations were (0.86±0.01), (0.65±0.03) and (0.59±0.01) (10^{-10} m^2 s^{-1}) for the 0% (liquid), 20% and 30% PVDF/PC/$LiBF_4$ (1.0M) samples, respectively at 283 K. It can be noted that there was a decrease with the addition of more polymer which was attributed to reducing the free volume the liquids can translate. However the fact that the decrease in the diffusion constant was not very significant strongly agrees with the hypothesis that the fluorine measurements are indeed the liquid electrolyte phase within the polymer gel electrolytes. There are likely BF_4 anions located in the solvated amorphous PVDF phase of the gels, however, the fact that only a single diffusion constant is obtained suggests that the measured diffusion constant is merely an average of all locations of the fluorine atoms.

As with the liquid electrolytes, Arrhenius plots have been employed here to determine the temperature dependence of the diffusion constants. Figure 5.9 shows the Arrhenius plot for both the 20% and 30% PVDF polymer gel electrolytes with 0.5M and 0.9M $LiBF_4$. As seen previously, the temperature dependence can be considered Arrhenius if the plot displays a linear relationship. It can be noted from figure 5.9 that there appears to be some possible curvature to the data at the extremes, however this was not significant and for this research it was assumed that the diffusion was exhibiting Arrhenius (linear) type dependence. The temperature dependence of the liquid electrolytes was found to be Arrhenius and therefore the assumption that the diffusion of the polymer gel electrolytes was simply diffusion of the liquid electrolyte contained within, it might then be expected to find the same temperature dependence. The measurements of the polymer gel electrolytes show more scatter than that of the liquid electrolyte, this was attributed to the difficulty in preparing the polymer gel electrolytes. It took trial and error in the production stage to hone the skill of making the polymer gel electrolytes with minimum solvent loss.

Since the assumption has been made that the temperature dependence was Arrhenius this

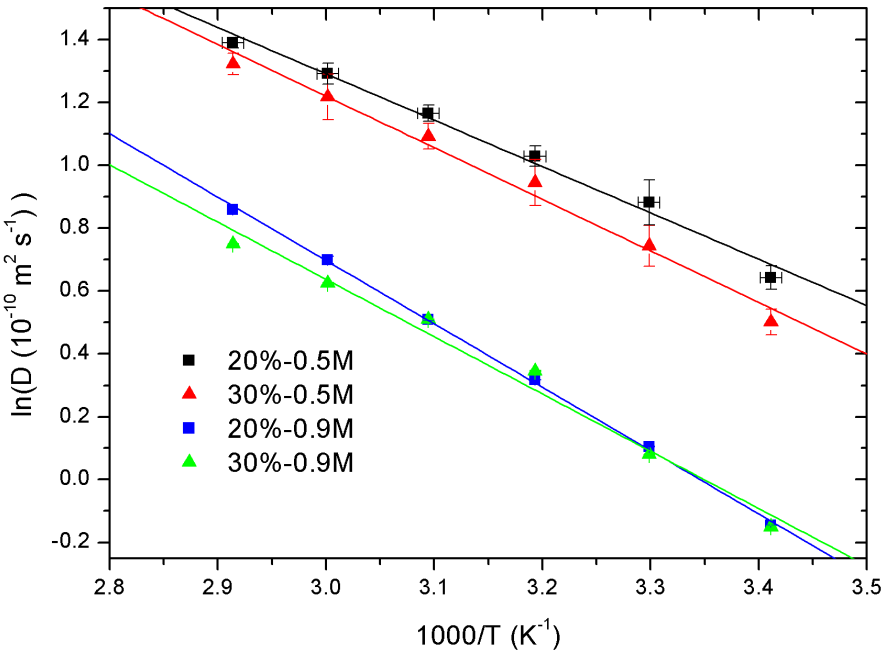

Figure 5.9: ^{19}F diffusion Arrhenius plot for 20% and 30% PVDF/PC/$LiBF_4$ (0.5M and 0.9M) polymer gel electrolytes.

allows calculation of the activation energy of the diffusion process. The activation energy can be determined from the gradient of the linear line of the Arrhenius plots. Table 5.11 shows the activation energies and the pre-exponential factor (D_∞), which relates to the diffusion constant at $T = \infty$, for both 20% and 30% PVDF/PC/$LiBF_4$ polymer gel electrolytes at various salt concentrations. The activation energies of the liquid electrolytes have also been displayed in table 5.11 as a basis for comparison. It can be readily noted that the activation energies were seen to increase with salt concentration, this trend was seen for both liquid and polymer gel electrolytes. The activation energy for the diffusion constant is the measure of the energy required by the diffusive species to translate through the medium in which it is contained. Therefore a high activation energy relates usually to a very viscous system where more energy would be needed to initiate diffusion. It can also be noted from table 5.11 that the activation energies for the polymer gel electrolytes are lower than the corresponding liquid electrolyte. This was counter intuitive as the diffusion constants for the polymer gel electrolytes were lower than the corresponding liquid, therefore suggesting a higher viscosity at higher polymer concentrations. The difference between the activation energies of the liquid and gels were however quite similar in value. As previously stated, the data for the gels was more scattered due to difficulty in producing the gels, this could be the cause of the discrepancy. The activation energy of the 20% and 30% PVDF gels were very similar with a value of (13.5±0.2) kJ mol^{-1} for both the 20% and 30% gels containing 0.1M $LiBF_4$. At higher salt concentrations (1.0M) there was a slight discrepancy between the two polymer concentrations as they yielded the values (17.6±0.2) kJ mol^{-1} and (18.0±0.2) kJ mol^{-1} for the 20% and 30% PVDF gels, respectively. A slightly higher activation energy of the 30% gel agreed with the suspected increased viscosity with more polymer.

	Activation Energy (kJ mol^{-1})			D_∞ (10^{-8} m^2 s^{-1})	
Salt Concentration (M)	Liquid	20%	30%	20%	30%
0.1	—	13.5	13.5	8.6	8.5
0.3	17.8	14.9	15.2	11.2	11.8
0.5	18.7	14.3	15.3	6.6	9.0
0.7	19.9	14.5	15.7	5.5	8.1
0.8	—	15.9	16.6	8.0	10.1
0.9	—	17.8	16.5	15.8	8.5
1.0	22.3	17.6	18.0	12.0	13.5

Table 5.11: ^{19}F Arrhenius fitting parameters, the pre-exponential factor (D_∞) and activation energies for self diffusion constants for 20% and 30% PVDF/PC/$LiBF_4$ polymer gel electrolytes.

	D_0 (10^{-10} m^2 s^{-1})			A_D (M)		
Temperature (K)	Liquid	20%	30%	Liquid	20%	30%
283	3.2	3.2	2.5	0.76	0.63	0.73
293	4.1	4.1	3.2	0.80	0.67	0.76
303	5.2	4.7	4.4	0.84	0.71	0.72
313	6.2	5.9	4.9	0.90	0.69	0.80
323	7.7	6.3	5.4	0.91	0.76	0.84
333	9.4	7.0	6.6	0.95	0.80	0.79
343	10.8	7.7	6.8	1.00	0.84	0.86
353	12.9	7.8	7.5	1.04	0.91	0.87

Table 5.12: ^{19}F salt concentration fitting parameters, pre-exponential factor (D_0) and exponential decay factor (A_D) for 0% (liquid), 20% and 30% PVDF/PC/$LiBF_4$ polymer gel electrolytes.

The salt concentration dependence of the liquid electrolytes were determined by fitting a simple exponential and noting the exponential decay factor. An decrease of the decay factor caused the diffusion to decrease faster with increasing salt concentration. This was used in Chapter 4 to determine the factors causing a decrease in diffusion with salt concentration. The same equation has been fitted to the diffusion data for the polymer gel electrolyte. For all polymer gel electrolytes the diffusion constants were seen to decrease with increasing salt concentration. A simple exponential equation was used in the form;

$$D(c) = D_0 exp\left[\frac{c}{A_D}\right] \tag{5.6}$$

where D_0 is the diffusion constant at infinite dilution and A_D is the exponential decay factor. The A_D factor was considered proportional to the viscosity as this was the most significant cause of the decrease in diffusion constant. However it is possible for other factors to affect this value such as the effective radius of the molecules.

Table 5.12 shows the salt concentration fitting parameters for the polymer gel electrolytes as well as for the liquid electrolyte results from Chapter 4. For the liquid electrolytes the diffusion constants were very well defined and therefore the diffusion as a function of salt concentration

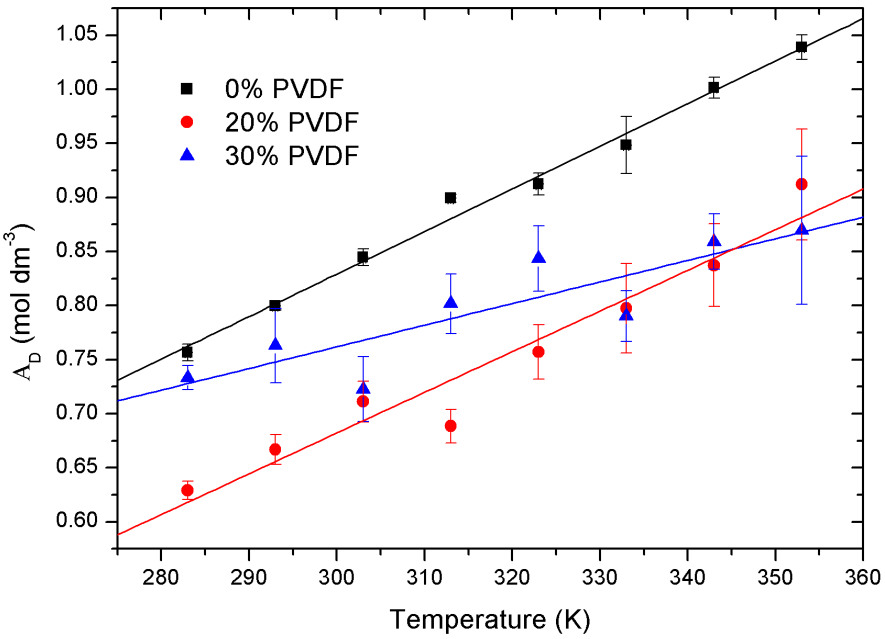

Figure 5.10: ^{19}F self diffusion salt concentration fitting parameter A_D for 0% (liquid), 20% and 30% PVDF/PC/$LiBF_4$ polymer gel electrolytes.

was a smooth exponential decay, producing an accurate fit to the data and hence accurate values of A_D. However the polymer gel electrolytes were much more difficult to consistently produce and therefore when plotting the diffusion data as a function of salt concentration the data was observed to be more scattered. The 20% gels were fairly consistent, it was the 30% gels that were the most scattered and this was reflected in the value of A_D. Figure 5.10 shows the exponential decay factor A_D as a function of temperature for the liquid and polymer gel electrolytes. The liquid electrolyte and 20% gel exhibit a linear relationship with temperature, whereas the data for the 30% gel was scattered and more difficult to analyse. The increase of this factor was attributed to the decrease in viscosity at higher temperatures.

To fully understand the dynamics of the polymer gel electrolytes it was important to compare the diffusion for the polymer gel electrolyte and corresponding liquid electrolytes. Since $D_{Liquid} > D_{Gel}$ each of the diffusion values for the polymer gel electrolytes were divided by the corresponding liquid diffusion, this ratio would take a value between 0 and 1. Taking the 20% PVDF polymer gel electrolytes as an example the D_{Gel}/D_{Liquid} values were (0.88±0.03), (0.86±0.03), (0.86±0.03) and (0.72±0.03) for 0.3M, 0.5M, 0.7M and 1.0M $LiBF_4$ respectively at 293 K. A value of one for this ratio would suggest that the polymer gel electrolytes were behaving in the exact same manner as the liquid electrolytes. It can be seen that the values for the 20% gels are quite close to one and therefore suggests that the polymer gel electrolytes were very similar to the liquid electrolytes. This supports the hypothesis that the gels consist predominatly of liquid electrolyte flowing through the polymer structure. The ratio was practically independent of salt concentration, therefore the viscosity effects with salt concentration were the same for both cases. The ratio was observed to decrease with temperature, suggesting that the diffusion of the liquids was increasing at a greater rate than the gels with increasing temperature. Since not

	D_{Gel}/D_{Liquid}							
	20% PVDF				30% PVDF			
Temperature (K)	0.3M	0.5M	0.7M	1.0M	0.3M	0.5M	0.7M	1.0M
283	0.88	0.88	0.90	0.75	0.83	0.78	0.78	0.69
293	0.88	0.86	0.86	0.72	0.77	0.75	0.77	0.72
303	0.85	0.85	0.79	0.69	0.83	0.74	0.74	0.68
313	0.81	0.79	0.75	0.66	0.79	0.73	0.72	0.68
323	0.79	0.74	0.70	0.65	0.75	0.69	0.66	0.65
333	0.71	0.69	0.61	0.62	0.66	0.64	0.57	0.57
343	0.69	0.62	0.59	0.60	0.61	0.58	0.54	0.54
353	0.65	0.55	0.53	0.55	0.58	0.52	0.48	0.47

Table 5.13: ^{19}F D_{Gel}/D_{Liquid} values for 20% and 30% PVDF/PC/$LiBF_4$ polymer gel electrolytes.

much is known about the phase seperation of the polymer gel electrolytes, so it was possible that the gel structure changed with increasing temperature. It has already been discussed that there are several phases including a crystalline, solvated amorphous and liquid phase of the gels, so it would be possible for the contribution of the phases to change with temperature, particularly the solvated amorphous polymer phase and pure liquid electrolyte phase. There was also the possibility of some correlated motion when measuring the liquids due to a temperature gradient in the samples, this was mainly seen at the highest temperature 353 K and therefore the ratio at high temperatures are considered to be not as accurate as the low temperature equivalents; the ratio of the diffusion values are summarised in table 5.13.

The 30% PVDF gels were also compared to the liquid diffusion in the same manner as the 20% PVDF gels. The values of D_{Gel}/D_{Liquid} were (0.77±0.03), (0.75±0.03), (0.77±0.03) and (0.72±0.03) for 0.3M, 0.5M, 0.7M and 1.0M $LiBF_4$, respectively at 293 K. Firstly, it should be noted that the values for the 20% and 30% PVDF gels were very similar with the 20% slightly larger than the 30% gels. Secondly, the 30% gels also do not exhibit any salt concentration dependence. Since the ratio decreased with increasing polymer concentration it was assumed that the addition of the polymer structure has introduced pockets of liquid electrolyte which are clearly less free than the liquid electrolyte. This decrease in diffusion has been observed in similar PVDF based polymer gel electrolytes [84].

The 30% PVDF gels also exhibited a decrease with increasing temperature mainly observed at the highest few temperatures, which again raised question of possible correlated motion of the diffusion of the liquid electrolytes at these temperatures. The polymer gel electrolytes were much less likely to display any correlated motion as they are considered to be in pockets of liquid and therefore each pocket would likely have the same temperature. Therefore not too much significane has been put on the decrease of this ratio with temperature. All D_{Gel}/D_{Liquid} ratios are displayed in table 5.13 for both the 20% and 30% PVDF polymer gel electrolytes with both temperature and salt concentration.

5.4.2 Lithium Measurements

In this section the lithium (^{7}Li) NMR diffusion measurements are displayed and discussed. The lithium nucleus was used to detect the cation of the salt. The same settings were used for the polymer gel electrolyte measurements as for the liquid ones. These measurements were taken on the 400 MHz NMR spectrometer and therefore the resonant frequency of the lithium nucleus was 155 MHz. The same power level was used which was 3 dB, for this power level the pulse duration was $\tau_{90} = 18.50\,\mu$s. The diameter of the NMR tubes for the lithium coil were 10 mm which was the same as for the fluorine coil and also the low field bench top spectrometer. As discussed previously, the polymer gel electrolytes were mounted into the glass tubes when in the polymer melt which allowed manipulation of the gels. For each gel made, the lithium and fluorine measurements were carried out on the same sample. To reduce the possibility of contamination, the samples were created and sealed within a nitrogen filled glove box. The samples were measured within 48 hours of creation to avoid any degradation of the sample with time. There was no reason to believe that the gels would degrade however this was simply a precautionary measure.

5.4.2.1 Multi-Phase Diffusion

The diffusion measurements were carried out by applying magnetic field gradients which gave the spins spatial encoding, by allowing a set time (diffusion time, Δ) for the spins to diffuse then removing the spatial encoding the intensity is then dependent on the average distance traveled by the spins. This theory has been addressed in Chapter 2, which showed that by applying increasing gradient strengths (G) the intensity of the NMR spectrum would be explained by equation 2.76. For the ease of the reader the equation will be restated here;

$$I = I_0 exp\left[-G^2 D\delta^2\left(\Delta - \frac{\delta}{3}\right)\right] \tag{5.7}$$

where δ was the duration of the gradient pulses which for all measurements in this research was 10 ms and Δ is the diffusion time (time between gradient pulses) and was set to 40 ms as standard for these measurements. For the liquid electrolytes this equation was found to fit the diffusion decay well, which was also the case for the polymer gel electrolyte fluorine diffusion measurements discussed in the previous section. On measuring the lithium diffusion constants for the polymer gel electrolytes it was found that equation 5.7 was not a sufficient fit to the data. This result suggests that the polymer gel electrolytes had other contributions to the diffusion than the liquid electrolyte equivalent.

It was decided that equation 5.7 needed to be altered to fit the data, and was assumed here that there were multiple distinctly different environments for the molecules containing lithium ions. Therefore it was assumed that these two environments were separate and another term was added in series to equation 5.7 to describe the second environment. The equation that was then fit to the data was in the form;

$$I(G) = I(0)_1 exp\left[-G^2 D_1\delta^2\left(\Delta - \frac{\delta}{3}\right)\right] + I(0)_2 exp\left[-G^2 D_2\delta^2\left(\Delta - \frac{\delta}{3}\right)\right] \tag{5.8}$$

where $I(0)_1$ and $I(0)_2$ are the intensity of the spectrum when the gradient was not present for the first and second environment respectively, with D_1 and D_2 as the diffusion constant for each

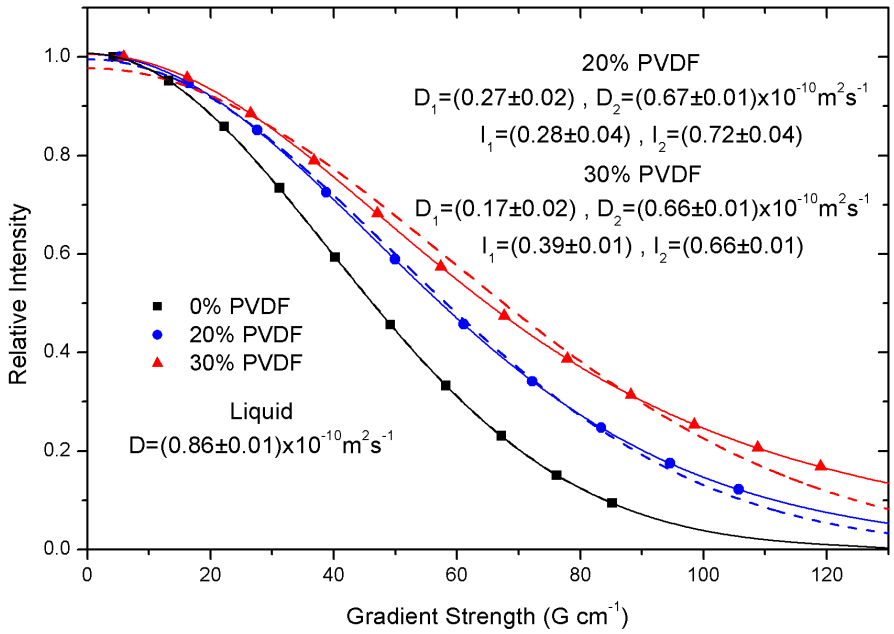

Figure 5.11: Intensity of the diffusion decay curve as a function of gradient strength for the lithium (^{7}Li) nucleus self diffusion constants for 0% (liquid), 20% and 30% PVDF/PC/$LiBF_4$ (1.0M) polymer gel electrolytes at 303K. A single exponential (dashed) and double exponential (solid) have been applied to the data.

phase. Since the intensity of all the diffusion decay curves were normalised to have a maximum value of 1 the intensities give an indication of the amount of each phase was present.

Figure 5.11 shows a typical diffusion decay curve with the intensity of the spectrum against the gradient strength of the magnetic field gradient pulses (G) for 0% (liquid), 20% and 30% PVDF/PC/$LiBF_4$ (1.0M) polymer gel electrolytes at 303 K. Fits to the data for both equation 5.7 (dashed) representing a single exponential component to the diffusion and equation 5.8 (solid) representing two distinct exponential components were employed. It can be readily observed that for the liquid electrolyte (black square) the two fits overlap one another and can be assumed that for the liquid electrolytes there was clearly only one component to the diffusion process. For the case of the polymer gel electrolytes, for both the 20% PVDF (blue circles) and the 30% PVDF (red triangles), the single exponential fit (dashed) was not a good fit to the data and became worse with increasing polymer concentration. However an interesting result was observed in the two exponential fitting of the gels which showed for both polymer concentrations that equation 5.8 fitted the data well.

The results from the fits in figure 5.11 were (0.86±0.01) for the liquid electrolyte diffusion, (0.27±0.02) and (0.67±0.02) for the 20% PVDF gels for D_1 and D_2, respectively and (0.17±0.01) and (0.66±0.01) for the 30% PVDF D_1 and D_2, respectively (all with units 10^{-10} m^2 s^{-1}). The two diffusion constants for each of the gels both yielded reasonable results for diffusion, with the slower (D_1) diffusion constant being around a quarter of the value of the faster component (D_2). It can be seen from the data in figure 5.11 that the diffusion of the liquid electrolyte and faster components of the polymer gel electrolytes were quite similar and that the fast components of

the two polymer concentrations were identical within the error. Therefore it was assumed that the faster diffusive species of the gels was due to the pure liquid electrolyte phase of the gels. The intensities $I(0)_1$ and $I(0)_2$ were (0.28±0.04) and (0.72±0.04), respectively for the 20% PVDF gels. This shows that the liquid electrolyte phase was dominant, however the slower diffusive species was not negligible. This was reasonable as the polymer gel electrolytes were made from between 70%-80% solvent so one would expect to have a dominant liquid phase.

The intensities for the 30% gel were (0.39±0.05) and (0.61±0.05) for $I(0)_1$ and $I(0)_2$, respectively. Therefore it can be seen that with an increase in polymer the intensity of the slower phase ($I(0)_1$) became more significant. Suggesting that the slower phase was dependent on the amount of polymer. The diffusion for this phase was still quite fast and therefore assumed not to be the crystalline polymer which would leave the amorphous phase of the gels. The increase in the intensity of the slower phase was intuitive as an increase amount of polymer would surely create more amorphous regions of the gel. It was assumed in this thesis that the second slower diffusion constant was due to the solvated amorphous polymer phase as discussed by Hubbard *et al* [18; 34]. If the intensity of the liquid phase in the 20% PVDF gel was (0.72±0.04), the total solvent was clearly 80%, it is likely that the loss of solvent has gone into the amorphous phase of the gel.

It has been previously observed by Magistris *et al* [41] that a PVDF-HFP polymer gel electrolytes can exhibit two diffusion constants. They attributed the two contributions to the $'swelled'$ polymer phase and a liquid electrolyte phase for the slow and fast diffusion constants, respectively. The same group has reported that they observe the same two phase diffusion in other PVDF solvent systems [114; 115], showing that for most solvents the faster diffusive phase has the larger intensity and therefore is in good agreement with the observation in this research. The authors also suggest that a single fit to the diffusion data would essentially be an average of the two phases.

It was important to assess the likelihood of two distinct diffusive species, as it was possible that the poor fit of the data in figure 5.11 of equation 5.7 was due to other factors. Firstly, there are likely to be different arrangements of molecules containing lithium ions. The lithium was known to be surrounded by a solvent shell of PC molecules and can also be associated with the anion of the salt (BF_4^-), among other arrangements, all of which would exhibit different diffusion constants. However all of these arrangements were contained within the liquid electrolyte, which only exhibited a single diffusion constant. Suggesting that the different arrangements had diffusion constants which were quite similar so the single diffusion constant of the liquids is an average of all of these arrangements, however this does not explain the second exponential factor found in the gels. Another possible explanation of the poor fit in figure 5.11 was if the pockets of liquids in the polymer structure are small the molecules could come into contact with the walls of the cavities and therefore the diffusion would have to be explained by a stretched exponential rather than equation 5.7 [116]. One way to test this hypothesis was to measure the diffusion of polymer gel electrolytes as a function of diffusion times (Δ). If the fit reduced to a single exponential component at low diffusion times then this would suggest that restricted diffusion was the cause of the second exponential. If the diffusion time was decreased then the molecules would have less time to diffuse and therefore less time to interact with the boundaries of the polymer structure.

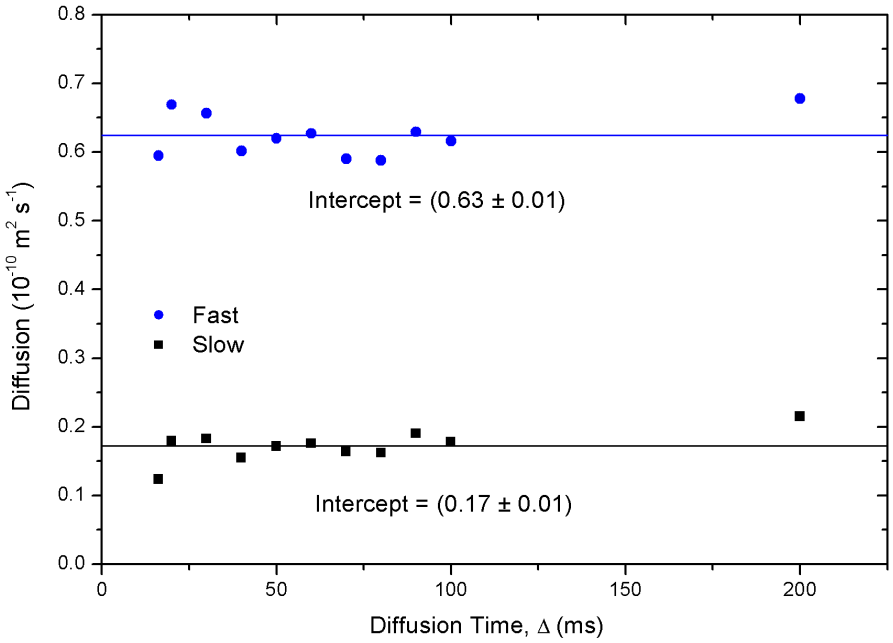

Figure 5.12: Lithium (^{7}Li) diffusion constants as a function of diffusion time for 20% and 30% PVDF/PC/$LiBF_4$ (1.0M) polymer gel electrolytes at 293 K. Average values of slow and fast diffusion constants given as (0.17±0.01) $\times 10^{-10}$ m^2 s^{-1} and (0.63±0.01) $\times 10^{-10}$ m^2 s^{-1} respectively.

The diffusion was measured for 20% and 30% PVDF/PC/$LiBF_4$ (1.0M) polymer gel electrolytes at various different diffusion times ranging from 16.25 ms to 200 ms. It was assumed that a random walk argument could be used here using the equation of the average distance travelled [105] (r) as;

$$r = \sqrt{6Dt} \tag{5.9}$$

where D is the diffusion constant which will arbitrarily be given as 1 $\times 10^{-10}$ m^2 s^{-1} and t is the time which will be the values of Δ used. This corresponds to an average distance traveled between 3 μm and 11 μm; it should be noted that in equation 5.9 r is actually the root mean square distance. At all diffusion times the second exponential term was present, suggesting that restricted diffusion was not a factor here and that the second diffusive species was real. Figure 5.12 shows the diffusion constants (D_1 and D_2) at the various diffusion times. It was observed that not only was the two diffusion fit valid at all diffusion times, but that the values were constant over the range. It was therefore assumed for the rest of this discussion that restricted diffusion was not a factor, and the two diffusion constants referred to two distinct phases on the length scale covered. It should be noted that although there is no indication of restricted diffusion on this length scale (i.e. μm) it is possible for the cavities in the polymer gel electrolytes to be on a smaller length scale. If this was the case here then the result shown in figure 5.12 could mean that the molecules were sufficiently restricted even at the lowest possible diffusion time. That being said, it has been shown by other research groups [35; 38; 41] that cavities and also spherulite sizes often exceed μm in size and therefore one would expect to observe some variance as the diffusion time was altered.

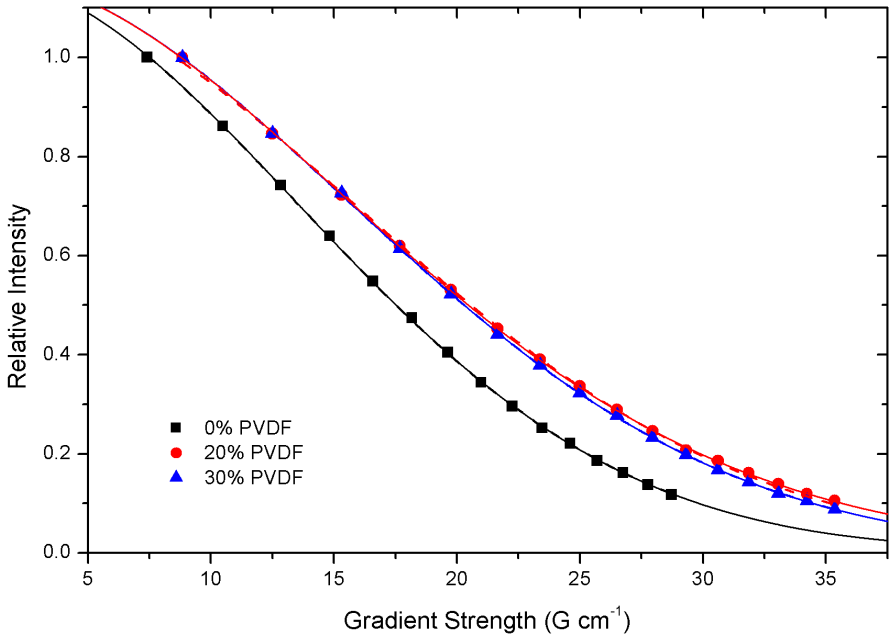

Figure 5.13: ^{19}F diffusion decay curve with single and double exponential fitting for 0% (liquid), 20% and 30% PVDF/PC/$LiBF_4$ (1.0M) polymer gel electrolytes at 293 K. A single exponential (dashed) and double exponential (solid) have been applied to the data.

It has been observed in diffusion measurements of PVDF based gels measured elsewhere that over several different polymer concentrations there was no change in the diffusion of the cationic species with increasing diffusion time[117]. The authors suggested that the presence of restricted diffusion would cause the diffusion constant to decrease as the measurement of diffusion is the distance from start to end of the diffusion time[118]. The authors concluded that instead of linked cavities of the polymer, the system was more likely that the carriers in solution diffuse around the polymer chains [117].

In the previous section, the fluorine diffusion for the polymer gel electrolytes was discussed, and it was assumed that there was only a single exponential factor to the diffusion decay curves, same as for the liquid electrolytes. Figure 5.13 shows the typical diffusion decay curves for the fluorine nucleus for for 0% (liquid), 20% and 30% PVDF/PC/$LiBF_4$ (1.0M) polymer gel electrolytes at 303 K. In figure 5.13, fits to equation 5.7 (dashed) and equation 5.8 (solid) have been employed. The fluorine data were fitted well to a single exponential factor for both liquid and polymer gel electrolytes, suggesting a single phase. However there was likely fluorine molecules in the solvated amorphous phase however the diffusion could not be distinguished and therefore the values measured were an average if all diffusion times weighted towards the liquid electrolyte phase. The values obtained from 5.13 were (1.19±0.01), (0.86±0.01) and (0.86±0.02) (10^{-10} m^2 s^{-1}) for the liquid, 20% PVDF gel and 30% PVDF gel, respectively. Suggesting that in each case the diffusion constant for the liquid electrolyte phase was measured and there was very little or no contribution from any other phase. The fluorine diffusion constants were consistently larger than the lithium measurements, thus strengthening the hypothesis that there was no restricted diffusion since the fluorinated BF_4 would surely interact with the boundaries faster

	Diffusion Constant (10^{-10} m^2 s^{-1})						
Temperature (K)	0.3M	0.5M	0.6M	0.7M	0.8M	0.9M	1.0M
283	—	0.21	0.18	0.23	0.16	0.19	0.24
293	—	0.31	0.26	0.36	0.24	0.27	0.29
303	0.69	0.49	0.51	0.54	0.42	0.34	0.41
313	0.97	0.65	0.73	0.68	0.56	0.46	0.53
323	1.18	0.97	0.99	0.89	0.78	0.68	0.59
333	1.52	1.13	1.20	1.19	0.99	0.88	0.81
343	1.75	1.36	1.38	1.48	1.14	1.01	0.93
353	2.07	1.63	1.75	1.75	1.54	1.23	1.30

Table 5.14: Slow phase ^{7}Li diffusion constants (D_1) for 20% PVDF/PC/$LiBF_4$ polymer gel electrolytes.

than the lithium ions if they are translating at a faster rate.

5.4.2.2 NMR-PFG Diffusion Results

The polymer gel electrolyte diffusion data can now be presented and discussed with the knowledge that there were two distinct diffusive species present in the polymer gel electrolytes. Fitting of the diffusion decay curves were carried out on the control computer of the NMR spectrometer which utilises the Levenberg-Marquardt algorithm which is a least squares iterative fitting process. The Bruker Topspin 1.5 software needed initial guesses of the diffusion constants, which for both species was usually entered as 1×10^{-10} m^2 s^{-1}. The fitting procedure gave reliable fits and therefore reliable measurements of the diffusion. For every measurement taken both equations 5.7 and 5.8 were fitted to give the single diffusion parameter and the dual fitting parameters, respectively. The single fit diffusion parameters were included here for completion, however it was assumed that there were two real diffusive species containing lithium ions which could be distinguished and that the single fit would essentially represent an average of these two phases.

It is important here to define the terminology that will be used for the remaining of this chapter. The lithium diffusion has been shown in the previous section that there are two distinct diffusive species, one that has been attributed to the liquid electrolyte phase of the gels and a second one which has been attributed to the solvated amorphous phase of the gel. The term $'slow'$ will be used to denote the solvated amorphous phase contribution and the term $'fast'$ was used to denote the liquid electrolyte component. These have been chosen due to the fact that the $'fast'$ component has a faster rate of diffusion. The term $'single'$ fit has been used to denote the fitting of equation 5.7 to the data which only includes a single exponential term and hence a single diffusion constant.

The diffusion constants for the slow and fast components for 20% PVDF/PC/$LiBF_4$ polymer gel electrolytes at all salt concentrations measured are displayed in tables 5.14 and 5.15 respectively. Firstly turning the attention to the slower diffusive species contained in the gels it was observed that the usual trends in diffusion were observed here, an increase with temperature and decrease with increasing salt concentration. These trends have been observed for all

	Diffusion Constant (10^{-10} m^2 s^{-1})						
Temperature (K)	0.3M	0.5M	0.6M	0.7M	0.8M	0.9M	1.0M
283	—	0.86	0.81	0.71	0.64	0.56	0.55
293	—	1.17	1.08	1.03	0.89	0.81	0.63
303	1.94	1.45	1.29	1.35	1.19	0.95	0.88
313	2.45	1.83	1.74	1.56	1.47	1.22	1.13
323	3.13	2.36	2.21	1.99	1.96	1.59	1.35
333	3.65	2.78	2.53	2.50	2.38	1.93	1.64
343	4.14	3.26	2.94	2.91	2.74	2.23	1.92
353	4.72	3.87	3.55	3.37	3.45	2.59	2.40

Table 5.15: Fast ^{7}Li diffusion constants (D_2) for 20% PVDF/PC/LiBF$_4$ polymer gel electrolytes.

diffusion measurements and can be explained by the thermal energy of the molecules as well as the viscosity of the system which will increase with salt concentration and decrease with temperature. When fitting the diffusion decay curves the values of the diffusion were at times quite erratic, mainly for the slower diffusive species; this was attributed to the fitting process. The fitting process allowed for the two intensity and two diffusion terms to be freely fitted therefore allowing some speculation of the results. However usually the variation in the values between repeat scans were not too far apart and were therefore trusted, but there was clearly an extra error contribution of the dual fitting rather than the liquid single fit of the diffusion decay curves. All of the diffusion values for the slower phase were seen to be of the order of 10^{-11} m^2 s^{-1} and at higher temperatures some of the diffusion reached 10^{-10} m^2 s^{-1}. It was considered possible to obtain a diffusional contribution from the lithium ions associating to the polymer backbone, as the lithium ions are positively charged and the fluorine of the PVDF was slightly negatively charged therefore allowing electrostatic interaction. However it was thought that the diffusion times measured for this phase were too fast for an ion connected to the polymer backbone itself, as even though the polymer will gyrate these movements will be on a different timescale to the diffusion observed for the liquid electrolyte regions. The $'slow'$ diffusive species measured were still quite substantial compared to the faster diffusive species, therefore both phases are considered to be relatively mobile.

It is possible to determine the diffusion constants by fitting a single exponential (equation 5.7) to the 20% and 30% PVDF/PC/LiBF$_4$ data, displayed in tables 5.16 and 5.17, respectively. As expected, the single diffusion constants behave as the slow and fast diffusion constants, i.e. they increase with temperature and decrease with salt concentration. As discussed in section 5.4.2.1, the single fitting of the diffusion decay curves for both 20% and 30% PVDF gels displayed some variance from the data points. Essentially, these values represent an average diffusion constant of the two distinct phases, which would clearly depend on the significance of each phase. Since the liquid electrolyte phase was considered the most prominent phase of the polymer gel electrolytes, the average would be weighted toward the liquid value. The diffusion constants for 20% PVDF/PC/LiBF$_4$ (1.0M) were (0.62±0.01), (0.41±0.05) and (0.88±0.03) (10^{-10} m^2 s^{-1}) for the single fit, slow and fast dual fit, respectively. Therefore it can be seen that the single diffusion fit falls between the two dual fit parameters. An estimate of the intensity can be calculated here

	Diffusion Constant (10^{-10} m^2 s^{-1})						
Temp. (K)	0.3M	0.5M	0.6M	0.7M	0.8M	0.9M	1.0M
303	1.29	0.98	0.91	0.85	0.77	0.71	0.62
313	1.59	1.26	1.17	1.10	0.99	0.92	0.82
323	2.00	1.61	1.48	1.39	1.28	1.18	1.05
333	2.36	1.94	1.79	1.66	1.56	1.45	1.26
343	2.84	2.27	2.13	1.99	1.88	1.72	1.51
353	3.29	2.71	2.52	2.34	2.22	2.01	1.84

Table 5.16: Single fit ^{7}Li diffusion constants for 20% PVDF/PC/$LiBF_4$ polymer gel electrolytes.

simply with the values given above. It is assumed that the single fit value of diffusion could be calculated by:

$$D_{Single} = I(0)_{Slow} D_{Slow} + I(0)_{Fast} D_{Fast} \tag{5.10}$$

where $I(0)_{Slow}$ and $I(0)_{Fast}$ are the intensities of the polymer and liquid phases, respectively. Since there were only two components to the diffusion it was logical that $I(0)_{Slow} + I(0)_{Fast} = 1$. Using the values for the 20% PVDF 1.0M gel results shown above, the intensities were calculated using equation 5.10 as 0.45 and 0.55 for the polymer and liquid phase, respectively. The intensities were recorded of each fit along with the corresponding diffusion values, the average of the three repeat measurements gave 0.41 and 0.59 as the intensities of the polymer and liquid phases respectively. This corresponds to the result from the calculated intensity and therefore the single fit can be seen as an average of the polymer and liquid phases. Therefore it was assumed that in most publications that do not express two distinct diffusive species they are observing merely an average of all phases represented here by the 'single' fits. The presence of the multiple phases in the gels are attributed to the significant amount of solvent contained. The higher the solvent concentration, the larger the cavities will be [26], therefore making the phases more distinct.

The diffusion of the liquid electrolytes containing PC/$LiBF_4$ (1.0M) exhibited a value of (0.61±0.01) at 283 K with the 20% PVDF gel result of (0.24±0.03) and (0.55±0.03) (10^{-10} m^2 s^{-1}) for the slow and fast components, respectively. It should be noted here that the faster gel component was very similar to the liquid electrolyte result. This point strongly correlates with the hypothesis that the liquid electrolyte flows throughout the polymer structure and that the faster diffusive species was most likely the lithium ions in the pure liquid phase of the gel. It was observed that for all of the diffusion measurements, the faster diffusive species correlated well with the liquid measurements at all temperatures. At the highest temperature the diffusion of the liquid electrolyte containing PC/$LiBF_4$ (1.0M) exhibited a value of (3.63±0.01) at 353 K and the 20% PVDF gel result was (1.30±0.03) and (2.40±0.03) (10^{-10} m^2 s^{-1}) for the slow and fast components, respectively. Therefore it can be seen that at higher temperatures there was some deviance of the liquid electrolyte result and the fast polymer species, however this has been attributed to the confinement of the liquid electrolyte phase, as seen with fluorine in the previous section.

The diffusion constants were also measured for 30% PVDF/PC/$LiBF_4$ polymer gel electrolytes, which also exhibited two distinct diffusive species and hence two diffusion constants,

	Diffusion Constant (10^{-10} m^2 s^{-1})						
Temp. (K)	0.3M	0.5M	0.6M	0.7M	0.8M	0.9M	1.0M
283	0.53	0.40	—	—	—	0.31	0.23
293	0.65	0.51	—	0.47	—	0.38	0.34
303	0.85	0.68	0.65	—	0.54	0.52	0.44
313	1.02	0.82	0.84	0.82	0.72	—	0.53
323	1.27	1.05	1.06	0.99	0.90	0.90	0.70
333	1.52	1.28	1.30	1.19	1.10	1.05	0.89
343	1.76	1.53	1.56	1.40	1.30	1.27	1.12
353	2.12	1.92	1.93	1.62	1.54	—	1.37

Table 5.17: Single fit ^{7}Li diffusion constants for 30% PVDF/PC/$LiBF_4$ polymer gel electrolytes.

	Diffusion Constant (10^{-10} m^2 s^{-1})						
Temperature (K)	0.3M	0.5M	0.6M	0.7M	0.8M	0.9M	1.0M
283	0.25	0.17	—	0.23	—	0.15	0.11
293	0.35	0.26	—	0.27	—	—	0.23
303	0.48	0.35	0.31	0.36	0.27	0.32	0.27
313	0.56	0.42	0.46	0.48	0.38	0.38	0.29
323	0.72	0.51	0.60	0.56	0.51	0.55	0.35
333	0.89	0.66	0.74	0.73	0.67	0.61	0.55
343	1.06	0.72	0.88	0.87	0.78	0.73	0.65
353	1.31	0.89	1.08	0.95	0.92	0.84	0.83

Table 5.18: Slow ^{7}Li diffusion constants (D_1) for 30% PVDF/PC/$LiBF_4$ polymer gel electrolytes.

	Diffusion Constant (10^{-10} m^2 s^{-1})						
Temperature (K)	0.3M	0.5M	0.6M	0.7M	0.8M	0.9M	1.0M
283	1.00	0.76	—	0.75	—	0.53	0.46
293	1.33	1.03	—	0.94	—	—	0.91
303	1.82	1.31	1.16	1.22	1.06	1.08	0.94
313	2.06	1.53	1.54	1.48	1.35	1.23	1.02
323	2.42	1.79	1.89	1.72	1.71	1.60	1.25
333	2.96	2.24	2.21	2.17	2.14	1.82	1.74
343	3.23	2.38	2.59	2.41	2.40	2.13	2.03
353	3.75	2.83	3.03	2.61	2.73	2.43	2.34

Table 5.19: Fast ^{7}Li diffusion constants (D_2) for 30% PVDF/PC/$LiBF_4$ polymer gel electrolytes.

the results of which are displayed in tables 5.18 and 5.19 for the slow and fast species, respectively. As one would expect, the temperature and salt concentration dependencies are the same as for the liquid and 20% PVDF gels. Taking the 1.0M $LiBF_4$ samples as an example, the 30% PVDF gel yielded a value of (0.11±0.03) for the slow diffusion component. Comparing this to the 20% PVDF result of (0.24±0.03), it can be noted that the increase of polymer causes a decrease in the diffusion constant in the solvated amorphous polymer phase. The fast diffusive species results were (0.55±0.03) and (0.46±0.03) (10^{-10} m^2 s^{-1}) for the 20% and 30% PVDF gels, respectively at 283 K. Therefore with the addition of more polymer the diffusion constants of both the faster (liquid) and slower (polymer) phases decreased; interestingly, the slower diffusive species decreased much more significantly than the faster phase. The addition of more polymer would increase the viscosity of the amorphous phase and therefore reduce the ionic mobility. However it is assumed that the viscosity of the liquid phase would not be directly effected by the addition of polymer, however the pockets of liquids would likely be smaller and therefore more confined. At higher temperatures it was seen that the liquid phase for the 20% and 30% PVDF gels, the diffusion was almost equal with values of (2.40±0.03) and (2.34±0.02) (10^{-10} m^2 s^{-1}) for the 20% and 30% PVDF gels, respectively.

Figure 5.14 shows an Arrhenius plot for the lithium diffusion constants for both the 20% and 30% PVDF/PC/$LiBF_4$ (0.5M) polymer gel electrolytes. Analysis of figure 5.14 reveals that the slower diffusive species was possibly non-Arrhenius as they displayed slight curvature, however the fast liquid phase exhibited a linear relationship suggesting Arrhenius type behaviour. It was decided that since there was not a clear curvature to figure 5.14 that it would be assumed that the temperature dependence was Arrhenius for both phases. This allowed determination of the activation energies from the linear relationship of the Arrhenius plot, the results of which can be found in table 5.20.

Table 5.20 displays the activation energy E_D and the fitting parameter D_∞ for the 20% and 30% PVDF/PC/$LiBF_4$ polymer gel electrolytes for all salt concentrations measured. The liquid activation energy has been added to table 5.20 as a basis for comparison. The activation energies of diffusion for the polymer (slow) phase were seen to be larger than the liquid (fast) phase. The solvated amorphous phase would be expected to have a significantly higher viscosity than the corresponding liquid electrolyte phase, therefore the molecules would require more

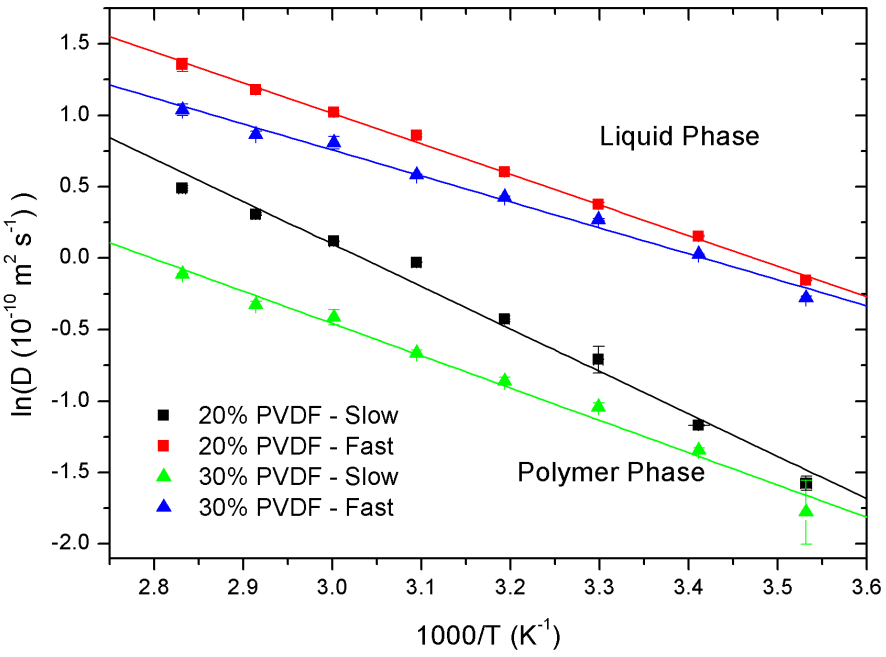

Figure 5.14: ^{7}Li diffusion Arrhenius plot for 20% and 30% PVDF/PC/$LiBF_4$ (0.5M) polymer gel electrolytes. Both slow (polymer) and fast (liquid) phases are included.

energy to translate through the sample. For both diffusive species the activation energies were seen to roughly increase with increasing salt concentration which has again been attributed to the viscosity of the system. The fitting parameters D_∞ have also been included in table 5.20, however there seems very little variance over the salt concentration covered. The physical meaning of D_∞ is the diffusion constant at an infinitely high temperature, as $D(T) = D_\infty$ when $exp\,[-E_D/T]$=1, therefore since the exponential of zero equals 1, D_∞ is the value of the diffusion constant when $-E_D/T = 0$ or at infinite temperature. No physical significance has been taken from the D_∞ value as there seems to be a lot of scatter between samples and was therefore considered simply a fitting parameter.

The liquid electrolyte phase of the gels exhibited similar activation energies for both polymer concentrations, which was attributed to the fact that the liquid electrolyte phase flows throughout the polymer structure and therefore would be similar in both cases. It can be seen in table 5.20 that for the PVDF/PC/$LiBF_4$ (0.3M) samples, the liquid phase activation energies were (15.8±0.8) kJ mol^{-1} and (14.2±0.7) kJ mol^{-1} for the 20% and 30% PVDF, respectively. From this result it was noted that the liquid phase activation energies were similar for both polymer concentrations. The corresponding polymer phase activation energies were (19.2±0.9) kJ mol^{-1} and (19.2±0.5) kJ mol^{-1} for the 20% and 30% PVDF gels, respectively, which are higher and therefore suggesting a more viscous environment for the molecules in the polymer phase. It should be noted that the activation energies of the solvated amorphous phase were the same for both polymer concentrations.

The activation energies of the longitudinal relaxation times have also been included in table 5.20 to allow comparison with the corresponding diffusional activation energies. As seen with

	E_{T_1} (kJ mol^{-1})		E_D (kJ mol^{-1})					D_∞ (10^{-10} m^2 s^{-1})			
Salt				20% PVDF		30% PVDF		20% PVDF		30% PVDF	
Conc. (M)	20%	30%	Liquid	Slow	Fast	Slow	Fast	Slow	Fast	Slow	Fast
0.3	9.4	—	19.4	19.2	15.8	19.2	14.2	1.51	1.07	0.92	0.49
0.5	8.7	7.5	20.4	24.7	17.8	17.2	15.1	8.32	1.71	0.31	0.50
0.6	12.5	8.6	—	21.2	17.5	21.3	16.6	2.47	1.42	1.58	0.88
0.7	9.9	9.2	21.5	23.9	18.1	17.7	15.3	6.53	1.64	0.42	0.50
0.8	8.7	8.3	—	26.6	19.7	21.9	17.1	14.28	2.87	1.70	0.98
0.9	10.7	—	—	22.9	18.1	17.3	14.9	3.21	1.26	0.32	0.39
1.0	11.1	10.3	21.9	19.6	18.3	19.1	19.2	0.95	1.22	0.51	1.68

Table 5.20: ^{7}Li diffusion Arrhenius activation energies and D_∞ for 20% and 30% PVDF/PC/$LiBF_4$ polymer gel electrolytes. Activation energy of the longitudinal relaxation times (E_{T_1}) have also been included.

the liquid electrolytes in Chapter 4, by comparing the T_1 and diffusion activation energies it was possible to obtain an indication of the relative contributions from the rotational and translational to the longitudinal relaxation. If the longitudinal relaxation was solely due to translational motion then it was thought that the activation energies for the two measurements would be equal since diffusion is a purely translational quantity. If the activation energy was smaller than the diffusion activation energy then it was assumed that there was also a rotational component to the relaxation. However in the case of the gels it is much more difficult to directly compare the activation energies as the longitudinal relaxation was an average of each phase, whereas the diffusion activation energies could be determined for the polymer and liquid phase separately.

The 20% PVDF/PC/$LiBF_4$ (0.5M) diffusion activation energies from table 5.20, were (24.7 ±0.9) kJ mol^{-1} and (17.8±0.4) kJ mol^{-1} for the polymer and liquid phases, respectively, with the longitudinal relaxation activation energy given as (8.7±0.4) kJ mol^{-1}. It was assumed that the longitudinal relaxation can validly represent both the liquid and polymer phases (as an average for both) which then allows a comparison between the two activation energies to be carried out. Ratios of the activation energies of the longitudinal relaxation and diffusion (E_{T_1}/E_D) were calculated and displayed in table 5.21. For the 0.5M samples which yielded values of (0.35±0.02) and (0.49±0.03) for the polymer and liquid phases, respectively. Since the diffusion is a purely translational process a ratio of one would suggest that the longitudinal relaxation was solely due to translational motion. Therefore this result suggests that there was a larger rotational component of the relaxation in the solvated amorphous polymer phase than the liquid electrolyte phase due to an increased viscosity. Therefore as the viscosity was increased the more difficult it becomes to undergo translational motion and therefore the rotational component becomes more significant. The ratio for the liquid electrolyte at the same salt concentration (0.5M) was determined to be (0.67±0.02), in Chapter 4. Therefore in the liquid electrolyte case, there was a dominant translational component of the longitudinal relaxation. The introduction of the polymer has increased the viscosity of the system causing the translational component of the relaxation becoming less significant in the liquid phase due to an increased energy required for translation. The solvated amorphous polymer phase was observed to be dominated by rotational

	E_{T_1}/E_D			
Salt Conc. (M)	20% PVDF		30% PVDF	
	Slow	Fast	Slow	Fast
0.3	0.49	0.59	—	—
0.5	0.35	0.49	0.44	0.50
0.6	0.41	0.71	0.40	0.52
0.7	0.41	0.55	0.52	0.60
0.8	0.33	0.44	0.38	0.49
0.9	0.47	0.59	—	—
1.0	0.57	0.61	0.54	0.54

Table 5.21: ^{7}Li ratio of longitudinal and diffusional activation energies (E_{T_1}/E_D) for 20% and 30% PVDF/PC/$LiBF_4$ polymer gel electrolytes.

motion.

The activation energies were fairly scattered with salt concentration for both longitudinal and diffusion activation energy and therefore these ratios are only to give an indication of the relative contributions from the translational and rotational components of the T_1 values. However since it was assumed that the longitudinal relaxation times was an average of both phases and that the diffusion activation energies of the polymer phase were always larger than the liquid phase, it can be concluded that the polymer phase exhibited a larger rotational component than the liquid electrolyte phase.

The 30% PVDF activation energies can be compared in the same manner as the 20% PVDF gels. By taking an example from table 5.21 for the 30% PVDF/PC/$LiBF_4$ (0.5M) polymer gel electrolyte sample the ratio of the activation energies were (0.44±0.02) and (0.50±0.03) for the polymer and liquid phases, respectively. The corresponding liquid ratio from Chapter 4 was (0.67±0.02). This result suggests that for both phases the contribution from the rotational motion was more significant than in the liquid electrolytes, and that the polymer phase has a larger rotational component than the liquid electrolyte phase of the polymer gel electrolytes.

The salt concentration dependence has been shown graphically in figure 5.15 for both 20% and 30% PVDF/PC/$LiBF_4$ for both polymer and liquid phases at 303 K. It can be observed for both polymer concentrations the diffusion of the amorphous polymer does not decrease significantly with increasing salt concentration. This result was considered reasonable as the viscosity of the amorphous region of the gels would likely be dominated by the presence of the polymer and not the salt concentration, therefore an increase in salt concentration would effect the viscosity, although not as significantly as the liquid counterparts.

5.4.2.3 Phase Intensity

In previous sections of this chapter the intensities of the dual exponential fit have been briefly discussed, however in this section they will be considered more closely. From the transverse relaxation measurements taken on the benchtop NMR spectrometer it was shown that hydrogen atoms could be found in at least three different phases within the polymer gel electrolyte.

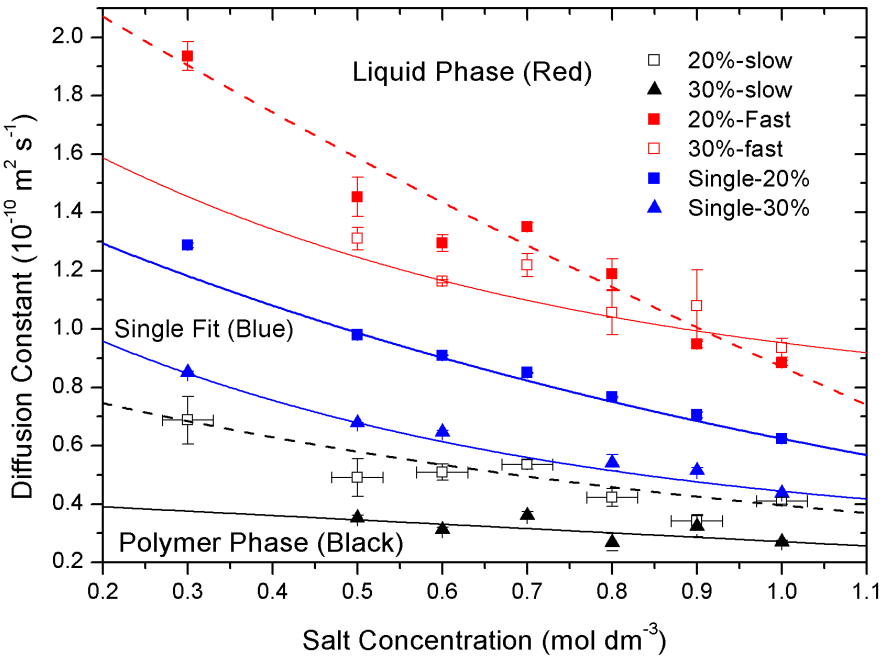

Figure 5.15: ^{7}Li diffusion constants as a function of salt concentration for 20% and 30% PVDF/PC/$LiBF_4$ polymer gel electrolytes at 303 K. Both slow (polymer) and fast (liquid) phases are included.

These phases have been attributed to the interlamellar amorphous polymer, solvated amorphous polymer and pure liquid electrolyte. For the fitting process of the transverse relaxation measurements an intensity was determined for each phase which gave an indication of the significance of the phase. It was noted that a small contribution gave a relaxation of the order of milliseconds which was attributed to the interlamellar amorphous regions of the spherulites. The next significant phase had relaxation times in the order of 100 ms which was attributed to the amorphous polymer phase which would most likely be mixed with liquid. The third phase was the most significant and exhibited relaxation times of the order of seconds which is characteristic of liquids and therefore was attributed to the liquid electrolyte phase.

The presence of two distinct diffusion constants was therefore logical as the mobility of each of the phases would be quite different. The gyration of the crystalline polymer would most likely cause very little contribution to the diffusion decay curve and therefore be negligible compared to the other two phases. For this reason the slower of the two diffusion phases has been attributed to the solvated amorphous polymer phase.

The diffusion decay curves were fitted with equation 5.8 which gave a value for the diffusion as well as the significance of the contribution of each phase which was labeled intensity, where $I(0)_1$ and $I(0)_2$ are the intensities for the solvated amorphous polymer and liquid phases, respectively. Table 5.22 shows the intensities of the liquid phase ($I(0)_2$) for all temperatures and salt concentrations measured for the 20% PVDF/PC/$LiBF_4$ polymer gel electrolytes. The values of the polymer intensity will not be displayed here as the polymer phase intensity can be easily calculated $(1 - I(0)_2)$ as the total intensity was normalised so $I(0)_1 + I(0)_2$=1. It

	20% PVDF Intensity, $I(0)_2$						
Temperature (K)	0.3M	0.5M	0.6M	0.7M	0.8M	0.9M	1.0M
283	—	0.9	0.8	0.8	0.8	0.7	0.6
293	—	0.8	0.8	0.7	0.8	0.7	0.7
303	0.7	0.7	0.7	0.6	0.6	0.8	0.6
313	0.6	0.7	0.6	0.6	0.7	0.7	0.6
323	0.6	0.6	0.6	0.6	0.6	0.7	0.7
333	0.6	0.7	0.6	0.5	0.6	0.6	0.7
343	0.6	0.7	0.6	0.5	0.7	0.7	0.7
353	0.6	0.7	0.6	0.5	0.6	0.7	0.6

Table 5.22: ^{7}Li liquid phase intensity I_2 for 20% PVDF/PC/$LiBF_4$ polymer gel electrolytes.

	30% PVDF Intensity, $I(0)_2$						
Temperature (K)	0.3M	0.5M	0.6M	0.7M	0.8M	0.9M	1.0M
283	0.6	0.7	—	0.5	—	0.6	0.6
293	0.6	0.7	—	0.6	—	—	0.4
303	0.6	0.6	0.6	0.6	0.6	0.6	0.5
313	0.6	0.7	0.6	0.6	0.6	0.7	0.6
323	0.6	0.7	0.6	0.6	0.6	0.6	0.7
333	0.6	0.7	0.6	0.6	0.6	0.7	0.6
343	0.6	0.7	0.6	0.6	0.6	0.7	0.6
353	0.6	0.8	0.6	0.7	0.6	0.7	0.6

Table 5.23: ^{7}Li liquid phase intensity I_2 for 30% PVDF/PC/$LiBF_4$ polymer gel electrolytes.

can be noted from table 5.22 that there was no significant trend with either temperature or salt concentration. Each intensity was determined from the average of three individual repeat readings. Since there was no obvious trend with temperature or salt concentration an average of all of the values in table 5.22 was taken to obtain an estimation of the contribution from the liquid electrolyte phase. The average value obtained from table 5.22 was (0.66±0.05) which implies that the average intensity of the polymer phase ($I(0)_1$) was (0.34±0.05). Therefore on average for the 20% PVDF/PC/$LiBF_4$ gels the liquid electrolyte phase contributed 66% of the diffusion decay and the polymer phase contributes 34%. Comparing these values to that obtained for the transverse relaxation measurements discussed earlier, the intensities of the three phases were (0.13±0.08), (0.36±0.06) and (0.52±0.06) for the interlamellar amorphous polymer, solvated amorphous polymer and liquid electrolyte, respectively. This corresponds to contributions of the solvated amorphous polymer and liquid electrolytes phases as 41% and 59%, respectively. Therefore the contributions from the liquid and polymer phase were similar from both the transverse relaxation and diffusion measurements.

The intensities of the liquid electrolyte phase ($I(0)_2$) for the 30% PVDF/PC/$LiBF_4$ polymer gel electrolytes are displayed in table 5.23. As with the 20% PVDF gels there was no clear trend with temperature or salt concentration therefore an average of all values in table 5.23 were

taken. The average value of the tintensity of the liquid phase was given as (0.61±0.05). Therefore the contributions from the solvated amorphous polymer and liquid phases were 39% and 61%, respectively for the 30% PVDF polymer gel electrolytes. The transverse relaxation time intensities for the 30% PVDF gels were (0.14±0.08), (0.42±0.04) and (0.44±0.04) for the interlamellar amorphous polymer, amorphous polymer and liquid phases, respectively. The contributions of the amorphous polymer and liquid phases were 49% and 51%, respectively. Therefore both the transverse relaxation and diffusion constant intensities show that the liquid electrolyte phase became less significant as the amorphous polymer phase became more significant. This was intuitive as an increase in polymer concentration would logically lead to a higher amorphous polymer region and hence less liquid electrolyte component.

5.4.3 Hydrogen Measurements

In this section the hydrogen (^{1}H) NMR diffusion measurements for the polymer gel electrolytes are reported. At the beginning of this chapter it was discussed that there were three distinct phases within the polymer gel electrolyte; an interlamellar polymer phase, a solvated amorphous polymer phase and a pure liquid electrolyte phase. These phases were detected via transverse relaxation measurements which also revealed the significance of each phase.

It has shown earlier, that the lithium PFG-NMR diffusion measurements revealed two distinct diffusive species which were attributed to the solvated amorphous polymer and liquid electrolyte phases. However for the fluorine nucleus it was found that there was only a single diffusive species that could be determined from fitting of the diffusion decay curves. It is therefore a possibility that there will be two hydrogen diffusive species for the 20% and 30% PVDF gels.

In section 5.1.1 the mounting of the polymer gel electrolyte into the 10 mm glass NMR tubes was discussed and it was determined that the best way to manipulate and mount the gels was to extract a sample and shape the gel as it cooled and hardened. The hydrogen coil had a 5 mm diameter and therefore 5 mm NMR glass tubes were used in these measurements. This was not an issue with the measurements of the liquid electrolytes as they were simply pipette into the tube. However the gels were practically solid at room temperature and extremely difficult to manipulate. As with the 10 mm tubes the gels were created by heating the ingredients to 160 °C and allowed to cool to form polymer gel electrolytes. While in the molten form, the samples were stirred using a clean stainless steel spatula and allowed to drip from the spatula onto a clean surface in a controlled manner. This allowed the gels to be formed to any thickness as the gels were dripped into the desired thickness. Although this preparation method seems uncontrolled it was deemed the best way to mount the gels. The only other viable method of mounting would be to cut the gels once cooled; however, since the sample size had to be very small, a significant amount of solvent would be lost from the sample. The dripping method provided an easy way to mount the gels within the tubes with minimal solvent loss.

The power level used for NMR measurements presented in this section was 0 dB which gave the values of the $\pi/2$ and π pulse durations as 6.47 μs and 12.94 μs, respectively. These durations were measured using the parameter optimisation ('*popt*') sequence which varies the value of the $\pi/2$ pulse duration and measures the resulting intensity of the FID. This is repeated over many values and the point at which the intensity is zero is defined as the pulse duration for a π pulse. The magnetisation can only be detected in the xy plane, therefore if the spins are flipped

perfectly to the $-z$ direction there would be zero magnetisation in the measurable xy plane.

The settings for the diffusion measurements were kept the same as for all of the previous diffusion measurements. The value of Δ the diffusion time was fixed at 40 ms for all measurements. The duration of the gradient pulse (δ) was fixed to 10 ms with the time between RF pulses and gradient pulses (δ_1) at 1 ms. The diffusion measurements were two dimensional experiments, as the experiment was repeated for several values of the gradient strength (G). The values of the gradient strength were determined based on the expected value of the diffusion measurement.

The 20% PVDF polymer gel electrolytes were measured in the salt concentration range 0.0-1.0M and temperature range of 283-353 K, however for some measurements the 283 K and 293 K temperatures were not attainable due to limitations of the NMR spectrometer. Since lithium exhibited two distinct diffusion constants a single fit and dual fit was employed using equations 5.7 and 5.8, respectively. It was found for the 20% PVDF gels that the dual diffusion fitting was applicable only for the 0.0M and 0.3M $LiBF_4$ salt concentrations. However even in these cases the fitting of the single exponential did not deviate very far from the data, suggesting a smaller contribution from the solvated amorphous phase in the hydrogen measurements. It was seen for the 0.3M $LiBF_4$ sample that the dual fitting reduced to the single fit at higher temperatures. It was assumed that restricted diffusion was not an issue here, as the effects of the restricted diffusion would presumably be worse at higher temperatures as the molecules are diffusing faster.

Figure 5.16 displays example diffusion decay curves for 20% and 30% PVDF/PC/$LiBF_4$ (0.5M) at 293 K. A single (dashed) and dual (solid) diffusion fits were employed for both the 20% and 30% PVDF gels. For the 20% PVDF polymer gel electrolyte the single fit was observed to vary slightly from the measured diffusion data, indicating a second diffusive species as seen for the lithium nucleus. The values obtained for the two fits for the 20% PVDF gels were (0.64±0.05) and (2.6±0.1) (10^{-10} m^2 s^{-1}) for the slow and fast diffusion constants, respectively. The intensity of the two phases were determined from the fitting in figure 5.16 were (0.12±0.08) and (0.87±0.08) for the polymer and liquid phase, respectively. As with the lithium measurements the faster diffusive species was attributed to the liquid electrolyte phase of the gel electrolytes which for this fit was seen to contribute around 87% of the decay curve. This percentage was higher than the corresponding liquid phase for the lithium diffusion measurements, an average value for the 20% PVDF gels was (0.66±0.01) (66%) for the liquid electrolyte phase. This result suggested that there was a stronger signal from the solvated amorphous phase in the lithium measurements than for the hydrogen. It proved difficult to determine the slower, less prominent diffusive species and as a result the values were quite scattered. Therefore the analysis of the diffusion of 20% PVDF/PC/$LiBF_4$ gels was considered to only have one contribution to the diffusion decay curve.

Figure 5.16 also shows the diffusion decay curve for the 30% PVDF/PC/$LiBF_4$ (0.5M) polymer gel electrolyte. The values obtained from fitting this data was (0.83±0.05) and (2.56±0.05) (10^{-10} m^2 s^{-1}) for the slow and fast dual diffusion fits respectively. It should be noted that the fast liquid electrolyte phase diffusion constants for the 20% and 30% PVDF gels were the same to one decimal place. This suggested again that the diffusion in the liquid electrolyte phase was similar for both polymer concentrations. The intensities for the polymer and liquid electrolyte phases were (0.31±0.03) and (0.69±0.03) respectively for the 30% PVDF gel. Therefore it can be noted that since the fluorine nucleus could be fitted with a single exponential it had the lowest presence in the amorphous polymer phase, followed by the hydrogen nucleus. The lithium

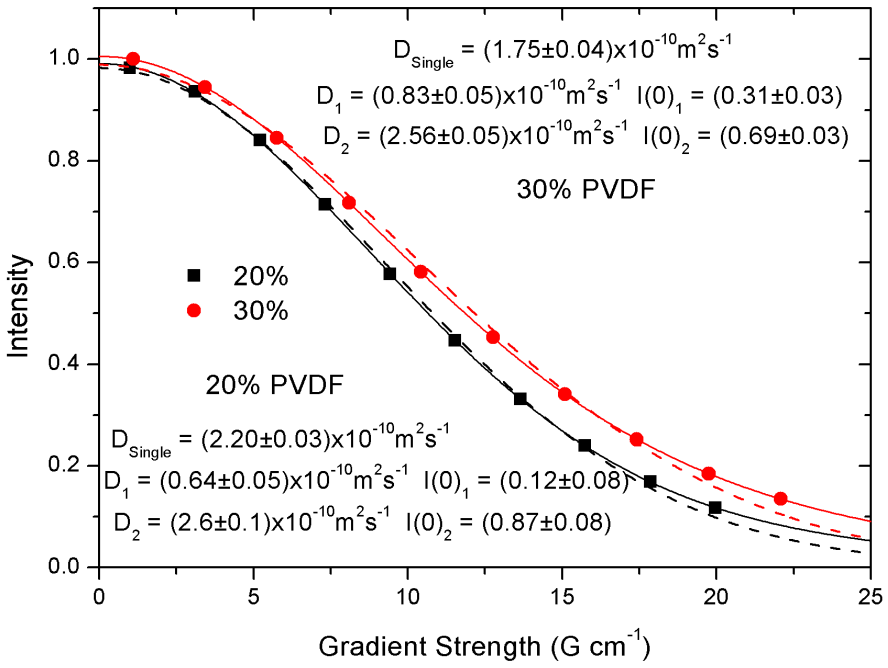

Figure 5.16: ^{1}H diffusion decay curves for 20% and 30% PVDF/PC/LiBF$_4$ (0.5M) polymer gel electrolytes at 293 K. Single (dashed) and double (solid) exponentials have been applied.

measurements had the largest deviance suggesting the most prominent polymer phase.

It was assumed for the analysis of the 20% PVDF/PC/LiBF$_4$ polymer gel electrolytes that there was only a single diffusion constant for the entire gel similar to the fluorine measurements. Table 5.24 shows the single fit diffusion constants for the 20% and 30% PVDF/PC/LiBF$_4$ gel electrolytes for all samples measured in the temperature range 283-353 K. The diffusion constants were seen to increase with temperature and decrease with salt concentration, which has been attributed to the change in viscosity with these two quantities. The diffusion constants for the 20% PVDF gels were higher than the corresponding 30% PVDF gels. This was attributed to the reduction of free volume with the increase in polymer concentration.

The temperature dependence of the single fit diffusion constants for the 20% and 30% gels can be determined in the same manner as the lithium and fluorine diffusion constants. Arrhenius plots were employed in figure 5.17 which shows an Arrhenius plot for the single diffusion for the 20% and 30% PVDF gels. It was shown that the Arrhenius plots exhibited a linear relationship and therefore an Arrhenius type temperature dependence which is consistent with the other diffusion measurements for both the liquid and polymer gel electrolytes. This allowed the determination of the activation energy of diffusion for the single fit values. However it was also of interest to determine the temperature dependence of the dual phase 30% PVDF gels.

The two exponential dual fitting was applied to the 30% gels in the same manner as the lithium measurements, in which two exponential components were added together in series to respresent the polymer and liquid phases of the gels. Where again the $'slow'$ and $'fast'$ terms are used to denoted the solvated amorphous polymer and liquid phases, respectively. The diffusion data for the two phases for the 30% PVDF gels is displayed in table 5.25 for all salt

	Diffusion Constant (10^{-10} m^2 s^{-1})									
	20% PVDF					30% PVDF				
Temp. (K)	0.0M	0.3M	0.5M	0.7M	1.0M	0.0M	0.3M	0.5M	0.7M	1.0M
303	3.80	3.09	2.69	2.19	1.67	2.53	2.15	2.12	1.76	1.19
313	4.66	3.87	3.36	2.78	2.18	3.00	2.62	2.68	2.21	1.55
323	5.53	4.68	4.15	3.46	2.73	3.86	3.20	3.21	2.76	1.95
333	6.48	5.48	4.94	4.09	3.31	4.50	3.85	3.89	3.23	2.42
343	7.31	6.43	5.65	4.86	3.86	5.40	4.49	4.63	3.83	2.86
353	8.24	7.36	6.52	5.63	4.57	6.03	5.26	5.42	4.48	3.33

Table 5.24: ^{1}H diffusion constants for single fit for 20% and 30% PVDF/PC/$LiBF_4$ polymer gel electrolytes.

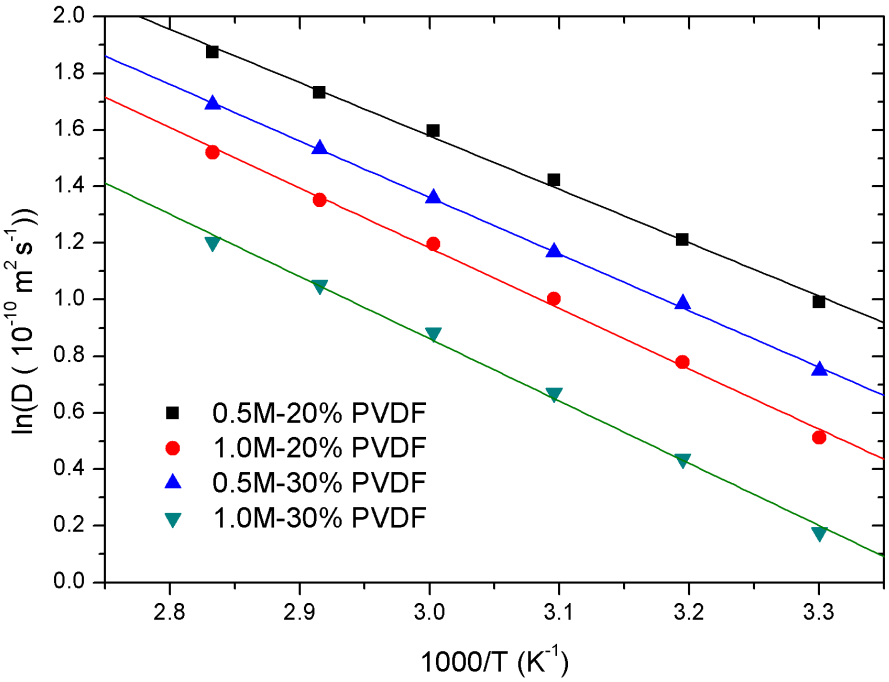

Figure 5.17: ^{1}H diffusion Arrhenius plot for 20% and 30% PVDF/PC/$LiBF_4$ (0.5M, 1.0M) polymer gel electrolytes. Linear fits suggest Arrhenius type temperature dependence at this temperature range.

	Diffusion Constant (10^{-10} m^2 s^{-1})									
	Slow (Polymer Phase)					Fast (Liquid Phase)				
Temp. (K)	0.0M	0.3M	0.5M	0.7M	1.0M	0.0M	0.3M	0.5M	0.7M	1.0M
303	1.45	1.08	0.83	0.70	0.62	3.69	3.15	2.77	2.18	1.74
313	2.12	1.50	1.59	1.35	0.70	6.02	4.05	3.94	3.03	2.12
323	2.40	2.10	2.19	1.86	1.23	6.65	5.26	5.21	3.90	3.02
333	2.65	2.52	2.61	2.17	1.66	7.33	6.12	6.02	4.48	3.94
343	2.97	3.00	2.89	2.43	2.01	8.18	7.02	6.67	5.15	4.48
353	3.46	3.50	3.63	3.02	2.29	9.56	8.04	7.90	6.05	4.94

Table 5.25: ^{1}H diffusion constants for slow (polymer) and fast (liquid) phases for 30% PVDF/PC/$LiBF_4$ polymer gel electrolytes.

	Intensity ($I(0)_2$)				
Temperature (K)	0.0M	0.3M	0.5M	0.7M	1.0M
303	0.8	0.7	0.8	0.8	0.7
313	0.4	0.6	0.6	0.6	0.7
323	0.5	0.5	0.6	0.6	0.6
333	0.6	0.6	0.6	0.6	0.5
343	0.6	0.5	0.6	0.6	0.5
353	0.6	0.5	0.6	—	0.5

Table 5.26: ^{1}H intensities for liquid phase ($I(0)_2$) for 30% PVDF/PC/$LiBF_4$ polymer gel electrolytes. Where $I(0)_1 = 1 - I(0)_2$ and $I(0)_1$ is the intensity of the polymer phase.

concentrations (0.0M, 0.3M, 0.5M, 0.7M and 1.0M) and temperatures. As with the lithium polymer diffusion constant, the hydrogen polymer phase diffusion was too fast to be considered to be the interlamellar amorphous phase or the crystalline polymer phase and therefore again is attributted to the solvated amorphous region of the polymer gel electrolytes.

Values of $I(0)_1$ and $I(0)_2$ the intensity of the polymer and liquid phases respectively were also determined from the fitting of the diffusion decay curves. The intensity refers to the contribution from each phase and has been normalised so that $I(0)_1$+$I(0)_2$=1. Table 5.26 shows the intensities of the liquid phase for the 30% PVDF/PC/$LiBF_4$ polymer gel electrolytes for all temperatures and salt concentrations measured. There was no clear trend of the intensity as a function of temperature or salt concentration as seen with the lithium measurements. The average value of the intensity was determined to be (0.59±0.01) which corresponds to the liquid contributing 59% and the solvated amorphous polymer phase contributing 41% to the total diffusion of the 30% PVDF gels. The intensity values determined for the lithium measurements were (0.61±0.01) for the 30% PVDF gels. Therefore the contributions of the liquid electrolyte phases for the 30% PVDF gel for the lithium and hydrogen nuclei were 61% and 59% respectively. Therefore these contributions were very similar suggesting that approximately the same proportion of hydrogen and lithium ions are present in the solvated amorphous polymer phase.

The temperature dependence of the dual polymer fits were quite scattered, this was considered

	E_D (kJ mol^{-1})				D_∞ (10^{-10} m^2 s^{-1})			
	20% PVDF	30% PVDF			20% PVDF	30% PVDF		
Salt Conc. (M)	Single	Single	Slow	Fast	Single	Single	Slow	Fast
0.0	13.7	15.9	11	10	898	1419	138	316
0.3	15.4	16.0	19	15	1404	1218	2285	1523
0.5	15.7	16.6	18	15	1394	1576	1512	1379
0.7	16.7	16.5	17	15	1705	1247	1094	1119
1.0	17.7	18.3	26	19	1963	1749	20845	3803

Table 5.27: ^{1}H diffusion Arrhenius fitting parameters, activation energy (E_D) and diffusion at infinite temperature (D_∞) for 20% and 30% PVDF/PC/$LiBF_4$ polymer gel electrolytes for both single fits and dual fit (slow and fast) for the 30% PVDF gels.

an artifact of the fitting process as it was a four parameter fitting procedure. However the trends with temperature and salt concentration were consistent with the other gel and liquid measurements as there was an increase with temperature and decrease with increasing salt concentration. The temperature dependence was assumed to be Arrhenius due to the linear relationship on the Arrhenius plots, therefore the activation energies were determined from the gradient of the Arrhenius plot multiplied by the universal gas constant. As seen with the lithium dual diffusion activation energies the slow polymer phase exhibited significantly higher activation energies, suggesting that the viscosity of this region was higher than the corresponding liquid electrolyte region.

In order to compare each nuclei, the single fit diffusion activation energies were considered. For the 20% PVDF/PC/$LiBF_4$ (0.3M) polymer gel electrolytes the activation energies were (15.4±0.2) kJ mol^{-1}, (16.8±0.3) kJ mol^{-1} and (14.9±0.6) kJ mol^{-1} for the ^{1}H, ^{7}Li and ^{19}F, respectively. It can be assumed that each nucleus experienced the same viscosity, and therefore a larger activation energy suggests a larger effective radius. It has been previously discussed that the order of diffusion was in general $D(^1H) > D(^{19}F) > D(^7Li)$ in the liquid electrolytes, suggesting that the PC molecules were on average the smallest entity followed by the fluorinated anions. The lithium ions were considered to have the largest effective radius. The larger the effective radius of the entity diffusing the more energy that would be needed to move though the medium. This agrees with the liquid and gel result as lithium was seen to have the largest activation energy with the fluorine and hydrogen being the same within the experimental error. It should also be noted that the fluorine and lithium activation energies converge at the higher salt concentration. In the liquid electrolytes it was observed that the diffusion constants for the lithium and fluorine species converged at higher salt concentrations suggesting a higher ionic association. This explanation could also be used here to describe the convergence of the activation energies at high salt concentration.

The 30% PVDF/PC/$LiBF_4$ (0.3M) polymer gel electrolyte gave (16.0±0.2) kJ mol^{-1}, (16.5 ±0.2) kJ mol^{-1} and (15.2±0.9) kJ mol^{-1} for the activation energies for the ^{1}H, ^{7}Li and ^{19}F nuclei, respectively. It can be concluded that with an increase in polymer concentration that the hydrogen and lithium activation energies increase, whereas the fluorine seemed independent. This was attributed to the fluorine gel measurements failing to exhibit a noticeable signal from

a slower polymer phase and therefore the single fit represents the liquid electrolyte phase. It has been discussed earlier that the liquid phase in the gels does not vary much with the increase in polymer concentration as the structure is believed to be a porous polymer structure with pockets of liquid electrolyte. Since the liquid electrolyte phase should be similar for the 20% and 30% PVDF gels, the fluorine molecules require similar energies to diffuse. For all nuclei, the activation energies were observed to increase with increasing salt concentration which was attributed to the increase in viscosity resulting in more energy required for activation of diffusion. It should also be noted again that as with the 20% PVDF gels, the lithium exhibited a significantly larger activation energy than the other nuclei which was attributed to an assumed larger effective radius of the lithium species due to solvation of the lithium ions. The effective radii of each of the nuclei will be discussed in greater detail in Chapter 7.

5.5 Conclusions

In this chapter, the results of the NMR measurements on the polymer gel electrolytes have been reported and discussed. Two different polymer concentrations were used which were 20% and 30% PVDF with 80% and 70% solvent by mass. The electrolyte used here was propylene carbonate mixed with lithium tetrafluoroborate ($LiBF_4$), so that the gels could be compared to the corresponding liquid electrolytes. The structure of the PGEs consists of a porous polymer structure with liquid electrolyte flowing throughout. The gels were considered to contain at four distinct phases corresponding to the crystalline polymer, interlamellar phase, an amorphous polymer phase and liquid electrolyte phase.

The transverse relaxation times were measured using the low field Bench top spectrometer. The transverse relaxation time measurements were able to distinguish between different phases in the gels. The introduction of a second exponential yielded a significantly improved fit to the data, however it was noted that for very short times the fit deviated from the data. With the introduction of the third exponential, the fitting was very good and fit all aspects of the data, therefore suggesting that there were three distinct phases of the polymer gel electrolytes containing hydrogen atoms. The three phases detected were attributed to the interlamellar phase, amorphous polymer-liquid and pure liquid electrolyte phases.

The transverse relaxation times were also measured using the lithium resonant frequency. It was found that the lithium relaxation decay curve required two exponential terms to describe the data. Therefore it was assumed that the lithium was located in two of the phases of the polymer gel electrolytes. The relaxation times were characteristic of the solvated amorphous polymer and liquid electrolyte phases. The intensities were found to be around 64% and 36% for the liquid and solvated polymer phases, respectively, which were in agreement with the hydrogen measurements.

The low field 50 MHz Maran bench top NMR spectrometer was used to measure the longitudinal and transverse relaxation times using the hydrogen (^1H) nucleus which represented the solvent molecules. Since these measurements were for the gels which contained PVDF there would also be a hydrogen signal from the polymer as it contains two hydrogen atoms per monomer ($[CH_2\text{-}CF_2]_n$). The very nature of the longitudinal relaxation times means that a single value was used to represent the whole system and therefore was an average of all phases in the gels. The

longitudinal relaxation times were observed to increase with temperature which suggested that the system was on the high temperature (low correlation time (τ_c)) of the minimum. The longitudinal relaxation times were observed to decrease with salt concentration dependence which saw the longitudinal relaxation times decrease with increasing salt concentration.

The 400 MHz Bruker Avance II Ultrashield NMR spectrometer was used to measure the diffusion and longitudinal relaxation times of the ^{1}H, ^{7}Li and ^{19}F which represents the solvent molecules, lithium cation and fluorinated anion (BF_4), respectively. The polymer used in this research was PVDF, which contained both hydrogen and fluorine ions on the chain, there would be signals from the polymer as well.

The fluorine diffusion was determined by fitting the exponential decay equation. The diffusion constants of the polymer gel electrolytes were observed to be similar to the corresponding liquid electrolytes and did not decrease much with the increase of polymer concentration which was attributed to the liquid electrolyte being simply contained within the polymer structure.

An interesting feature of the lithium diffusion measurements was observed that the standard diffusion equation was not sufficient to fit the data. Therefore a second exponential was added in series and refitted, this resulted in a very good fit to the diffusion decay curve. This suggested that there were two distinct diffusion constants for the polymer gel electrolytes. This result was considered reasonable since there were three phases observed in the hydrogen transverse relaxation measurements. The two lithium diffusion constants were attributed to the amorphous-liquid phase and the pure liquid electrolyte phases, respectively, as the diffusion constants were too large to correspond to the crystalline polymer phase. The diffusion constants were measured for varying diffusion times, in the range of 16.25-200 ms. For both the 20% and 30%, the two diffusion constants were present, suggesting that restricted diffusion was not occuring. The individual values for two phase diffusion were independent of the diffusion time. Since the liquid electrolyte measurements were fit very well to the single exponential the addition of the polymer was considered the source of the second diffusion constant.

The intensity of the diffusion fits here were in good agreement with the hydrogen transverse relaxation times. The intensity of the polymer phase ($I(0)_1$) and liquid phase ($I(0)_2$) were normalised so that the sum of the two equals unity. There was no clear trend of this intensity with either salt concentration of temperature and therefore an average for the 20% and 30% PVDF gels was taken. The transverse relaxation yielded intensity values comparable to these which showed that the liquid phase was always the most dominant, however the polymer phase became more prominent at the higher polymer concentration.

The hydrogen diffusion measurements also displayed two distinct diffusive species. However unlike the lithium measurements, the 20% PVDF gels only exhibited them at low salt concentration. The 20% PVDF gels produced a better single fit at higher temperatures, this therefore discounts the notion of restricted diffusion as it was more likely to be an issue when the molecules are moving faster. The intensities of the dual fits were (0.12±0.08) and (0.87±0.08) for the polymer and liquid phases, respectively. These intensities of the polymer phase were lower than the corresponding lithium measurements.

All of the diffusion constants for all nuclei were seen to increase with increasing temperature and decrease with salt concentration. Comparing the single fits for all nuclei the values of the activation energy were seen to be in the order of $^{19}\text{F}\approx{}^{1}\text{H}<{}^{7}\text{Li}$ suggesting that the lithium

had the largest effective radius, with the fluorine and hydrogen exhibiting similar radii. As a standard result, the slower phase exhibited a higher activation energy for both hydrogen and lithium measurements. This result was attributed to the likely higher viscosity of the amorphous polymer phase requiring more energy for each molecule to diffuse.

The longitudinal relaxation times were measured for the lithium polymer gel electrolytes. The activation energies were compared to the corresponding diffusion activation energies as this can give insight into the relative contributions of rotational and translational motion. However this was much more simple for the liquid electrolyte measurements as there was a single relaxation time for the entire gel which would essentially be an average of all phases, where as the diffusion values were for each phase independently. The values of E_{T_1}/E_D were (0.57±0.02) and (0.61±0.02) for the polymer and liquid phases, respectively. This suggests that the lithium molecules were dominated by translational motion in each phase; however, there was also a significant rotational component which was more prominent for the polymer phase.

Chapter 6

Conductivity Measurements

In this chapter the ionic conductivity measurements taken for the liquid and polymer gel electrolytes are discussed. As mentioned in Chapter 3, the conductance has contributions from the electronic and ionic conductivity, however with liquid electrolytes the ionic conductivity is much greater than the electronic conductivity and the latter is therefore considered negligible; therefore the term conductivity and ionic conductivity are synonymous.

6.1 Liquid Electrolytes

The research carried out here will have its main focus on liquid electrolytes and polymer gel electrolytes based on PC, $LiBF_4$ and PVDF. The conductivity of liquid electrolytes has been a popular area of research due their use within batteries. The solvents which are commonly used are organic, with high dielectric constants which are well characterised and include ethylene carbonate (EC), diethyl carbonate (DEC), dimethyl carbonate (DMF), γ-butyrolactone (GBL) and, of course, propylene carbonate (PC) [43; 56; 63; 99; 100; 119]. Although commercial electrolytes often have mixed solvents [45; 91; 98; 120], a single solvent (PC) was chosen here for a better understanding of the core physical concepts. PC exhibits a high dielectric constant of 61.7 [80] and therefore helps to dissociate the cation and anion. The conductivity of liquid electrolytes containing PC have been studied extensively [56; 103; 121].

In this research, conductivity measurements have been taken for liquid electrolytes at various temperatures and salt concentrations. The conductivity has been measured for temperatures in the range of 253-353 K, chosen due to realistic operational temperatures of the primary application of use in advanced lithium batteries. There was also some consideration that the solvent has a freezing temperature of around 218 K and that the cryostat system employed here could only achieve around 233 K. The upper temperature limit was chosen to ensure safety regulations were not violated, as the Novocontrol BDS1200 has a maximum operational temperature of 723 K (450 °C) [87]; however the outer casing made from stainless steel also heats up, so 353 K was chosen as a safe medium.

When considering the range of salt concentrations to be used here it was important to ensure that for all samples the salt is completely miscible with the solvent, and had not saturated. The range used was between 0.1-1.5M, the same range used for the diffusion measurements.

	Ionic Conductivity (mS cm^{-1})									
Temp. (K)	0.1M	0.3M	0.5M	0.7M	0.8M	0.9M	1.0M	1.1M	1.3M	1.5M
253	—	0.93	0.92	0.81	0.74	0.77	0.70	0.55	0.47	—
263	0.70	1.30	1.38	1.28	1.23	1.23	1.13	0.97	0.82	—
273	0.93	1.70	1.92	1.84	1.80	1.77	1.66	1.51	1.28	1.05
283	1.20	2.20	2.53	2.49	2.47	2.39	2.29	2.13	1.83	1.51
293	1.47	2.74	3.18	3.21	3.20	3.08	2.99	2.82	2.47	2.06
298	1.62	3.01	3.52	3.57	3.57	3.44	3.36	3.18	2.82	2.36
303	1.77	3.30	3.90	3.97	3.98	3.84	3.78	3.57	3.20	2.69
313	2.09	3.91	4.69	4.80	4.85	4.66	4.65	4.44	3.99	3.40
323	2.43	4.54	5.52	5.59	5.77	5.54	5.58	5.32	4.87	4.18
333	2.77	5.17	6.38	6.54	6.74	6.55	6.56	6.29	5.79	5.01
343	3.11	5.86	7.25	7.41	7.72	7.46	7.58	7.33	6.78	—
353	—	6.59	8.18	8.38	8.69	8.38	8.67	8.30	7.80	—

Table 6.1: Conductivity for PC/$LiBF_4$ (0.1-1.5M) liquid electrolytes in temperature range of 253-353 K.

6.1.1 Liquid Electrolyte Temperature Dependence

In this section we will observe the temperature dependence of the conductivity for the liquid electrolytes based on PC/$LiBF_4$. Table 6.1 shows the conductivity of PC/$LiBF_4$ (0.1-1.5M) liquid electrolytes with temperature. As the temperature is increased the ions will have more thermal energy and can thus gain more translational motion. It is very well known that the conductivity will increase with temperature, usually described by an exponential function.

It can be seen that the conductivity increases as the temperature is increased. This was attributed to the lowering of viscosity and increase in the thermal energy of the conducting ions. It is important to understand the mechanism for this conduction. A first approach would be to observe the type of exponential governing the conductivity. This usually falls into two categories, firstly Arrhenius which is a simple exponential in the form;

$$\sigma(T) = \sigma_0 exp\left[-\frac{E_\sigma}{RT}\right] \tag{6.1}$$

where E_σ is the activation energy of the conducting ions at temperature T, with the conductivity at infinite temperature (σ_0) and R is the universal gas constant. The other type of temperature dependence commonly used to describe the conductivity for liquid electrolytes when Arrhenius type behaviour cannot explain the data is the Vogel-Tamman-Fulcher (VTF) equation [94–96], which has the form:

$$\sigma(T) = \sigma_0 exp\left[-\frac{E'_\sigma}{R\{T - T_0\}}\right] \tag{6.2}$$

where T_0 is the ideal glass transition temperature and E'_σ is a temperature dependent energy term, distinct from E_σ, the activation energy of conduction. In order to determine which equation was most appropriate for the conductivity an Arrhenius plot was employed. By taking the natural

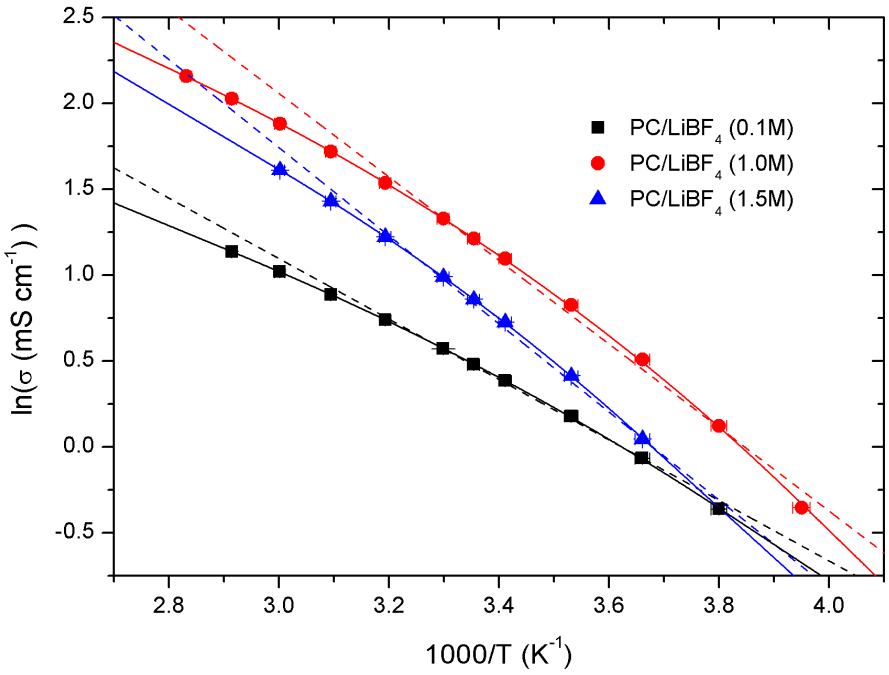

Figure 6.1: Conductivity Arrhenius plot for PC/$LiBF_4$ (0.1M, 1.0M and 1.5M) liquid electrolytes. Linear (dashed) and non-linear (solid) fits used.

log of both sides of equation 6.1 it can then be written as;

$$ln\left(\sigma(T)\right) = ln\left(\sigma_0\right) - \frac{E_\sigma}{RT} \tag{6.3}$$

therefore by plotting ln(conductivity) against 1000/T would yield a linear relationship with the gradient being equal to $E_\sigma/1000R$. However if this Arrhenius plot exhibits a non-linear response then it is most likely controlled by VTF type temperature dependence. In Chapters 4 and 5, it was shown that the diffusion constants exhibited an Arrhenius type temperature dependence for the liquid and polymer gel electrolytes respectively. Since the two mechanisms are related it was logical to assume that the conductivity measurements would exhibit the same temperature dependence.

Figure 6.1 shows an Arrhenius plot for PC/$LiBF_4$ liquid electrolytes at three different salt concentrations over the entire range of temperatures (253-353 K). Linear (dashed) and non-linear (solid) lines have been fitted to the data in order to determine the temperature dependence type. For all salt concentrations the non-linear fits were seen to be much better than the linear counterparts and therefore Arrhenius type dependence can be discounted. It is likely that the conductivity has VTF type behaviour for the liquid electrolytes, a trend that has been observed for liquid electrolytes measured elsewhere [122]. Since the diffusion measurements displayed Arrhenius type temperature dependence it was assumed that the conductivity would also exhibit this type of temperature dependence. However the diffusion measurements were taken over a temperature range of 283-353 K as opposed to the conductivity which used a temperature range of 253-353 K. It can usually be stated that VTF dependence is seen when the temperatures get close to the glass transition temperature of the sample. Therefore the difference in dependencies

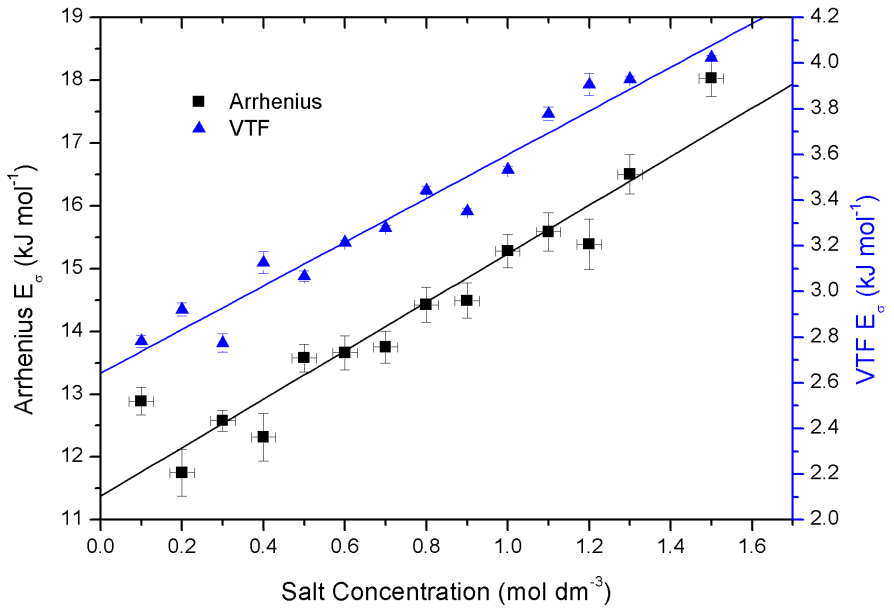

Figure 6.2: VTF conductivity energy term (E'_σ) and reduced temperature range Arrhenius activation energy (E_σ) as a function of salt concentration for PC/$LiBF_4$ liquid electrolytes. For the VTF fitting the T_0 value was held constant at 155K.

between the conductivity and diffusion measurements was assumed to be due to the different temperature ranges used. It was not possible to measure the diffusion values at less that 283 K on the NMR spectrometer used. In Chapter 4, it was also observed that the longitudinal relaxation measurements (T_1) exhibited VTF type temperature dependence which were measured over the same temperature range as the conductivity.

Now that the type has been identified each of the salt concentrations can be fitted with equation 6.2 in order to determine the activation energy (E_σ) and the conductivity pre-exponential factor (σ_0). The fitting procedure was executed using an iterative process based on the Levenberg-Marquardt method [78; 79]. The value of T_0 was initially allowed to freely change in the fitting process, the result of which showed it be independent of salt concentration. Therefore all data was refitted holding T_0 constant at the average value obtained from the initial fitting which yielded (T_0=155 K). It has been previously seen that T_0 is independent of salt concentration in other polymer systems containing poly(ethylene glycol) with $LiCF_3SO_3$, $LiClO_4$, $NaClO_4$, $LiBF_4$ and $NaBF_4$ [11]. Since the activation energies for the diffusion measurements were for the Arrhenius fitting the conductivity temperature can be reduced and fitted in the same manner in order to compare the two values.

Figure 6.2 shows the activation energies for PC/$LiBF_4$ liquid electrolytes against salt concentration for both the reduced temperature Arrhenius and VTF fitting. The Arrhenius activation energy was considered to be constant over the temperature range, whereas the VTF equation describes a system with an activation energy which is scaled by the ideal transition temperature. The activation energy was seen to increase with increasing salt concentration, this is intuitively reasonable due to the inevitable increase in viscosity with increasing salt concentration. This

	Activation Energy (kJ mol^{-1})					σ_0 (mS cm^{-1})	
	Conductivity		Diffusion			Conductivity	
Salt Conc. (mol dm^{-3})	VTF	Arrhenius	^{1}H	^{7}Li	^{19}F	VTF	Arrhenius
0.1	2.8	12.9	—	—	—	19.7	291
0.2	2.9	11.7	—	—	—	32.7	281
0.3	2.8	12.6	16.9	19.4	17.8	36.8	484
0.4	3.1	12.3	—	—	—	52.7	478
0.5	3.1	13.6	17.5	20.4	18.7	55.8	850
0.6	3.2	13.7	—	—	—	64.2	899
0.7	3.3	13.8	17.9	21.5	19.9	67.0	924
0.8	3.4	14.4	—	—	—	77.7	1215
0.9	3.4	14.5	—	—	—	69.7	1200
1.0	3.5	15.3	19.9	21.9	22.3	80.3	1615
1.1	3.8	15.6	—	—	—	92.7	1727
1.2	3.9	15.4	—	—	—	102.1	1609
1.3	3.9	16.5	20.6	23.6	22.2	94.7	2214
1.5	4.0	18.0	22.5	24.0	23.2	86.6	3418

Table 6.2: VTF and Arrhenius fitting parameters E_σ and σ_0 for PC/$LiBF_4$ (0.1-1.5M) liquid electrolytes. The activation energies for the Arrhenius diffusion measurements have been included in order to compare the values.

increased viscosity would mean that the conducting ions would need more energy in order to displace the liquid electrolyte and hence an increased activation energy. The relationship is seen to be linear with salt concentration. The pre-exponential factor (σ_0) was also observed to increase linearly with increasing salt concentration. This factor has been linked to the number of ions in solution which would therefore rationalise the result.

Table 6.2 shows the Arrhenius and VTF fitting parameters E_σ and σ_0 for PC/$LiBF_4$ (0.1-1.5M) liquid electrolytes. The diffusion activation energies determined from the Arrhenius fitting from Chapter 4 have been included here in order to compare the two mechanisms. It was found that $E_\sigma(Arr) > E'_\sigma(VTF)$, which was attributed to the VTF activation energy being scaled by the ideal glass transition temperature. Therefore in order to compare the diffusion and conductivity mechanisms the Arrhenius activation energies of the two measurements have to be compared. Taking a low salt concentration from table 6.2 it can be seen that the activation energies for the 0.3M $LiBF_4$ samples were 12.6, 16.9, 19.4 and 17.8 (kJ mol^{-1}) for the conductivity and ^{1}H, ^{7}Li and ^{19}F diffusion activation energies, respectively. It can be noted that the conductivity activation energy was comparable to the corresponding diffusion energies. However the conductivity activation energies were noticeably lower than the diffusion energies. Although the two mechanisms describe the mobility of the liquid electrolytes there are differences between the two values. For instance the ionic association would form neutral pairs and therefore not contribute to the conductivity, however these pairs still contribute to the average diffusion. This would therefore be the likely cause of the discrepancy between the two activation energies.

6.1.2 Liquid Electrolyte Salt Concentration Dependence

In this section the behaviour of the conductivity with the salt concentration is addressed. There are three main factors that are known to affect the conductivity; the viscosity of the solution, number of ions and the ionic association. The ionic association refers to the fraction of ions that are non-conducting via anion-cation association. Figure 6.3 shows the conductivity against salt concentration for PC/$LiBF_4$ liquid electrolytes at several different temperatures (253 K, 273 K, 293 K, 313 K and 333 K).

All temperatures exhibited a peak in the conductivity with salt concentration. The initial increase in conductivity at low salt concentrations was attributed to the increase in the number of ions or charge carriers. However the viscosity is also being increased with increasing salt concentration and will act as a deterrent to the conductivity and will eventually dominate the whole system and therefore causes the conductivity to decrease. The ionic association also has an effect on the position of the maximum which will be discussed later in Chapter 7. The existence of a peak is of importance to the major application of this research in use for the advanced lithium batteries, as there is no advantage to using a salt concentration higher than the critical concentration as it would hinder the conductivity and raise manufacturing costs. It is therefore informative to determine accurate values of these critical concentrations.

In order to fit the conductivity as a function of salt concentration the Casteel-Amis equation has been employed [123]. This semi-empirical equation used to fit the salt concentration dependence of the conductivity in liquid electrolyte solutions of the form;

$$\sigma = c^a exp\left[-bc^2 + dc + e\right] \tag{6.4}$$

where σ is the electrolytic conductivity, c is the concentration of salt contained in solution and a, b, d, e are four fitting parameters. It was shown by Casteel and Amis that equation 6.4 can be mathematically transformed to replace the d and e parameters with σ_p and c_p in the form;

$$\sigma_r = c_r^a exp\left[-bc_p^2(c_r - 1)^2 - a(c_r - 1)\right] \tag{6.5}$$

where the physical meaning of σ_p was the maximum conductivity observed with salt concentration and c_p is the concentration at which $\sigma = \sigma_p$ and where $\sigma_r = \sigma/\sigma_p$ and $c_r = c/c_p$. This form is often used as the parameters σ_p and c_p have a clear physical meaning. For the ease of notation the parameters σ_p and c_p will be denoted as σ_{max} and c_{max} respectively for the rest of this work. By expanding the σ_r and c_r terms equation 6.5 becomes;

$$\sigma = \sigma_{max}\left(\frac{c}{c_{max}}\right)^a exp\left[-b\left(c - c_{Max}\right)^2 - \frac{a}{c_{Max}}\left(c - c_{Max}\right)\right] \tag{6.6}$$

where a and b are fitting parameters. Equation 6.6 has been shown to fit liquid data very well elsewhere[124–126]. The fitting process allowed all four parameters a, b, σ_{max} and c_{max} to be free, which yielded very good fits to the data with reasonable maximum conductivity and concentration values. The solid lines in figure 6.3 were produced from fitting the Casteel-Amis equation in the form of equation 6.6 and can be observed to fit the data well. A fit of the locus of the position of the peak has been added to figure 6.3 to highlight that the position of the maximum is dependent on the absolute temperature of the sample. The values of c_{max} and σ_{max} were observed increase with temperature, in the case of c_{max} this was a linear relationship.

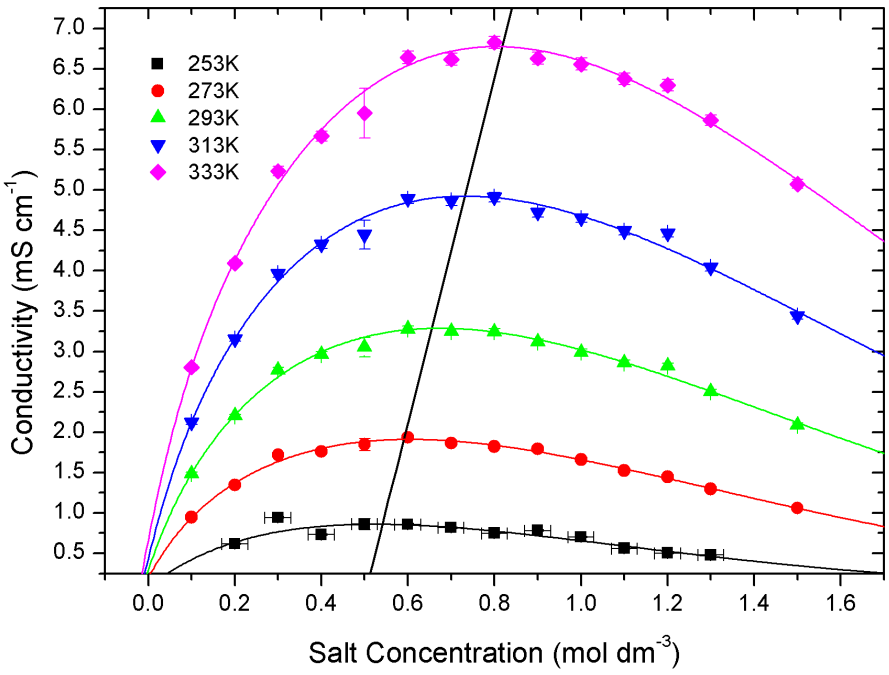

Figure 6.3: Conductivity against salt concentration for PC/$LiBF_4$ liquid electrolytes. Data fitted to Casteel-Amis equation (equation 6.6). The black line is a locus of the max conductivities.

It has been shown for 20 different aqueous solutions measured elsewhere that the c_{max} values increased linearly with increasing temperature [125].

When observing the salt concentration dependence of the conductivity at various temperatures it was noted that the position of the peak was not constant with changes in temperature. Therefore by using the Casteel-Amis fits an accurate value of c_{max} was determined for each temperature, shown in figure 6.4. Figure 6.4 shows that the position of the peak (c_{max}) increases linearly with increasing temperature. This result is reasonable when considering that the viscosity decreases with increasing temperature so would be logical to assume that more salt could be added before the hindering effect of the viscosity becomes dominant at higher temperatures. Another logical conclusion of this result is that the ionic association would also affect the position of the peak as more associated ions would cause the value of c_{Max} to decrease yielding;

$$c_{Max}(T) \propto \frac{1}{\alpha\eta} \tag{6.7}$$

where α is the ionic association and η is the viscosity of the system. The effect of ionic association will be considered further in Chapter 7.

Each temperature has a unique value of both c_{max} and σ_{max}, it is therefore possible to take all of the conductivity measurements and scale them according to their relevant value of c_{max} and σ_{max}. This graph is known as a Casteel-Amis plot can be used with all conductivity data; where the conductivity scaled by the maximum conductivity is plotted against the concentration scaled by the maximum concentration [126].

Figure 6.5 shows a Casteel-Amis plot for all PC/$LiBF_4$ liquid electrolyte conductivity data. It can be observed that all of the data can be fitted with a single value of a and b, implying

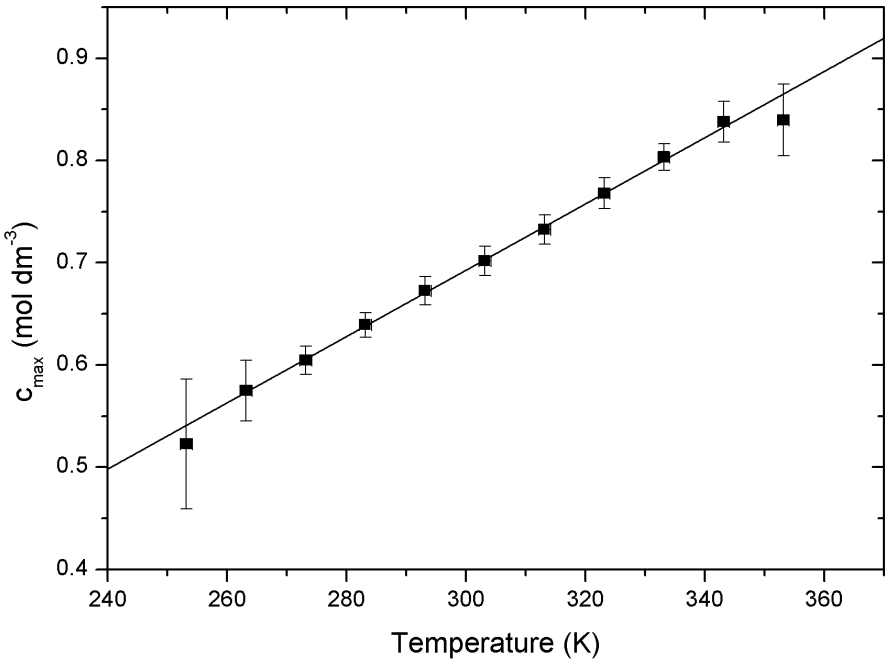

Figure 6.4: Concentration at which $\sigma = \sigma_{Max}$ against temperature for PC/$LiBF_4$ liquid electrolytes.

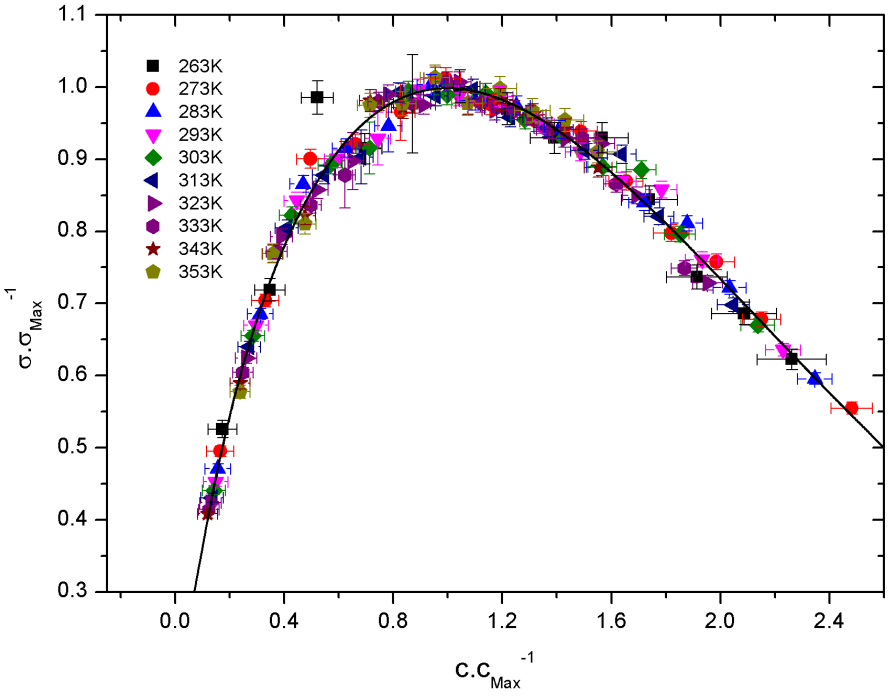

Figure 6.5: Casteel-Amis plot for all PC/$LiBF_4$ liquid electrolyte conductivity data. All data has been normalised by the relevant c_{Max} and σ_{Max}.

that the conductivity mechanism is the same regardless of temperature of salt concentration. This has been shown for other liquid electrolyte systems [127] containing $LiClO_4$ in propylene carbonate and γ-Butyrolactone (GBL). It is therefore of interest to employ this plot for the polymer gel electrolytes to verify if the conductivity mechanism is the same as for the liquid electrolytes (see figure 6.9 below).

6.2 Polymer Gel Electrolytes

In this section the conductivity measurements for polymer gel electrolytes based on PVDF/PC/ $LiBF_4$ are considered. This section will frequently refer back to section 6.1.2 on the liquids as it is a logical progression to consider the liquids prior to the PGEs which are based on the liquids. Song *et al* have concluded that the ionic conductivity of a porous membrane is thought to be essentially the same conductivity as the electrolyte solution contained within the porous structure [61]. Since this is the case, the conductivity can be affected by the properties of the membrane such as the porosity, tortuosity and the thickness of the cell membrane [60]. That being said, it has also been observed elsewhere that the structure of the gels exhibited hysteresis whereas the ionic conduction did not, suggesting that the ionic conductivity is independent of the mechanical state of the gel [48], however this refers to the crystallinity rather than the size of the cavities.

In Chapter 5, it was extensively discussed that the polymer gel electrolytes contained multiple phases. It was shown elsewhere by Hubbard *et al* using $T_{1\rho}$ measurements that there are several phases including a crystalline polymer, amorphous interlamellar, solvated amorphous and liquid electrolyte phases [18; 34]. From the results presented in Chapter 5 it was shown that there was at least three phases present for the hydrogen ions which were attributed to the crystalline PVDF, solvated amorphous and liquid electrolyte phases. For the lithium measurements, at least two phases were seen in both the longitudinal relaxation and diffusion measurements corresponding to the solvated amorphous and liquid electrolyte phases. Therefore since ions have been found in two phases of the polymer gel electrolytes it is of interest if the ions in the amorphous phase contribute to the ionic conductivity. Ideally there would be no loss of solvent or salt to the polymer structure as this would hinder the conductivity of the sample. It is expected that there will be some loss of conductivity by adding the polymer to the system, caused by the reduction of free volume for the ions to translate and likely tortuous paths of the polymer channels. However, this loss in conductivity is less significant than the mechanical properties gained. The mechanical properties are of interest but are not included in this research.

Two different polymer concentrations have been chosen here which are 20% and 30% PVDF by mass of solvent ($m_{PVDF}/(m_{PC} + m_{PVDF})$ =0.2 or 0.3). It was not reasonable to add less than 20% PVDF as this does not allow the gelation process to occur successfully. Furthermore, with more than 30% by mass the gels become very brittle and become difficult to manipulate. As with the liquid electrolytes both the temperature and salt concentration dependences will be considered.

	σ (mS cm^{-1})									
	20% PVDF					30% PVDF				
Temp. (K)	0.1M	0.3M	0.5M	0.7M	1.0M	0.1M	0.3M	0.5M	0.7M	1.0M
253	0.20	0.38	0.40	0.38	0.28	0.12	0.17	0.18	0.23	0.20
263	0.32	0.59	0.64	0.62	0.50	0.20	0.27	0.31	0.40	0.35
273	0.45	0.84	0.93	0.95	0.78	0.29	0.38	0.47	0.60	0.55
283	0.61	1.12	1.27	1.30	1.12	0.39	0.51	0.64	0.83	0.79
293	0.77	1.42	1.63	1.80	1.51	0.50	0.66	0.84	1.09	1.07
303	0.94	1.77	2.00	2.19	1.97	0.63	0.83	1.06	1.38	1.38
313	1.12	2.14	2.41	2.63	2.46	0.75	1.03	1.30	1.69	1.73
323	1.31	2.53	2.83	3.09	2.96	0.89	1.32	1.57	2.01	2.12
333	1.50	2.93	3.26	3.60	3.51	1.05	1.57	1.84	2.32	2.50
343	1.70	3.33	3.70	4.13	4.10	1.19	1.83	2.14	2.65	2.90
353	1.92	3.57	4.12	4.71	4.69	1.31	2.07	2.45	2.97	3.26

Table 6.3: Conductivity for 0%, 20% and 30% PVDF/PC/$LiBF_4$ (0.1M, 0.5M and 1.0M) polymer gel electrolytes in the temperature range of 253-353 K.

6.2.1 PGE Temperature Dependence

Table 6.3 shows the conductivity of 20% and 30% PVDF/PC/$LiBF_4$ polymer gel electrolytes at salt concentrations between 0.1-1.0M $LiBF_4$. The conductivity of the PGEs were seen to increase with temperature in the same manner as the liquid electrolytes. At the low temperature of 263 K the values of the conductivity were 1.13, 0.50 and 0.35 mS cm^{-1} for 0% (liquid), 20% and 30% PVDF/PC/$LiBF_4$ (1.0M), respectively. As predicted, the conductivity decreased with increasing polymer concentration, therefore the general trend that can be noted here was $\sigma_{30\%} < \sigma_{20\%} < \sigma_{0\%}$. This result can be explained by considering the reduction of the relative free volume the ions have to move through the solution with the addition of the polymer. Taking the above solution as an example, the ratio of the liquid conductivity to the 20% PVDF gel conductivity ($\sigma_{20\%}/\sigma_{0\%}$) is around 0.5; this decrease is much more significant than the pure volume fraction decrease of the liquid and can not solely be due to a decrease in free volume as some of the ions are being lost to the polymer in some manner. Since it has been shown that the ions are contained within the solvated amorphous polymer and liquid electrolyte phases it was considered reasonable that both of these phases contributed to the total ionic conductivity. Another conclusion worth noting from Chapter 5 was that the activation energy of the solvated amorphous phase was greater than the corresponding liquid electrolyte phase. This result indicated that the viscosity of the solvated amorphous phase was higher than the liquid phase. This means that the conductivity corresponding to the amorphous phase of the gel would contribute less to the total ionic conductivity than the corresponding liquid phase.

The temperature dependence of the polymer gel electrolytes was classified in the same manner as the liquid electrolytes as either VTF or Arrhenius. An Arrhenius plot was used in order to determine if it yields a linear (Arrhenius) or non-linear (VTF) response. The linear fits (dashed) were not suitable, therefore suggesting that the conductivity is exhibiting VTF type temperature

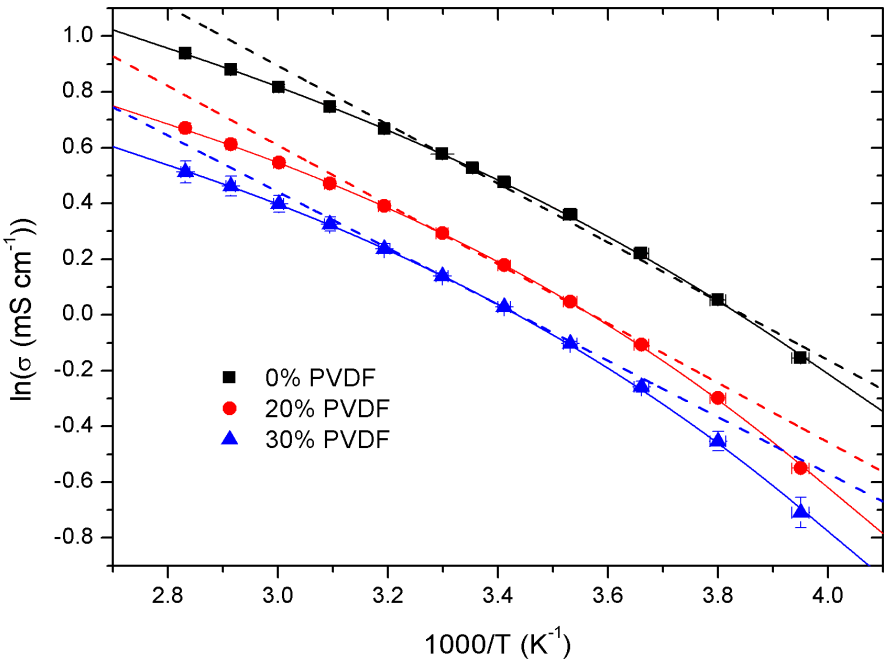

Figure 6.6: Conductivity Arrhenius plot for 0% (liquid), 20% and 30% PVDF/PC/$LiBF_4$ (1.0M) polymer gel electrolytes. Linear (dashed) and non-linear (solid) fits used.

dependence. This result was plausible, as the most significant contribution to the conductivity was the liquid phase and would therefore exhibit the same temperature dependence as the liquid electrolytes measurements.

Table 6.4 shows the reduced temperature range Arrhenius fitting and VTF conductivity parameters for 0%(liquid), 20% and 30% PVDF/PC/$LiBF_4$ polymer gel electrolytes with the value of T_0 fixed at 155K for all data, determined by fitting equation 6.2. The activation energy of the polymer gel electrolytes were seen to be higher than for the corresponding liquid electrolytes, which was likely due to an effective increase of the average viscosity of the medium due to some of the ions being located in the solvated amorphous PVDF phase. At low salt concentration (0.1M) the values of E_σ are 12.9, 13.0 and 13.9 kJ mol^{-1} for the 0% (liquid), 20% and 30% PVDF gels, respectively, for the reduced temperature range Arrhenius fitting. Therefore these values are comparable suggesting a very similar medium in each case with a slight increase due to the addition of the polymer. The further increase in the activation energies observed for the 30% PVDF gels was attributed to more of the ions being located in the solvated amorphous phase therefore increasing the effective viscosity of the whole gel. The same trend was observed at higher salt concentrations (1.0M) where the activation energies were 15.3, 16.2 and 16.1 kJ mol^{-1} for the 0% (liquid), 20% and 30% PVDF gels, respectively. The general trend for the activation energies was $E_{0\%} < E_{20\%} < E_{30\%}$ within the error of the value. The pre-exponential factor σ_0 was observed to increase with increasing salt concentration, attributed to the increase in ions with the addition of salt.

From the data in this section it can be surmised that the polymer gel electrolytes behave in a very similar way to the liquid electrolytes due to the gels containing mostly liquid electrolyte,

	$E_\sigma(arr)$ (kJ mol^{-1})			$E'_\sigma(VTF)$ (kJ mol^{-1})			$\sigma_0(arr)$ (mS cm^{-1})		
Salt Conc. (mol dm^{-3})	0%	20%	30%	0%	20%	30%	0%	20%	30%
0.1	12.9	13.0	13.9	2.8	3.9	4.1	291	165	152
0.2	11.7	12.8	14.0	2.9	3.8	3.9	281	247	220
0.3	12.6	13.4	16.7	2.8	3.9	4.3	483	364	645
0.4	12.3	13.4	14.2	3.1	3.9	4.1	478	409	375
0.5	13.6	13.3	15.3	3.1	4.0	4.4	850	397	466
0.6	13.7	14.4	15.2	3.2	4.3	4.3	898	643	554
0.7	13.8	13.7	14.3	3.3	4.3	4.4	924	513	402
0.8	14.4	16.0	15.6	3.4	4.7	4.6	1215	1130	747
0.9	14.5	16.0	15.4	3.4	4.7	4.6	1200	1188	643
1.0	15.3	16.2	16.1	3.5	4.8	4.8	1615	1186	812

Table 6.4: Reduced temperature range conductivity Arrhenius parameters $E_\sigma(arr)$ and $\sigma_0(arr)$ and also VTF fitting parameter $E'_\sigma(VTF)$ for 0%(liquid), 20% and 30% PVDF/PC/$LiBF_4$ polymer gel electrolytes.

however, there were clearly ions contained within the solvated amorphous phase which were assumed to contribute to the ionic conductivity with a smaller contribution than the corresponding liquid phase due to the viscosity of the phases.

6.2.2 PGE Salt Concentration Dependence

In this section the effect of salt concentration of the polymer gel electrolytes is determined and compared to the results of the liquid electrolytes. There were limitations to the amount of salt that can be dissolved here. As a result of introducing the polymer, the solvent can not dissolve as much salt ($LiBF_4$), therefore there now exists a competition between the salt and polymer. The maximum amount of salt that can be dissolved here was around 1.1M $LiBF_4$, after this the gels do not undergo gelation properly and there is some phase separation, called syneresis. The range of polymer gel electrolytes analysed here was salt concentrations in the range of 0.1-1.1M and 0.1-1.0M for the 20% and 30% PVDF polymer gel electrolytes, respectively.

The conductivity of the PGEs as a function of salt concentration is shown in figure 6.7, showing that, as with the liquids, the PGEs exhibit a peak in conductivity with salt concentration. It can be seen that the peak occurs at different salt concentrations depending on the polymer concentration. As the polymer content is increased the peak shifts to lower salt concentration. As with the liquids the value of c_{max} can be determined by fitting the Casteel-Amis equation to the PGE conductivity.

Figure 6.8 shows the maximum conductivity (c_{Max}) at different temperatures for the 0% (liquid), 20% and 30% PVDF/PC/$LiBF_4$ polymer gel electrolytes. As with the liquid electrolytes the PGE c_{Max} values were observed to increase linearly as the temperature was raised. This is again attributed to the fall in viscosity with increasing temperature which would mean more salt can be dissolved before viscosity dominates the system and therefore causes the peak in conductivity. Since it seems that the PGEs behave in a very similar manner to the liquid

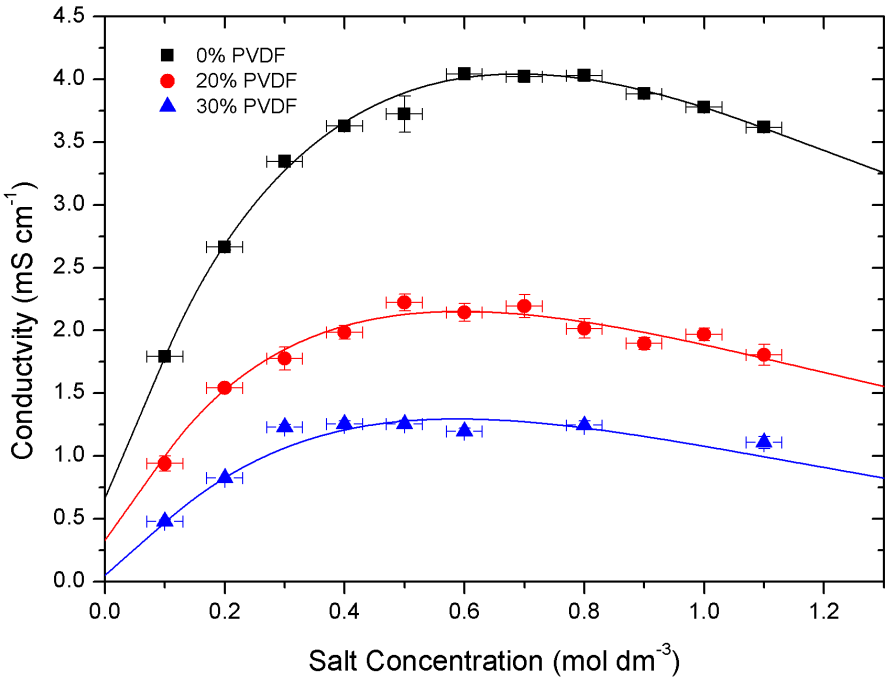

Figure 6.7: Conductivity against salt concentration for 0%(liquid), 20% and 30% PVDF/PC/$LiBF_4$ polymer gel electrolytes at 303 K. Data fitted with Casteel-Amis equation (equation 6.6).

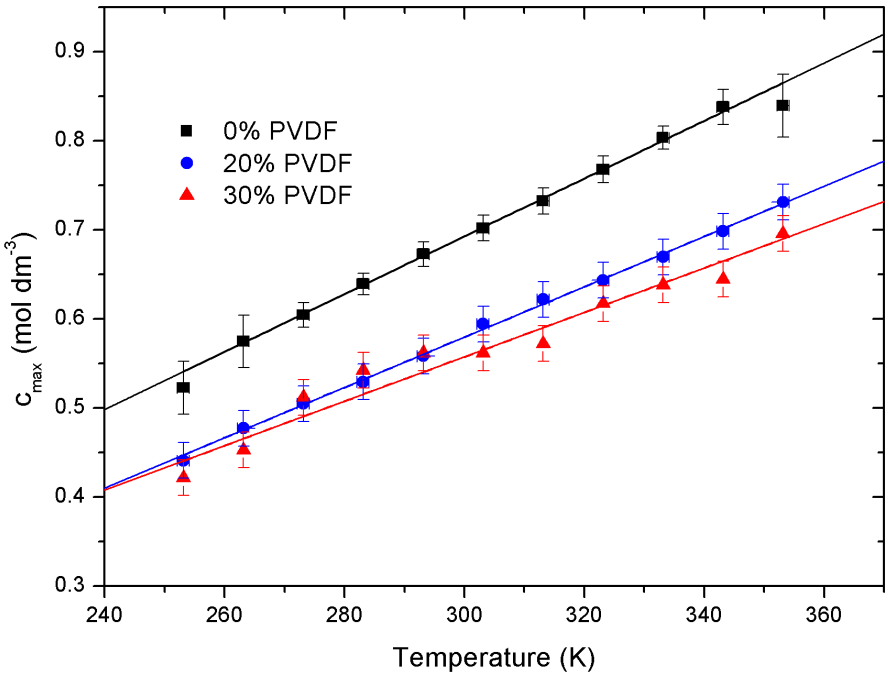

Figure 6.8: Position of maximum conductivity (c_{max}) as a function of temperature for 0% (liquid), 20% and 30% PVDF/PC/$LiBF_4$ polymer gel electrolytes.

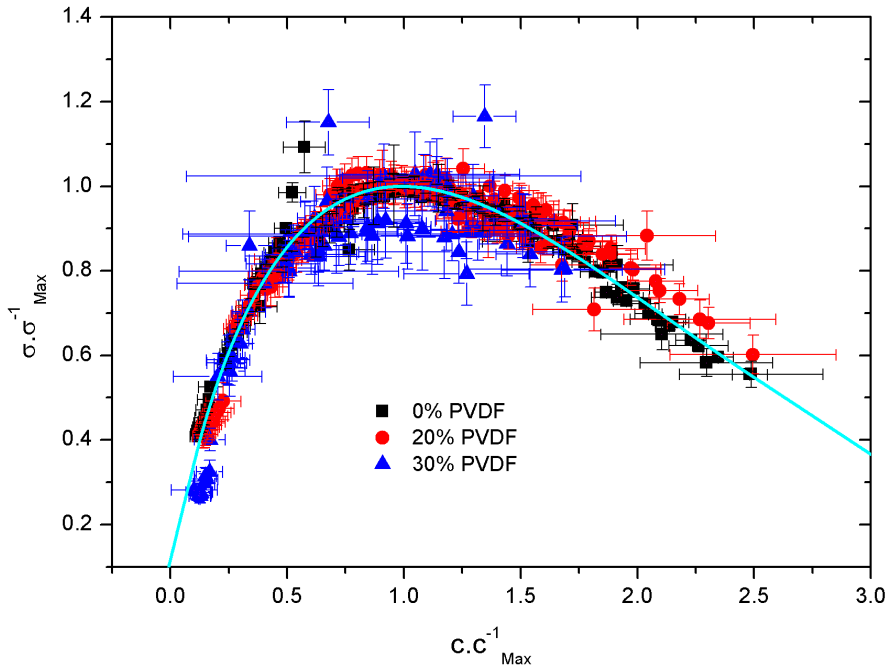

Figure 6.9: Casteel-Amis plot for 0% (liquid), 20% and 30% PVDF/PC/$LiBF_4$ polymer gel electrolytes (340 data points used). Data fitted using the Casteel-Amis equation.

electrolytes, a Casteel-Amis plot can be produced in order to see if all of the data overlaps.

Figure 6.9 shows the Casteel-Amis plot for the 0%, 20% and 30% PVDF/PC/$LiBF_4$ PGEs. It can be seen that all of the data from both the liquid and polymer gel electolytes overlap, suggesting that the conductivity mechanism is indeed similar in both systems. The solid line in figure 6.9 is a fit of the Casteel-Amis equation to all of the data. The values otained for a and b from figure 6.9 are (0.73±0.02) and (0.07±0.01), respectively. The values of a and b for just the liquid electrolytes were (0.67±0.01) and (0.10±0.01) and therefore similar values. This universal value of a and b once again confirms that the conductivity mechanism for the liquid electrolyte and PGEs are very similar. There was some deviance for the 30% PVDF gels which was attributed to the presence of a second phase of the polymer gel electrolytes which became more significant with the increasing polymer concentration.

6.3 Liquid-PGE Comparison

In this section the liquid and polymer gel electrolytes are compared with both temperature and salt concentration. By taking a ratio of the gel conductivity (σ_{PGE}) and the liquid conductivity (σ_{Liquid}) for the same salt concentration and temperature the two systems can be compared. If the decrease in the conductivity is caused by only volumetric considerations then it would be logical to assume that the value of $\sigma_{PGE}/\sigma_{Liquid}$ would be around 0.8 and 0.7 for the 20% and 30% PVDF PGEs, respectively. Figure 6.10 shows the ratio of the gel and liquid conductivity ($\sigma_{PGE}/\sigma_{Liquid}$) for a 20% and 30% PVDF/PC/$LiBF_4$ (1.0M) polymer gel electrolyte. It can be

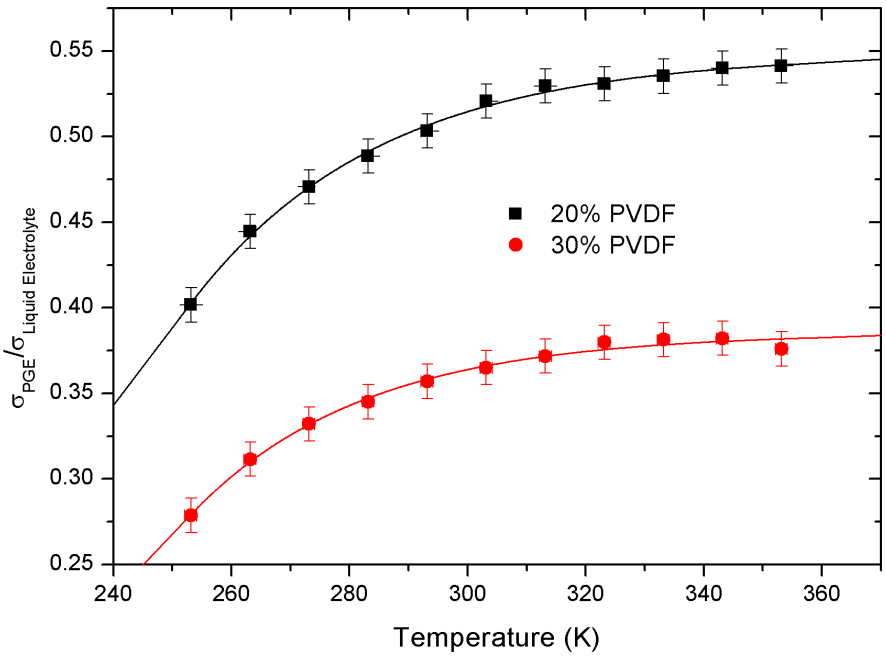

Figure 6.10: Ratio of PGE conductivity (σ_{PGE}) and the liquid conductivity (σ_{Liquid}) against temperature for 20% and 30% PVDF/PC/$LiBF_4$ (1.0M) polymer gel electrolytes.

seen that for both the 20% and 30% PVDF gels the ratio of the conductivities increases with increasing temperatures. At low temperatures (253 K) the ratio was around 0.4 which levels out to around 0.55 at 353 K for the 20% PVDF sample. The 30% PVDF gels also show this behaviour with ratios of 0.27 and 0.35 at 253 K and 353 K, respectively.

The surprising result is that at low temperatures the ratio is at even lower values and increases to a plateau at around 310 K for both gels. This result implies that there are some ions that are not contributing to the conductivity at low temperature, which become available at elevated temperatures. One possible explanation is that some of the lithium ions are associated to the polymer in some manner, or alternatively they are trapped in the polymer structure. The PVDF structure has negatively charged fluorine ions on the polymer backbone, it would therefore be possible for the positively charged conducting lithium ions to electrostatically interact with the fluorine on the PVDF molecule. Another, possibly more accurate interpretation of this result is to consider that the polymer gel electrolytes have been shown to contain multiple phases with lithium being located in the solvated amorphous and liquid electrolyte phases. The activation energies of the diffusion and conductivity have suggested that the viscosity of the solvated amorphous region of the PVDF is higher than the corresponding liquid electrolyte phase. Therefore it is assumed that the conductivity from the liquid phase would be on average higher due to the lower viscosity. Since the ratio of the gel and liquid conductivity showed an increase with temperature it may be the case that the conductivity contribution from the amorphous PVDF phase converges with the liquid phase with temperature. This result would be possible if the viscosity of the amorphous polymer phase decreased faster than the corresponding liquid electrolyte phase with increasing temperature. This explanation seemed the most reasonable

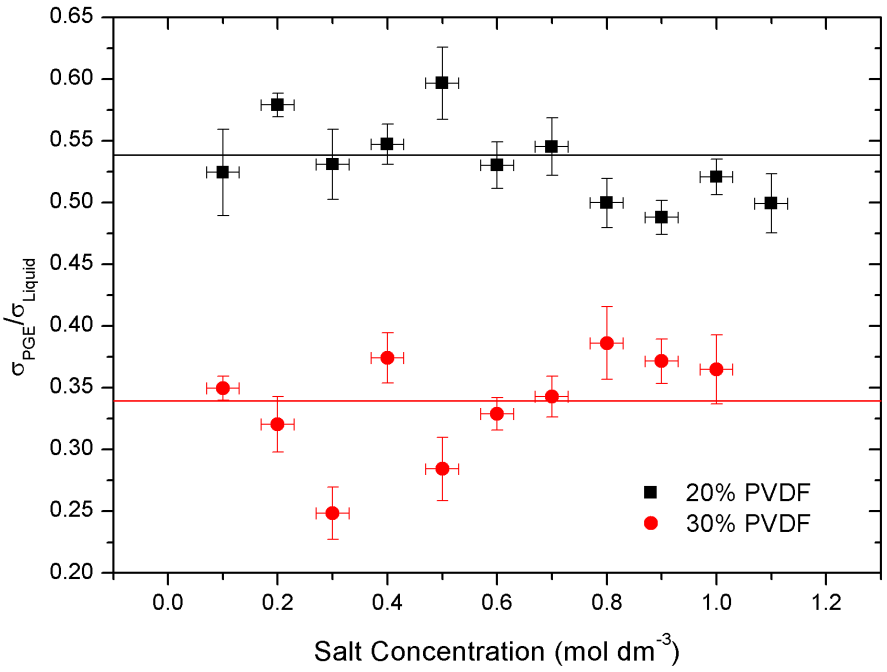

Figure 6.11: Ratio of PGE conductivity (σ_{PGE}) and the liquid conductivity (σ_{Liquid}) against salt concentration for 20% and 30% PVDF/PC/$LiBF_4$ polymer gel electrolytes at 293 K.

and explains the trends observed from the data of the diffusion and conductivity measurements.

Figure 6.11 shows the salt concentration dependence for the 20% and 30% PVDF gels at 293 K. The ratio of the conductivities ($\sigma_{PGE}/\sigma_{Liquid}$) was seen to have no trend with salt concentration and is roughly constant over the range of salt concentrations used. This result suggests that the amount of salt lost to the polymer is the same regardless of salt concentration, meaning that at this temperature the salt had already reached a plateau by 293 K. It would be informative to observe the ratios at low temperatures as these are the temperatures which the ratio of the conductivities changes most significantly.

It was found that at all temperatures, the ratio of the conductivities ($\sigma_{PGE}/\sigma_{Liquid}$) was independent of salt concentration. If the reduction in conductivity was attributed to the lithium ions associating with the polymer backbone, then it might be expected that at higher salt concentrations, more salt would be associated. However, if the reduction of the conductivity was attributed some of the ions being in located in the amorphous phase, the salt concentration independent ratio suggested a similar increase in viscosity for both phases. The temperature effect of the ratio in figure 6.10 has been attributed to a difference in viscosity for the amorphous and liquid phases. So as the temperature was increased the solvated amorphous phase conductivity contribution increased at a faster rate than the corresponding liquid electrolyte.

6.4 Diffusion Ratio

The calculations of ionic radii found in Chapter 7 revealed that there was no significant trend of the relative radii in either phase within the polymer gel electrolyte for the PC molecules,

	D_{Slow}/D_{Fast}							
	^{1}H				^{7}Li			
Temperature (K)	0.3M	0.5M	0.7M	1.0M	0.3M	0.5M	0.7M	1.0M
283	0.27	0.28	0.38	—	0.25	0.22	0.31	0.24
293	0.31	0.30	0.32	—	0.26	0.25	0.29	0.25
303	0.34	0.30	0.45	0.36	0.26	0.27	0.30	0.29
313	0.37	0.40	0.48	0.33	0.27	0.28	0.32	0.28
323	0.40	0.42	0.48	0.41	0.30	0.29	0.33	0.28
333	0.41	0.43	0.47	0.42	0.30	0.29	0.34	0.32
343	0.43	0.43	—	0.45	0.33	0.30	0.36	0.32
353	0.44	0.46	0.50	0.46	0.35	0.32	0.36	0.35

Table 6.5: ^{1}H and ^{7}Li ratio of slow (amorphous polymer) and fast (liquid phase) diffusive species (D_{Slow}/D_{Fast}) for 30% PVDF/PC/$LiBF_4$ polymer gel electrolytes.

lithium ions and BF_4^- anion. In this section the ratio of the diffusion of the slow (amorphous polymer phase) and fast (liquid phase) phases were calculated. Since most of the Stokes-Einstein equation was assumed constant by taking the ratio of the diffusion of the relative phases the trend of the viscosity in each of the phases can be determined as $D \propto 1/\eta$. The D_{Slow}/D_{Fast} values for the 30% PVDF/PC/$LiBF_4$ polymer gel electrolytes are shown in table 6.5 for the ^{1}H and ^{7}Li measurements.

Firstly considering the hydrogen measurements, it can be seen that there was no salt concentration dependence of the diffusion ratio, however there was a fairly strong temperature dependence. Since it is well known that the diffusion constants increase with temperature, the rise in the ratio means that the diffusion of the slower polymer phase was increasing more significantly than the corresponding liquid phase with temperature. The physical meaning of this result is that the viscosity of the amorphous polymer phase decreases more significantly than the viscosity of the liquid electrolyte phase of the gels. The same result was determined from the ratio of the diffusion of the slow and fast phases of the lithium measurements as shown in table 6.5.

The data in table 6.5 was for the 30% PVDF/PC/$LiBF_4$ gels, it was possible to perfom these calculations for the 20% PVDF gels also in the case of the lithium measurements. However since hydrogen measurements only exhibited a single diffusion constant for the 20% gels it was not possible to make the calculations for the hydrogen nucleus. The ratio of diffusion constants for the 20% PVDF gels are displayed in table 6.6. As with the 30% PVDF gels there was a strong positive correlation between the diffusion ratio and temperature, again suggesting that the viscosity of the amorphous polymer phase of the gels decreases more significantly than the corresponding liquid electrolyte phase of the gels.

In section 6.3 the ratios of the conductivity of the polymer gel electrolytes (PGE) and liquid electrolytes ($\sigma_{PGE}/\sigma_{Liquid}$) were calculated and displayed in figure 6.10. The result of this ratio was that it increased with increasing temperature, suggesting that the gel conductivity increased at a more significant rate than the corresponding liquid electrolytes. If the amorphous polymer phase contributed to the conductivity then it is reasonable to assume that as the temperature

	D_{Slow}/D_{Fast}						
Temperature (K)	0.3M	0.5M	0.6M	0.7M	0.8M	0.9M	1.0M
283	—	0.24	0.22	0.32	0.25	0.33	0.44
293	—	0.27	0.24	0.35	0.27	0.33	0.46
303	0.36	0.34	0.39	0.40	0.36	0.36	0.46
313	0.40	0.36	0.42	0.43	0.38	0.38	0.47
323	0.38	0.41	0.45	0.45	0.40	0.43	0.44
333	0.42	0.40	0.47	0.48	0.42	0.46	0.49
343	0.42	0.42	0.47	0.51	0.42	0.45	0.48
353	0.44	0.42	0.49	0.52	0.45	0.47	0.54

Table 6.6: Ratio of slow (amorphous polymer) and fast (liquid phase) diffusive species (D_{Slow}/D_{Fast}) for 20% PVDF/PC/$LiBF_4$ polymer gel electrolytes for ^{7}Li nucleus.

increased then the contribution to the conductivity would also increase. This would provide an explanation for the increase in the conductivity ratio ($\sigma_{PGE}/\sigma_{Liquid}$). It can be assumed that the liquid electrolyte conductivity behaves in the same manner as the liquid phase of the gels and therefore any change in the ratio of conductivities would be as a result of the amorphous polymer phase. At low temperatures, if the viscosity was higher for the polymer phase than the pure liquid phase, then this would reduce the conductivity. However, if the viscosity of the amorphous phase had a larger temperature dependence than the liquid phase, then as the temperature increased viscosities of the two phases would converge, resulting in an increase in the ratio of the conductivities. This validates the explanation offered earlier in this chapter for the trends of the polymer gel electrolyte conductivity.

Figure 6.12 shows the ratio of the two diffusion phases (D_{Slow}/D_{Fast}) and ratio of the conductivity of the liquid and gel ($\sigma_{PGE}/\sigma_{Liquid}$) for a 30% PVDF/PC/$LiBF_4$ (0.5M) polymer gel electrolyte for the measured temperatures. It can be readily observed that the two values increase at roughly the same rate. Therefore it can be concluded that both of the phases observed in diffusion measurements contribute to the ionic conductivity. It can also be concluded from this result that the viscosity of the two diffusion phases have different temperature dependencies which causes the ratio of $\sigma_{PGE}/\sigma_{Liquid}$ to exhibit an increase with increasing temperature.

6.5 Conclusions

In this chapter, the conductivity was measured for the liquid and polymer gel electrolytes. The liquid electrolytes were produced in the salt concentration range of 0.1-1.5M as up to this point the salt was miscible with the solvent. With the polymer gel electrolytes the solvent had to dissolve both the salt and polymer and was therefore a competition between the two. This has the effect of reducing the amount of salt that was able to be dissolved, thus the salt concentration range for the PGEs was set to no more than 1.1M. Exceeding this limit caused syneresis, a process which causes the gel to phase separate into part gel and part liquid.

It was observed that the conductivity increased with temperature for both the liquid electrolytes and the PGEs, this result is well understood due to the increased temperature providing

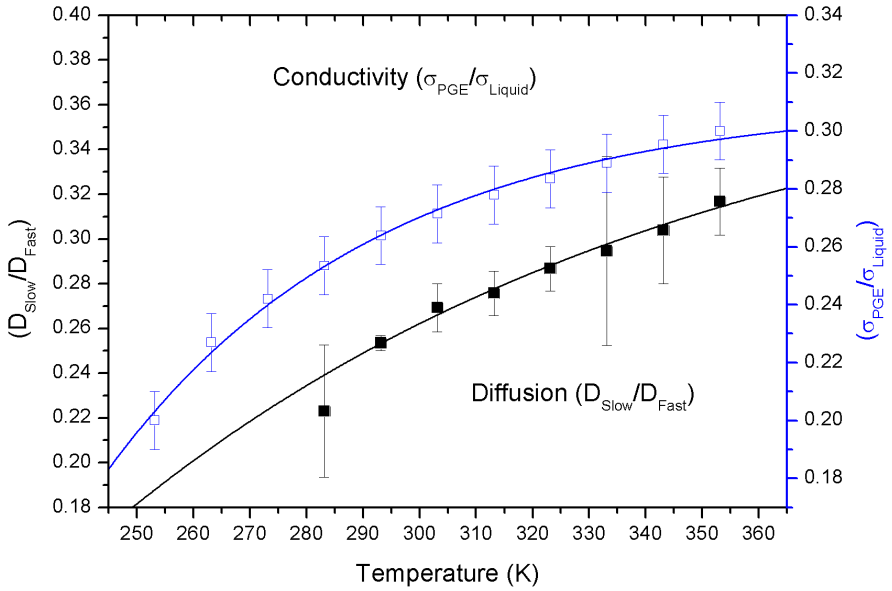

Figure 6.12: D_{Slow}/D_{Fast} and $\sigma_{PGE}/\sigma_{Liquid}$ for a 30% PVDF/PC/$LiBF_4$ (0.5M) polymer gel electrolyte.

more thermal energy and a reduced viscosity. To understand the conductivity mechanism, it was important to classify the temperature dependence as either Arrhenius or Vogel-Tamman-Fulcher (VTF) type behaviour. This was achieved by plotting Arrhenius plots (ln(conductivity) against $1000/T$) for both the liquids and PGEs. The Arrhenius plots illustrated that for the liquids and PGEs the fit was non-linear, suggesting that the behaviour was likely VTF. The diffusion measurements of liquid (Chapter 4) and polymer gel electrolytes (Chapter 5) exhibited Arrhenius type temperature dependence. The difference between the conductivity and diffusion was due to the different temperature ranges used for each measurement. The conductivity measurements were in the range of 253-353 K whereas the diffusion measurements were limited to a temperature range of 283-353 K, therefore the reduced temperature range Arrhenius fitting was employed, as well as the VTF fitting.

The activation energy can be determined for the VTF dependence by fitting equation 6.2 to the conductivity data of the liquids and gels. The reduced temperature range Arrhenius activation energy was determined using Arrhenius plots ($\ln(\sigma)$ against $1000/T$). It was established that the activation energies of the liquids and gels were seen to increase roughly linearly with increasing salt concentration. This result is explained by the increase in viscosity with salt concentration thus making it more difficult for the ions to translate through the medium and therefore requiring more energy. The activation energies of the liquids and gels were also comparable to each other, suggesting that the ions are in a similar medium when translating. This supports the hypothesis that the polymer forms a porous structure during phase separation with the liquid electrolyte flowing throughout the structure. However the general trend of the activation energies was $E_{30\%} > E_{20\%} > E_{0\%}$ which implied that as the polymer concentration increased the effective viscosity increased. It was assumed that the viscosity increase was due to the solvated amorphous phase which was observed to have a higher viscosity than the liquid

phase.

In this chapter we have also reported the conductivity as a function of salt concentration. The conductivity shows an initial increase at low salt concentration and then at some critical concentration (c_{Max}) the conductivity starts to decrease resulting in a peak in the conductivity. Initially the conductivity increases due to an increase in the number of ions able to conduct, however as the salt concentration is increased the viscosity of the system is also increased thus hindering the motion of the conducting ions. Therefore at the critical concentration c_{Max} the viscosity becomes the dominating factor and causes the conductivity to fall.

The Casteel-Amis equation (equation 6.6) is a semi-empirical equation which has been used previously to fit conductivity data as a function of salt concentration. This equation allowed the determination of the critical concentration as a function of temperature. It was observed that the value of c_{Max} increased linearly with increasing temperature. Since c_{Max} is the point at which the increase in ions is overcome by viscous effects, it was considered reasonable that as the temperature was increased the viscosity also decreased and therefore c_{Max} increases, allowing more salt to be entered into the system before viscosity dominates.

If each value of conductivity and salt concentration are scaled by the systems relevant σ_{Max} and c_{Max} respectively then a Casteel-Amis plot can be produced. A plot can be found in figure 6.5 for liquids and figure 6.9 for both liquids and PGEs. In figure 6.9 there are 340 points in total spanning over the 0% (liquid), 20% and 30% PVDF/PC/$LiBF_4$ polymer gel electrolytes. This plot illustrates that all of the values roughly overlap suggesting that they can be described by a universal equation and therefore are exhibiting the same conductivity mechanism. This again supports the theory that the liquid electrolytes are free flowing through the gels.

The ratio of the PGE (σ_{PGE}) and liquid (σ_{Liquid}) conductivity has been calculated as a function of temperature. If the drop in conductivity was simply due to volumetric factors then it might be expected that the ratio would be unaffected by a change in temperature; however an initial increase was observed at low temperatures which plateaus at around 310 K for both 20% and 30% PVDF gels. This result has been attributed to some of the lithium ions being associated to the polymer in some manner and is therefore an important consideration to understand the transport properties in these gels.

In the final section of this chapter the ratio of the diffusion for the slow (amorphous polymer) and fast (liquid phase) phases of the polymer gel electrolytes was calculated. An interesting result was shown for both the hydrogen and lithium measurements that this ratio increased with increasing temperature. This results suggested that since the ionic radii increases were observed to be nominal then the difference must be due to the relative viscosity. Therefore this result suggests that the viscosity of the amorphous polymer phase decreased faster than the corresponding liquid electrolyte phase with temperature. A graph was produced showing the ratio of the gel conductivity and measured conductivity ($\sigma_{Gel}/\sigma_{Liquid}$) and the ratio of the diffusion (D_{Slow}/D_{Fast}). This graph showed that the increases of the two parameters were very similar. The importance of this result is that not only must the amorphous polymer phase contribute to the conductivity that it must also converge to the liquid electrolyte system at higher temperatures.

Chapter 7

Ionic Association and Solvation Dynamics

7.1 Introduction

In this chapter, the diffusion and conductivity data are used to determine the ionic association in both liquid and polymer gel electrolytes. It is possible to predict the conductivity based on the self diffusion constants which can be compared to the measured conductivity to determine the degree of ionic association. The viscosity of the liquid electrolytes for the PC/$LiBF_4$ are also displayed and discussed. It was possible to calculate the ionic radii of each of the diffusive species by using the diffusion and viscosity measurements along with the Stokes-Einstein. However there are some implications of this as the micro-diffusion and macro-viscosity are used which can cause discrepancies.

7.2 Ionic Association

In this section the degree of ionic association was determined for the liquid and polymer gel electrolytes. This parameter is important as it dictates the level of ions that are contributing to the ionic conductivity. The Einstein relationship is developed from Fick's law of diffusion which is given by;

$$J = -D\frac{dc}{dx} \tag{7.1}$$

where J is the flux of matter through a given cross-section, D is the translational diffusion constant and dc/dx is the concentration gradient of the system which is driving the diffusion of the ions. This equation arises from the fact that the flux is driven by a concentration gradient and therefore the two are proportional with the diffusion constant being the constant of proportionality. The molecules moving through a cross-sectional area (A) and are translating at a speed equal to the drift velocity (ν_d). Any molecule within a distance of $\Delta t\nu_d$ will pass through the area and therefore all the molecules in the volume of $\Delta t\nu_d A$ will pass through the area, where Δt is an arbitrary change in time. Therefore the total number of moles of molecules that will

pass through this volume per area per second (i.e. the flux) is;

$$J = \frac{\nu_d \Delta\, t\, A\, c}{\Delta t\, A} = \nu_d c \tag{7.2}$$

where c is again the concentration of the system. Therefore combining equations 7.1 and 7.2 gives equation 7.3.

$$\nu_d c = -D\frac{dc}{dx} \tag{7.3}$$

The opposing force to diffusion is equal to the chemical potential gradient at constant temperature and pressure;

$$F = -\left(\frac{\delta\mu}{\delta x}\right)_{P,T} \tag{7.4}$$

where μ is the chemical potential at position (x). This force describes the motion of molecules as they disperse due to the second law of thermodynamics. Therefore diffusion is the process by which the molecules move to increase the entropy of the system.

The chemical potential of a system can be given by

$$\mu = \mu^0 + RT\, lna \tag{7.5}$$

where μ^0 is the chemical potential at standard conditions and a is the activity of the system. Therefore the thermodynamic force is now given by;

$$F = -\frac{RT}{a}\left(\frac{\delta a}{\delta x}\right)_{P,T} \tag{7.6}$$

where the activity a can be exchanged with the molar concentration c. Therefore equation 7.6 can be written as;

$$F = -\frac{RT}{c}\left(\frac{\delta c}{\delta x}\right)_{P,T} \tag{7.7}$$

therefore by rearranging equation 7.7 and combining with equation 7.3 yields equation;

$$\nu_d = \left(\frac{-D}{c}\right)\left(\frac{-F\, c}{RT}\right) = \frac{DF}{RT} \tag{7.8}$$

where the drift velocity is proportional to the diffusion constant and the thermodynamic force. The thermodynamic force of a charged ion in an electric field can be described by;

$$F = zeE \tag{7.9}$$

where z is the number of electrons of charge e (charge on an electron) and E denotes the electric field. Where the force per mole can be written;

$$F = N_A zeE \tag{7.10}$$

since the mobility (u) of the system is the constant of proportionality of the drift velocity and electric field. Therefore the mobility is given by;

$$u = \frac{DzN_A e}{RT} \tag{7.11}$$

where this is known as the Einstein relation.

Now in order to obtain a relationship for the diffusion of the ions and the conductivity of the system the Nernst-Einstein relationship can be used. The limiting conductivity (λ) is defined by;

$$\lambda = zuN_Ae \tag{7.12}$$

where u is the mobility, e is the charge on an electron and N_A is the Avagadro number. The limiting conductivity corresponds to the limit of infinite dilution. Therefore by rearranging equation 7.12 for the mobility and substituting into equation 7.11 and rearranging for molar limiting conductivity gives;

$$\lambda = \frac{Dz^2}{RT}N_A^2e^2 \tag{7.13}$$

it was found by Kohlrausch that the limiting conductivity of a strong electrolyte of anions and cations are additive. A strong liquid electrolyte is one that is assumed to fully dissociate the cation and anion. Therefore the limiting conductivity can be given by;

$$\Lambda_m^0 = v_+\lambda_+ + v_-\lambda_- \tag{7.14}$$

where λ_+ and λ_- are the limiting molar conductivity of the cation and anion respectively and the v_+ and v_- are the number of ions per formula unit of electrolyte. Therefore in the case of this system for the $LiBF_4$ salt the values of $v_+ = v_- = 1$. Therefore the limiting molar conductivity can be given by;

$$\Lambda_m^0 = \frac{N_A^2e^2}{RT}\left[v_+D_+z_+ + v_-D_-z_-\right] \tag{7.15}$$

where the D_+ and D_- are the diffusion constants for the cation and anion respectively. In this case $LiBF_4$ was used in the electrolytes and therefore the cation and anion were the lithium and BF_4 ions respectively. Therefore for this system equation 7.15 can be expressed as;

$$\Lambda_m^0 = \frac{N_A^2e^2}{RT}\left[D_+ + D_-\right] \tag{7.16}$$

where the ionic conductivity is defined as $\Lambda_m^0 = \sigma/c$ and therefore the ionic conductivity can be written as;

$$\sigma = \frac{N_Ae^2c}{k_BT}\left[D_{Li} + D_{BF_4}\right] \tag{7.17}$$

where this equation is known as the Nernst-Einstein equation and is used to determine the conductivity of a system based on diffusion measurements. Therefore this equation was used to calculate the conductivity of the electrolytes. This equation is for a strong electrolyte which assumes complete dissociation and therefore is an ideal conductivity.

7.2.1 Liquid Electrolytes

The conductivity has been predicted for the liquid electrolytes containing PC and $LiBF_4$ using the Nernst-Einstein relationship along with the diffusion constants displayed in Chapter 4. The values of the predicted conductivity have been displayed in table 7.1. It should be noted that the conductivity values predicted from the Nernst-Einstein relation were much higher than that of the measured conductivity. Taking for example a PC/$LiBF_4$ (0.5M) liquid electrolyte at 283 K the conductivity values were given as (5.27±0.06) mS cm^{-1} and (2.53±0.03) mS cm^{-1} for the predicted and measured values, respectively, therefore it can be seen that the difference is

	Predicted Conductivity (mS cm^{-1})					
Temperature (K)	0.3M	0.5M	0.7M	1.0M	1.3M	1.5M
283	4.0	5.3	5.7	5.8	5.1	4.5
293	5.2	6.8	7.6	7.8	7.2	6.5
303	6.4	8.6	9.8	10.3	9.6	8.8
313	7.8	10.5	12.1	12.9	12.3	11.4
323	9.3	12.5	14.7	15.6	15.2	14.3
333	11.1	14.7	18.2	19.1	18.8	18.0
343	13.4	17.7	20.7	22.5	22.7	22.3
353	—	22.8	25.3	27.0	28.2	28.0

Table 7.1: Predicted conductivity using the Nernst-Einstein relationship for PC/$LiBF_4$ liquid electrolytes.

significant. This difference is attributed to the fact that the Nernst-Einstein is only valid for perfect dissociation of the cation and anion in the solution, so any association that would take place in a real system would cause the predicted conductivity deviate from the measured value.

The same trends were observed with the predicted conductivity that were discussed in Chapter 6 for the measured values, the conductivity increased with temperature and exhibited a peak with increasing salt concentration. This was attributed to the diffusion constants decreasing with increasing salt concentration and increasing with temperature which was in turn attributed to the viscosity of the system. Figure 7.1 shows the conductivity as a function of salt concentration for PC/$LiBF_4$ liquid electrolytes at 293 K. It can be readily observed that the predicted conductivity is significantly higher than the corresponding measured conductivity. Both curves have been fitted with the Casteel-Amis equation 6.6 which is the semi-empirical equation used to describe the specific conductivity of liquid electrolytes as a function of salt concentration. In figure 7.1 the position of the maximum (c_{Max}) was determined from the Casteel-Amis fitting and has been noted as (0.64±0.01) M and (0.88±0.01) M for the measured and predicted conductivity, respectively. Therefore it can be seen that not only was the predicted conductivity higher than the measured but also significantly shifted the position of the maximum. In Chapter 6 it was discussed that the c_{Max} value was dependent on the viscosity of the system. If the viscosity of the system decreased then it would be intuitive to assume that more salt could be added to the electrolyte before the viscosity dominated the conductivity and therefore c_{Max} would increase with decreasing viscosity. This result was supported by observing the c_{Max} values as a function of temperature.

Since the c_{Max} value was significantly higher for the predicted conductivity, the position of the maximum must also be dependent on the ionic association since the difference between the predicted and measured conductivities was the association. Therefore it can be stated that as the ionic association is increased the position of the maximum decreased and that c_{Max} maybe stated as;

$$c_{Max} \propto \frac{T}{\alpha} \propto \frac{1}{\eta\alpha} \tag{7.18}$$

where α is the degree of ionic association. The c_{Max} values were determined for the predicted

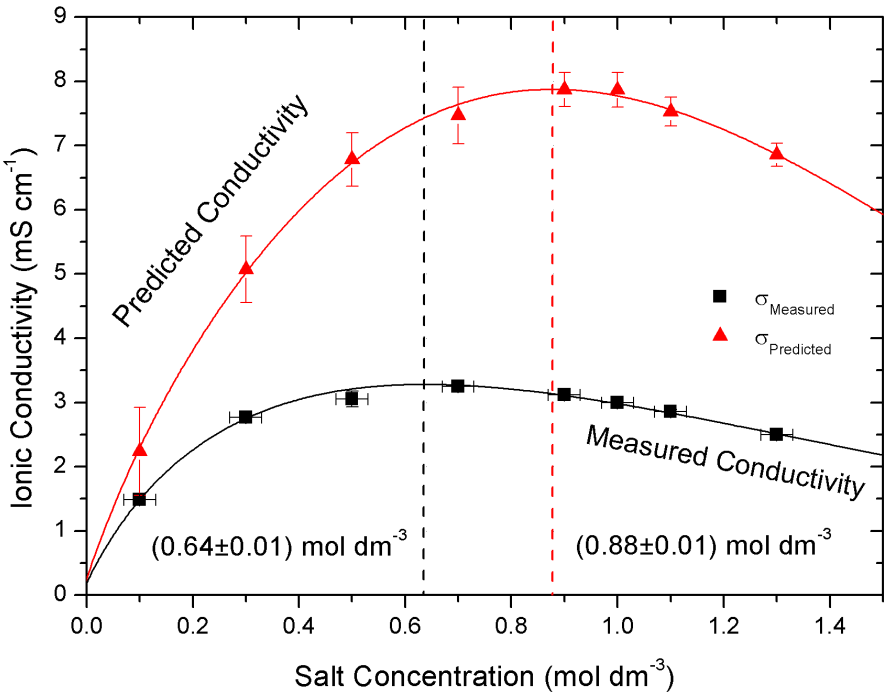

Figure 7.1: Predicted and measured conductivity as a function of salt concentration for PC/$LiBF_4$ at 293 K. The dashed lines are to indicate the position of the maximum for both the measured (black) and predicted (red) curves.

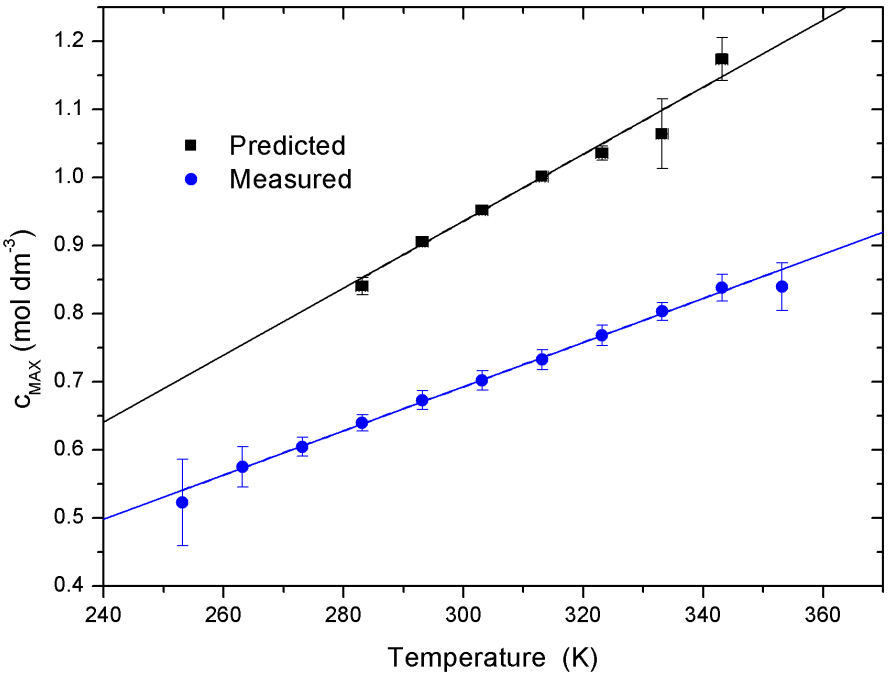

Figure 7.2: Position of ionic conductivity (c_{Max}) as a function of temperature for measured and predicted (Nernst-Einstein) conductivity of PC/$LiBF_4$ liquid electrolytes.

	Ionic Association					
Temperature (K)	0.3M	0.5M	0.7M	1.0M	1.3M	1.5M
283	0.45	0.52	0.57	0.60	0.64	0.67
293	0.47	0.53	0.58	0.62	0.66	0.68
303	0.49	0.55	0.59	0.63	0.67	0.69
313	0.50	0.55	0.60	0.64	0.68	0.70
323	0.51	0.56	0.62	0.64	0.68	0.71
333	0.54	0.57	0.64	0.66	0.69	0.72
343	0.56	0.59	0.64	0.66	0.70	—
353	—	0.64	0.67	0.68	0.72	—

Table 7.2: Ionic association (α) for PC/$LiBF_4$ liquid electrolytes.

conductivity and compared with the values for the measured conductivity in Chapter 6 as a function of temperature in figure 7.2. It can be observed that the value of c_{Max} increases with temperature for both the predicted and measured conductivities. This agrees with theory that the position shifts to higher concentrations as the viscosity is lowered. The gradients of the linear relationships shown in figure 7.2 were (4.9±0.2) mM K^{-1} and (3.24±0.06) mM K^{-1} for the predicted and measured conductivities, respectively. The predicted conductivity c_{Max} increased at a faster rate with temperature, which was attributed to an increase of ionic association of the measured conductivity with temperature.

The ionic association can be defined as a ratio of the predicted and measured conductivity since the Nernst-Einstein is for a strong electrolyte which is fully dissociated and is given by;

$$\alpha = 1 - \left(\frac{\sigma_{Measured}}{\sigma_{Predicted}} \right) \tag{7.19}$$

where the $\sigma_{Measured}$ and $\sigma_{Predicted}$ are the measured and predicted ionic conductivities respectively. Therefore α the ionic association can take values between 0 and 1, where a value of 0 represents a fully dissociated system i.e. when $\sigma_{Measured} = \sigma_{Predicted}$ and a value of 1 represents a fully associated system which would yield a conductivity of zero as all cations and anions have formed neutral pairs. For a real system a value between these two extremes is expected. The ionic association for the PC/$LiBF_4$ liquid electrolytes are displayed in table 7.2.

It can be readily observed from table 7.2 that the ionic association increases with increasing temperature [43]. This is somewhat counter intuitive as it might be expected that as the temperature was increased the molecules would have more kinetic energy and therefore would disrupt the formation of ion pairs leading to dissociation. The increase with temperature has been seen for other electrolyte systems, this was attributed to the lowering of the free energy of ionic association at higher temperatures, therefore actually favoring association [43]. It has been stated by Olender *et al* [128] that for the chemical reaction $MA \rightleftharpoons M^+ + A^-$ the equilibrium constant takes the form of;

$$K = exp\left[-\frac{\Delta G^0}{RT} \right] \tag{7.20}$$

where K is the equilibrium constant and ΔG^0 is the difference between the standard molar

Gibbs free energies of reactants and products [128]. The difference in free energy takes the form;

$$\Delta G^0 = \Delta H^0 - T\Delta S^0 \tag{7.21}$$

where ΔH^0 and ΔS^0 are the change in enthalpy and entropy of the system, respectively. The enthalpy can be written in the form;

$$\Delta H = \Delta E + P\Delta V \tag{7.22}$$

where ΔE is a positive energy term corresponding to promoting dissociation and P and ΔV are the pressure and change in volume due to the reaction, respectively. It was stated by Olender *et al* [128] that the volume term can outweigh the positive energy term and can also be negative due to electrostriction [43; 128]. It has also been shown that the dielectric constant can decrease with increasing temperature which would result in an increase in ionic association [129].

The ionic association was also observed to increase with increased salt concentration. This has been seen to occur for six different lithium based salts in γ-butyrolactone (GBL) where the authors showed that the ionic dissociation $(1-\alpha)$ decreased with salt concentration[56]. The order of ionic association of those six salts were $LiSO_3CF_3$>$LiBF_4$>LiBETI≈ LiBOB≈ LiTFSI≈ $LiPF_6$ and therefore can be seen that the $LiBF_4$ exhibits a high ionic association relative to other lithium based salts. The physical significance of α is the fraction of neutral $LiBF_4$ pairs that are contained in the liquid electrolyte, and the ionic dissociation ($\delta = 1-\alpha$) is the fraction of ions which are 'free' contributing to the ionic conductivity.

The ionic association is an important consideration from an engineering standpoint because for the practical battery application it is preferable to have as high conductivity as possible and therefore very low ionic association is desired. This was a fairly straightforward calculation for the liquid electrolytes. The same calculations can be performed for the polymer gel electrolytes, however they have a much more complex structure and the ionic association are harder to determine.

7.2.2 Polymer Gel Electrolytes

The predicted conductivity of the polymer gel electrolytes can be determined in the same way as the liquid electrolytes. However unlike the liquids, the lithium cation measurements were observed to produce two distinct diffusion constants which were assumed to correspond to two distinct phases in the gels, as shown in section 5.4.2.1. The D_{Li} term in equation 7.17 must now be altered in order to include both phases. The intensity of each of the diffusion measurements was determined for every measurement where the two intensities were normalised to equal unity. Therefore the lithium diffusion (D_{Li}) was given by;

$$D_{Li} = I(0)_1 D_1 + I(0)_2 D_2 \tag{7.23}$$

where $I(0)_1$ and D_1 are the intensity and diffusion of the polymer phase, respectively and $I(0)_2$ and D_2 are the intensity and diffusion of the liquid electrolyte phase. Since the fluorine measurements only exhibited a single diffusion constant the diffusion constant was unchanged.

The predicted conductivities of the 20% PVDF/PC/$LiBF_4$ polymer gel electrolytes are displayed in table 7.3. The same trends were observed as with the liquid electrolytes; there was

	Predicted Conductivity (mS cm^{-1})									
	20% PVDF					30% PVDF				
Temp.(K)	0.3M	0.5M	0.7M	0.9M	1.0M	0.3M	0.5M	0.7M	0.9M	1.0M
283	—	4.3	4.8	4.4	4.2	3.0	3.7	4.0	4.0	3.6
293	—	5.6	6.1	5.9	5.3	3.6	4.6	5.2	—	5.2
303	5.1	6.6	7.2	7.2	6.6	4.7	5.7	6.5	6.9	6.3
313	6.0	7.6	8.5	8.8	8.1	5.4	6.7	7.8	8.0	7.7
323	7.1	8.8	9.9	10.6	9.7	6.1	7.6	8.8	9.4	9.1
333	7.8	9.9	11.2	11.7	11.4	6.7	8.6	10.0	10.7	10.3
343	8.7	10.8	12.3	13.7	13.0	7.1	9.3	10.9	12.1	11.7
353	9.3	11.8	13.4	15.1	14.8	7.8	10.3	11.7	13.2	12.7

Table 7.3: Predicted conductivity from Nernst-Einstein equation for 20% and 30% PVDF/PC/$LiBF_4$ polymer gel electrolytes.

an increase with temperature due to a decrease in viscosity and a peak with increasing salt concentration. The same trends were seen with the 30% PVDF/PC/$LiBF_4$ polymer gel electrolytes which are displayed in table 7.3. As for the liquid electrolytes the predicted conductivity values were significantly higher than the measured values. A plot of predicted and measured conductivity as a function of salt concentration is displayed in figure 7.3 which shows again that the value of c_{Max} has shifted. It should also be noted that the difference in predicted and measured conductivities was much more signifcant than for the liquid electrolytes.

The position of the maximum in figure 7.3 for the liquid electrolyte was (0.64±0.01) M and (0.88±0.01) M for the measured and predicted conductivities, respectively. For the 20% PVDF gel the peaks were at (0.57±0.06) M and (0.72±0.04) M for the measured and predicted, and for the 30% PVDF gels the peaks were (0.61±0.06) M and (0.70±0.08) M for the measured and predicted, respectively. This result suggested that the position of the maximum was dependent on the ionic association for both the liquids and gels.

The ionic association values of the 20% and 30% PVDF/PC/$LiBF_4$ polymer gel electrolytes are displayed in table 7.4. It can be observed that there was no trend with salt concentration for the polymer gel electrolytes. It can also be noted that there was a decrease with increasing temperature which is the inverse of the case in the liquid electrolytes. In the case of the polymer gel electrolytes the ionic association was not as straightforward. In the case of the liquid electrolytes α was the fraction of cations and anions which formed neutral pairs or clusters which would not contribute to the ionic conductivity. However, in the case of the polymer gel electrolytes, all that can be stated from the ionic association is that it is the fraction of ions which do not contribute to the ionic conductivity. It was shown in Chapter 6 that the ratio of $\sigma_{Gel}/\sigma_{Liquid}$ with temperature was seen to increase and plateau. This suggested that some ions were being released with the increase of temperature which were then available to contribute to the ionic conductivity. Therefore it is plausible that some ions are associated with the polymer which cannot contribute to the ionic conductivity which is not strictly ionic association. Since the ionic association decreases with temperature for the gels this means that some ions are being made available for conduction. This therefore agrees with the ratio of the conductivities as

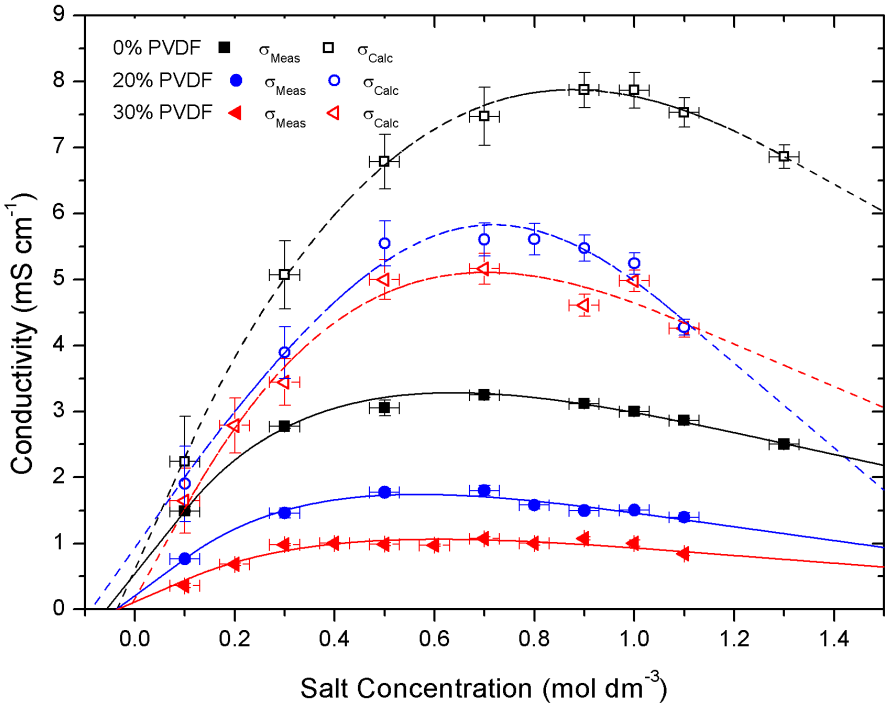

Figure 7.3: Predicted (hollow) and measured (solid) conductivity for 0% (liquid), 20% and 30% PVDF/PC/$LiBF_4$ gel electrolytes at 293 K. All data has been fitted with Casteel-Amis equation, solid lines for measured conductivity and dashed lines for predicted conductivity.

	Ionic Association									
	20% PVDF					30% PVDF				
Temp.(K)	0.3M	0.5M	0.7M	0.9M	1.0M	0.3M	0.5M	0.7M	0.9M	1.0M
283	—	0.71	0.73	0.71	0.73	0.83	0.83	0.79	0.79	0.78
293	—	0.71	0.71	0.72	0.71	0.82	0.82	0.79	—	0.79
303	0.65	0.70	0.70	0.71	0.70	0.82	0.81	0.79	0.79	0.78
313	0.64	0.68	0.69	0.70	0.70	0.81	0.80	0.78	0.78	0.78
323	0.64	0.68	0.69	0.70	0.70	0.79	0.79	0.77	0.77	0.77
333	0.63	0.67	0.68	0.68	0.69	0.77	0.78	0.77	0.77	0.76
343	0.62	0.66	0.66	0.68	0.69	0.74	0.77	0.76	0.76	0.75
353	0.62	0.65	0.65	0.66	0.68	0.73	0.76	0.75	0.75	0.74

Table 7.4: Ionic association (α) for 20% PVDF/PC/$LiBF_4$ polymer gel electrolytes.

discussed in section 6.4.

The ionic association for PVDF/PC/$LiBF_4$ (0.5M) at 303 K were (0.55±0.01), (0.70±0.01) and (0.81±0.08) for the 0% (liquid), 20% and 30% PVDF, respectively. As the polymer was increased the ionic association increased; this was true for all temperatures and salt concentrations measured. This result was attributed to some of the ions being located in the solvated amorphous phase which has been shown to have a higher effective viscosity which would therefore cause the ionic association value to increase. The 0% (liquid), 20% and 30% PVDF gel ionic association data as a function of salt concentration at 303 K is displayed in figure 7.4.

It can be readily seen from figure 7.4 that the 30% PVDF gels exhibit no trend with increasing salt concentration. However, the 20% gels seem to have an increase initially much like the liquid electrolyte association. Since the gels are predominantly cavities of liquid electrolytye it might be expected that a similar trend would be observed between the liquid and polymer gel electrolyte. The dotted red line in figure 7.4 has been fitted with a simple exponential of the same for as the liquid electrolyte curve, which fits the data well.

7.3 Viscosity Measurements

The viscosity has been measured for the PC/$LiBF_4$ liquid electrolytes in a salt concentration range of 0.0-1.5M $LiBF_4$. An Ostwald viscometer ('U' tube) was used to measure the bulk viscosity of the liquid electrolytes which was placed inside a water bath to maintain the temperature, however this method of temperature control was limited to 293-333 K. Using viscometers to measure the viscosity requires the use of a calibration sample of a well known solvent. The time taken for the calibration liquid to fall through a fixed volume was measured for each temperature. By taking a ratio of the sample measurement and calibration solvent there was no need to know the geometric constants of the 'U' tube used as shown in Chapter 3 in equation 3.37, restated here;

$$\frac{\eta_{Sample}}{\eta_{Calibration}} = \frac{t_{Sample}\rho_{Sample}}{t_{Calibration}\rho_{Calibration}} \tag{7.24}$$

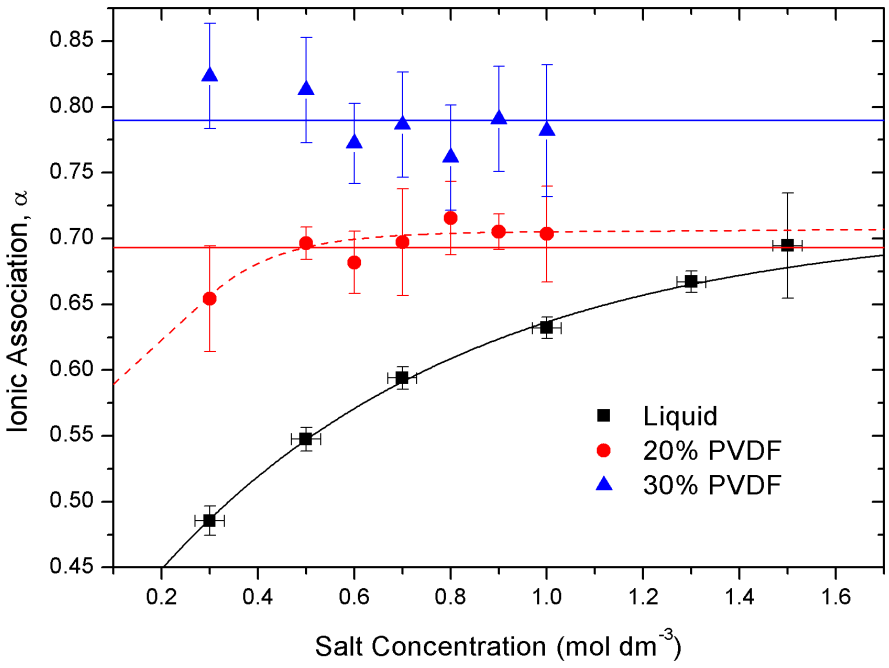

Figure 7.4: Ionic association as a function of salt concentration for 0%, 20% and 30% PVDF/PC/$LiBF_4$ polymer gel electrolytes at 303 K.

where η is the viscosity, t is the time taken to fall the fixed volume and ρ is the density. Therefore in order to determine the viscosity the density and time taken to fall the fixed volume must be known, along with all of the calibration solvent parameters. Here the calibration liquid was pure propylene carbonate as the viscosity of the pure solvent is well defined. The density and viscosity taken from Barthel *et al* [93] as a function of temperature can be found in table 7.5. The density was taken from reference [93] and extrapolated to the relevant temperatures as the density was linear with temperature.

It is important to have a constant volume when using a capillary viscometer. Since the density changes with temperature this can be difficult to achieve, however across the temperature range measured here there was not a significant volume change and therefore this effect can be assumed negligible. From equation 7.24 it can be observed that since the calibration viscosity and densities were known, only the time for the liquid to fall through the fixed volume for both the calibration liquid and sample liquid must be measured along with the density of the sample liquid. These were then used along with equation 7.24 in order to determine the dynamic viscosity of the liquid electrolytes.

The density was measured using two 10 ml volumetric flasks which were placed in the water bath along side the viscometer. Two flasks were used in order to take two independent density measurements to reduce errors. The mass was measured using a balance which was accurate to five decimal places. The final value of the density was an average of the two densities calculated from the two different volumetric flasks. Between each different salt concentration the flasks were throughly cleaned with acetone and allowed to dry in an oven at 50°C which was chosen so that the glass did not warp. The density at four different temperature was taken at 298 K,

Temperature (K)	Density (g cm^{-3})	Viscosity (mPa s)
293	1.205	2.786
298	1.200	2.514
303	1.194	2.281
308	1.189	2.080
313	1.184	1.905
318	1.178	1.753
323	1.173	1.619
328	1.168	1.500
333	1.162	1.395

Table 7.5: Propylene carbonate density and viscosity used for viscosity calibration. The viscosity and density were taken from a reference [93] by Barthel *et al*, where the density was extrapolated from the data.

308 K, 318 K and 328 K and was extrapolated from linear fits to the data. The density of the PC/$LiBF_4$ liquid electrolytes are displayed in figure 7.5.

The density values were extrapolated to all temperatures measured. The density was not measured at every temperature as the volume was adjusted by eye and a 5 K change was quite difficult to determine, so the density was taken every 10 K. The fits in figure 7.5 were seen to be linear and therefore the density was easily extrapolated. The viscosity values for the liquid electrolytes are displayed in table 7.6. It can be immediately noted that the viscosity increases with salt concentration and decreases with increasing temperature.

7.3.1 Temperature Dependence

It has been noted in the previous section that the viscosity values were observed to decrease with increasing temperature. This is a very well understood property and in this section the temperature dependence was determined as well as the activation energy which were compared to the diffusion activation energies in Chapter 4. As with the diffusion and conductivity the viscosity data was analysed in the same manner. A plot of $ln(\eta)$ against $1000/T$ is an Arrhenius plot, if the resulting relationship is linear then the temperature is considered to be Arrhenius and can be fitted with;

$$\eta(T) = \eta_\infty exp\left[\frac{E_\eta}{RT}\right] \tag{7.25}$$

where E_η is the activation energy of the bulk viscosity and η_∞ is the viscosity at infinite temperature (i.e. when $exp\left[\frac{E_\eta}{RT}\right] = 0$). If the Arrhenius plot exhibited a non-linear relationship then it is likely that the temperature dependence is described by the VTF equation of the form;

$$\eta(T) = \eta_\infty exp\left[\frac{E_\eta}{R(T - T_0)}\right] \tag{7.26}$$

where T_0 is the ideal glass transition temperature. An Arrhenius plot is shown for the PC/$LiBF_4$ liquid electrolyte viscosity data in figure 7.6.

The Arrhenius plot exhibits strongly linear relationships for all salt concentrations. The diffusion and conductivity measurements also exhibited Arrhenius type temperature dependence

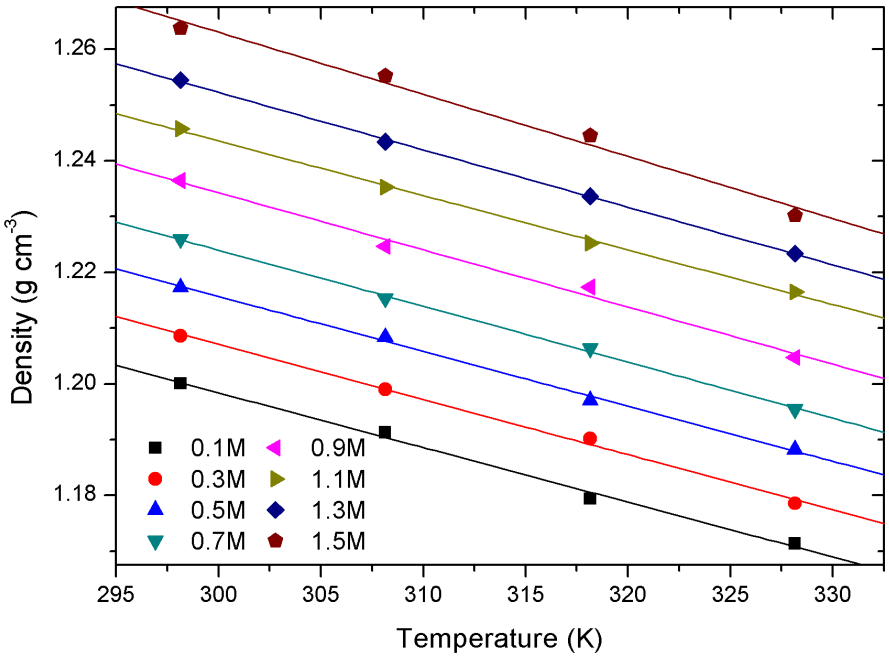

Figure 7.5: Density as a function of temperature for PC/$LiBF_4$ liquid electrolytes.

Salt Conc. (M)	Viscosity (mPa s)								
	293	298	303	308	313	318	323	328	333
0.1	—	2.91	2.54	2.30	2.09	1.92	1.78	1.65	1.52
0.2	—	3.03	2.74	2.49	2.26	2.08	1.91	1.75	1.67
0.3	—	3.31	3.04	2.68	2.46	2.24	2.03	1.88	1.75
0.4	4.19	3.68	3.35	2.95	2.73	2.48	2.24	2.05	1.91
0.5	4.53	4.03	3.64	3.18	2.90	2.65	2.37	2.19	2.03
0.6	4.95	4.44	3.96	3.48	3.19	2.84	2.62	2.38	2.18
0.7	5.56	4.89	4.36	3.80	3.47	3.13	2.79	2.54	2.35
0.8	—	5.44	4.93	4.29	3.87	3.46	3.10	2.83	2.57
0.9	—	6.17	5.53	4.74	4.25	3.86	3.47	3.10	2.84
1.0	—	7.39	6.31	5.42	4.88	4.38	3.87	3.52	3.25
1.1	8.46	7.67	6.89	6.01	5.22	4.58	4.16	3.72	3.38
1.2	9.72	8.66	7.70	6.72	5.85	5.09	4.61	4.12	3.73
1.3	10.96	9.63	8.45	7.34	6.35	5.59	5.03	4.46	4.03
1.4	12.42	10.97	9.53	8.18	7.10	6.22	5.58	4.93	4.43
1.5	14.47	12.55	10.83	9.36	7.97	7.07	6.24	5.64	5.10

Table 7.6: Viscosity for PC/$LiBF_4$ liquid electrolytes in the temperature range 293-333 K.

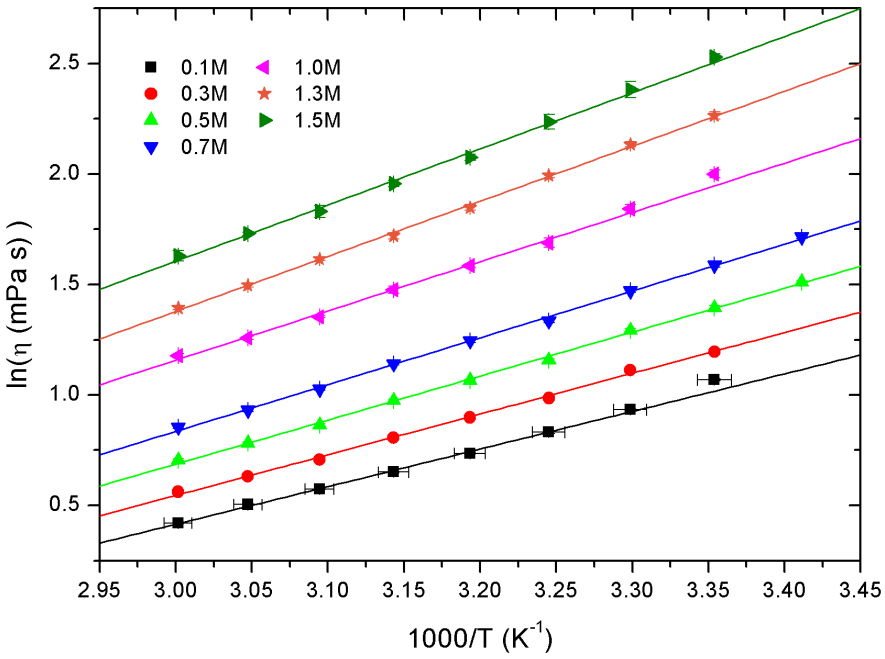

Figure 7.6: Viscosity Arrhenius plot for PC/$LiBF_4$ liquid electrolytes with linear fits applied to the data.

in the temperature range of the viscosity measurements. However the conductivity was also shown to exhibit VTF type temperature dependence at lower temperatures. It was therefore reasonable to assume that the viscosity would also exhibit VTF temperature dependence if measurements at lower temperatures were analysed. Since the viscosity exhibited Arrhenius temperature dependence equation 7.25 could be fitted to the data. The Arrhenius parameters, activation energy (E_η) and the viscosity at infinite temperature (η_∞) were determined from the linear fits of the Arrhenius plots. The fitting parameters are displayed in table 7.7 for PC/$LiBF_4$ liquid electrolytes.

The activation energy was observed to increase with increasing salt concentration. This was attributed to the increase in viscosity resulting in the molecules requiring more energy to translate through the solution. This trend was also observed for the diffusion and conductivity for the same reason. The value of η_∞ represented the viscosity at infinite temperature, in table 7.7 this value was observed to decrease with increasing salt concentration. This result was reasonable as the maximum viscosity would likely decrease as the salt concentration increased as this was the same trend observed for the viscosity measurements. It should be noted that the values of viscosity in table 7.6 are in units of mPa s and the units of the η_∞ were displayed in μPa s and were three orders of magnitude smaller than the viscosity values measured. It was possible to compare the activation energies of the diffusion constants measured in Chapter 4 with the activation energy of viscosity displayed in this chapter. It would be reasonable to assume that the activation energies of diffusion and viscosity should be similar as they both correspond to translational motion. However the diffusion is the motion of the ions in solution and the viscosity measurements are of the bulk motion of the solution.

Salt Conc. (M)	E_η (kJ mol^{-1})	η_∞ (μPa s)
0.1	14.9	7.0
0.2	14.4	9.1
0.3	15.3	6.9
0.4	15.7	6.6
0.5	16.5	5.1
0.6	16.8	5.0
0.7	17.6	4.0
0.8	17.9	4.0
0.9	18.4	3.6
1.0	19.3	3.0
1.1	19.8	2.7
1.2	20.3	2.4
1.3	20.8	2.2
1.4	21.5	1.8
1.5	21.5	2.1

Table 7.7: Viscosity Arrhenius fitting parameters activation energy (E_η) and the viscosity at infinite temperature (η_∞) for PC/$LiBF_4$ liquid electrolytes.

Taking the low salt concentration example (0.3M) the activation values were 16.9 kJ mol^{-1}, 19.4 kJ mol^{-1} and 17.8 kJ mol^{-1} for the diffusion of hydrogen, lithium and fluorine species respectively compared to the activation of viscosity which was 15.3 kJ mol^{-1}. Therefore it can be noted that, although the diffusion activation energies were always larger than the viscosity activation energies, the two are comparable. This difference was attributed to the fact that the diffusion concerns the motion on a microscopic scale whereas the viscosity is a macroscopic measurements. It can be observed from these results that the viscosity and hydrogen diffusion activation energies were very similar. Since the hydrogen measurements corresponded to the solvent molecules this result was intuitive as the solutions consisted of a vast majority of solvent. The activation energies of a PC/$LiBF_4$ (1.0M) were 19.9 kJ mol^{-1}, 21.9 kJ mol^{-1} and 22.3 kJ mol^{-1} for the hydrogen, lithium and fluorine nuclei, respectively, with the viscosity energy determined as 19.3 kJ mol^{-1}. This result was very similar to the low concentration example with the hydrogen diffusion and viscosity being similar with the lithium and fluorine activation energies being noticeably higher. This result was again seen for the high salt concentration measurements (1.3M) which gave values of 20.6 kJ mol^{-1}, 23.6 kJ mol^{-1} and 22.2 kJ mol^{-1} for the hydrogen, lithium and fluorine, respectively, and the viscosity energy as 20.8 kJ mol^{-1}. With these measurements it was observed that in this case the hydrogen activation energies, the diffusion and viscosity were the same within the error (around 0.3 kJ mol^{-1}).

7.3.2 Salt Concentration Dependence

The salt concentration dependence of viscosity is not fully understood and commonly different empirical equations have been used to describe different electrolyte systems. The original em-

pirical equations used were by Falkenhagen-Onsager-Fuoss [130; 131] and Debye-Huckel-Onsager [132] predicted a square root concentration dependent in the form of;

$$\frac{\eta}{\eta_0} = 1 + A\sqrt{c} \tag{7.27}$$

where η and η_0 are the viscosities of the sample and pure solvent, respectively, and where c is the concentration of salt. The fitting parameter A is related to the interactions and mobilities of solute ions and can be calculated. However equation 7.27 was found to be valid only for very dilute electrolytes (c <0.05M), therefore this equation did not fit the data well as concentrations between 0.0M and 1.5M were used.

Jones and Dole [133] proposed an empirical model for liquid electrolytes which could be used for higher salt concentrations. This was achieved by adding another term to equation 7.27 in the form;

$$\frac{\eta}{\eta_0} = 1 + A\sqrt{c} + Bc \tag{7.28}$$

where A and B are fitting parameters where A has the same meaning as in equation 7.27 and B corresponds to the interactions between the solvent and ions. Equation 7.28 was only valid for salt concentrations c <0.1M [134]. The A parameter is a constant which is always positive by definition, however the B value can be positive or negative depending if the salt impedes or enhances the mobility [135; 136].

For electrolytes at higher salt concentrations extra terms at higher orders of magnitude were introduced to accommodate the concentration range used here. Jones and Talley [137] and Kaminsky [138], among others, introduced a quadratic term to equation 7.28 in the form;

$$\frac{\eta}{\eta_0} = 1 + A\sqrt{c} + Bc + Dc^2 \tag{7.29}$$

where D is another parameter, where the Dc^2 term includes all solute-solvent and solute-solute interactions that were previously unaccounted for in equations 7.27 and 7.28. However the concentration range for this equation is c <0.2M, therefore this is again not sufficient for the data measured here and more terms must be added. It has been shown for aqueous solutions containing water with LiCl that the system was better described by adding a further term to equation 7.29[136] in the form;

$$\frac{\eta}{\eta_0} = 1 + A\sqrt{c} + Bc + Dc^2 + Fc^{\frac{5}{2}} \tag{7.30}$$

where F is another fitting parameter.

A modified version of the Angell equation [139] has been used by Afanas'ev *et al* [140] for Et_4NBF_4 in propylene carbonate of the form;

$$\eta = \eta_0 exp\left[\left(\frac{C_0^2}{K'}\frac{1}{c} - \frac{C_0}{K'}\right)\right] \tag{7.31}$$

where K' is an arbitrary fitting parameter and C_0 is the hypothetical concentration at which the glass transition occurs in the system at the current temperature [140].

Another approach used in a recent publication on liquid electrolytes containing $LiClO_4$ and $NaClO_4$ in propylene carbonate and GBL[127] which showed that equation 7.29 was not sufficient to fit the data as the salt concentrations used were in excess of 1.5M. Therefore they proposed

that instead of adding more terms to equation 7.29, to change the Dc^2 term to Dc^3. They also suggested that the use of the $A\sqrt{c}$ term was redundant as it only explains the first 0.05M dependence, resulting in equation 7.29 being written as;

$$\frac{\eta}{\eta_0} = 1 + B'c + D'c^n \tag{7.32}$$

where B' and D' are fitting constants that which are different to B and D in equation 7.29 and n is the order of the polynomial. It was observed for the system mentioned above[127] that $n = 3$ was needed to fit the data well. Therefore this equation was easily rearranged to;

$$\frac{\eta_r - 1}{c} = B' + D'c^{n-1} \tag{7.33}$$

where η_r is the ratio of the sample and pure solvent viscosities. Therefore plots of $(\eta_r - 1)/c$ against c^{n-1} should produce a straight line if the equation is sufficient to fit the data here. The gradient being D' and the intercept of the straight line being B'. Figure 7.7 shows the fitting of equation 7.33 with $n = 2$ and $n = 3$ for the PC/$LiBF_4$ liquid electrolytes at 298K. The fits have both been shown in figure 7.7, this was achieved by plotting c on the x-axis for $n = 2$ and c^2 for $n = 3$. It can be readily observed from figure 7.7 that the $n = 2$ fit does not display a linear relationship and therefore is insufficient to explain the data. The $n = 3$ case does however yield a much more linear relationship suggesting that it could be used to fit the data here. The fitting parameters obtained from figure 7.7 were (1.01±0.01) M^{-1} and (0.71±0.01) M^{-3} for the B' and D' values respectively. The values for the B' and D' for $LiClO_4$ in PC were 1.077 M^{-1} and 1.293 M^{-3} respectively at 298 K[127]. There are also many other empirical fits to salt concentration dependence of the viscosity data of liquid electrolytes including equations by Vand, Afzal, Othmer, Kestin, Klugman, Feldenkamp and Einstein, a summary of which is in references [141] and [142].

In Chapter 4 it was shown that the diffusion constants with salt concentration could be described by equation 4.9 which had the form;

$$D(c) = D_0 exp\left[\frac{-c}{A_D}\right] \tag{7.34}$$

where D_0 is the diffusion for infinitely dilute electrolytes and A_D is a fitting constant. It was shown that all three nuclei measured fit well to this equation which is a simple exponential. Since $D \propto \eta$ then it might be the case that the viscosity can also be described by an equation of this form. Therefore it was proposed that the viscosity should be fitted with an equation of the form;

$$\eta(C) = \eta_0 exp\left[\frac{c}{A_\eta}\right] \tag{7.35}$$

where η_0 is the viscosity of the pure solvent and A_η is a fitting parameter. Equation 7.35 can be rearranged in the form;

$$ln(\eta) = ln(\eta_0) + \frac{c}{A_\eta} \tag{7.36}$$

therefore if $ln(\eta)$ is plotted against the salt concentration c then the data should exhibit a linear relationship if this equation is valid with gradient $\frac{1}{A_\eta}$ and intercept $ln(\eta_0)$.

Figure 7.8 shows the fitting of equation 7.36 to the viscosity data as a function of salt concentration for the PC/$LiBF_4$ liquid electrolytes. It can be seen that the relationship was

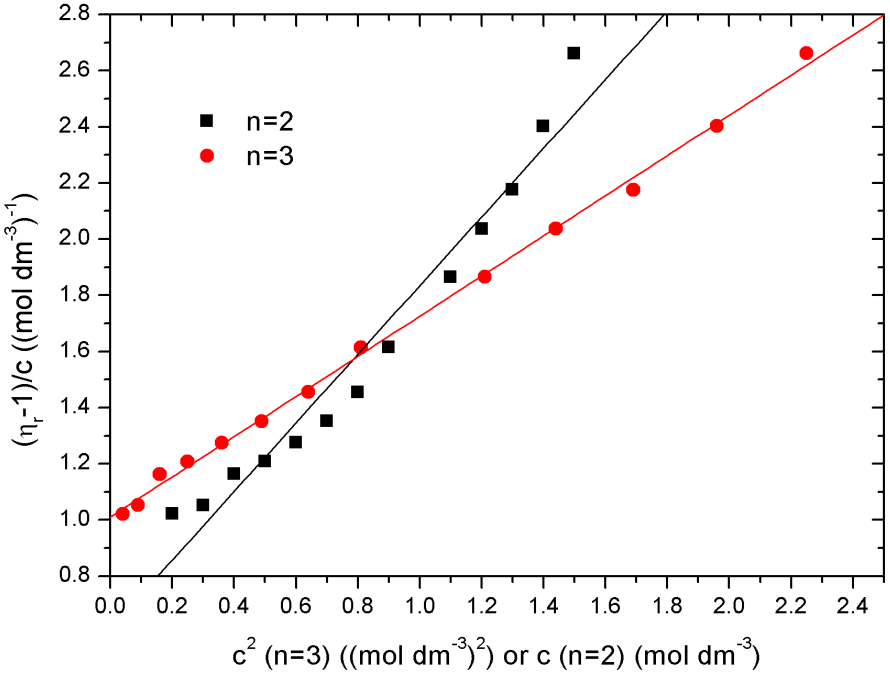

Figure 7.7: Viscosity salt concentration fitting of $(\eta_r - 1)/c$ against c $(n = 2)$ or c^2 $(n = 3)$ for $PC/LiBF_4$ liquid electrolytes at 298 K.

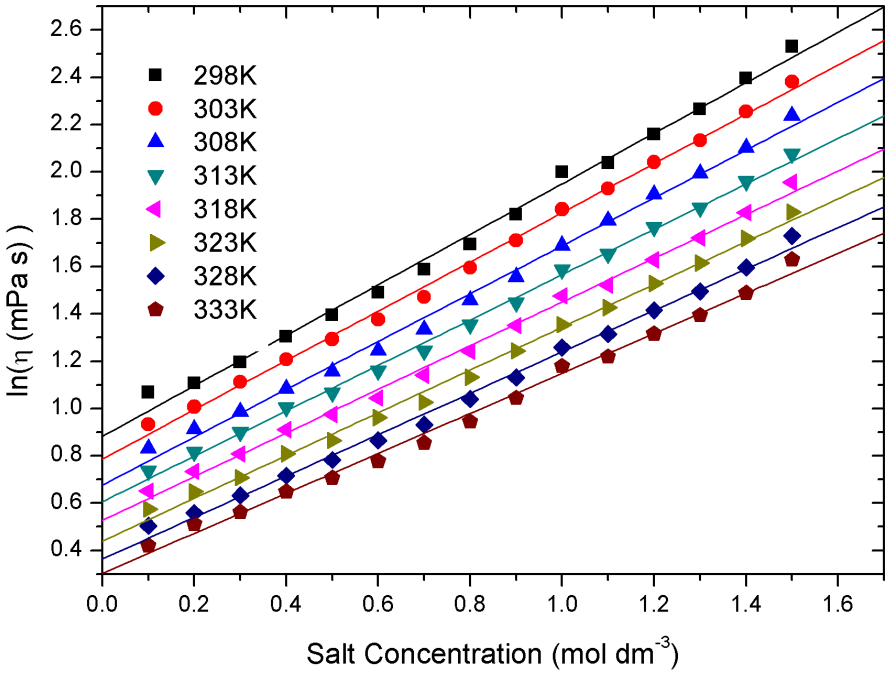

Figure 7.8: Exponential viscosity fitting of $ln\,(\eta)$ against the salt concentration for $PC/LiBF_4$ liquid electrolytes.

		η_0 ($\pm$0.05 mPa s)	
Temperature (K)	A_η (M)	Extrapolated	Measured
298	0.94	2.42	2.51
303	0.96	2.20	2.28
308	0.99	1.97	2.08
313	1.04	1.83	1.91
318	1.08	1.69	1.75
323	1.11	1.55	1.62
328	1.14	1.44	1.50
333	1.18	1.35	1.40

Table 7.8: Viscosity salt concentration fitting parameters A_η and viscosity of pure PC (η_0) for PC/$LiBF_4$ liquid electrolytes. Both extrapolated η_0 values and those measured by Barthel *et al* are included [93].

very linear and the fits were significantly better than the fitting of the cubic polynomial in figure 7.7. Equation 7.35 was chosen to fit the viscosity as a function of salt concentration. The fitting parameters A_η and η_0 are displayed in table 7.8, and the measured values of η_0 by Barthel *et al* [93] which were used for calibration are also included. It was noted that the extrapolated η_0 values from the fitting procedure were similar to the actual measured values of pure PC. For example, at 298 K the values were (2.42$\pm$0.05) mPa s and 2.51 mPa s for the extrapolated and measured values, respectively. Therefore the measured value was within two time the error and 4% away from the measured value. The errors on the values of parameters of the fitting process were determined from the deviance from the fit and were found to be $\pm$0.05 mPa s for the η_0 values and therefore for all values of the extrapolated η_0 were within at least twice the error. This highlights the validity of the fit as it was able to produce the viscosity of the pure solvent from a free parameter fitting procedure. The values of A_η were observed to increase with temperature from (0.94$\pm$0.02) M at 298 K upto (1.18$\pm$0.02) M at 333 K. The diffusion salt concentration dependence shown in Chapter 4 showed that the parameter A_D also increased with temperature, which was attributed to the decrease in viscosity with temperature. The physical implication of the parameter A_η increasing with temperature, was at high temperatures each increase in salt concentration raises the viscosity by less. This is intuitive since at higher temperatures the viscosity is lower and therefore the increasing salt concentration would have a lesser effect of the viscosity.

Figure 7.9 shows the exponential fitting parameters of the salt concentration dependence of the viscosity (A_η) and diffusion (A_D) for the PC/$LiBF_4$ liquid electrolytes. The three different nuclei diffusion and viscosity data showed an increase with temperature. If the diffusion decrease with increasing salt concentration was solely due to an increase in viscosity then one would expect to have $A_D = A_\eta$, however this was not the case which is highlighted in figure 7.9. If $A_D < A_\eta$, this suggested that the decrease of diffusion with salt concentration is more significant than from viscosity alone. Since $D \propto \frac{T}{\eta a}$ (a is the ionic radius) and the temperature for each value was constant, the only other thing affecting the diffusion constant would be the ionic radius of the molecules. Therefore if $A_D < A_\eta$ then it was assumed that the ionic radius of the molecule

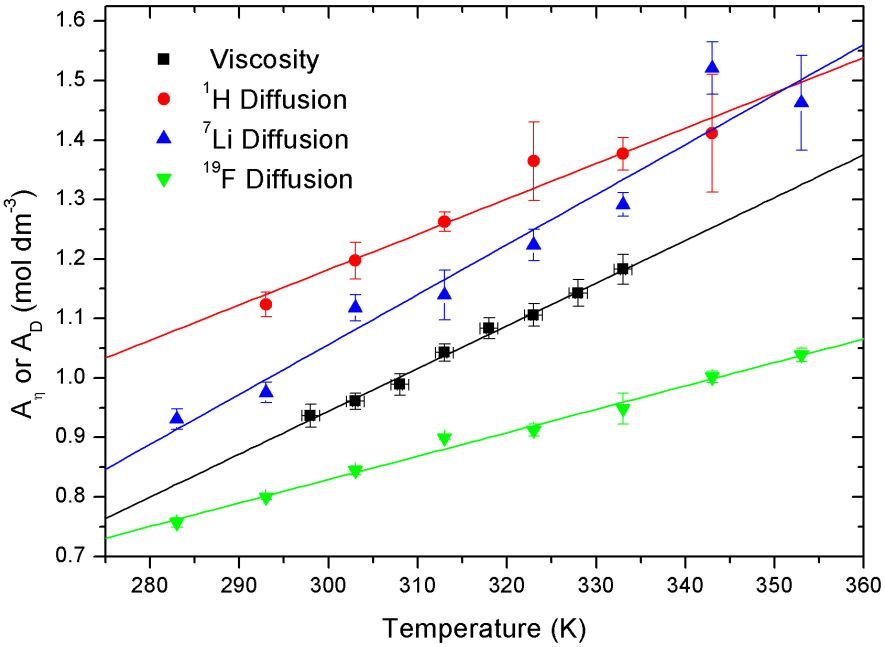

Figure 7.9: Salt concentration viscosity (A_η) and diffusion (A_D) fitting parameters for PC/$LiBF_4$ liquid electrolytes as a function of temperature.

in question was increasing, therefore causing a higher effective viscosity and reducing A_D. The inverse can be concluded if $A_D > A_\eta$, then it was assumed the ionic radii were decreasing. Figure 7.9 shows the values of A_D for all nuclei and the A_η values as a function of temperature. It can be observed that the lithium and hydrogen A_D parameters are greater than the A_η parameter and therefore suggests that the ionic radius decreased with salt concentration, whereas the fluorine A_D was less than A_η and was assumed to increase with salt concentration.

Since all of the parameters in figure 7.9 increased linearly with temperature it was possible to determine the gradient easily. The gradient of the viscosity parameter A_η was found to be (7.2±0.2) mM K^{-1} and the diffusion gradients were (5.9±0.7) mM K^{-1}, (8.4±0.8) mM K^{-1} and (3.9±0.2) mM K^{-1} for the hydrogen, lithium and fluorine, respectively. It was assumed that if the gradient of A_D was lower than the gradient of A_η then the radius was decreasing with temperature and vice versa. The hydrogen and fluorine gradients were lower than the viscosity gradient, suggesting that the solvent molecules and anion radii increased with increasing temperature. Whereas the lithium gradient was greater than the viscosity gradient, suggesting that the lithium cations ionic radii were decreasing with increasing temperature. The fluorine radii seemed to change most significantly of all nuclei. It is possible to directly obtain an estimation of the ionic radius using the Stokes-Einstein equation.

7.4 Ionic Radius

The ionic radius can be determined using the Stokes-Einstein equation which relates the translational diffusion to the bulk viscosity of the system. The mobility (u) of a charged ion in solution

is inversely related to the frictional force F_f, the mobility can therefore be stated to be;

$$u = \frac{ze}{F_f} \tag{7.37}$$

where z is the number of charges of charge e and F_f is some frictional force of a molecule in solution. If we assume that the molecules translating through the solution are spherical then the frictional force can be taken as Stoke's law which is defined as;

$$F_f = 6\pi\eta a\nu \tag{7.38}$$

where η is the viscosity of the medium, ν is the velocity and a is the hydrodynamic radius of the spherical molecules in solution. The actual Stokes' law contains two terms which give equation 7.38 of the form;

$$F_f = 4\pi\eta a\nu_\infty + 2\pi\eta a\nu_\infty \tag{7.39}$$

where the first term is the friction drag acting tangentially to the translating sphere and the second term describes the drag normal to the molecule[143]. If the ions had a shape much different from a hard sphere then the second term is greatly reduced. Therefore it was suggested that there be a term which corrects for any discrepancy of the geometry of the ions. Equations 7.37 and 7.38 can be combined to give the mobility in the form;

$$u = \frac{ze}{6\pi\eta a} \tag{7.40}$$

now by substituting equation 7.40 into the Einstein relation (equation 7.11) for the mobility and rearranged for diffusion yields;

$$D = \frac{RT}{6\pi\eta a N_A} \tag{7.41}$$

where $\frac{R}{N_A} = k_B$ the Boltzmann constant and therefore equation 7.41 becomes;

$$D = \frac{k_B T}{6\pi\eta a} \tag{7.42}$$

this is known as the Stokes-Einstein equation and expresses the translational diffusion in terms of the temperature, viscosity and hydrodynamic radius.

The calculated PC molecular radii using ^{1}H NMR are displayed in table 7.9 using the Stokes-Einstein relationship (equation 7.42) using the viscosity measured by Barthel *et al* [93] and the measured NMR PFG hydrogen diffusion. The ionic radii here are assumed to be unaffected by temperature as in the pure PC sample the only constituent are single PC molecules. The use of equation 7.42 requires several assumptions, firstly that the PC molecules are perfect hard spheres and also that the boundary between the particle and fluid is non-slippy otherwise the second term ($2\pi\eta a\nu_\infty$) in equation 7.39 disappears [83]. It can be seen that temperatures in the range of 293-323 K were practically the same, with the only measurement that varies is the 333 K value. This has been attributed to a slightly higher effective diffusion due to convection caused by a temperature gradient in the sample, which was only seen in low concentrations at high temperatures. The radius of a PC molecule was determined elsewhere using molecular mechanics (MM2) calculations as 2.76 Å[83]. The average value of the ionic radii expressed in table 7.9 was (1.53±0.04) Åwhich was significantly lower than the radii measured elsewhere.

Temp. (K)	η (mPa s)	D(^{1}H) (10^{-10} m^2 s^{-1})	Radius (Å)	ξ
293	2.79	4.96	1.55	0.56
303	2.28	6.18	1.57	0.57
313	1.91	7.73	1.56	0.56
323	1.62	9.23	1.58	0.57
333	1.40	12.7	1.38	0.50

Table 7.9: Viscosity, hydrogen (^{1}H) diffusion, calculated ionic radius and micro-viscosity factors for pure PC. Viscosity measured by Barthel *et al* [93].

This discrepancy was attributed to a deviance from a hard sphere model for the PC molecule. By taking a ratio of the measured value and the value calculated elsewhere, a correction factor can be obtained, which had the value of (0.55±0.01). This factor was used to correct the PC molecules deviation from the hard sphere model, including considerations for geometry and boundary conditions. The previously measured value of the radius of PC was determined using molecular mechanics calculations, which was also used to determine the size of the x, y and z axis independently, labeled a, b and c, respectively. The authors suggested that if there was a difference between the a, b and c then the molecule was not a sphere and the best way to determine the deviance was to take the ratio c/a. They found that a =0.781 and c =0.430 which yielded the value c/a =0.55. This coincides perfectly with the constant that was determined in this thesis by taking the ratio of the determined radius and the one calculated from MM2 calculations [83]. This result suggests that the PC molecules deviate quite significantly from the hard sphere model. A micro-viscosity factor of (ξ =0.56) was also found for an electrolyte system containing tetraglyme (TG) and lithium triflate ($LiCF_3SO_3$) [77]. It was also determined from MM2 calculations that the same factor for the BF_4^- ion was c/a =0.89 and c/a =0.92 from crystallographic data and MM2 calculations respectively [83]. Therefore the anion was much closer to the hard sphere model than the PC molecules.

This correction factor can be incorporated into Equation 7.42, which becomes;

$$D = \frac{k_B T}{c_s \pi \eta a} \tag{7.43}$$

where c_s (6ξ) is the correction factor which deals with the change in geometry of the ions and molecules in solution and any deviation from the hard sphere model. This correction factor (c_s) will be set as 3.3, 5.4 and 5.7 for the hydrogen, fluorine and lithium measurements, respectively. A factor of 5.7 for lithium has been used as one could not be determined so easily and therefore the assumption has been made that the lithium ions were well described by the hard sphere model [83]. The ionic radii for the molecules containing hydrogen nuclei are displayed in table 7.10 for the liquid electrolytes at various salt concentration and temperatures. The radius of the PC molecules were observed to exhibit a slight increase with temperature and a decrease with salt concentration. The average radius over all measurements for the PC molecule was determined to be (2.60±0.04) Å. This was very similar to the measured PC radius of 2.76 :AA elsewhere [83]. It is known that the PC molecules would likely solvate the lithium ions and therefore one might expect to observe a radius which was larger than the value obtained. However it was calculated in Chapter 3 that for a PC/$LiBF_4$ liquid electrolyte the ratio of

	Ionic Radius (Å)						
Temperature (K)	0.0M	0.3M	0.5M	0.7M	1.0M	1.3M	1.5M
293	2.82	2.69	2.69	2.62	2.19	2.41	2.18
303	2.86	2.68	2.70	2.65	2.29	2.34	2.14
313	2.83	2.74	2.75	2.68	2.41	2.40	2.29
323	2.88	2.82	2.88	2.86	2.48	2.54	2.37
333	2.51	2.85	2.89	2.82	2.57	2.61	2.40

Table 7.10: Calculated ionic radius using Stokes-Einstein equation for molecules containing ^{1}H nuclei for PC/$LiBF_4$ liquid electrolytes.

	Ionic Radius (Å)					
Temperature (K)	0.3M	0.5M	0.7M	1.0M	1.3M	1.5M
293	3.68	3.64	3.57	3.04	3.27	3.08
303	3.59	3.49	3.46	3.12	3.10	3.01
313	3.58	3.55	3.48	3.17	3.19	3.12
323	3.64	3.63	3.57	3.27	3.23	3.16
333	3.62	3.61	3.58	3.24	3.30	3.08

Table 7.11: Calculated ^{7}Li ionic radii using Stokes-Einstein equation for PC/$LiBF_4$ liquid electrolytes.

number of PC molecules to lithium ions was around 11. Therefore even if every lithium ion was solvated by four PC molecules (the maximum number of PC molecules around one lithium ion) there would still be around 64% of PC molecules translating unsolvated. It might expected that the average radius would be comparable to the radius of a single PC molecule, which was the case for here. The values displayed in figure 7.10 are not strictly the absolute values of the ionic radius as there were still assumptions made, however the trends with salt concentration and temperature show physical significance.

The calculated ionic radii of the lithium species are displayed in table 7.11. The ionic radius of a single lithium ion has been determined elsewhere to be 0.76 Å[83; 144] and 0.78 Å[104]. The ionic radii calculated in table 7.11 are significantly higher than the radius of a single lithium ion and therefore has to be solvated. It has been shown elsewhere that the maximum number of PC molecules that can solvate a single lithium ion was around four at high salt concentrations [82; 103]. The radius of $LiPC_4^+$ has been found elsewhere to be around 3.7 Å[100]. The maximum ionic radius calculated in table 7.11 was found to be (3.49±0.03) Å. This value was smaller than the average radius of the lithium ion solvated by four PC molecules, however as observed for the ionic association some of the lithium ions are associated with the anion (BF_4^-). The average radius would therefore have to be somewhere between the radius of a lithium ion solvated by four PC molecules and that of the lithium associated with the BF_4^-. The radius of the BF_4^- molecule has been measured elsewhere to be 2.29 Å[83]. All values of the ionic radius of the lithium ions were between the radius of the fully solvated lithium ion and the neutral pair of $LiBF_4$.

	Ionic Radius (Å)					
Temperature (K)	0.3M	0.5M	0.7M	1.0M	1.3M	1.5M
293	2.22	2.39	2.51	2.32	2.65	2.61
303	2.26	2.38	2.52	2.44	2.63	2.61
313	2.30	2.48	2.59	2.52	2.75	2.74
323	2.30	2.55	2.65	2.66	2.83	2.80
333	2.21	2.55	2.45	2.56	2.81	2.73

Table 7.12: Calculated ^{19}F ionic radii using Stokes-Einstein equation for PC/$LiBF_4$ liquid electrolytes.

The ionic radius of the fluorinated molecules are displayed in table 7.12 for the PC/$LiBF_4$ liquid electrolytes. In the PC/$LiBF_4$ liquid electrolytes the fluorine ions are only found in the BF_4^- anion. As previously stated the ionic radius of the BF_4^- anion was found elsewhere to be 2.29 Å[83]; it has also been measured as 2.32 Å[145] and 2.78 Å[146]. All of the ionic radii measured here using the fluorine nuclei were found to be between 2.22 Åand 2.80 Å. This result suggests that anion was not solvated by the PC molecules and that the only structures were either anion dissociated or associated with the lithium ion, where the radius of the $LiBF_4$ would be larger than the BF_4^- anion.

It was observed that the ionic radius of the species containing lithium ions decreased with increasing salt concentration. This has been attributed to the increase in ionic association observed in figure 7.4, which showed that there was a non-linear increase in the ionic association with increasing salt concentration. If there are more $LiBF_4$ neutral pairs contained within the electrolyte at higher salt concentration then it stands that the lithium ions that associate with the anions would lose their solvation shell, therefore the lithium radii would be observed to decrease with increasing salt concentration. The reverse could be stated about the fluorine nuclei. The addition of the lithium ions onto the BF_4^- ion would have the effect of increasing the effective radius of the fluorine measurements. This was observed in figure 7.10 which shows that there is a roughly linear decrease in the lithium effective radii and a linear increase in the fluorine radii. This result was consistent with the theory that as the ionic association increases the anion increases in size due to the addition of the lithium ion and lithium ions lose their solvation shell reducing the lithium effective radii.

The lithium and fluorine ionic radii were fitted with linear equations in figure 7.10. The gradients were found to be (-0.51±0.06) m M^{-1} and (0.27±0.06) m M^{-1} for the lithium and fluorine radii, respectively. This result suggests that the lithium radii decrease more significantly than the fluorine radii. This result was consistent with the hypothesis that the change in radii was due to association, as the loss of the solvation shell around the lithium caused a more significant change than the BF_4^- gaining a lithium ion. The intercept values from figure 7.10 were (3.75±0.06) Å and (2.24±0.07) Å for the lithium and fluorine radii, respectively. If the change in radii for the two nuclei was purely due to ionic association between the cation and anion then at infinite dilution it would be assumed that there would be zero ionic association. The intercept values of figure 7.10 therefore refer to the radii of the solvated lithium ion and BF_4^- molecule for the lithium and fluorine measurements, respectively. The effective radius of a lithium ion solvated

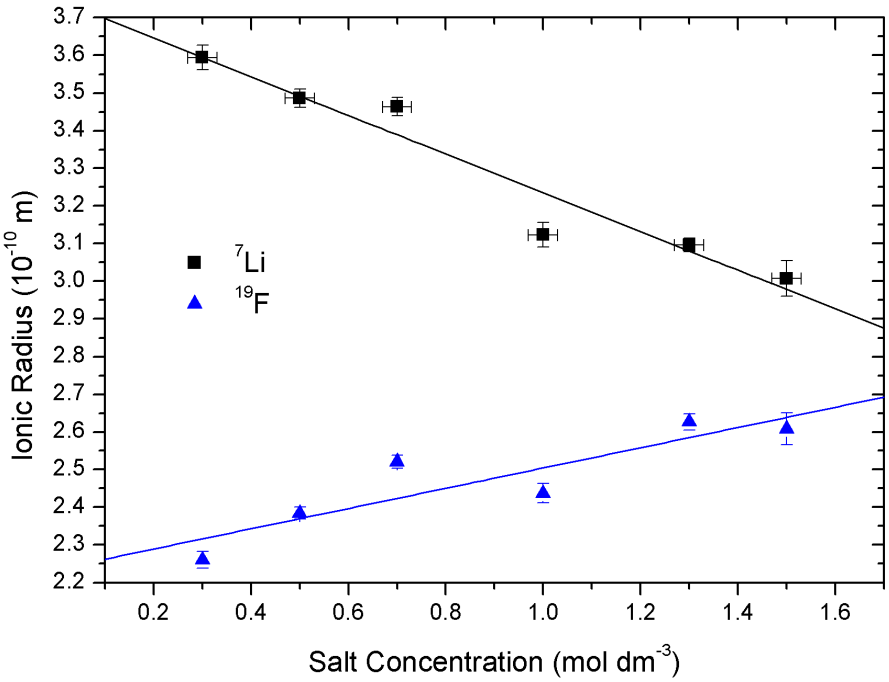

Figure 7.10: Ionic radius calculations for ^{7}Li and ^{19}F for PC/$LiBF_4$ liquid electrolytes as a function of salt concentration at 303 K.

by four PC molecules was determined elsewhere to be 3.7 Å[100], which corresponds well to the intercept, which gave (3.75±0.06) Å. It should be noted that the absolute values mentioned here are estimates, as there are a number of assumptions made in these calculations. The data therefore indicate that the maximum number of PC molecules that can solvate the lithium ion was four, however different numbers of PC molecules can solvate the lithium ion. It has been seen elsewhere that the solvation number of the PC molecule with lithium was an average value of 3.2[83]. The BF_4^- molecule was measured elsewhere as 2.29 Å[83], which was very close to the value determined here for the fluorine intercept (2.24±0.07 Å), assumed to be effective radius of the BF_4^- anion, since it was assumed there was no association at infinite dilution.

It can clearly be observed from figure 7.10 that there was a point at which the radius of the fluorine and lithium effective radii are equal, assuming that the radius will keep rising linearly. Since both radii were described by linear equations, they can be rearranged easily to find the point at which the two lines cross over;

$$C_r = \frac{I_{19F} - I_{7Li}}{g_{7Li} - g_{19F}} \tag{7.44}$$

where C_r is the concentration at which the two radii are equal, I_{19F} and I_{7Li} are the intercept values for the fluorine and lithium radii, respectively, and g_{7Li} and g_{19F} are the gradient values of the lithium and fluorine, respectively. The resulting concentration from equation 7.44 was determined as 1.94M which corresponded to a radius of (2.76±0.05) Å. This value was assumed to be the radius of the $LiBF_4$ molecule, however there was a lot assumptions in calculating this value, the most significant of which was that the ionic radii would carry on to increase linearly; however this value was considered reasonable for the radius of the $LiBF_4$ molecule.

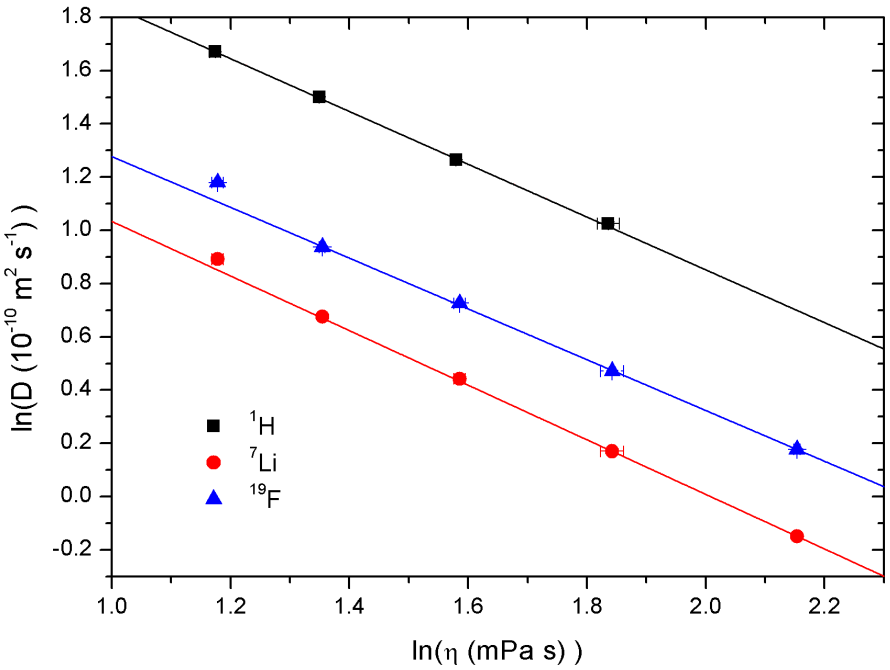

Figure 7.11: ln-ln plot of self diffusion coefficients against viscosity for all nuclei used (^{1}H, ^{7}Li and ^{19}F) for PC/$LiBF_4$(1.0M) liquid electrolytes at various temperatures. The gradients determined were -0.99, -1.03 and -0.95 for ^{1}H, ^{7}Li and ^{19}F, respectively.

There is another major assumption that has not been addressed so far which is that the diffusion corresponds to micro-diffusion whereas viscosity was a macroscopic measurement. These two were different timescales and therefore might not be applicable to compare the two values to calculate the ionic radius. It is possible to assess the validity of this effect by comparing the natural log of the diffusion and viscosity. If a plot of ln(diffusion) against ln(viscosity) is plotted then the resulting relationship should be linear with the gradient on one and since the diffusion decreases as the viscosity increases the gradient would be negative. Figure 7.11 shows a typical plot of ln(diffusion) against ln(viscosity) for the ^{1}H, ^{7}Li and ^{19}F nuclei for PC/$LiBF_4$ (1.0M) liquid electrolyte. The relationship was found to be linear for all nuclei with gradients of (-0.99±0.01), (-1.03±0.01) and (-0.95±0.01) for ^{1}H, ^{7}Li and ^{19}F, respectively, therefore suggesting that using the Stokes-Einstein equation with the micro-diffusion and macro-viscosity gives a good approximation of the ionic radius.

7.5 Solvation Number

In the previous section it was discussed that lithium exhibited an ionic radius much larger than a single lithium ion and therefore must be solvated by the PC molecules. It was also concluded that the BF_4^- anion exhibited a radius which was consistent with the single radius of the anion and therefore showed no sign of associating with the solvent molecules. It would be informative to have a quantitative measure of the number of PC molecules that were solvating each lithium ion.

	R_{Li}					
Temperature (K)	0.3M	0.5M	0.7M	1.0M	1.3M	1.5M
293	2.36	2.34	2.35	2.40	2.34	2.44
303	2.32	2.23	2.25	2.35	2.28	2.43
313	2.25	2.23	2.24	2.28	2.30	2.36
323	2.23	2.17	2.16	2.28	2.20	2.30
333	2.20	2.16	2.19	2.18	2.18	2.22
343	—	2.04	2.18	—	2.08	2.11

Table 7.13: Ratio of lithium and hydrogen diffusion ($R_{Li} = D_{solvent}/D_{ion}$) for PC/$LiBF_4$ liquid electrolytes.

7.5.1 Liquid Electrolytes

A paper by Hayamizu *et al* [99; 101; 120] has suggested that by using the Stokes-Einstein equation it was possible to obtain a semi-quantitative understanding of the solvation of the cation and anion. They stated that the Stokes-Einstein for the solvent could be written as;

$$D_{solvent} = \frac{k_B T}{c_s \pi \eta a_{solvent}} \tag{7.45}$$

where the radius $a_{solvent}$ is assumed to be the Stokes radius as opposed to the Van der Waals radius where c_s is a constant depending on the geometry. Similarly the ion diffusion can be given by;

$$D_{ion} = \frac{k_B T}{c_s \pi \eta a_{ion}} \tag{7.46}$$

where again D_{ion} and a_{ion} are the ion diffusion and Stoke's radii respectively. Hayamizu *et al* stated that taking a ratio of equation 7.45 and 7.46 can be denoted R of the form;

$$R = \frac{D_{solvent}}{D_{ion}} \propto \frac{a_{ion}}{a_{solvent}} \tag{7.47}$$

therefore by calculating the R value a semi-quantitative understanding can be obtained for the solvation of the anion and cation. The values of R_{Li} ($D_{solvent}/D_{ion}$) are displayed in table 7.13 for the PC/$LiBF_4$ liquid electrolytes.

The van der Waals radii of the lithium ion and PC molecules are 0.76 Å and 2.76 Å[83] and therefore if the diffusion constant was for a single lithium ion and PC molecule then it would be assumed that the lithium diffusion would be almost four times that of the hydrogen diffusion. However since the lithium diffusion constant was significantly lower than the hydrogen measurements it can be concluded that the lithium ions are solvated by the PC molecules. In the previous section the constant c_s was assumed to be different for the lithium and PC molecules as it has been observed previously that for lithium c_s=5.7 was used whereas the PC molecule was determined from taking the ratio of the measurements of pure PC and the van der Waals radius (2.76Å) which yielded c_s=3.3. For the calculated R_{Li} values in table 7.13, the c_s value was assumed to be constant for both the PC molecules and the solvated lithium ions. This was a reasonable assumption as the PC molecule is much larger than the lithium ion then the c_s value would most likely take a value close to that for the PC molecule (c_s=3.3). The values

	RR_{anion}					
Temperature (K)	0.3M	0.5M	0.7M	1.0M	1.3M	1.5M
293	0.99	1.07	1.16	1.27	1.33	1.44
303	1.02	1.07	1.14	1.28	1.35	1.47
313	1.01	1.09	1.16	1.26	1.38	1.44
323	0.98	1.06	1.11	1.29	1.34	1.42
333	0.94	1.06	1.05	1.20	1.30	1.37
343	—	1.03	1.07	—	1.27	1.38

Table 7.14: Ratio of ^{19}F and ^{1}H diffusion normalised by the van der Waals radii (RR_{anion}) for PC/$LiBF_4$ liquid electrolytes.

of R_{Li} in table 7.13 range from 2.08 to 2.40 depending on salt concentration and temperature. This suggests that the lithium ions are solvated by around an average of two PC molecules on the timescale of the experiment diffusion time Δ. A very similar result was observed elsewhere for PC/$LiN(SO_2CF_3)_2$ where the average R_{Li} value was found to be 2.3 [120].

So in the case of the anions it was previously assumed that the BF_4^- was not solvated by the PC molecules, therefore the c_s values would take a different value for the BF_4 anion and the PC molecules. It is therefore proposed that the ratio R_{anion} should be calculated using;

$$R_{anion} = \frac{D_{solvent} c_{s(PC)}}{D_{anion} c_{s(BF_4)}} \tag{7.48}$$

where $c_{s(PC)}$ and $c_{s(BF_4)}$ are the c_s correction factors for the PC molecule (3.3) and the anion (5.4), respectively. It was found for the PC/$LiBF_4$ (0.3M) liquid electrolyte that the R_{anion} value was (0.82 ± 0.01). The ratio of the van der Waals radii (r_{BF4}/r_{PC}) where the radii were 2.29 Å and 2.76 Å for the BF_4 anion and PC molecules, respectively, which yielded a ratio of 0.86. Therefore the ratio of van der Waals radii was practically equal to the R_{anion} value which suggests that the anion was not solvated by the PC molecules. It is considered very informative to normalise the R_{anion} values by the ratio of the van der Waals radii which is denoted as RR_{anion} [56]. The RR_{anion} values were calculated using;

$$RR_{anion} = \frac{D_{solvent} c_{s(PC)}}{D_{anion} c_{s(BF_4)}} \frac{r_{PC}}{r_{BF_4}} \tag{7.49}$$

where r_{PC} and r_{BF_4} are the van der Waals radii of the PC and BF_4^- molecules respectively. The values of RR_{anion} have been displayed in table 7.14 for the PC/$LiBF_4$ liquid electrolytes. A value of $RR_{anion} \approx 1$ suggests that the BF_4^- was not solvated by the solvent molecules.

It can be readily observed from table 7.14 that the RR_{anion} values increased with increasing salt concentration. This result could suggest that the solvent started to solvate the anion at higher salt concentration, however this is unlikely. The much more likely explanation of this increase in RR_{anion} was due to the increase of the BF_4^- due to ionic association with the lithium ions. It has been observed in a ethylene carbonate (EC)/$LiPF_6$ liquid electrolyte system that the R_{anion} was greater than the ratio of the Van der Waals radii, which was assumed to be due to an incomplete dissociation of the salt [63]. It was noted in figure 7.4 that the ionic association between the lithium ions and the BF_4^- anion increased with increasing salt concentration and

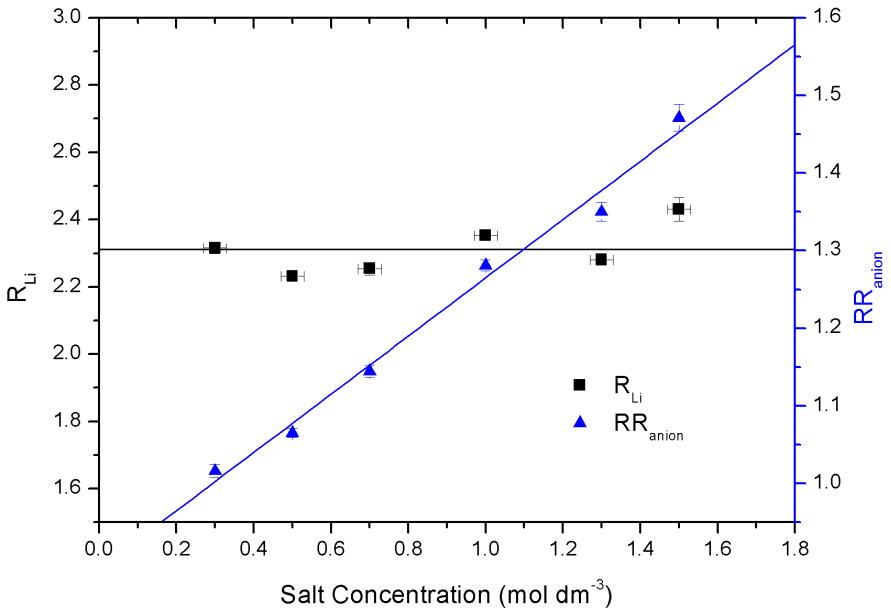

Figure 7.12: R_{Li} and RR_{anion} values as a function of salt concentration for the PC/$LiBF_4$ liquid electrolytes at 303K.

would therefore explain the increase in the RR_{anion} value here. There was not a significant change in RR_{anion} with an increase in temperature. The same salt concentration dependence was observed in a GBL/$LiBF_4$ liquid electrolyte system [56]. The salt concentration dependence of the RR_{anion} and R_{Li} are shown in figure 7.12. It can be observed that the RR_{anion} values increased linearly with salt concentration. The R_{Li} values were observed to be independent of salt concentration, which has been seen with other salt systems in PC [56; 63; 120].

7.5.2 Polymer Gel Electrolyte

It was not possible to calculate the ionic radii directly for the polymer gel electrolytes as even though the faster diffusing phase was assumed to be pure liquid electrolyte this would not likely have the same viscosity as the corresponding electrolyte sample. However it is possible to calculate R_{Li} and RR_{anion} values for the polymer gel electrolytes. It was shown in Chapter 5 that there were two diffusive species for the lithium ions and the hydrogen ions for 30% PVDF gels it was possible to calculate the R_{Li} values for both the amorphous polymer and liquid electrolyte phases. Since the fluorine only exhibited a single diffusion constant which was attributed to the liquid electrolyte phase. Therefore the RR_{anion} value could only be calculated for the liquid electrolyte phase.

The calculated R_{Li} values for the amorphous polymer and liquid phases are displayed in table 7.15 for the 30% PVDF/PC/$LiBF_4$ polymer gel electrolytes. The amorphous polymer R_{Li} values were calculated by taking a ratio of the diffusion of the amorphous phase of the hydrogen measurements with the amorphous polymer lithium phase diffusion. Likewise the liquid R_{Li} were calculated by taking a ratio of the liquid phase diffusion. Firstly considering the liquid phase R_{Li} values, it was observed that there was no clear trend with either temperature or salt

	R_{Li}							
	Amorphous Polymer				Liquid Phase			
Temperature (K)	0.3M	0.5M	0.7M	1.0M	0.3M	0.5M	0.7M	1.0M
283	3.0	3.7	2.9	—	2.81	2.89	2.40	—
293	3.3	3.3	2.5	—	2.84	2.75	2.32	—
303	2.3	2.4	3.7	2.3	1.73	2.12	2.48	1.86
313	2.7	3.8	3.9	2.4	1.96	2.57	2.63	2.09
323	2.9	4.3	3.9	3.5	2.17	2.91	2.61	2.41
333	2.8	3.9	3.3	3.0	2.07	2.68	2.37	2.27
343	2.8	4.0	—	3.1	2.17	2.81	—	2.21
353	2.7	4.1	3.2	2.8	2.14	2.80	2.32	2.11

Table 7.15: Ratio of ^{7}Li and ^{1}H diffusion constants (R_{Li}) for 30% PVDF/PC/$LiBF_4$ polymer gel electrolytes.

concentration. This result was consistent with the results for the liquid electrolyte R_{Li} in the previous section. An average value of R_{Li} was taken as (2.40±0.06) for the liquid phase of the polymer gel electrolytes. The average value of R_{Li} for the liquid electrolyte measurements in the previous section was given as (2.25±0.02). These values were similar in value suggesting that the solvation process was almost identical in the liquid electrolytes and the liquid phase of the polymer gel electrolytes.

The R_{Li} values for the polymer phase of the gels were quite scattered, which was attributed to the scattered nature of the diffusion measurements due to the fitting process of the diffusion decay curves. As with the liquid phase there was no clear trend with either temperature or salt concentration. The average R_{Li} for the amorphous polymer phase of the polymer gel electrolytes was (3.2±0.1), this value was larger than the corresponding liquid phase. A larger value of R_{Li} suggests that the lithium was now solvated by around three PC molecules. However it was also possible that there was some association of the lithium with the polymer creating a larger average effective radius of the lithium. All that can be concluded for certain is that in the lithium ions on average have an even larger radius in the amorphous polymer phase than in the corresponding liquid phase or at least a higher viscosity.

The RR_{anion} values for the 30% PVDF/PC/$LiBF_4$ polymer gel electrolyte are shown in table 7.16. Since only one phase was observed in the fluorine diffusion measurements which was attributed to the liquid phase of the gels the RR_{anion} values in table 7.16 refer to the liquid phase. A value of RR_{anion}=1 means that the radius of the fluorine measurements were equal to a single BF_4 anion. As with the R_{Li} values in table 7.15 the values of the RR_{anion} were fairly scattered and no clear trend was present with temperature. The values of RR_{anion} were observed to increase with increasing salt concentration as shown in figure 7.16. The same trend was observed in the liquid electrolyte calculations and was attributed to the increase in ionic association at higher salt concentrations as shown earlier in the chapter. This result again highlights that the liquid phase of the polymer gel electrolytes are very similar to the liquid electrolytes themselves.

	RR_{anion}			
Temperature (K)	0.3M	0.5M	0.7M	1.0M
283	1.15	1.26	1.35	—
293	1.26	1.26	1.23	—
303	0.77	0.97	1.35	1.18
313	0.84	1.13	1.41	1.11
323	0.93	1.29	1.41	1.34
333	0.98	1.31	1.42	1.55
343	1.04	1.31	—	1.56
353	1.08	1.40	1.38	1.57

Table 7.16: Ratio of ^{19}F and ^{1}H diffusion normalised by the van der Waals radii (RR_{anion}) for 30% PVDF/PC/$LiBF_4$ polymer gel electrolytes.

7.6 Conclusions

In this chapter, the NMR and conductivity data were used to gain further analysis into the dynamics of the liquid and polymer gel electrolytes. Firstly it was possible to use the NMR-PFG diffusion measurements along with the Nernst-Einstein equation to predict the ionic conductivity of the system. The calculated conductivities were observed to be significantly higher than the measured conductivity due to the absence of ion pairs. Therefore by comparing the measured and calculated conductivity a value for the degree of ionic association was determined.

The ionic association for the liquid electrolytes was observed to increase with increasing temperature. This was counter intuitive as one would expect that an increase of temperature would introduce more energy to each molecule and therefore promote dissociation. This trend has been observed for other lithium based salts in polar solvent and was attributed to the lowering of free energy of ionic pairing at elevated temperatures. The ionic association was observed to increase with increasing salt concentration and was attributed to the increase of ions reducing the average distance between each ion and therefore promoting ionic association.

The ionic association was also determined for the polymer gel electrolytes. However in the gel case the results were much harder to interpret. For the liquid case there is the simple case of either ions dissociated or ions associated creating neutral pairs which do not contribute to the conductivity. However in the gel case it has been observed that there are ions in at least three different phases and there was no indication from results whether or not the ions in the amorphous polymer and crystalline polymer phase contributed. It was assumed that indeed the amorphous polymer phase contributed to the ionic conductivity however there are other factors which could reduce the conductivity such as a relative viscosity difference between the two phases. With temperature the ionic association was observed to decrease rather than increase as in the liquid electrolyte case. This was assumed not to be an ion pairing factor but rather a relative viscosity shift between the solvated amorphous polymer and pure liquid phases.

It was noted that not only did the predicted conductivity exhibit a peak with salt concentration but that it occurred at a much higher salt concentration than the measured conductivities. Which was attributed to the ionic association as it is a detrimental factor to the conductivity,

much like the viscosity and therefore a decrease in the maximum conductivity position suggests a higher ionic association or viscosity or both.

The viscosity measurements of the PC/$LiBF_4$ liquid electrolyte have been reported in this chapter. These measurements were taken to further understand the dynamics of the system. It was observed that the viscosity increased exponentially with increasing temperature which is a characteristic feature of viscosity. The temperature dependence was observed to be Arrhenius in the temperature range studied. The activation energy was observed to increase with salt concentration. This was intuitive, as the salt concentration increased it would require more energy for the ions to translate through the solution therefore increasing the activation energy.

The salt concentration of the viscosity was much more difficult to define. There exists no exact theory to fit the viscosity of liquid electrolytes and rather empirical equations are often used. There are many different equations favoured by different research groups, some of which have been discussed here. It was found that for this system a simple exponential was the best fit to the data, in the same form the diffusion with salt concentration was analysed. From this fitting, an exponential factor A_η was determined for each temperature. This parameter was observed to increase with increasing temperature. The physical meaning of this parameter was that it determined the rate of increase in viscosity with salt concentration. Plots were made here comparing the A_η parameter with the similar diffusion parameter A_D. It was shown that for the fluorine diffusion $A_D < A_\eta$, suggesting that the diffusion was decreasing faster with salt concentration than could be defined by the viscosity and therefore an increase in the ionic radii of the fluorine was assumed. The inverse was observed for the lithium and hydrogen and therefore it was expected that the ionic radii of the two nuclei decreased with increasing salt concentration.

The ionic radius was calculated by using the Stokes-Einstein equation. It is commonly known that using the standard equation with the factor of 6 arising from Stokes law was not a good model for real system as it assumed that the molecules were perfect hard spheres. It is much more likely that the correction factor c_s would take the value of between 4 and 6 for a perfect slip or stick boundary condition, respectively. The correction factor was determined for the PC molecule empirically by using a ratio of the calculated radius using the standard factor of 6 for the pure solvent (1.55 Å) and the known value of van der Waals radii (2.76 Å). The correction factor of PC was therefore determined as 3.3, where the correction factor for BF_4^- was determined elsewhere to be 5.4 and lithium to be 5.7.

The calculated radii for the PC molecules were observed to be very similar to the van der Waals radii of 2.76 Å, which was attributed to the fact that even though the PC molecules are known to solvate the lithium ions there are still many more PC molecules than lithium ions and so an average would reveal the radius of a single PC molecule. The fluorine radii were observed to be either similar to the van der Waals radius of BF_4^- 2.29 Å or slightly above. The slight increase was attributed to ionic association with the lithium ions. The lithium ions were observed to exhibit ionic radii significantly higher than that of a single lithium ion (0.76 Å), which was attributed to a solvation shell around the lithium. It was difficult to assign the average number of PC molecules around each lithium via this method and was found easier by using a ratio of the diffusion constants.

It has been suggested in many publications by Hayamizu *et al* that it was possible to deter-

mine an approximation of the solvation number by taking a ratio of the solvent diffusion and the ion diffusion, a factor denoted R ($R = D_{solv}/D_{ion}$). In the calculation of the R_{Li} values it was assumed that since the lithium was surrounded by PC molecules that it would take on the same correction factor of c_s=3.3. This parameter was observed to be unchanged in the liquid electrolytes with salt concentration or temperature and yielded an average value of 2.3. This suggests that since the lithium ions are so small compared to the PC molecules that on the timescale of the diffusion the average solvation number of the lithium ions was 2.3, this result has been observed with many different lithium salts dissolved in PC.

With the anions it was not so simple as the PC molecules and BF_4 anions have different correction factors and therefore were accounted for in the calculation of the parameter. It was also stated that since the BF_4 (2.29 Å) had a comparable size to the PC molecules (2.76 Å) that the R_{anion} parameter must be normalised by the ratio of the van der Waals radii and denoted RR_{anion}. A value of RR_{anion}=1 would suggest that there are no PC molecules solvating the anion. The RR_{anion} values were found to be close to one at low salt concentrations and were observed to increase with salt concentration. However this increase was not significant enough to be a PC molecule solvating the anion but rather due to the increased ionic association with salt concentration.

The same parameters were determined for the polymer gel electrolytes as well. However it was only possible to calculate them for the 30% PVDF/PC/$LiBF_4$ gels as solvent diffusion was needed for both phases and only the 30% PVDF gels exhibited two phases in the hydrogen measurements. It was found by calculating R_{Li} for the liquid electrolyte phase of the gel that the value was very similar to the liquid electrolyte measurements with an average value of (2.40±0.06). In the case of the amorphous polymer phase the resulting R_{Li} was observed to be higher with an average of around (3.2±0.1). This suggests that in the amorphous polymer phase there was an effective increase in the ionic radius compared to the solvent molecules in the same phase. This was assumed to be on average a larger PC solvation shell, however could be an association of the lithium with the amorphous polymer.

The RR_{anion} values were determined using the liquid electrolyte phase hydrogen diffusion constant and the single diffusion constant determined for the fluorine measurements. The values of RR_{anion} were observed to be only slightly higher than in the liquid electrolyte case and was again assumed to be association at higher concentrations. This was different to the calculated ionic association in the first section of this chapter which showed that the ionic association was not salt concentration dependent. This was attributed to the ionic association not fully describing the system for the polymer gel electrolytes.

Chapter 8

Conclusions

This thesis has been concerned with the dynamics of liquid electrolytes and the polymer gel electrolytes on which they are based. Several different practical experimental techniques were employed to probe the dynamics of the systems. The most significant technique used in this research was nuclear magnetic resonance (NMR). Other techniques measured involved ionic conductivity via impedance spectroscopy and viscosity measurements of the liquid electrolytes. The liquid electrolytes studied in this work comprised lithium tetrafluoroborate ($LiBF_4$) in the organic solvent propylene carbonate (PC). The polymer added to these liquids to produce polymer gel electrolytes was poly(vinylidene) fluoride (PVDF). The choice of constituents is important to enhance the conductivity of the final gels. Since ionic dissociation is a desired property of these gels, a solvent with a high dielectric constant is preferred. Lithium based salts are commonly used due to the large charge density. The anion choice is also important as a large anion aids dissociation, these are commonly fluorinated anions. PVDF is a desirable polymer as it miscible with the chosen solvent and salt, and is a non chemically cross-linked semi-crystalline polymer which allows the creation of thermo-reversible gels [85]. The thermo-reversible nature is important for processing using a extrusion lamination system developed at the University of Leeds which allows commercial production of batteries based on these materials [31; 32]. However, in the actual batteries PC cannot be solely used as the solvent as it causes a passivation layer on the anode, which led to loss of lithium ions to the anode.

8.1 Liquid NMR

In Chapter 4 the results for the several NMR based techniques were reported and discussed for the liquid electrolytes. Three nuclei were used; hydrogen (^{1}H), lithium (^{7}Li) and fluorine (^{19}F) which were used to observe the PC molecules, cation and fluorinated BF_4 anion, respectively. The longitudinal and transverse relaxation times were measured using the 50MHz Maran bench top NMR spectrometer using the resonant frequency for hydrogen (^{1}H). The values of the two relaxation times were observed to be very similar ($T_1 \approx T_2$), which is characteristic of molecules that have very low correlation times, i.e. molecules in non-viscous liquids. The 500 MHz Bruker Avance Ultrashield NMR spectrometer was also used to measure the hydrogen longitudinal relaxation. The high field machine allowed distinction between the different hydrogen sites of

the PC molecules; each peak of the NMR spectrum exhibited different relaxation times. The different relaxation times were attributed to different internuclear distances of the hydrogen sites of the PC molecules. An alternative explanation is that there was an anisotropic molecular reorientation, i.e. as the molecule 'tumbled' each site experienced a different interaction. All relaxation times exhibited Arrhenius type temperature dependence in the temperature range 293-353 K. VTF type dependence was observed at temperatures which converged to the glass transition temperature of the system.

The diffusion constants were measured using pulsed-field gradient NMR (PFG-NMR). All diffusion constants exhibited Arrhenius type temperature dependence. The order of diffusion was $D_H > D_F > D_{Li}$, since all constituents experienced the same bulk viscosity the order of ionic radii was assumed to be, $a_{Li} > a_F > a_H$. Because the size of a single lithium ion is significantly smaller than the other two species, it was clear that the lithium ions must have a large solvation shell. The activation energies of the three nuclei support this conclusion. The diffusion for each nuclei decreased with increasing salt concentration, this dependence was fitted with a simple exponential. The three nuclei yielded different values for the decay constant, suggesting that the viscosity increase was not the only factor effecting the diffusion.

By comparing the activation energies of the diffusion and the longitudinal relaxation, the translational and rotational contributions of the relaxation times were determined. Three different methods were employed which were from a similar strategy from previous work carried out at the University of Leeds by Williamson *et al* [57]. The three methods included ln$D$-lnT_1 plots, comparing the normalised values of the two quantities and comparing the activation energies. It was concluded that the hydrogen and lithium relaxation times were dominated by translational motion, and the fluorine relaxation had a dominant rotational component. However all nuclei displayed significant contributions for both translational and rotational. It was found that the translational contribution decreased with increasing salt concentration for all measurements.

8.2 Polymer Gel Electrolyte NMR

In Chapter 5 the results for the polymer gel electrolyte NMR were discussed. The polymer gel electrolytes are a much more complex system than the corresponding liquid electrolytes. Polymer gel electrolytes of this type are believed to form smooth spherulites [35; 36; 38; 39] which aggregate to form a porous polymer structure. These spherulites consist of radial crystalline lamellae which are held together by interlamellar amorphous PVDF into a spherical structure. Gels with over 50%wt solvent have been shown to contain pores which are usually of the order of microns in size [41]. It has been shown in work carried out previously that the polymer gel electrolytes contain multiple phases [18; 34; 41; 84], including a crystalline PVDF, interlamellar PVDF, solvated (swollen) amorphous PVDF and pure liquid electrolyte phases.

Transverse relaxation measurements were carried out using the hydrogen nucleus. The measurements highlighted that there are at least three phases present in the 20% and 30% PVDF gels. The longest relaxation time was attributed to the liquid phase of the gel, the shortest relaxation time was attributed to the interlamellar amorphous PVDF phase and the intermediate time was attributed to the solvated amorphous phase. The intensities of the three phases for the 20% PVDF gel were 0.13 and 0.36 and 0.51 for the interlamellar amorphous PVDF, solvated

amorphous PVDF and liquid electrolyte phases, respectively. The intensities for the 30% PVDF gel were 0.14, 0.42 and 0.44 for the interlamellar amorphous PVDF, solvated amorphous PVDF and liquid electrolyte phases, respectively. Therefore, with an increase in polymer concentration, the liquid phase became less prominent. The crystalline regions of the polymer gel electrolytes would likely exhibit tranvserse relaxation times of the order of 20 μs. Therefore it is believed here that the timescale for the crystalline regions were too short to be measured accurately.

The lithium transverse relaxation times were also determined for a 30% PVDF gel. As with the hydrogen, a single exponential was insufficient to fit the data. It was found that the lithium displayed two distinct phases. The relaxation times were 840 ms and 260 ms with corresponding intensities of 0.64 and 0.36, respectively. The longer relaxation time was attributed to the liquid electrolyte phase and the other phase the solvated amorphous phase. It might be expected that the crystalline phase and interlamellar amorphous PVDF phase were missing from the lithium transverse relaxation time measurements, as there was no indication that any lithium would be bound to the crystalline polymer.

Longitudinal relaxation measurements were also taken for the polymer gel electrolytes for the hydrogen and lithium nuclei. The longitudinal relaxation times only exhibited a single time which was attributed to a fast energy exchange, therefore the values measured were an average of all phases. All of the relaxation times exhibited Arrhenius type temperature dependence.

The PFG-NMR diffusion measurements were carried out for all three nuclei. The fluorine measurements exhibited a single diffusion constant, attributed to the liquid phase of the polymer gel electrolyte. An interesting feature of the lithium diffusion measurements was the presence of two distinct diffusion constants. This has been reported in publications elsewhere for PVDF based gel electrolytes [41; 84]. The faster diffusive species was attributed to the liquid phase contained in the cavities of the gel and the slower diffusion constant was too mobile to be associated with the crystalline or interlamellar amorphous polymer phases and therefore attributed to the solvated amorphous phase. The intensities of the two phases were independent of salt concentration and temperature, where an average was taken as 0.66 and 0.34 for the liquid and solvated amorphous phase, respectively for the 20% PVDF gels. The average intensities for the 30% PVDF gels were 0.61 and 0.39 for the liquid and amorphous phases, respectively. As with the T_2 measurements an increase in polymer corresponded in a reduction of the pure liquid electrolyte phase. The intensities of the lithium T_2 and diffusion were 0.64 and 0.61 respectively for the 30% PVDF gels, therefore these two measurements are in good agreement with each other. It was noted that the diffusion constants for the liquid phases of the gels were comparable to the liquid electrolyte measurements discussed in Chapter 4.

The hydrogen diffusion measurements also exhibited two distinct diffusive species, however only in the 30% PVDF gels; the second phase was not observed in the 20% PVDF gels. The intensities for the 30% PVDF hydrogen measurements were 0.59 and 0.41 for the liquid and amorphous polymer phases, respectively; the intensity for the hydrogen and lithium were therefore comparable.

Since the liquid was contained in a cavity or pore of some unknown size there was the possibility of restricted diffusion occurring and thus lowering the measured diffusion. To test this theory, the lithium diffusion was measured for a 30% PVDF gel at varying diffusion times (Δ). It was found that the diffusion of both phases were unaffected by the change in diffusion

time. Suggesting that, on the timescale of the diffusion measurements, there was no interaction between the ions and cavity walls.

8.3 Conductivity

In Chapter 6 the ionic conductivity measurements were taken for the liquid and polymer gel electrolytes. The liquid electrolyte conductivities exhibited VTF type temperature dependence much like the relaxation times in Chapter 4. The temperature range for the conductivity measurements was 253-353 K which went to temperatures 40K lower than the diffusion measurements. It can be concluded that the liquids and gels exhibit VTF dependence once they are taken to around 273 K, VTF dependence is often observed at low temperatures close to the glass transition temperature of the system due to reduced mobility.

There was a peak in the conductivity of the liquid and polymer gel electrolytes as a function of salt concentration. This was attributed to the competition between the increase in the number of ions and the increase in viscosity of the system. However, there is another contribution to this peak which is the fraction of ions that are in ion pairs, and cannot contribute to the ionic conductivity; known as the ionic association. It was found that the semi-empirical Casteel-Amis equation [123] provided a good fit to the data. This equation allowed the determination of the maximum conductivity (σ_{max}) and the concentration when $\sigma = \sigma_{max}$ (c_{max}), i.e. the position of the peak. The c_{max} values increased with increasing temperature. This result was attributed to the decrease in viscosity at higher temperatures, ultimately shifting the peak to higher salt concentration.

The polymer gel electrolytes exhibited similar trends to the corresponding liquid electrolytes, with both temperature and salt concentration. The values of c_{max} were observed to decrease with increasing polymer concentration, suggesting that the c_{max} values were dependent on the mobility of the ions in solution. The conductivity measurements also decreased with the introduction of polymer. Since multiple phases were observed for the lithium diffusion and T_2 measurements, this means that some of the charge carriers are present in the solvated amorphous regions of the polymer gel electrolytes. It is assumed that the viscosity of the amorphous phase was higher than the corresponding liquid phase of the gels and would therefore affect the ionic conductivity, assuming that the ions within the polymer phase contributed to the conductivity.

The ratio of the liquid and gel conductivity ($\sigma_{PGE}/\sigma_{Liquid}$) was determined with varying salt concentration and temperature. A decrease was expected in the conductivity with addition of polymer, since conductivity of a porous membrane is dependent on factors such as the porosity, tortuosity and thickness of the membrane. However, the reduction in conductivity was much more significant than expected due to reduction in free volume. The ratio of gel to liquid conductivity was observed to increase with increasing temperature. There was no trend of this parameter with salt concentration at both high and low temperatures. The conclusion of this result was that the viscosity of the amorphous polymer phase decreased more significantly than the corresponding liquid electrolyte phase with increasing temperature.

In the final section of Chapter 6 the ratio of the fast and slow diffusion constants was calculated as a function of temperature and salt concentration. The motivation behind this was to determine if there was a viscosity difference between the two phases. If the viscosity temperature

dependence was the same in both phases, then the ratio of diffusion constants (D_{slow}/D_{fast}) would not change with temperature. The interesting result of this ratio was that it also increases much like the ratio of conductivities. The implication of this result is that not only can it be said that the amorphous polymer phase is contributing to the total conductivity but that its contribution is temperature dependent, due to relative viscosity effects and the two phases converge at higher temperatures.

8.4 Ionic Association and Ionic Radius Calculations

The ionic association is the fraction of ions which are neutral due to ion pairing and therefore not contributing to the ionic conductivity. This parameter is important with considerations of the practical use of these gels within lithium batteries, where clearly a low ionic association is desired. The ionic conductivity was predicted using the Nernst-Einstein equation which relates the conductivity to the diffusion of the charge carriers. The predicted conductivity has no term to account for the ionic association and as a result, is much higher than the directly measured conductivity; the difference in these two values being the ionic association.

For the liquid electrolyte, the ionic association increased with both temperature and salt concentration. The temperature dependence was somewhat counter intuitive since an increased temperature would be expected to disrupt the ion pairs and separate them. However this temperature dependence has been attributed to the lowering of the free energy of ion pair formation at high temperatures due to a volume increase caused by electrostriction. The salt concentration increase was attributed to the increase in the density of ions.

The polymer gel electrolyte ionic association values were not as straightforward as the corresponding liquid electrolytes. Since the ionic association is essentially a measure of ions that are not conducting, this does not strictly mean ionic association in the case of the polymer gel electrolytes. The trend with temperature for the gels was the inverse of the liquids and decreased with increasing temperature. Increasing the temperature causes the viscosity of the amorphous phase to decrease, converging with the liquid phase, therefore essentially increasing the ionic association value, although this is not considered a real shift in the ionic association. The ionic association for the gels were independent of salt concentration. It can be concluded that the ionic association of the gels was higher than the corresponding liquid electrolytes, meaning that more ions are not available for conduction.

In Chapter 7 the viscosity of the liquid electrolytes was measured using an Ostwald viscometer. The temperature dependence was Arrhenius, much like the diffusion and conductivity in the same temperature range. The salt concentration dependence was difficult to define as no set method exists to analyse the dependence, several empirical models were assessed, however, it was found that the data was fitted best by a simple exponential, as with the liquid diffusion salt concentration dependence. This allowed a temperature dependent exponential factor (A_η) to be determined. By comparing this factor with the factor determined for the diffusion measurements (A_D), some insight into the ionic radii was established. If the decrease in diffusion with salt concentration is solely due to viscosity effects then it can be assumed that $A_\eta = A_D$. It was observed that for the hydrogen and lithium diffusion measurements $A_D < A_\eta$, which suggests that the fall in diffusion is not as fast as the increase in viscosity and therefore only a decrease in radius

could account for this deviance. The inverse can be stated for fluorine diffusion measurements which yielded $A_D > A_\eta$, suggesting an increase in ionic radius with salt concentration.

The ionic radii were calculated directly using the Stokes-Einstein equation. In order to achieve this, a correction factor had to be used which accounted for both 'stick' and 'slip' conditions as well as deviances away from the hard sphere model, initially used in deriving the Stokes-Einstein equation. The correction factors were 3.3 (empirically determined in this thesis), 5.7 (taken from reference [83]) and 5.4 (taken from reference [83]) for the PC molecule, lithium and BF_4^- ions, respectively. As predicted by comparing the decrease in diffusion against the increase in viscosity with salt concentration, the average fluorine radii increased and the average radii of the hydrogen and lithium decreased with increasing salt concentration. The values of the BF_4^- was 2.22 Åat low temperature and concentration where the known value is 2.29 Å[83] and is therefore in very good agreement. The same was observed for the hydrogen radii, the average of which was determined to be 2.60 Åwith the known value of 2.76 Å[83]. The lithium ionic radii was observed to be around four times larger than would be expected from a single lithium ion and therefore can be concluded that there was a significant solvation shell around the lithium ions.

The final section of Chapter 7 was also concerned with the ionic radius, however this time the solvation was estimated by taking ratios of the diffusion constants, as previously shown with other systems by Hayamizu *et al* [99; 101; 120]. By taking a ratio of the solvent and ion diffusion ($R_{Li} = D_{solvent}/D_{ion}$), a solvation number can be determined due to the large size difference between the single lithium ion and PC molecule. It was observed that the value of R_{Li} was independent of salt concentration and gave an average value of around 2.3, suggesting on the timescale of the experiment each lithium ion was solvated by two PC molecules. The same could be calculated for the anion; however since the natural size of the anion was comparable to the PC molecule, the value had to be scaled by the relevant van der Waals radii (RR_{anion}). The result for the anion was $RR_{anion} \approx 1$, suggesting that the anions (BF_4) were unsolvated by the PC molecule. RR_{anion} increased with the increase with salt concentration, which was attributed to the increase in ionic association between the anion and cation.

8.5 Future Work

It can be concluded from the work summarised above that with the use of three key techniques (NMR, impedance spectroscopy and viscosity), the system dynamics can be understood well in principle. However, there are areas which would benefit from further work. For instance, the ionic association in the polymer gel electrolytes was not very informative as it was unclear the contributions from the ionic association and the ions interacting with the polymer. There is a technique by Kataoka *et al* [117] which measures the diffusion via PFG-NMR, however they have applied a direct current through the sample. The effect of this is to change the diffusion of the charged ions and leave the neutral pairs unaffected. Therefore, the ionic association could be determined in this way, which would be able to distinguish between actual ionic association and loss of ions to the polymer.

In Chapter 5 it was briefly stated that measurements of similar systems have undergone $T_{1\rho}$ measurements [34]. This technique is similar to the relaxation measurements carried out in Chapters 4 and 5, however it makes use of a 'locking' pulse which is applied for various amount

of time, the longer the amount of time the 'locking' pulse is applied for the lower the intensity of the experiment. It has been shown that this method can provide better phase information than via transverse relaxation times. The very short times characteristic of the crystalline polymer are difficult to detect in the transverse relaxation measurements, but are shifted to longer times for $T_{1\rho}$, and therefore could become accessible. This might allow determination of more phases than detected in the course of this research.

As mentioned previously, the materials used in the practical battery applications generally use mixed solvents. It is also possible to enhance the conductivity using mixtures of salts, therefore it is of interest to understand these more complex systems. Some preliminary measurements were taken for EC:PC mixed solvents which showed promising results, they were not reported in this work. The conductivity values were significantly higher at room temperature and investigation into the optimum composition of these more complex systems would be very useful from the application side of this research.

The future work discussed here is certainly not exhaustive, but gives some possible directions for the current work to take, to obtain a broader understanding of the ion dynamics.

References

[1] P.M. Richardson, A.M. Voice, and I.M. Ward. Pulse-field gradient NMR self diffusion and ionic conductivity measurements for liquid electrolytes containing LiBF4 and propylene carbonate. *Electrochimica Acta*, 130:606–618, 2014.

[2] P.M. Richardson, A.M. Voice, and I.M. Ward. NMR T_1 relaxation time measurements and calculations with translational and rotational components for liquid electrolytes containing $LiBF_4$ and propylene carbonate. *The Journal of Chemical Physics*, 139:214501, 2013.

[3] P.M. Richardson, A.M. Voice, and I.M. Ward. Two distinct lithium diffusive species for polymer gel electrolytes containing LiBF4, propylene carbonate (PC) and PVDF. *International Journal of Hydrogen Energy*, 39(6):2904–2908, 2013.

[4] M.H. Levitt. *Spin Dynamics: Basics of Nuclear Magnetic Resonance*. John Wiley & Sons, 2008.

[5] A.M. Stephan. Review on gel polymer electrolytes for lithium batteries. *European Polymer Journal*, 42(1):21–42, 2006.

[6] P.V. Wright. Electrical conductivity in ionic complexes of poly(ethylene oxide). *British Polymer Journal*, 7(5):319–327, 1975.

[7] P.V. Wright. Recent trends in polymer electrolytes based on poly(ethylene oxide). *Journal of Macromolecular Science-Chemistry*, A26(2-3):519–550, 1989.

[8] M. Armand. Polymer solid electrolytes - an overview. *Solid State Ionics*, 9-10:745–754, 1983.

[9] J.E. Weston and B.C.H. Steele. Thermal history : conductivity relationship in lithium salt-poly (ethylene oxide) complex polymer electrolytes. *Solid State Ionics*, 2(4):347–354, 1981.

[10] C. Berthier, W. Gorecki, M. Minier, M.B. Armand, J.M. Chabagno, and P. Rigaud. Microscopic investigation of ionic conductivity in alkali metal salts-poly(ethylene oxide) adducts. *Solid State Ionics*, 11(1):91–95, 1983.

[11] J. Cruickshank, H.V.St.A. Hubbard, N. Boden, and I.M. Ward. The role of ionic salts in determining tg and ionic conductivity in concentrated PEG electrolyte solutions. *Polymer*, 36(19):3779–3781, 1995.

[12] D.J. Bannister, G.R. Davies, I.M. Ward, and J.E. McIntyre. Ionic conductivities of poly(methoxy polyethylene glycol monomethacrylate) complexes with LiSO3CH3. *Polymer*, 25(11):1600–1602, 1984.

[13] P.G. Hall, G.R. Davies, J.E. Mcintyre, I.M. Ward, D.J. Bannister, and K.M.F. Le Brocq. Ion conductivity in polysiloxane comb polymers with ethylene glycol teeth. *Polymer communications*, 27(4):98–100.

[14] D. Fish, I.M. Khan, E. Wu, and J. Smid. Polymer electrolyte complexes of LiClO4 and comb polymers of siloxane with oligo-oxyethylene side chains. *British Polymer Journal*, 20(3):281–288, 1988.

[15] A. Nishimoto, M. Watanabe, Y. Ikeda, and S. Kohjiya. High ionic conductivity of new polymer electrolytes based on high molecular weight polyether comb polymers. *Electrochimica Acta*, 43(10-11):1177–1184, 1998.

[16] I.E. Kelly, J.R. Owen, and B.C.H. Steele. Poly(ethylene oxide) electrolytes for operation at near room temperature. *Journal of Power Sources*, 14(1-3):13–21, 1985.

[17] S.A. Dobrowski, G.R. Davies, J.E. Mclntyre, and I.M. Ward. Ionic conduction in poly(n,n-dimethylacrylamide) gels complexing lithium salts. *Polymer*, 32(16):2887–2891, 1991.

[18] I.M. Ward and H.V.St.A. Hubbard. *Polymer electrolytes: conduction mechanisms and battery applications, Chapter 21, in Ionic interactions in natural and synthetic macromolecules*. Wiley and Sons Inc., 2012.

[19] Y. Aihara, G.B. Appetecchi, B. Scrosati, and K. Hayamizu. Investigation of the ionic conduction mechanism of composite poly(ethyleneoxide) peo-based polymer gel electrolytes including nano-size SiO2. *Physical Chemistry Chemical Physics*, 4(14):3443–3447, 2002.

[20] S. Abbrent, S.H. Chung, S.G. Greenbaum, J. Muthu, and E.P. Giannelis. Nuclear magnetic resonance studies of nanocomposite gel electrolytes. *Electrochimica Acta*, 48(14-16):2113–2121, 2003.

[21] A.M. Stephan, K.S. Nahm, M.A. Kulandainathan, G. Ravi, and J. Wilson. Electrochemical studies on nanofiller incorporated poly(vinylidene fluoride-hexafluoropropylene) (PVdF-HFP) composite electrolytes for lithium batteries. *Journal of Applied Electrochemistry*, 36(10):1091–1097, 2006.

[22] A.M. Voice, J.P. Southall, V. Rogers, K.H. Matthews, G.R. Davies, J.E. McIntyre, and I.M. Ward. Thermoreversible polymer gel electrolytes. *Polymer*, 35(16):3363–3372, 1994.

[23] Z. Jiang, B. Carroll, and K.M. Abraham. Studies of some poly(vinylidene fluoride) electrolytes. *Electrochimica Acta*, 42(17):2667–2677, 1997.

[24] F. Boudin, X. Andrieu, C. Jehoulet, and I.I. Olsen. Microporous PVdF gel for lithium-ion batteries. *Journal of Power Sources*, 81-82:804–807, 1999.

[25] M.J. Williamson, H.V.St.A. Hubbard, and I.M. Ward. NMR measurements of self diffusion in polymer gel electrolytes. *Polymer*, 40(26):7177–7185, 1999.

[26] C. Capiglia, Y. Saito, H. Kataoka, T. Kodama, E. Quartarone, and P. Mustarelli. Structure and transport properties of polymer gel electrolytes based on PVdF-HFP and LiN(C2F5SO2)2. *Solid State Ionics*, 131(3-4):291–299, 2000.

[27] J.M. Song, H.R. Kang, S.W. Kim, W.M. Lee, and H.T. Kim. Electrochemical characteristics of phase-separated polymer electrolyte based on poly(vinylidene fluoride-co-hexafluoropropane) and ethylene carbonate. *Electrochimica Acta*, 48(10):1339–1346, 2003.

[28] F. Croce, S.D. Brown, S.G. Greenbaum, S.M. Slane, and M. Salomon. Lithium-7 NMR and ionic conductivity studies of gel electrolytes based on polyacrylonitrile. *Chemistry of Materials*, 5(9):1268–1272, 1993.

[29] O. Bohnke, G. Frand, M. Rezrazi, C. Rousselot, and C. Truche. Fast ion transport in new lithium electrolytes gelled with PMMA. 1. influence of polymer concentration. *Solid State Ionics*, 66(1-2):97–104, 1993.

[30] S. Ramesh and A.K. Arof. Ionic conductivity studies of plasticized poly(vinyl chloride) polymer electrolytes. *Materials Science and Engineering: B*, 85(1):11–15, 2001.

[31] H.V.St.A. Hubbard, I.M. Ward, P.L. Carr, and W.F. Tyldesley. Uk patent application pct/gb01/03937. 2001.

[32] I.M. Ward, H.V.St.A. Hubbard, S.C. Wellings, G.P. Thompson, J. Kaschmitter, and H.P. Wang. Separator-free rechargeable lithium ion cells produced by the extrusion lamination of polymer gel electrolytes. *Journal of Power Sources*, 162(2):818–822, 2006.

[33] J.Y. Song, Y.Y. Wang, and C.C. Wan. Review of gel-type polymer electrolytes for lithium-ion batteries. *Journal of Power Sources*, 77:183–197, 1999.

[34] H.V.St.A. Hubbard and I.M. Ward. *Polymer Preprints*, 49(1):709–710, 2008.

[35] B.S. Kim, S.T. Baek, K.W. Song, I.H. Park, J.O. Lee, and N. Nemoto. Thermoreversible gelation of poly(vinylidene fluoride) in propylene carbonate. *Journal of Macromolecular Science, Part B*, 43(4):741–754, 2005.

[36] C.M. Chou and P.D. Hong. Scattering modeling of nucleation gels. *Macromolecules*, 41:6540–6545, 2008.

[37] C.M. Chou and P.D. Hong. A novel aspect on structural formation of physical gels. *Macromolecules*, 36:7331–7337, 2003.

[38] H. Shimizu, Y. Arioka, M. Ogawa, R. Wada, and M. Okabe. Sol-gel transitions of poly(vinylidene fluoride) in organic solvents containing LiBF4. *Polymer Journal*, 43(6):540–544, 2011.

[39] M. Tazaki, R. Wada, M. Okabe, and T. Homma. Crystallization and gelation of poly(vinylidene fluoride) in organic solvents. *Journal of Applied Polymer Science*, 65(8):1517–1524, 1997.

[40] H.C. Yang, Q.Y. Wu, H.C. Liang, L.S. Wan, and Z.K. Xu. Thermally induced phase separation of poly(vinylidene fluoride)/diluent systems: Optical microscope and infrared spectroscopy studies. *Journal of Polymer Science Part B: Polymer Physics*, 51(19):1438–1447, 2013.

[41] A. Magistris, E. Quartarone, P. Mustarelli, Y. Saito, and H. Kataoka. Pvdf-based porous polymer electrolytes for lithium batteries. *Solid State Ionics*, 152-153:347–354, 2002.

[42] M.M.E Jacob and A.K. Arof. FTIR studies of DMF plasticized polyvinyledene fluoride based polymer electrolytes. *Electrochimica Acta*, 45(10):1701–1706, 2000.

[43] M.J. Williamson, J.P. Southall, H.V.St.A. Hubbard, G.R. Davies, and I.M. Ward. Pulsed field gradient n.m.r. diffusion measurements on electrolyte solutions containing LiCF3SO3. *Polymer*, 40(14):3945–3955, 1999.

[44] M.S. Ding and T.R. Jow. How conductivities and viscosities of PC-DEC and PC-EC solutions of LiBF4, LiPF6, LiBOB, Et4NBF4, and Et4NPF6 differ and why. *Journal of The Electrochemical Society*, 151(12):A2007–A2015, 2004.

[45] M.S. Ding. Conductivity and viscosity of PC-DEC and PC-EC solutions of LiBF4. *Journal of The Electrochemical Society*, 151(1):A40–A47, 2004.

[46] M.S. Ding, K. Xu, and T.R. Jow. Conductivity and viscosity of PC-DEC and PC-EC solutions of LiBOB. *Journal of The Electrochemical Society*, 152(1):A132–A140, 2005.

[47] S.S. Zhang, K. Xu, and T.R. Jow. Enhanced performance of li-ion cell with LiBF4-PC based electrolyte by addition of small amount of LiBOB. *Journal of Power Sources*, 156:629–633, 2006.

[48] A.M. Voice, G.R. Davies, and I.M. Ward. Structure of poly(vinylidene fluoride) gel electrolytes. *Polymer Gels and Networks*, 5(2):123–144, 1997.

[49] A.M. Stephan and Y. Saito. Ionic conductivity and diffusion coefficient studies of PVdF-HFP polymer electrolytes prepared using phase inversion technique. *Solid State Ionics*, 148(3-4):475–481, 2002.

[50] E.O. Stejskal and J.E. Tanner. Spin diffusion measurements: Spin echoes in the presence of a Time-Dependent field gradient. *The Journal of Chemical Physics*, 42(1):288, 1965.

[51] G. Annat, D.R. MacFarlane, and M. Forsyth. Transport properties in ionic liquids and ionic liquid mixtures: The challenges of NMR pulsed field gradient diffusion measurements. *The Journal of Physical Chemistry B*, 111(30):9018–9024, 2007.

[52] R.M. Cotts, M.J.R. Hoch, T. Sun, and J.T. Markert. Pulsed field gradient stimulated echo methods for improved NMR diffusion measurements in heterogeneous systems. *Journal of Magnetic Resonance*, 83:252–266, 1989.

[53] Y. Saito, H. Yamamoto, O. Nakamura, H. Kageyama, H. Ishikawa, T. Miyoshi, and M. Matsuoka. Determination of ionic self-diffusion coefficients of lithium electrolytes using the pulsed field gradient NMR. *Journal of Power Sources*, 81-82:772–776, 1999.

[54] I.M. Ward, M.J. Williamson, H.V.St.A. Hubbard, J.P. Southall, and G.R. Davies. NMR studies of ionic mobility in polymer gel electrolytes for advanced lithium batteries. *Journal of Power Sources*, 81-82:700–704, 1999.

[55] K. Hayamizu, Y. Aihara, and W.S. Price. Nmr and ion conductivity studies on cross-linked poly(ethylene oxide-propylene oxide) and branched polyether doped with LiN(SO2CF3)(2). *Electrochimica Acta*, 46:1475–1485, 2001.

[56] Y. Aihara, T. Bando, H. Nakagawa, H. Yoshida, K. Hayamizu, E. Akiba, and W.S. Price. Ion Transport Properties of Six Lithium Salts Dissolved in γ-Butyrolactone Studied by Self-Diffusion and Ionic Conductivity Measurements. *Journal of The Electrochemical Society*, 151(1):A119–A122, 2004.

[57] M.J. Williamson, J.P. Southall, and I.M. Ward. Nuclear magnetic resonance relaxation measurements in electrolyte solutions containing LiCF3SO3. *The Journal of Chemical Physics*, 109(18):7893, 1998.

[58] H. Kikuko, S. Tsuzuki, S. Seki, and Y. Umebayashi. Nuclear magnetic resonance studies on the rotational and translational motions of ionic liquids composed of 1-ethyl-3-methylimidazolium cation and bis(trifluoromethanesulfonyl)amide and bis(fluorosulfonyl)amide anions and their binary systems including lithium salts. *The Journal of Chemical Physics*, 135(8):084505–084505–11, 2011.

[59] F. Ali, M. Forsyth, M.C. Garcia, M.E. Smith, and J.H. Strange. A 7Li and 19F NMR relaxation study of LiCF3SO3 in plasticised solid polyether electrolytes. *Solid State Nuclear Magnetic Resonance*, 5(3):217–225, 1995.

[60] K.M. Abraham. Directions in secondary lithium battery research and development. *Electrochimica Acta*, 38(9):1233–1248, 1993.

[61] J.Y. Song, Y.Y Wang, and C.C. Wan. Conductivity study of porous plasticized polymer electrolytes based on poly(vinylidene fluoride) a comparison with polypropylene separators. *Journal of The Electrochemical Society*, 147(9):3219–3225, 2000.

[62] I.M. Ward, N. Boden, J. Cruickshank, and S.A. Leng. NMR studies of ionic mobility and molecular mobility in polymer electrolytes. *Electrochimica Acta*, 40(13-14):2071–2076, 1995.

[63] K. Hayamizu. Temperature dependence of self-diffusion coefficients of ions and solvents in ethylene carbonate, propylene carbonate, and diethyl carbonate single solutions and ethylene carbonate + diethyl carbonate binary solutions of LiPF6 studied by NMR. *Journal of Chemical & Engineering Data*, 57(7):2012–2017, 2012.

[64] H. Kataoka, Y. Saito, T. Sakai, S. Deki, and T. Ikeda. Ionic mobility of cation and anion of lithium gel electrolytes measured by pulsed gradient Spin-Echo NMR technique under direct electric field. *The Journal of Physical Chemistry B*, 105(13):2546–2550, 2001.

[65] H. Kataoka and Y. Saito. New approached for determining the degree of dissociation of a salt by measurements of dynamic properties of lithium ion electrolytes. *The Journal of Physical Chemistry B*, 106(50):13064–13068, 2002.

[66] S.A. Leng. *University of Leeds*. PhD thesis, 1988.

[67] F. Bloch. Nuclear induction. *Physical Review*, 70(7-8):460–474, 1946.

[68] E. Fukushima and S.B.W. Roeder. *Experimental Pulse NMR: A Nuts and Bolts Approach*. Addison-Wesley, 1993.

[69] J.W. Hennel and J. Klinowski. *Fundamentals of nuclear magnetic resonance*. Longman Scientific & Technical, 1993.

[70] V.I. Bakhmutov. *Practical Nuclear Magnetic Resonance Relaxation for Chemists*. John Wiley & Sons, 2005.

[71] J. Kowalewski and L. Maler. *Nuclear Spin Relaxation in Liquids: Theory, Experiments, and Applications*. CRC Press, 2006.

[72] N. Bloembergen, E.M. Purcell, and R.V. Pound. Relaxation effects in nuclear magnetic resonance absorption. *Physical Review*, 73(7):679–715, 1948.

[73] P. Gerothanassis and C.G. Tsanaktsidis. Nuclear electric quadrupole relaxation. *Concepts in Magnetic Resonance*, 8(1):63–74, 1996.

[74] E.L. Hahn. Spin echoes. *Physical Review*, 80(4):580–594, 1950.

[75] H.Y. Carr and E.M. Purcell. Effects of diffusion on free precession in nuclear magnetic resonance experiments. *Physical Review*, 94(3):630–638, 1954.

[76] S. Meiboom and D. Gill. Modified Spin-Echo method for measuring nuclear relaxation times. *Review of Scientific Instruments*, 29(8):688, 1958.

[77] M.J. Williamson, J.P. Southall, H.V.St.A. Hubbard, S.F. Johnston, G.R. Davies, and I.M. Ward. NMR measurements of ionic mobility in model polymer electrolyte solutions. *Electrochimica Acta*, 43(10-11):1415–1420, 1998.

[78] K. Levenberg. A method for the solution of certain non-linear problems in least squares. *Quarterly of Applied Mathematics*, 2:164–168, 1944.

[79] D. Marquardt. An algorithm for least-squares estimation of nonlinear parameters. *SIAM Journal on Applied Mathematics*, 11 (2):431441, 1963.

[80] M.S. Ding. Liquid phase boundaries, dielectric constant, and viscosity of PC-DEC and PC-EC binary carbonates. *Journal of The Electrochemical Society*, 150(4):A455–A462, 2003.

[81] H.L. Yeager, J.D. Fedyk, and R.J. Parker. Spectroscopic studies of ionic solvation in propylene carbonate. *Journal of Physical Chemistry*, 77 (20):2407–2410, 1973.

[82] H. Ohtani, Y. Hirao, A. Ito, K. Tanaka, and O. Hatozaki. Theoretical study on thermochemistry of solvated lithium-cation with propylene carbonate. *Journal of Thermal Analysis Calorimetry*, 99:139–144, 2010.

[83] M. Ue. Mobility and Ionic Association of Lithium and Quaternary Ammonium Salts in Propylene Carbonate and γ-Butyrolactone. *Journal of The Electrochemical Society*, 141(12):3336–3342, 1994.

[84] Y. Saito, C. Capiglia, H. Kataoka, H. Yamamoto, H. Ishikawa, and P. Mustarelli. Conduction properties of PVDF-type polymer electrolytes with lithium salts, LiN(CF3SO2)2 and LiN(C2F5SO2)2. *Solid State Ionics*, 136-137:1161–1166, 2000.

[85] J.E. McIntyre, I.M. Ward, H.V.St.A. Hubbard, and V. Rogers. Uk patent application pct/gb92/01781. 1992.

[86] W. Xu, K.S. Siow, Z. Gao, and S.Y. Lee. AC impedance study on the interface of lithium and polymer electrolyte based on lithium-n(4-sulfophenyl) maleimide. *Solid State Ionics*, 112:1–8, 1998.

[87] Novocontrol. *BDS1200 Sample cell technical manual*.

[88] M.J. Williamson. *University of Leeds*. PhD thesis, 1998.

[89] L. Coury. Conductance measurements part 1: Theory. *Current Separations*, 18(3):1–8, 1999.

[90] P.H. Daum and D.F. Nelson. Bipolar current method for determination of solution resistance. *Analytical Chemistry*, 45:463–470, 1973.

[91] M.S. Ding. Electrolytic conductivity and glass transition temperatures as functions of salt content, solvent composition, or temperature for LiBF4 in propylene carbonate + diethyl carbonate. *Journal of Chemical & Engineering Data*, 49(4):1102–1109, 2004.

[92] D.B. Viswanath, T.K. Ghosh, D.H.L. Prasad, N.V.K. Dutt, and K.Y. Rani. *Viscosity of Liquids: Theory, Estimation, Experiment, and Data*. Springer, 2007.

[93] J. Barthel, R. Neueder, and H. Roch. Density, relative permittivity, and viscosity of propylene carbonate plus dimethoxyethane mixtures from 25 degrees c to 125 degrees c. *Journal of Chemical and Engineering Data*, 45:1007–1011, 2000.

[94] H. Vogel. The temperature dependence law of the viscosity of fluids. *Physikalische Zeitschrift*, 22:645–646, 1921.

[95] G.S. Fulcher. Analysis of recent measurements of the viscosity of glasses. *Journal of the American Ceramic Society*, 8(6):339–355, 1925.

[96] G. Tammann and W. Hesse. The dependency of viscosity on temperature in hypothermic liquids. *Zeitschrift Fur Anorganische Und Allgemeine Chemie*, 156(4), 1926.

[97] K. Hayamizu and W.S. Price. A new type of sample tube for reducing convection effects in PGSE-NMR measurements of self-diffusion coefficients of liquid samples. *Journal of Magnetic Resonance*, 167(2):328–333, 2004.

[98] C. Capiglia, Y. Saito, H. Kageyama, P. Mustarelli, T. Iwamoto, T. Tabuchi, and H. Tukamoto. Li-7 and f-19 diffusion coefficients and thermal properties of non-aqueous electrolyte solutions for rechargeable lithium batteries. *Journal of Power Sources*, 8182:859862, 1999.

[99] K. Hayamizu, Y. Aihara, S. Arai, and C.G. Martinez. Pulse-gradient spin-echo 1H, 7Li, and 19F NMR diffusion and ionic conductivity measurements of 14 organic electrolytes containing LiN(SO2CF3)2. *The Journal of Physical Chemistry B*, 103(3):519–524, 1999.

[100] Y. Saito, H. Yamamoto, H. Kageyama, O. Nakamura, T. Miyoshi, and M. Matsuoka. Investigation of the solution condition of lithium electrolyte solutions with LiCF3SO3 salt. *Journal of Materials Science*, 35(4):809–812, 2000.

[101] Y. Aihara, K. Sugimoto, W.S. Price, and K. Hayamizu. Ionic conduction and self-diffusion near infinitesimal concentration in lithium salt-organic solvent electrolytes. *The Journal of Chemical Physics*, 113(5):1981–1991, 2000.

[102] T. Fromling, M. Kunze, M. Schonhoff, J. Sundermeyer, and B. Roling. Enhanced lithium transference numbers in ionic liquid electrolytes. *The Journal of Physical Chemistry B*, 112(41):12985–12990, 2008.

[103] K. Kondo, M. Sano, A. Hiwara, T. Omi, M. Fujita, A. Kuwae, M. Iida, K. Mogi, and H. Yokoyama. Conductivity and solvation of li+ ions of LiPF6 in propylene carbonate solutions. *The Journal of Physical Chemistry B*, 104(20):5040–5044, 2000.

[104] J. Barthel, H.J. Gores, G. Schmeer, and R. Wachter. Non-aqueous electrolyte-solutions in chemistry and modern technology. *Topics in Current Chemistry*, 111:33–144, 1983.

[105] W. Jost. *Diffusion*. Academic, New York, 1960.

[106] A. Abragam. *The Principles of Nuclear Magnetism*. Oxford Sciences Publications, 1969.

[107] Y.G. Andreev, V. Seneviratne, M. Kahn, W.A. Henderson, R.E. Frech, and P.G. Bruce. Crystal structure of poly(eythene oxide)3:libf4 and (diglyme)n:libf4 (n=1,2). *Chemistry of Materials*, 17:767–772, 2005.

[108] H. Tsunekawa, A. Narumi, M. Sano, A. Hiwara, M. Fujita, and H. Yokoyama. Solvation and ion association studies of LiBF4 - propylene carbonate and LiBF4 - propylene carbonate - trimethyl phosphate solutions. *Journal of Physical Chemistry B*, 107:10962–10966, 2003.

[109] D.C. Douglass, V.J. McBrierty, and T.T. Wang. The use of NMR linewidths to study baxis distributions in poled and unpoled PVDF. *The Journal of Chemical Physics*, 77(11):5826–5835, 1982.

[110] C. Capiglia, Y. Saito, H. Yamamoto, H. Kageyama, and P. Mustarelli. Transport properties and microstructure of gel polymer electrolytes. *Electrochimica Acta*, 45(8-9):1341–1345, 2000.

[111] N. Boden, S.A. Leng, and I.M. Ward. Ionic conductivity and diffusivity in polyethylene oxode/electrolyte solutions as models for polymer electrolytes. *Solid State Ionics*, 45(3-4):261–270, 1991.

[112] Y. Aihara, S. Arai, and K. Hayamizu. Ionic conductivity, dsc and self diffusion coefficients of lithium, anion, polymer, and solvent of polymer gel electrolytes: the structure of the gels and the diffusion mechanism of the ions. *Electrochimica Acta*, 45(8-9):1321–1326, 2000.

[113] K. Hayamizu, Y. Aihara, S. Arai, and W.S. Price. Self-diffusion coefficients of lithium, anion, polymer, and solvent in polymer gel electrolytes measured using 7Li, 19F, and 1H pulsed-gradient spin-echo NMR. *Electrochimica Acta*, 45(8-9):1313–1319, 2000.

[114] H. Kataoka, Y. Saito, T. Sakai, E. Quartarone, and P. Mustarelli. Conduction mechanisms of pvdf-type gel polymer electrolytes of lithium prepared by a phase inversion process. *The Journal of Physical Chemistry B*, 104(48):11460–11464, 2000.

[115] Y. Saito, H. Kataoka, and A.M. Stephan. Investigation of the conduction mechanisms of lithium gel polymer electrolytes based on electrical conductivity and diffusion coefficient using NMR. *Macromolecules*, 34(20):6955–6958, 2001.

[116] R. Metzler and J. Klafter. The random walk's guide to anomalous diffusion: a fractional dynamics approach. *Physics Reports*, 339(1):1–77, 2000.

[117] H. Kataoka, Y. Saito, Y. Miyazaki, and S. Deki. Ionic mobilities of PVDF-based polymer gel electrolytes as studied by direct current NMR. *Solid State Ionics*, 152-153:175–179, 2002.

[118] W.S. Price. *Gradient NMR. In: Annual Reports on NMR Spectroscopy*, volume 32. Academic Press., 1996.

[119] J.P. Southall, H.V.St.A. Hubbard, S.F. Johnston, V. Rogers, G.R. Davies, J.E. McIntyre, and I.M. Ward. Ionic conductivity and viscosity correlations in liquid electrolytes for incorporation into PVDF gel electrolytes. *Solid State Ionics*, 85(1-4):51–60, 1996.

[120] K. Hayamizu and Y. Aihara. Ion and solvent diffusion and ion conduction of PC-DEC and PC-DME binary solvent electrolytes of LiN(SO2CF3)2. *Electrochimica Acta*, 49(20):3397–3402, 2004.

[121] A.M. Christie and C.A. Vincent. Conductivities of selected lithium salt complexes in propylene carbonate. *The Journal of Physical Chemistry*, 100(11):4618–4621, 1996.

[122] K. Hayamizu, A. Matsuo, and J. Arai. A divalent lithium salt Li2B12F12 dissolved in propylene carbonate studied by NMR methods. *Journal of The Electrochemical Society*, 156(9):A744–A750, 2009.

[123] J.F. Casteel and E.S. Amis. Specific conductance of concentrated solutions of magnesium salts in water-ethanol system. *Journal of Chemical and Engineering Data*, 17(1):55–59, 1972.

[124] A. de Diego, J.M. Madariaga, and E. Chapela. Conductivity of concentrated aqueous solutions of several fluorine-containing electrolytes in a wide range of concentrations and temperatures. *Journal of Chemical & Engineering Data*, 42(1):202–208, 1997.

[125] A. de Diego, J.M. Madariaga, and E. Chapela. Empirical model of general application to fit (k,c,t) experimental data from concentrated aqueous electrolyte solutions. *Electrochimica Acta*, 42(9):1449–1456, 1997.

[126] M.S. Ding. Casteel-Amis equation: Its extension from univariate to multivariate and its use as a two-parameter function. *Journal of Chemical & Engineering Data*, 49(5):1469–1474, 2004.

[127] K. Kuratani, N. Uemura, H. Senoh, H.T. Takeshita, and T. Kiyobayashi. Conductivity, viscosity and density of MClO4 (M=Li and Na) dissolved in propylene carbonate and γ-butyrolactone at high concentrations. *Journal of Power Sources*, 223:175–182, 2013.

[128] R. Olender and A. Nitzan. Ion solvation and association in complex solvents: Theoretical considerations. *Electrochimica Acta*, 37(9):1505–1509, 1992.

[129] M. Forsyth, V.A. Payne, M.A. Ratner, S.W. de Leeuw, and D.F. Shriver. Molecular dynamics simulations of highly concentrated salt solutions: Structural and transport effects in polymer electrolytes. *Solid State Ionics*, 53-56, Part 2:1011–1026, 1992.

[130] H. Falkenhagen and M. Dole. The internal friction of electrolytic solutions and their significance according to debye's theory. *Physikalische Zeitschrift*, 30:611–622, 1929.

[131] L. Onsager and R.M. Fuoss. Irreversible processes in electrolytes. diffusion, conductance and viscous flow in arbitrary mixtures of strong electrolytes. *The Journal of Physical Chemistry*, 36(11):2689–2778, 1931.

[132] P. Debye and E. Huckel. Remarks on a rate concerning cataphoretic appearances in suspended parts. *Physikalische Zeitschrift*, 25:49–52, 1924.

[133] G. Jones and M. Dole. The viscosity of aqueous solutions of strong electrolytes with special reference to barium chloride. *Journal of the American Chemical Society*, 51(10):2950–2964, 1929.

[134] H. Jenkins, B. Donald, and Y. Marcus. Viscosity b-coefficients of ions in solution. *Chemical Reviews*, 95(8):2695–2724, 1995.

[135] J. Jiang and S.I. Sandler. A new model for the viscosity of electrolyte solutions. *Industrial & Engineering Chemistry Research*, 42(25):6267–6272, 2003.

[136] I.M. Abdulagatov, A.B. Zeinalova, and N.D. Azizov. Experimental viscosity b-coefficients of aqueous LiCl solutions. *Journal of Molecular Liquids*, 126(1-3):75–88, 2006.

[137] G. Jones and S.K. Talley. The viscosity of aqueous solutions as a function of the concentration. *Journal of the American Chemical Society*, 55(2):624–642, 1933.

[138] M. Kaminsky. *Z. Phys. Chem.*, 12:206, 1957.

[139] C.A. Angell and R.D. Bressel. Fluidity and conductance in aqueous electrolyte solutions. approach from the glassy state and high-concentration limit. i. calcium nitrate solutions. *The Journal of Physical Chemistry*, 76(22):3244–3253, 1972.

[140] V.N. Afanas'ev, E.Y. Tyunina, and M.D. Chekunova. The influence of temperature and concentration on viscous flow of solutions of Et4NBF4 in propylene carbonate. *Russian Journal of Physical Chemistry A*, 83(12):2069–2073, 2009.

[141] G. Hefter, P.M. May, P. Sipos, and A. Stanley. Viscosities of concentrated electrolyte solutions. *Journal of Molecular Liquids*, 103-104:261–273, 2003.

[142] A.L. Horvath. *Handbook of aqueous electrolyte solutions: physical properties, estimation and correlation methods*. Ellis Horwood, 1985.

[143] K. Umemoto N. Matsuura. Formulation of stokes radii in DMF, DMSO and propylene carbonate with solvent structure cavity size as parameter. *Bulletin of The Chemical Society of Japan*, 48(8):2253–2257, 1975.

[144] M. Ue. Ionic radius of (CF3SO2)3C - and applicability of stokes law to its propylene carbonate solution. *Journal of The Electrochemical Society*, 143(11):L270–L272, 1996.

[145] H.D.B. Jenkins and K.P. Thakur. Reappraisal of thermochemical radii for complex ions. *Journal of Chemical Education*, 56(9):576, 1979.

[146] S. Tobishima and T. Okada. Lithium cycling efficiency and conductivity for high dielectric solvent/low viscosity solvent mixed systems. *Electrochimica Acta*, 30(12):1715–1722, 1985.